Manchester Metropolitan University

e-space

Manchester Metropolitan University's Research Repository

Please cite the Published Version

Ekpo, Sunday (2019) Engineering Subsystems Analysis of Adaptive Small Satellites. Doctoral thesis (PhD), Manchester Metropolitan University.

Downloaded from: https://e-space.mmu.ac.uk/625392/

Usage rights: Creative Commons: Attribution-Noncommercial-No Derivative Works 4.0

Additional Information: Doctor of Philosophy by Published Work

Enquiries:
If you have questions about this document, contact openresearch@mmu.ac.uk. Please include the URL of the record in e-space. If you believe that your, or a third party's rights have been compromised through this document please see our Take Down policy (available from https://www.mmu.ac.uk/library/using-the-library/policies-and-guidelines)

Engineering Subsystems Analysis of Adaptive Small Satellites

A thesis submitted in partial fulfilment of the requirements of Manchester Metropolitan University for the degree of Doctor of Philosophy by Published Work (Route 2)

2019

Sunday Cookey Ekpo

Department of Engineering

Contents

Contents 2
List of Figures 4
List of Tables 5
Abstract 6
Declaration 7
Statement of Ownership 8
Dedication 9
Acknowledgement 10
List of Abbreviations 11
Chapter One 13
Introduction 13
1.1 Motivation 13
1.2 Background Statement 22
1.3 Spacecraft System and Missions Design Tools Review 26
1.4 Spacecraft System Engineering Design 28
1.5 Aim and Objectives of the Research 32
1.6 Thesis Overview 33
1.7 Summary 34
Chapter Two 35
Adaptive Small Satellite Subsystems Engineering 35
2.1 Introduction 35
2.2 Adaptive Subsystem Design Methodology 35
2.3 Adaptive Multifunctional Architecture Design 37
2.4 HASS Subsystems Engineering 38
2.5 Adaptive Beamformer and Communication Link 39
2.6 Adaptive Subsystems Operational Times Analysis 40
Chapter Three 42

Technical Publications **42**
3.1 Introduction 42
3.2 Published Works 42
3.2.1 Paper 1 [SE1] 42
3.2.2 Paper 2 [SE2] 53
3.2.3 Paper 3 [SE3] 64
3.2.4 Paper 4 [SE4] 74
3.2.5 Paper 5 [SE5] 82
3.2.6 Paper 6 [SE6] 93
3.2.7 Paper 7 [SE7] 97
3.2.8 Paper 8 [SE8] 115
3.2.9 Paper 9 [SE9] 120
3.2.10 Paper 10 [SE10] 132
3.2.11 Paper 11 [SE11] 154
3.2.12 Paper 12 [SE12] 161
Chapter Four **166**
Conclusion and Future Work **166**
4.1 Overview of Research Contributions 166
4.2 Future Work 167
References **169**
Appendices **177**
Appendix 1 177
A. Statistical Analysis of Mass-based PERs for LEO Satellites 177

List of Figures

Figure 1.1.1. Types, Shapes and Properties of Earth Orbit 16
Figure 1.1.2. A Multifunctional Communications and Radar System [21] 19
Figure 1.2.1. Effect of a Charged Particle on a Semiconductor in LEO 23
Figure 1.2.2. Effect of a Neutron on a Semiconductor in LEO 24
Figure 1.4.1. The Vee Diagram of a System Design Process. 30

List of Tables

Table 1.1.1. Space Payloads by Orbit and Mass [1] 15

Table 1.3.1. Major Spacecraft Systems Engineering Design Tools [31] 27

Abstract

The current point-based satellite electronic subsystem engineering design process is insufficient to address the dynamic operations and post-mission reuse of small satellites. Also, space systems and missions require an adaptive architecture(s) that can withstand the radiation-prone flight environment and respond to in-situ environmental changes using onboard resources while maintaining optimal performance. This enormous conceptual design variables space/task of highly adaptive small satellite (HASS) system can be too large to explore, study, analyse and qualify.

This research involved a parametric electronic subsystem engineering design process and methodology development for the production of sustainable capability-based small satellites. Consequently, an adaptive multifunctional architecture with five levels of in-orbit spacecraft customisations that eliminate subsystem boundaries at the system level is presented. Additive manufacturing methods are favoured to fabricate the proposed adaptive multifunctional monolithic structures. The initial system engineering analyses reveal that the HASS system has mass-, cost- and power-savings over the conventional small satellite implementation.

An adaptive small satellite link performance improvement satisfying a less than 2 dB link margin loss for a 0.1 dB in-band noise figure ripple has been established. Moreover, a power budget model for HASSs that ensures a reliable solar array design and eliminates undue equipment oversizing has been developed. An adaptive broadband beamformer that can improve the satellite link margin has been designed. Also, an estimating relationship has been developed and practically validated for the operational times analysis of small satellite subsystems. The reported novel findings promise to enable capability-based, adaptive, cost-effective, reliable, multifunctional, broadband and optimal-performing space systems with recourse to post-mission re-applications.

Declaration

No portion of the work referred to in this thesis has been submitted in support of an application for another degree or qualification of this or any other university or other institution of learning.

Statement of Ownership

I certify

1. that this Thesis is my own account, based upon work actually carried out by me and that all sources of material, not resulting from my own investigation, including observational information, have been clearly indicated.

2. that no part of the work incorporated in the Thesis is a quotation from published or unpublished sources, except where it has been clearly acknowledged as such, and that any specific direction or advice received is also properly acknowledged.

Signed.....

Dedication

This research project is dedicated to the
Lord Jesus Christ for His great grace and fulfilling love in my life.

Acknowledgement

In the accomplishment of this project, tremendous assistance has been drawn from many persons. To them, too numerous to mention, the researcher wishes to acknowledge their unflinching support.

My eternal gratitude goes to my beloved wife for her focused and comforting love and faith that give me the strength, courage and resilience to soar through life. I remain profoundly thankful to our sons – Jior, Jiog and Jiop – for their soothing love, joyfulness and presence always.

I owe a great debt of gratitude to my advisor, Prof Andy Gibson, for his professional and academic guidance, advice, attentiveness and valuable suggestions which have enhanced the successful completion of my PhD by Published Work; his divinely-inspired professional counsel, academic tutelage, judicious advice, indelible academic research initiative and motivating encouragement are deeply appreciated.

The accomplishment of this research work at the relevant institution(s) would have been impossible without the sustained and committed sponsorship by the Akwa Ibom State Government of Nigeria and the Akwa Ibom State University of Technology (AKUTECH). My friends at the AKUTECH deserve a special recognition for their unalloyed counsel, kindness and encouragement.

I would also like to thank The Manchester Metropolitan University for granting me the required facilities to carry out this fulfilled research documentation. Furthermore, my invaluable appreciation goes to my colleagues for their direct and indirect support of my research effectiveness to achieve novel life-transforming outputs.

Finally, the spiritual support I received from the Deeper Christian Life Ministry Inc., UK deserves my indelible gratitude.

List of Abbreviations

ADC	Attitude determination and control
AESA	Active electronically scanned array
AIAA	American Institute of Aeronautics and Astronautics
ALNA	Adaptive low noise amplifier
ALO	Adaptive local oscillator
AMA	Adaptive multifunctional architecture
AMSU	Adaptive multifunctional structural unit
ARMA	Adaptive reconfigurable multifunctional architecture
ASIC	Application-specific integrated circuit
AWR	Adaptive wideband receiver
BOL	Beginning-of-life
CASE	Complex adaptive systems engineering
CBM	Core bus module
CDR	Critical design review
CDS	Command and data subsystem
CER	Cost estimating relationship
CFP	Customer-furnished payload
CoDR	Conceptual design review
DSS	Distributed satellite system
EOL	End-of-life
FPGA	Field programmable gate array
FRR	Flight readiness review
GEO	Geostationary orbit
HAA	Highly adaptive attosatellite
HAC	Highly adaptive CubeSat
HAF	Highly adaptive femtosatellite
HAM	Highly adaptive microsatellite
HAN	Highly adaptive nanosatellite

HAP	Highly adaptive picosatellite
HASS	Highly adaptive small satellite
LEO	Low Earth orbit
LNA	Low noise amplifier
MCM	Multichip module
MEMS	Microelectromechanical system
MEO	Medium Earth orbit
MGT	Multi-gigabit serial transceiver
MMIC	Monolithic microwave integrated circuit
NASA	National aeronautics and space administration
PCB	Printed circuit board
PDR	Preliminary design review
PER	Power estimating relationship
PMR	Power-to-mass ratio
PNG	Portable network graphics
PRISM	Packet router interface switch matrix
PRR	Preshipment readiness review
RCIC	Reconfigurable cooperative intelligent control
RER	Reliability estimating relationship
SiP	System-in-package
SoC	System-on-chip
SoP	System-on-package
STP	Spacecraft team's payload
WMM	Worldwide mission model

Chapter One

Introduction

1.1 Motivation

The advances in electronic subsystems technologies have continued to enable multipurpose capabilities for terrestrial and space communications applications and reuse. The device standards onboard space equipment have been greatly influenced by very large scale integration (VLSI) and embedded systems spanning active and adaptive semiconductor devices technologies.

Multifunctional complex satellite subsystems can be realised as an integrated entities design [SE1]. Multifunctional structures [SE2, 1, 2] enable volume and mass savings of a spacecraft to be about 80 % and 90 % respectively; the combined assembly and rework labour also decreases by up to 50 % [1].

Furthermore, the widespread adoption of additive manufacturing (AM) techniques and/or unitisation construction processes has enhanced the timely and cost-effective fabrication of complex satellite structures with stringent requirements [1, 2]. It is 3D printing in an industry scale. AM provides the facility to investigate new manufacturing and materials technologies prior to effecting the large capital investments associated with the component- and system-levels production. Innovative design processes (such as multifunctional structures) that are not feasible and/or economical using conventional machining techniques can be implemented with the design and flexibility enabled by AM. Hence, it is possible to fabricate subsystems with internal layers and/or features. This is very desirable for miniaturised multifunctional small satellite electronics, sensors and thermal regulators [2].

The consequence is the accomplishment of multipurpose space missions enabled by light-weight smaller satellites which are reliable, optimal and economical.

The prevailing applications and/or opportunities for this research work span the following thus:

- The need for an electronic subsystems engineering analysis tool for the combined conceptual and mission design of adaptive small satellites [SE1];
- In-orbit satellite reconfiguration for quality and reliability [SE2, SE9];
- Advanced radio access technology(s) [e.g., the fifth-generation (5G standard)] for integrated space-terrestrial communication networks [SE3–SE6];
- Advanced additive manufacturing of multifunctional small satellites for very rapid manufacturing and significant cost reduction [1, 2, SE10];
- Post-mission satellite reapplication [SE1, SE11, SE12];
- Satellite subsystems operational times reconfiguration [SE2, SE10];
- Availability of digitised analogue subsystems design tools [SE5, SE6];
- Seamless ubiquitous global communication [SE5, SE6]; and
- Emerging markets and use cases: [SE1–SE3, SE5]:
    - Increasing access to broadband (internet);
    - High speed and secure data networks;
    - Increased connectivity in dense or remote areas; and
    - Internet of Things (IoTs).

The Worldwide Mission Model (WMM) [3] has been developed to assess and predict the future space payloads market each year. A snapshot of future payloads for the period 2011 – 2030 (released in 2011) indicates that 2,315 proposed payloads are underway; this is 14 % and 4 % greater than the 2009 and 2010 figures respectively. The WMM further reveals that a considerable growth in the space payloads market is expected to be from the small satellite programmes spanning mini-, micro-, nano-, pico- and

femtosatellites (Table 1.1.1) [1]. The dominant orbits (Figure 1.1.1) for deployment are the low-Earth orbit (LEO) (1,465) and geostationary orbit (GEO) (532) by 2030.

Table 1.1.1. Space Payloads by Orbit and Mass [1]

Payloads	Yearly total		
By orbit	2011	2012	2013
Low Earth orbit	246	268	245
Geostationary orbit	56	94	63
Medium Earth orbit	12	9	13
Deep space	24	24	13
Elliptical orbit	13	2	1
Total	351	397	335
By mass (kg)			
1 – 500	157	172	181
501 – 2,000	106	118	86
2,001 – 4,000	28	37	22
4,001 – 6,500	42	22	31
Over 6,500	18	18	15
Total	351	397	335

Small satellite research has been around for approximately thirty years [1–11]; the present challenge is that of making it more application-independent with attendant merits. The National Aeronautics and Space Administration (NASA) has proposed five goals for small satellites such as nanosatellites: [8]

- Advanced capabilities;
- Advanced system architecture and practical;
- Less cost for launching and shorter period for fabrication;
- Ability to verify new design scheme(s);

- Adoption of application-specific integrated micromachines (ASIMs); and
- Ability to propel the application of some commercial technologies.

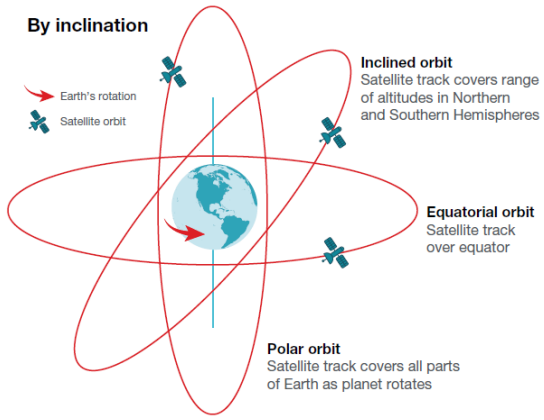

(a) By Inclination

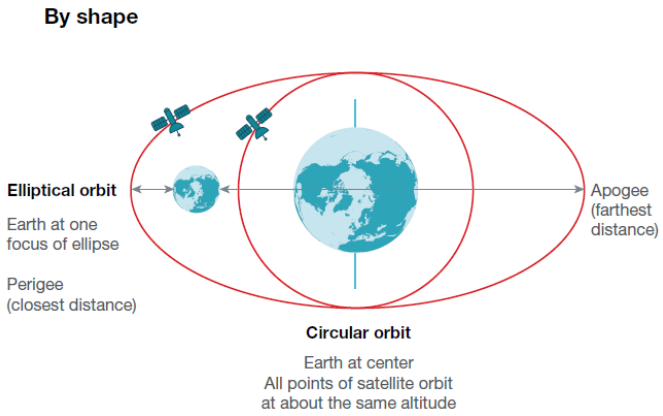

(b) By Shape

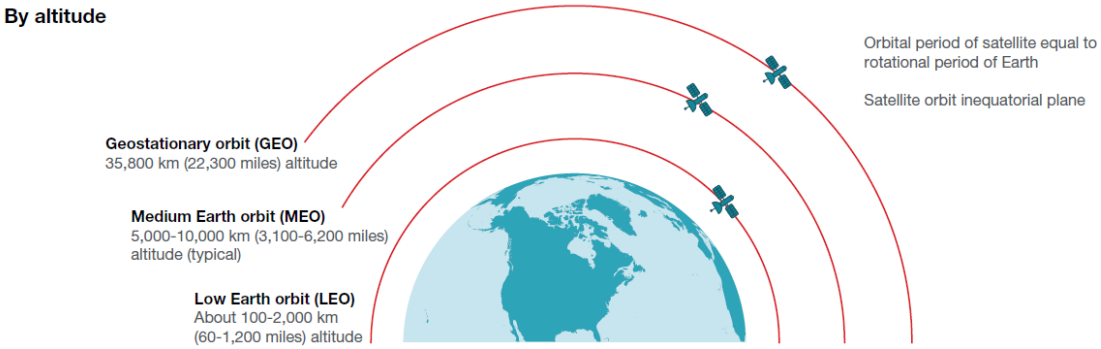

(c) By Altitude

Figure 1.1.1. Types, Shapes and Properties of Earth Orbit

The above objectives can only be realised through an intelligent selection and adoption of emerging subsubsystem, subsystem and system design and

integration technologies and architectures. This would also encompass using scaling strategies [SE10] to enhance spacecraft design [SE1] and manufacturing [1, 2]. For instance, CHIPSAT or satellite-on-the-chip development is an area of research that houses the conventional satellite subsystems [4–12] on a small microelectromechanical system (MEMS) substrate [13]. Application-specific integrated circuits (ASICs), field programmable gates arrays (FPGAs) [12, 14], monolithic microwave integrated circuits (MMICs) and MEMS are the present driving technologies behind CHIPSAT and further advances in these areas reveal a promising future for this novelty [15–20]. Technology drivers for small satellite systems revolve around CMOS-based integrated circuits (ICs), printed circuit board (PCB) integration of ICs, sophisticated ASICs, FPGAs, MEMS, multichip module (MCM), system-in-package (SiP), system-on-package (SoP) and additive manufacturing. These advanced design technologies, architectures, production approach and packaging techniques have enabled novel research pursuits in the design of heterogeneous multisubsystem system-on-chip (SoC) [15]. The SoC architecture bears less number of off-chip and interchip connections. This greatly enhances its reliability and reduces power consumption. The MCM technique enables unpackaged ICs to be integrated on different substrates onboard a SoC; the interconnects linking the components together are finer than a PCB implementation. MCM comes in grades: MCM-L is akin the conventional PCBs with no allowance for multicomponent embedding in multiple layers; MCM-C (ceramic substrate) and MCM-D (thin-film substrate) allow multicomponent embedding. In a SiP implementation, the SoC design features a system-level function in a chip package; passives and silicon devices (dies) are all mounted on the same substrate. This increases the quality of the functional unit and requires very few external component footprints to accomplish the mission. The SoP integrates device-level technologies for multipurpose applications. It houses the SiP and external components in a single module. The components are

codesigned and fabricated together at the IC and package levels; the SoP is a system that harnesses the best features of these two scaling strategies. Several digital, analogue, optical, sensor and control functions are implemented on the same substrate platform [15].

Micro- and nanosatellites make use of VLSI and embedded systems technologies [20, 21]. These also lend great credence to MEMS substrate and could be designed to be application-specific or field-programmable [22]. Active devices employing the hybrid MIC have not been greatly used in the past for developing small satellites due to their inherent limitations – narrowband, weight and size. The advent of the MMIC technology has ushered in tremendous breakthroughs in this area especially in the design of reliable reconfigurable switches and active antennas [22, 23]. Also, field programmable gate arrays (FPGAs) can enable the key performance traits of ASICs and microprocessor-based devices [12, 14, 19, 20]. It does system configuration and real-time reconfiguration for diverse custom hardware platforms; this is very attractive for a small satellite design.

Moreover, the applications of radio frequency subsystems in satellite communication systems have continued to expand with attendant challenging system-level performance requirements. For instance, the performance constraints of a RF transmitter include, but are not limited to, handling multiple carrier frequencies, widely varying RF power levels, differing modulation formats and linearity specifications and varying impedance provided by the antenna [22]. A power amplifier that operates on any frequency band adds value to the spacecraft system reliability and availability [23–30]. Hence, achieving the same performance at broadband as in narrowband frequencies is highly desirable. This would involve retuning the power amplifier subsubsystem onboard the spacecraft at the different frequencies rather than using one broadband amplifier. Some of the benefits of adaptive amplifiers [21] onboard a spacecraft include:

- Reconfiguration to support different spacecraft mission objectives (such as switching from communication to radar applications; a typical architecture is shown in Figure 1.1.2 [21].

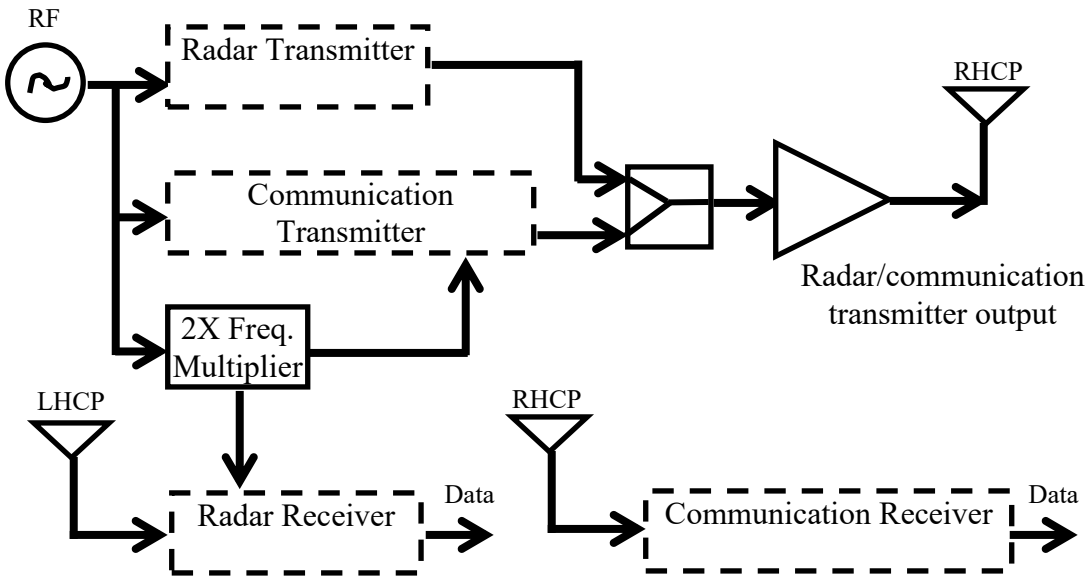

Figure 1.1.2. A Multifunctional Communications and Radar System [21]

In Figure 1.1.2, quasi-orthogonal linear-frequency-modulated (LFM) waveforms are used for both the communications and radar subsystems; the LFM waveforms obviate the need for time-division multiplexing. Modern systems (such as personal digital assistants and cell phones) deploy multifunctional architectures to enable simultaneous operations of different multicomponent systems. A multifunctional system also benefits from low cost and reduced size and volume. These advantages have been exploited by the military in the development of broadband RF antenna systems that have the capabilities for simultaneous radar, electronic warfare and communication operations [21]. The multifunctional communications and radar system has been implemented at a centre frequency of 750 MHz. With the simultaneous operations, an instantaneous bandwidth of 500 MHz was achieved. A radar pulse width of 1.5 ns, pulse repetition frequency of 150 MHz and data rate of

1 Mbps were used by the investigators to conduct a performance test; the probability of detection, probability of false alarm and BER were measured as 99 %, 7 % and 2 x 10^{-3} respectively [22]. The communications and radar functions are accomplished through a shared aperture or single transmit antenna. The communication receiver employs a right-hand circularly polarised (RHCP) helical antenna and the radar receiver, left-hand circularly polarised (LHCP) helical antenna. Opposite antenna polarities were used for the radar receiver and transmitter to check the effect of reflection while operating in the bistatic radar configuration.

- Onboard tuning after manufacturing; this obviates manual tuning and associated cost, relaxes component tolerances and reduces amplifier's susceptibility to temperature variations/aging.
- Nominal operating conditions can be selected as opposed to worst case design margins. Hence, tuning and bias conditions are adapted to system demand to improve efficiency and linearity of the amplifier.

Considerable work has been ongoing for over ten years in achieving adaptive circuits for microwave subsubsystems, subsystems and systems. Operational requirements such as variable microwave output frequency, variable output power level, variable modulation formats, variable antenna impedance and variable interference sources and constraints characterisation have been developed [21].

A key issue surrounding spacecraft in orbits is the impact of the solar radiation on the onboard semiconductor devices [17]. Hence, it is not enough for a system to be adaptive, it must survive in the unpredictable environment where it is deployed. Consequently, radiation-tolerant adaptive devices (such as field programmable gate array (FPGA)) have been developed and qualified as independent and integrated subsystems for control and signal processing applications. The monolithic integration of FPGA and GaAs-based RF/microwave subsystems promises to enable reliable deterministic satellite operations [SE10].

Though space systems and subsystems technologies have recorded unprecedented advances in the last forty years [3, 17], the system-level focus of the conceptual design phase for any given spacecraft requires optimality and not feasibility. Thus, the design model of the spacecraft must have cost and performance elasticity to changes in system requirements and applications for optimal results. Adaptive and multifunctional systems enable the reconfiguration of their functions and/or characteristics to meet various operational margins and emergent environments. This is why system resources adaptation and optimisation must be objectised for reliable space applications [SE1–SE4].

The fundamental motivations for the highly adaptive small satellite (HASS) concept are, but are not limited to, in-orbit adaptability, reliability, multifunctionality, enhanced portability, system-level simulation of spacecraft, reduced manufacturing and integration complexities, cost-effectiveness, safety, low carbon footprint, post-mission re-application and flexibility in deployments [SE1–SE8]. This capability-based space system design [SE1, SE2] will gain increasing and expanding applications in future deployments of constellations of small satellites. The novel HASS system architecture has an in-built redundancy and radiation shield for onboard semiconductor components which can be re-engineered while in orbit.

The categories of highly adaptive small satellites [SE1, SE2] are highly adaptive microsatellites (HAMs), highly adaptive nanosatellites (HANs), highly adaptive picosatellites (HAPs), highly adaptive femtosatellites (HAFs) and highly adaptive attosatellites (HAAs); this thesis focused on the first four categories. Moreover, the mass of each category follows the mass classification convention used for traditional small satellites.

1.2 Background Statement

The conceptual design of satellites involves several modelling and simulation approaches that span single person calculations to multiple organisations employing complex and advanced interconnected computer models for optimised solutions [SE1, 13]. The four design approaches that are currently utilised within the space community include back-of-the envelope techniques; single-use, computer-aided models; serial processes; and integrated concurrent engineering [SE1, 13]. These techniques can be combined to meet the customer's needs or a hybrid of several design methods may be implemented. Whatever the adopted design approach, a single solution or specific mission design interests may be the focus.

The conceptual design is influenced by several factors and design constraints and has no unique "right" technique [SE1, SE2, 13]. Issues ranging from the project manager's background, corporate culture, team leadership, cultural differences, and dynamics also determine the choice of a conceptual design approach for a spacecraft mission [SE1, 13].

The increase in the number of spacecraft launched each year has necessitated a reassessment of the system engineering margins governing their design, production and operation [SE1, 13, 15, 17, 25–30]. Technical and environmental constraints [SE1] have also prompted a review of existing SE procedures used for spacecraft programmes [SE4, 13, 15, 17, 31–33]. Satellites are generally deployed in orbits with mission-limited self-generated power margin and electronics-degrading radiation environment [13, 15]. For instance, the majority of artificial and communication satellites are placed in the LEO; this has an altitude span of 160–2000 km and houses small satellites such as microsatellites and nanosatellites [15]. As a non-geostationary orbit, LEO contains satellites that form a constellation to provide continuous coverage [15, 30–39]. They experience atmospheric drag (due to gases in the thermosphere) and harsh radiation environment. Below

600 km, the orbital lifecycle of a satellite is constrained by atmospheric friction and unpredictable. The satellite's lifecycle increases with the altitude of the orbit by design. The high-altitude satellites enjoy wide coverage due to the increase in the footprint angle. A disadvantage with high altitude flight is the increase in radiation resulting from the Van Allen belts; this damages semiconductor subsystems and decreases their lifetime [11, 15–18].

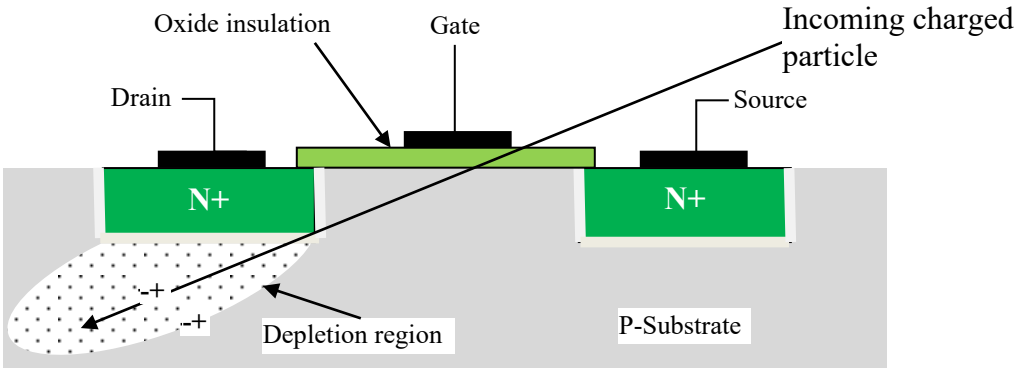

Figure 1.2.1. Effect of a Charged Particle on a Semiconductor in LEO

Moreover, incoming charged particles (such as an alpha particle or heavy ion) impact semiconductors leaving trails of ionisation through the substrate. Consequently, a momentary current pulse proportional to the incoming energy state is set up in nearby transistors (Figure 1.2.1). This can change the data states of memory cells and flip-flops in semiconductor devices [11, 15, 18].

Similarly, cosmic rays and heavy charged particles streaming out from the sun in the solar wind react with gases in the upper atmosphere to produce high energy neutrons. A neutron impact on a semiconductor device may collide with a silicon atom in the substrate. A cloud of heavy ions may be ejected resulting in a current pulse in the electronic device (Figure 1.2.2). These neutrons impact on the onboard semiconductor devices to produce unpredictable in-orbit failures in semiconductor subsubsystems and subsystems. For instance, the current pulse, which varies as the energy level

of the incoming neutron, can cause data in memory cells and flip-flops of complementary metal-oxide semiconductors (CMOS) integrated circuits (ICs) to change [14, 17]. As a result, the space systems in LEO have a potential replacement timeframe of 10 years [15, 16]. This translates into a huge investment cost that could be avoided through a judicious post-launch and post-mission system-level re-engineering.

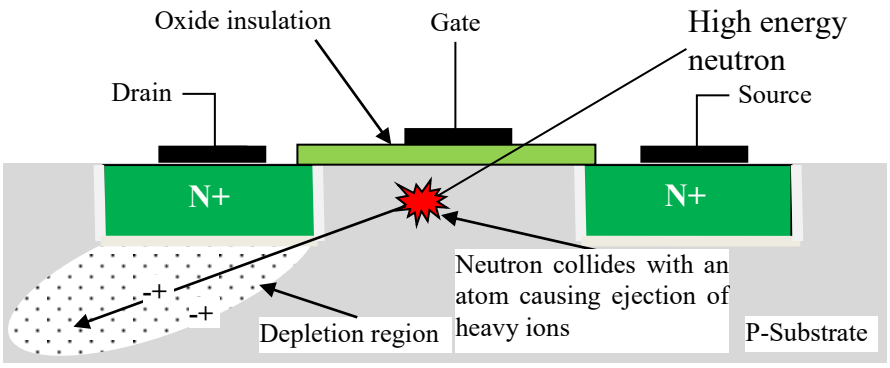

Figure 1.2.2. Effect of a Neutron on a Semiconductor in LEO

Furthermore, limited frequency spectrum and spatial capacity (orbital slots), high equipment cost, increased space debris [34] and expanding global broadband connectivity require capability-based space systems [SE2, SE4, SE7].

Satellite attitude control and space situational awareness are of great concern within the space community [SE5, 34]. A good number of spacecraft system issues bordering on real-time space surveillance are yet to be qualified for satellite applications [SE5]. Technologies such as active electronically scanned array (AESA) radar [35, 36] and mm-wave low noise amplifiers (LNAs) [SE7, 37–43] have been qualified for flexible, proactive and reactive beamforming [SE3] and image detection. These are also considered possible options for reliable and secure space operations.

A satellite procurement programme often starts with the design and development phase [6, 9, 11, 13]. This includes the analysis and design of the various systems, subsystems and units of a satellite; the mechanical models development; and test platforms for innovation certification prior to deployment [43-48[. Furthermore, a priori deployment requirements also involve various tests bordering on temperature variations, acoustic vibration levels and acceleration levels. These form an integral part of the overall engineering model standard tests for space equipment [15, 16].

The development of the highly adaptive small satellite (HASS) seeks to overcome the enormous technological and operational challenges of space programmes cost-effectively [SE1, SE2, SE7]. A HASS is a reconfigurable, multifunctional and adaptive small space satellite that has capabilities for dynamic space applications and operations while retaining its designed optimal performance [SE1, SE2, SE5]. Existing SE procedures [13, 15] are insufficient to give a complete analysis of this type of space system. Hence, the need to review the existing SE with respect to the emerging space satellite architectures, technologies and applications [SE1 – SE3]. To achieve appropriate link budget and system engineering analyses of capability-based small satellites missions, an objective assessment and computation of the component-, subsystem-, and system-levels parameters requirements must be carried out. This thesis presents the measurement-derived parametric models for the system engineering analysis of communication, meteorology, planetary, and other small satellite programmes with recourse to the initial mission, conceptual design, and post-mission objectives. Mass and power margins constitute the critical resources under investigation besides the link contingencies [SE8] and operational times [SE2].

1.3 Spacecraft System and Missions Design Tools Review

Novel attempts have been made to design space systems based on single and multidisciplinary designs optimisation and architecting resulting in useful existing systems engineering tools [SE7, 3, 25, 31, 32, 41, 42]. These techniques are utilised in the space industry to optimise satellite constellation architectures and spacecraft designs; spacecraft missions such as NASA's Near Earth Asteroid Rendezvous (NEAR) attest to the application of this technique for the conceptual design of spacecraft and distributed satellite systems (DSS) [17]. Furthermore, a dynamic programming approach has been utilised to assess the impact of subsystem technologies on the overall performance and cost of spacecraft missions [17]. The Ball Aerospace and Technologies Corporation have also developed reconfigurable multifunctional spacecraft architectures (RMA) [9]. Though their work advances space systems engineering beyond the traditional discrete component-oriented design approach, it fails to emphasise the enabling technology of the multifunctional modules to higher-level mission-specific functions. Moreover, the RMA concept does not address the system-level implications of the multifunctional structural units that contain the embedded electronics, wiring, thermal control and required discrete devices.

The majority of the spacecraft systems works have been on individual spacecraft and constellations designs and management issues [13, 15, 49-59] without an obvious recourse to a capability-based spacecraft adaptation [SE1, SE2]. Thus, the HASS system is a new spacecraft design approach that incorporates capability-based space systems, subsubsystem-, subsystem- and system-levels technologies, cost and system-level performance, adaptability, reliability, multifunctionality and reconfigurability in its mission accomplishment [SE1, SE6–SE8]. Spacecraft systems engineering design is a complex integration of interdisciplinary fields, technologies and specialties

[13, 15, 60-70]. Table 1.3.1 lists some of the dominant system engineering design tools in common use today by space systems design experts [17, 58–68]. Some of the tools were developed for private use and unique applications and therefore not available for the public.

Table 1.3.1. Major Spacecraft Systems Engineering Design Tools [31]

Tool	Use
Modsat	A software for small satellite design; interactive execution, defining alternative hardware configuration, feasibility verification, performance testing, utility sizing and optimisation.
ASSESS	Rapid spacecraft architecture analysis, concept exploration, and cost estimation.
STK	A suite of analysis software tools that addresses all phases of satellite system's life cycle, including policy development and design phases.
COBRA	Automated assessment of program cost risk and schedule risk as a function of spacecraft complexity for interplanetary missions.
Concurrent Engineering Methodology (CEM)	Mapping of "what if" cost and performance trade studies for Air Force missions.
ESSAM	Small satellite bus component selection.
GENSAT	Object-oriented software that interconnects existing commercial satellite subsystem tools (STK, CAD, IDEAS, etc.) and component databases for systems design.
ICE	Concept definition of novel space missions via integrated information systems.
MERIT	Automated assessment of the cost and performance implications of inserting existing s. new technologies into spacecraft bus.
MIDAS	Analysis of Proposed spacecraft designs via integrated tool executions on distributed machines.
Modelsat	Cost and mass modelling for communications satellites.

Project Trades Model (PTM)	Cost and performance prediction of novel interplanetary and space science missions.
QUICK	Spacecraft design programming language with extensive component databases and scaling relationship for conceptual spacecraft design.
ISSODMA	Combines STK with designing, analysing, certifying and optimising the project of satellite orbit design during the proposal research stage.
SCOUT	Single spacecraft mission bus component and launch vehicle selection.
SMALLSAT	Earth observation spacecraft senor and satellite bus configuration.
SMAD	Software automation of the calculations in Larson and Wertz's Space Mission Analysis Design.
SpaSat	A preliminary spacecraft sizing, cost estimating and orbital analysis tool for Ball Aerospace missions.

The HASS system engineering design process and analysis has been developed and presented in this thesis as an additional SE tool that enables the design of capability-based spacecraft. The HASS SE process/methodology bridges the gap between traditional spacecraft SE and complex adaptive spacecraft SE [SE1, SE2, SE7, SE8]. It serves as a tool for a full-scale conceptual design and analysis of modern and future adaptive small satellites [SE1, 15]. The procedure can be extended to cover large spacecraft systems [13] employing the adaptive architecture [SE10].

1.4 Spacecraft System Engineering Design

System engineering (SE) involves the specification of the objectives of a system and the qualification of the components and subsystems needed to satisfy its requirements cost-effectively. Hence, the customer requirement(s)

comes first before the selection of the relevant technologies mix or system that satisfies it.

An understanding of a system is essential for developing a sustainable and reliable SE procedure. The context, behaviour and subsystems of a system explain its purpose and essence. A complex system comprises integrated networks of functional hardware, software, firmware and human resources. Each layer of a complex system is a system in its own right. Thus, each layer of a complex system contains the context, behaviour and subsystems (called subsubsystems) unique to it. Consequently, this results in a system of systems (SoS). As an example, consider a spacecraft constellation or formation flying in which spacecraft, international space station engineers and scientists, ground station controllers/mission operation team work together using telemetry, engineering data, command and data signal, radar and communication systems to maintain satellites in the correct orbit in an unpredictable environment throughout their lifecycles. Each functional member of the system is a unique system with qualifying and quantifiable engineering attributes and/or characteristics [14, 17, 25, 27–30].

A SoS is, therefore, defined as "a set or arrangement of systems that are related to or connected to provide a given capability. The loss of any part of the system will degrade the performance or capabilities of the whole" [29]. According to the Department of Defence (DoD) Guide for SoS, a SoS refers to "a set or arrangement of systems that results when independent and useful systems are integrated into a larger system that delivers unique capabilities" [29]. These two definitions of SoS recognise the constituent parts of a system and their unique attributes that enable the system to achieve the intended purpose. Advances in adaptive and reconfigurable subsubsystems, subsystems and systems devices, designs and architectures have enabled the development of multifunctional and deterministic SoS [SE1, SE5, 10]. A complex system has its constituent elements as subsystems which in-turn have subsubsystems within their boundaries. The "Vee diagram" gives a

complete level-by-level breakdown of a complex system (or SoS) and the process of design, build and test to develop, qualify and deploy the system. This top-down process for complex systems or SoS design is called the SE process [29, 30].

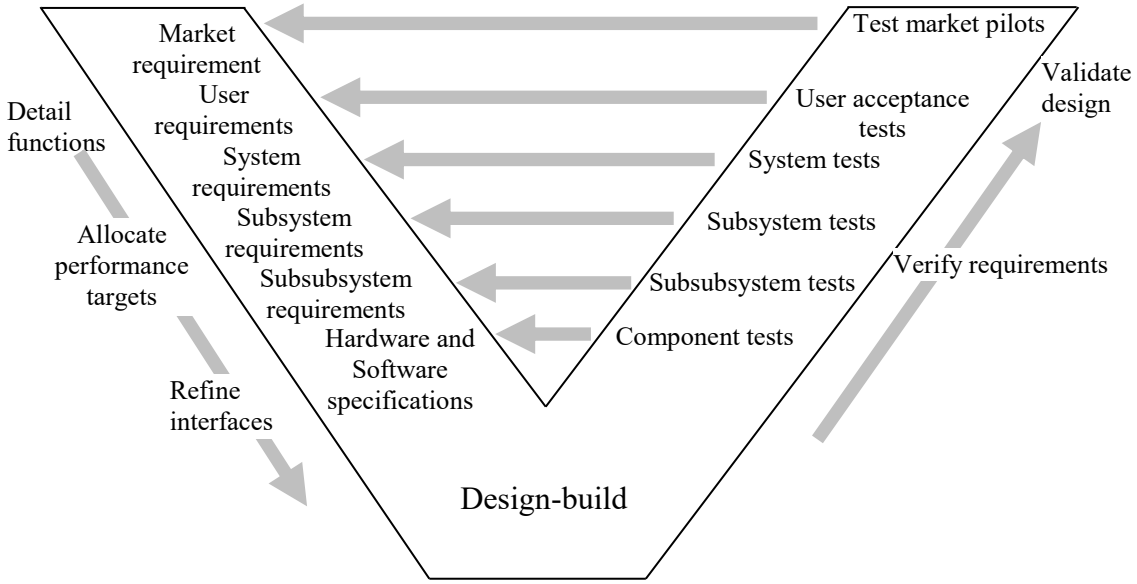

Figure 1.4.1. The Vee Diagram of a System Design Process.

The V diagram is shown in Figure 1.4.1 [29]. It is the acceptable design process with no recourse to the backtrackings and parallel nature of activities that take place in complex systems. For example, spacecraft engineers may develop smart constellation payloads but are not entirely sure of how the in-orbit operation will be following an adopted integration architecture. The detailed functions, performance targets allocation and interface refinement are explained on the left-hand side of the V. This process is applied to each subsystem and subsubsystem until the attributes and/or specifications are stated. The design-build domain at the base of the V houses where engineers develop and proffer solutions that meet the stated system constraints or specifications. Design validation and qualification occur on the right-hand side of the V. Tests are conducted at each component integration level to

ascertain compliance with the objectives of the design mission; respective components and modules tests precede the system-level integration tests and verification. The final verification and/or validation tests involve the customer (and market)'s response to the design; this indicates whether the objectives of the mission have been met by the design.

The international council of systems engineering (INCOSE) has defined the relevant steps in the complete SE process. It is a structured process and begins with stating the problem relating to the customer needs/requirements. The end is a solution or an output in terms of a system that delivers the requirements or a product resulting from having the system in place. The SIMILAR process for SE [16] is summarised thus:

- State the problem;
- Investigate alternatives;
- Model the system;
- Integrate;
- Launch the system;
- Assess performance; and
- Re-evaluate the steps with respect to stakeholder needs.

For instance, consider a communication spacecraft system developed for the LEO. The key drivers for the requirement that the system is expected to satisfy can be stated as follows:

- the market, the people and the organisations requiring the communication capability;
- identification of the locations for deployment/delivery of the communications; and
- characterisation of the services available such as voice, video and data.

System engineering of spacecraft involves the functional development of the detailed engineering tasks in a spacecraft design. It begins with the complete requirements that should characterise the satellite system together with the choice of key aspects that satisfy those requirements. In spacecraft

sizing, the technology choices and redundancy levels form the input for satisfying the payload requirements and core bus subsystems; the spacecraft sizing model uses these information and the chosen launch vehicle data to determine the power, mass and size of the spacecraft. In satellite system engineering, key performance parameters are tracked and assessed based on the observed system-level changes. Subsystem failures and/or issues revealed during final system integration are redressed by simulation/modelling. Vital technical adjustments are then carried out to ascertain the desired system-level functional margins [SE5, SE12].

1.5 Aim and Objectives of the Research

This research aims to establish a design routine that will enable the development and construction of capability-based small satellites for next-generation multipurpose space applications based on the enabling and emerging adaptive and active devices technologies. The attendant merits of reduced launch time and cost, reliability and multifunctionality are amongst the expected benefits from this novelty [SE1, SE2, SE6, SE10, SE12].

The main objectives of the proposed research work follow:

- To identify emerging space systems technologies for applications requiring adaptive spacecraft systems;
- To develop a design methodology and a technology framework for the conceptual design of an adaptive small satellite system. The methodology will search the trade space (design variables) and reveal the best solutions following the metric(s) of choice;
- To develop an adaptive multifunctional architecture for capability-based spacecraft systems that are reconfigurable while in orbit;
- To establish adaptive spacecraft design models for each small satellite subsystem for various space applications; and
- To provide a novel, inventive and adaptable small spacecraft electronic subsystem engineering design approach for different operational constraints

thereby establishing a sustainable technology platform for the space community.

1.6 Thesis Overview

A system engineering design methodology was developed to establish a small satellite electronic subsystem engineering design procedure and architecture [SE1, SE2, SE5, SE10]. The implementation of the developed research methodology for this PhD study work was formulated around technical publications that demonstrate "a strong academic career evidenced by publication." Hence, the method adopted for this study is a compilation of the analytical commentary of the published and prevailing research works in the subject area of the research project. This entails detailing the relevant peer-reviewed and refereed publications that show convincing evidence of the capacity to pursue research and scholarship and make an original contribution and substantial addition to the pool of knowledge. The adopted research project methodology involves a careful study, statistical analysis (Appendix 1) and implementation of the enabling and emerging space system technologies, architectures and design concepts for realising adaptive small satellites for space applications [SE1, SE4]. This work focuses on the power and mass budgets as the premium resources for spacecraft system engineering margins design [SE1, SE2, 13, 15]. The small satellite subsystems constitute its functional blocks. The eight subsystems of a typical satellite system to be considered are the propulsion; attitude and control; electrical power supply; thermal control; communication; command and data; structure and mechanisms; and payload.

Chapter one critically introduces the motivation and background statement behind the adaptive small satellite design for space applications research. The background statement critically examines the challenges of the spacecraft mission project and shortcomings of the conventional approaches in addressing them. Spacecraft systems engineering and design tools are

covered. The highly adaptive small satellite (HASS) has been proposed to reliably, sustainably and cost-effectively accommodate the electronic subsystems concerns of the space community.

Chapter two presents the full narrative of the research and highlights the contributions to the pool of knowledge in the subject area and the allied fields.

Chapter three contains the full paper contents of the published works that demonstrate the novelty of this research.

The conclusion and future work surrounding this thesis/analytical commentary are presented in chapter four. The pertinent contributions of the research are explained here. The future research works possible with the novel highly adaptive small satellite system are contained in this chapter. Moreover, the statistical analysis for mass-based power estimating relationships for LEO satellites is stated in Appendix 1.

1.7 Summary

The motivation for the adaptive small satellite design for space applications research has been explained in this chapter. Key emerging space applications; enabling existing technologies and architectures; payloads; and advanced production techniques(s) have been explored. The background statement gives a critical analysis of the implementation constraints encountered in a given spacecraft mission project; the incapability of the traditional small satellite design approaches in addressing the challenges has been stated. The highly adaptive small satellite (HASS) has been proposed for capability-based missions with recourse to in-orbit system re-engineering for post-mission re-application. The major system engineering design tools have been critically studied, compared with the HASS system and presented in this chapter. Moreover, this chapter contains the aim and objectives of the thesis.

Chapter Two

Adaptive Small Satellite Subsystems Engineering

2.1 Introduction

This chapter contains the full narrative and the key contributions of the research work. It is arranged into adaptive subsystems design methodology; adaptive multifunctional architecture design; adaptive subsystems engineering analysis; adaptive beamformer for small satellites; impact of noise figure on a satellite link; adaptive small satellite customisations; and adaptive subsystems operational times analysis.

2.2 Adaptive Subsystem Design Methodology

This section presents the system engineering design and analysis methodology for highly adaptive small satellites developed for the conceptual design and validation of the mass and power budgets of HASS electronic subsystems.

The design, development and implementation of conventional satellite systems emphasise the problem analysis methodology required of a holistic systems engineering [2, 4, 13]. The traditional satellite subsystems design methodology is point-based and non-reconfigurable with no recourse to multifunctional mission applications and reuse. Whilst conventional multifunctional structures designs do exist, they are based on a mission-specific methodology [1, 2]. The HASS subsystem methodology incorporates multifunctional analysis and design engineering [SE1, SE10] of a system into a capability-based space satellite programme. Hence, two systems engineering design methodology concepts have been contributed to the

existing pool of knowledge, viz: systems engineering design process and systems engineering design analysis. The contributed systems engineering design process refers to the inherent interrelated multifunctional system of systems architecture adopted for a capability-based satellite system design. Similarly, the systems engineering design analysis refers to the inherent interrelated capability-based systems engineering design resources considerations and trade-offs for a capability-based satellite system design [SE1, SE2].

The developed adaptive subsystem methodology [SE10] considered enabling and emerging technologies and so can be extended and scaled-up to address the mission definitions requirements of medium and large spacecraft [SE1, SE2, SE4]. The HASS design approach [SE10] eliminates the prevailing limitations of conventional satellite design methods – which are wholly based on pre-set requirements and non-components-level reconfigurations [2, 4, 14]. The developed HASS methodology is founded on the fundamental satellite systems engineering design process and generalised information network analysis model [SE1, SE5]. The functional definitions of the HASS methodology allow for the spacecraft mission and conceptual design objectives to be studied within a capability-based framework [SE1]. It is an iterative process that defines and combines the mission requirements with recourse to the space system transformation. Subsubsystem-level technologies are chosen for integrated applications with allowance for trade-offs and performance assessment [SE8]. Capability-based mission objectives are supported and implemented using a reconfigurable satellite architecture platform [SE1, SE8]. Furthermore, the quality of service metrics for the relevant mission is assigned and the system design variables space explored for a solution. This is followed by HASS-based multicriteria studies aimed at qualifying the optimal system architectures [SE7–SE9]. This adaptive space system-level platform allows the designer to optimise device technologies, systems and subsystems configurations and architectures in an integrated

environment [SE2, 15]. In a typical HASS system implementation [SE5], radiation effects are mitigated using radiation-hardening by design [14, 15]. Current and future spacecraft systems engineering analyses can be accomplished using the HASS methodology for an objective satellite mission study and development [SE1, 13, 15].

2.3 Adaptive Multifunctional Architecture Design

Traditional satellite architectures follow a subsystem-oriented design approach [13, 15]. The adaptive multifunctional architecture (AMA) design concept [SE5] utilises multifunctional satellite scaling techniques to implement subsystemless architectures. The design process accomplishes functions [SE5, SE7] and eliminates conventional subsystem boundaries [13–17]. It focuses on the identification and specification of subsystem-level functional requirements. In this approach, the functions of several subsystems are implemented on a single circuit card.

The AMA design platform enables deterministic applications and lends credence to real-time performance. It contains point-to-point links that provide inter- and intra-subsystem communication and lower latency. The term "deterministic" connotes "real-time" and is widely used to describe systems employing FPGAs for various reconfigurable applications. In the case of HASS systems, the deterministic multifunctional architecture (DMA) approach allows for relocating system functionalities across and within the monolithic FPGA-RF/microwave subsystems. Thus, multiple mission capabilities can be sustained by changing parts of the adaptable architecture without interrupting the running functionality(s). The DMA implements reliable, flexible and high bandwidth links without undue population of FPGA I/O pins that characterise non-HASS systems. For instance, the HASS system is able to assign spacecraft resources to essential (such as attitude

determination and control) and non-essential (such as offline image or audio signal processing) functionalities without any overheads and/or penalties.

The AMA uses the modularity and high/low integration lightweighting strategies to achieve an efficient small satellite design [SE5]. It uses functional modules [SE5, SE10, SE11] to realise high-level mission-specific and non-specific functions. The functional design paradigm employs the functional modules for a small satellite design. These modules give the satellite system modularity that supports the high-level functionality(s) required for customised and re-engineered space missions [SE10, SE12]. Each adaptive multifunctional structural unit comprises a composite panel that provides mechanical, electrical and thermal functionalities. Compared with traditional and existing functional design-based satellites, physically replaceable/upgradeable components of the AMSU are fewer; this is a huge cost benefit for any space mission. The benefits of the AMSU implementation onboard a HASS system includes, but are not limited to, the elimination of massive wire harnesses and connectors, increased system-level reliability, fast design re-engineering, streamlined subsystem integration and test process and cost-effective mass production.

2.4 HASS Subsystems Engineering

The success of the satellite subsystems engineering depends on the optimal design, modelling, simulation, and validation of the deliverables of the conceptual and mission design objectives. Moreover, the design and development of capability-based and adaptive multifunctional small satellites require a reliable subsystems engineering procedure. In Papers SE1 and SE7, HASS-based parametric system engineering design estimating relationships have been developed. The emerging technology-based subsystem engineering design procedure [SE1] can be utilised for the conventional small satellites programmes [15] respecting the relevant resources assignment

adjustments. The is a major contribution to the space community as it enables the conceptual and mission objectives of spacecraft missions [13, 15] to be validated prior to the full system implementation. The presented adaptive subsystem engineering for mass and power budgets for HASS systems can accommodate space missions applications and post-mission reuse in the GEO, MEO and LEO [SE1, SE7, SE11]. The cost reduction is more for HASS systems compared with the conventional satellite design architectures and concepts. The HASS novelty is in the SE design and emergent missions capabilities enablement with the attendant economies of scale over the traditional satellite systems.

2.5 Adaptive Beamformer and Communication Link

Small satellite communication links are required to be stable for optimal temporal and spatial data transmissions. A key requirement of an adaptive sensor array involves the ability to deterministically adjust the directional response of the array to reduce noise, null interferences and enhance the gain and quality of the desired signal. A low-carbon adaptive broadband beamforming algorithm has been developed [SE3]. It enhances the desired signal based on the noise conditions of the individual omnidirectional sensors deployed in a complex dynamic environment that is prone to steering errors. The adaptive beamformer can accurately estimate the Doppler frequency for applications involving satellite navigation system receivers of vehicles under varying environmental conditions. Ubiquitous seamless inter-satellite and satellite-to-ground data transmissions for integrated terrestrial-space communications require the implementation of adaptive beamforming algorithms [SE3, SE5]. Moreover, distributed satellite networks (including satellite constellation, formation flying spacecraft, fractionated spacecraft and swarms/clusters) [SE13] require adaptive broadband beamforming

capabilities [SE5]. Given these stringent requirements, the regulated-Frost beamformer [SE5] is an ideal candidate for HASS missions. Also, its antenna subsystem can be additively manufactured [3] with the onboard HASS electronic subsystems for high quality reliable data transmissions and receptions.

Furthermore, adaptive low-noise amplifiers [SE6, SE8] enable reconfigurable satellite links to be realised for cost-effective and sustainable data communication applications. In this research, the impact of noise figure on the carrier and data links performances of a HASS application has been established and quantified [SE6]. The findings would enable reconfigurable subsystems for reliable, dynamic, broadband and adaptive space operations.

2.6 Adaptive Subsystems Operational Times Analysis

A further contribution of this research is in the multiple power modes and operational times that can be realised onboard the HASS system. A real-time reconfiguration of the operational times of multifunctional satellite subsystems [2] is an emerging research interest within the space community [13, SE2, SE9]. The operational times of spacecraft subsystems overpower modes can be reconfigured in orbit to reliably sustain the operating conditions of the capability-based satellite components for ubiquitous communication. The subsystems of space satellites experience different orbital and eclipse periods. Hence, an in-orbit operational times reconfiguration design process [SE2, SE9] has been developed for all categories of HASS subsystems and systems to ensure optimal mission operations. This represents a major contribution to the pool of space technology knowledge that would benefit the space community. The basic power-storing and overpower modes can be implemented while a HASS system is in orbit and performing a given mission [SE2]. The capability-based

architecture enables power modes spanning power-storing, communications (uplink and downlink) and payload processing to be carried out with recourse to the prevailing orbital pattern(s) of the HASS mission. Hence, different operational times for the various power modes and feasible missions can be adaptively reconfigured for key mission operations including data capturing, onboard processing and transmission. This would enable LEO satellites to adapt their mission objectives to the stringent (10 minutes) temporal data transmission window during their orbital period; this occurs when an Earth station is within the footprint of the satellite. For propulsive missions, the HASS system enables integrated multiple operational modes [SE1, SE2, SE5] for miniature solar electric propulsion and cold-gas micropropulsion subsystems [SE4, 15] to be reliably and cost-effectively incorporated. A switch between passive and active phases for the ADC and the thermal control provides a hybrid optimal operational margin for the satellite system [SE2]. The HASS system has the capability to enhance the performance of primary and secondary satellite payloads by providing component-level reconfigurations for optimal mission accomplishment [SE1, SE5].

Chapter Three

Technical Publications

3.1 Introduction

The relevant peer-reviewed and refereed published works that demonstrate the novelty of this research are stated in this chapter.

3.2 Published Works

3.2.1 Paper 1 [SE1]

Parametric System Engineering Analysis of Capability-based Small Satellite Missions, *IEEE Systems Journal*, pp. 1–10, May 2019.

DOI: http://dx.doi.org/10.1109/JSYST.2019.2919526.

Sunday Cookey Ekpo
Department of Engineering, Manchester Metropolitan University, UK

This subsection is an exact copy of Paper 1.

Parametric System Engineering Analysis of Capability-Based Small Satellite Missions

Sunday Cookey Ekpo, *Member, IEEE*

***Abstract*—To achieve appropriate link budget and system engineering analyses of capability-based small satellites missions, an objective assessment and computation of the component-, subsystem-, and system-levels parameters requirements must be carried out. This paper presents the measurement-derived parametric models for the system engineering analysis of communication, meteorology, planetary, and other small satellite programs with recourse to the initial mission, conceptual design, and postmission objectives. Mass and power margins are the critical resources under investigation besides the link contingencies and operational times. The case study spacecraft systems engineering analyses indicate a transmit power for data transmission uplink and downlink of at least 33 dBm for the generic communication, meteorology, and planetary missions applications. The presented parametric models also reveal a signal-to-noise ratio of at least 16 dB per radio communication link for worst case noise floor and path loss. For a 30-W power utilization, a two-power communication-overpower mode mission operates for an extra 8.3 min compared with a three-power payload-overpower mode mission. This holds a great promise for the development of adaptive subsystems for reconfigurable multiband, and multistandard transponders for multipurpose missions and postmission applications.**

***Index Terms*—Adaptive systems, capability engineering, parametric study, satellite communication, system engineering.**

I. Introduction

THE conceptual design of satellites involves several modeling and simulation approaches that span single person calculations to multiple organizations employing complex and advanced interconnected computer models for optimized solutions [1]. The four design approaches that are currently utilized within the space community include back-of-the envelope techniques, single-use, computer-aided models, serial processes, and integrated concurrent engineering [1]–[4]. These techniques can be combined to meet the customer's needs or a hybrid of several design methods may be implemented. Whatever the adopted design approach, a single solution or specific mission design interests may be the focus.

The conceptual design is influenced by several factors and design constraints and has no unique "right" technique. Issues ranging from the project manager's background, corporate culture, team leadership, cultural differences, and dynamics also determine the choice of a conceptual design approach for a spacecraft mission.

The fundamental motivations for the capability-based space satellites (CSSs) (such as a highly adaptive small satellite (HASS) [1]) concept include, but are not limited to, in-orbit adaptability, reliability, multifunctionality, enhanced portability, system-level simulation of spacecraft, reduced manufacturing and integration complexities, cost-effectiveness, safety, low carbon footprint, postmission re-application, and flexibility in deployments. A HASS is a reconfigurable, multifunctional, and adaptive small space satellite that has capabilities for dynamic space applications and operations while retaining its designed optimal performance. This capability-based space system design paradigm will gain increasing and expanding applications in the future deployments of constellations of small satellites [1]–[6]. A HASS system architecture has an in-built redundancy and radiation shield for onboard semiconductor components that can be re-engineered while in orbit. The adaptive multifunctional architecture does not follow a subsystem-oriented design approach; it embraces the small satellites scaling techniques [2], [7]. The design process accomplishes functions and eliminates conventional subsystem boundaries. It focuses on the identification and specification of subsystem-level functional requirements. In this approach, the functions of several subsystems are implemented on a single circuit card [6].

Moreover, a capability-based satellite system is developed as a network of functions with reconfigurable intra- and inter-subsystem and module links. This eliminates a single point of failure, enhances a deterministic operation, and/or helps to sustain a real-time performance. The functionality of a module and/or subsystem can be seamlessly transferred to another module and/or subsystem via the adaptable point-to-point network of the adaptive satellite system [6]–[9]. Thus, all the HASS subsystems can directly access the resources of the other subsystems. In this paper, mass and power margins are the critical resources under investigation for achieving an optimal, economical, reliable, and sustainable capability-based small satellite mission [1], [8], [9].

The existing conventional parametric models for system engineering analysis of small satellite missions are based on the work of Charles Brown [3]. Other documented small satellite missions have been mission-based and application-specific [6] with no particular published guiding system engineering design principles. Moreover, the integrated cost, size, weight, and power

Manuscript received July 14, 2017; revised January 31, 2018, April 24, 2018, July 5, 2018, and March 2, 2019; accepted May 24, 2019. Date of publication June 11, 2019; date of current version August 23, 2019. The author wishes to thank the Akwa Ibom State Government of Nigeria for sponsoring this research at The University of Manchester, Manchester, U.K., and Engineering & Materials Science Research Centre, Manchester Metropolitan University, Manchester, U.K. for sponsoring extra research equipment through its open bid scheme.

The author is with the Department of Electrical and Electronic Engineering, Manchester Metropolitan University, Manchester M1 5GD, U.K. (e-mail: scekpo@ieee.org).

Digital Object Identifier 10.1109/JSYST.2019.2919526

1932-8184 © 2019 IEEE. Translations and content mining are permitted for academic research only. Personal use is also permitted, but republication/redistribution requires IEEE permission. See http://www.ieee.org/publications_standards/publications/rights/index.html for more information.

(C-SWaP) limitations of small satellites are not the core system-level design considerations [8] since commercial-off-the-shelf components are often favored for this type of mission. Ekpo and George [5] and Waseem and Sadiq [10] provide small satellite architecture technologies, and model-based systems engineering in conceptual design of small satellites that satisfy delineated "all-analog" and "all-digital" system designs only.

Ekpo and George [1] introduces a common design procedure for capability-based small satellite systems engineering but focuses on a system engineering analysis of various categories of highly adaptive small satellites for a meteorology satellite (METSAT) mission. Ekpo and George [5] considers the design methodology of adaptive small satellites that enables an optimal architecture for a mission. Ekpo and George [5] and and Ekpo *et al.* [11] explore the fact that an adaptive small satellite design problem is a multicriteria optimization design problem that must be judiciously assessed for a cost-effective first-pass success. The parametric models presented in this paper cover other satellite missions as well with an allowance for adapting the models to suit next- and future-generation satellite system engineering design processes. The developed and validated models can be adapted to suit any mission of choice with allowance for assessing the impact of integrated emerging device to system-level technologies.

The parametric models presented in this paper allow for "integrated digitized analog" satellite systems [5] and can be adapted to meet the user and the system requirements definitions for delineated "all-analog" and "all-digital" satellite designs if required. Within the scope of this paper, the system engineering of capability-based small satellite missions is analyzed with recourse to the industry-standard parametric estimation of the subsystems design characteristics. This research work provides comprehensive spacecraft system simulation parameters models that are measurement derived for precision mission programs. Moreover, the operational times of the capability-based satellite subsystems can be modeled for accurate near real-time orbital dynamics assessment. Furthermore, the communication link budget and payload operational times can be reliably assessed with recourse to the high-level performance requirements of spacecraft mission and postmission systems. This paper provides a parametric system engineering analysis of capability-based small satellite missions respecting the enabling and emerging space satellite technologies. The frontal objective of this paper is to develop and present estimating spacecraft power and mass relationships that can be utilized to provide reliable and sustainable mission and conceptual system engineering decisions to satisfy performance definitions and budget constraints. This is important because of the increasing dependence on cost-effective, reconfigurable space-borne assets [especially in the low-earth orbit (LEO)] to complement terrestrial radio access technologies. The focus of this paper is to provide the quantitative engineering principles platform for the subsystems design parameters of sustainable small satellites based on their systems definitions and requirements.

This paper is organized as follows. Section II explains the satellite system engineering estimating relationships and margins for the communication, meteorology, planetary, and other mission applications. Section III details the postmission satellite mission applications including the operational time. The capability-based small satellite communication link budget analysis is presented in Section IV. Section V concludes this paper.

II. Satellite System Engineering

Single-use, computer-aided models for conceptual design represent a system engineering design process tool for the entire spacecraft modules and their respective integrated subsubsystems and subsystems [2], [3], [11]–[13]. This approach allows for a more detailed analysis of the spacecraft subsystems and their interdependencies than the back-of-the-envelope technique. The historical data of spacecraft (including mass, power, size, data link margins, and orbit parameters) are required to establish this technique. This involves utilizing appropriate statistical curve-fitting algorithms (such as linear programming) to obtain equations that define a design resource of interest as explicit parametric functional relationships of other independent variables that strongly determine it. Depending on the coefficient of determination that fits the spacecraft model of interest, an estimating relationship can be a simple linear function; logarithmic equation; or a complex, higher order polynomial. Systems engineers find this method to be particularly helpful for sizing subsystems that require expert inputs following their basic conceptual design definitions. For instance, the sizing of the solar panel and structure as functions of the spacecraft's mass or thermal control subsystem as a function of the spacecraft's power and mass. Also, a physical quantity such as the subsystems' power consumption can be expressed as a function of the spacecraft's mass. It is worthwhile to note that the accuracy of this technique depends largely on the consistency of the mathematical relationships of the subsystems (i.e., the plotted historical spacecraft data lie closely with the curve-fit).

The empirical mass and power estimating relationship (PER) approach is relatively simple and easy. This approach has been adopted in the development of the system engineering design process for the HASS systems using the data of past space programs of built systems. Adaptive and active devices strongly influence the system-on-chip and multichip design paradigms for HASS systems. To ensure that the developed system engineering (SE) design process model works well for the presented adaptive satellite architecture (i.e., integrated digitized radio frequency (RF)/microwave analog systems substrates), the design parameters (such as cabling harnesses, subsystems integration, system configurations, and technology options) are modified to reflect the technological advancements for the estimating relationships. This has revealed a good technical agreement between the reported system design parameters (such as payload mass fraction) and those of past space programs. The results of the power and mass budgets analyses for the meteorology, communication, and planetary missions using HASS systems are presented here. The SE analysis for each considered mission is based on the functional relationships and derivations.

The choice of the payload- and mass-based PER models for each spacecraft mission is informed by the combined statistical analysis of past and current spacecraft missions with

recourse to the emerging small satellite technologies. For instance, given the limited size, weight and power generation capability of small satellites, the payload design for the meteorology mission in LEO is modeled using the PERs [1]. Similarly, the business needs of communication and planetary missions limit the spacecraft category to the higher end of the microsatellites and beyond.

The subsystem mass reduction M_{SMR} of a capability-based small satellite based on the satellite category and cabling factor is given by

$$M_{\mathrm{SMR}} = M_{\mathrm{ODM}} C_{\mathrm{MF}} \tag{1}$$

where M_{ODM} is the on-orbit dry mass of a conventional satellite in kilogram, and C_{MF} is the cable mass factor. The corresponding HASS subsystems (core bus and payload modules) mass for allocation M_{SSH} in kg is given by

$$M_{\mathrm{SSH}} = \frac{M_{\mathrm{ODM}}\left(1 - C_{\mathrm{MF}}\right)}{1 + C_f} \tag{2}$$

where C_f is the mass contingency factor. The mass margin for HASS systems is obtained as $M_{\mathrm{Hmargin}} = C_f M_{\mathrm{SSH}}$ [1], [3]. Furthermore, the equivalent on-orbit dry mass M_{HODM} of the capability-based small satellite is given by [1]

$$M_{\mathrm{HODM}} = M_{\mathrm{ODM}}\left(1 - C_{\mathrm{MF}}\right). \tag{3}$$

The abovementioned analysis was applied in the derivation of the mass allocation of HASS systems for communication, planetary, and meteorology missions based on past spacecraft historical database/missions and the American Institute of Aeronautics and Astronautics guidelines [1]–[3], [8].

To demonstrate how the power margin of LEO satellites as a function of the generated solar array power is derived, the following definitions apply:

x = maximum spacecraft power available from the solar array, W, and

y = actual core bus and payload subsystems power, W.

The power contingency P_{margin} is therefore derived thus

$$yC_f = P_{\mathrm{margin}} \tag{4}$$

$$x - y = P_{\mathrm{margin}}. \tag{5}$$

From (4) and (5), the power margin becomes

$$P_{\mathrm{margin}} = \frac{xC_f}{\left(1 + C_f\right)}. \tag{6}$$

Equation (6) assumes that the payload subsystem is developed along with the core bus subsystems. A capability-based satellite system employs an adaptive device(s) in its architecture. Following the preceding analyses and discussions, the power contingency function for a capability-based application cannot follow the conventional definition. Hence, the power budget of a HASS is modeled with recourse to the requirements of the subsystems and the mission. It is a system capability-based model and the total in-orbit power P_T of a HASS system is given by [1]

$$P_T = P_{pl} + P_{\mathrm{bus}} + P'_{\mathrm{margin}} \tag{7}$$

TABLE I
CORE BUS SUBSYSTEMS POWER ALLOCATION FOR HASS MISSIONS

	Percentage of Total Core Bus Subsystems Power Allocation (%)							
	Communication		Planetary		Meteorology		Other	
Subsystem	STP	CFP	STP	CFP	STP	CFP	STP	CFP
Thermal	30.5	30.5	28.8	28.8	48.8	48.8	33.2	30.1
ADC	28.5	28.5	20.6	20.6	19.3	19.3	11.1	11.1
EP	14.6	14.6	7.5	7.5	3.5	3.5	1.5	1.6
CDH	19.3	19.3	17.5	17.5	13.2	13.2	15.1	15.1
Comms	0	0	23.6	23.6	15.2	15.2	30.1	30.1
Propulsion	7.1	7.1	1	1	0	0	4.0	4.0
Mechanism	0	0	1	1	0	0	5.0	5.0

where P'_{margin} is the power margin, and P_{bus} is the core bus power. The corresponding power contingency P'_{margin} is given by

$$P'_{\mathrm{margin}} = P_{\mathrm{margin}} + \delta P \tag{8}$$

where δP is the maximum differential power (W) resulting from the dynamic operation and application of a HASS system.

Combining (7) and (8) together, we obtain the final in-orbit payload-based HASS power budget function as

$$P_T = P_{pl} + \left(1 + C_f\right) P_{\mathrm{bus}} + \delta P. \tag{9}$$

As observed in (9), the adaptive power margin function P'_{margin} is dependent upon the deterministic system application. Since P_{margin} is defined for the conventional spacecraft without any obvious recourse to the adaptive power regimes, P'_{margin} must be greater or equal to P_{margin}. Hence, the constraint on (9) for a capability-based small satellite system is given by

$$P_{\mathrm{margin}} \leq P'_{\mathrm{margin}} \leq \left(P_{\mathrm{margin}} + \delta P\right). \tag{10}$$

Consequently, for a capability-based satellite system, (9) becomes

$$P_T = f\left(P_{pl}\right) + kf\left(M\right) + C_f P_{\mathrm{bus}} + \delta P + C \tag{11}$$

where k is the power per unit mass or specific power (W/kg) for each satellite category, $f(P_{pl})$ is the payload power (W), and C is a mission-based power constant (W) [1], [3]. Equation (11) represents the complete in-orbit total spacecraft power budget function for the conceptual design of a capability-based small satellite system.

Table I states the core bus subsystem power allocation for capability-based small satellite systems (such as a HASS) [1]. The presented analysis covers thermal, attitude determination and control (ADC), electrical power (EP), command and data handling (CDH), communications, propulsion, and mechanism subsystems.

A. Meteorology Mission

A judicious analysis of PERs with recourse to the orbital patterns must be carried out to understand and validate the operational times of capability-based satellite systems' modules, subsystems, and subsubsystems. Two case studies are considered in this paper. Case study 1 represents a spacecraft team payload (STP), and case study 2, represents customer-furnished payload (CFP).

From (11), the total in-orbit PERs of capability-based small satellites for meteorology missions in LEO are presented as follows:

1) Microsatellites

Case study 1

$$P_T = 0.522M_{\mathrm{HAM}} + 0.5(P_{\mathrm{pl}} + (1 + C_f) \times (1 - C_{lf})(P_t - P_{\mathrm{pl}})) + 7.78 \quad (12)$$

where C_{lf} is the cable loss factor, and C_f is the contingency factor.

Case study 2

$$P_T = 0.522M_{\mathrm{HAM}} + 0.5P_t(1 + C_f)(1 - C_{lf}) + 7.78. \quad (13)$$

2) Nanosatellites

Case study 1

$$P_T = 1.13M_{\mathrm{HAN}} + 0.5(P_{\mathrm{pl}} + (1 + C_f)(1 - C_{lf}) \times (P_t - P_{\mathrm{pl}})) + 1.72. \quad (14)$$

Case study 2

$$P_T = 1.13M_{\mathrm{HAN}} + 0.5(1 + C_f)(1 - C_{lf})P_t + 1.72. \quad (15)$$

3) Picosatellites

Case study 1

$$P_T = 2.5M_{\mathrm{HAP}} + 0.5(P_{\mathrm{pl}} + (1 + C_f)(1 - C_{lf}) \times (P_t - P_{\mathrm{pl}})) + 0.35. \quad (16)$$

Case study 2

$$P_T = 2.5M_{\mathrm{HAP}} + 0.5(1 + C_f)(1 - C_{lf})P_t + 0.35. \quad (17)$$

4) Femtosatellites

Case study 1

$$P_T = 5.15M_{\mathrm{HAF}} + 0.5(P_{\mathrm{pl}} + (1 + C_f)(1 - C_{lf}) \times (P_t - P_{\mathrm{pl}})) + 0.0835. \quad (18)$$

Case study 2

$$P_T = 5.15M_{\mathrm{HAF}} + 0.5(1 + C_f)(1 - C_{lf})P_t + 0.0835. \quad (19)$$

A good and reliable system engineering analysis reveals the design margins that can be sustained in the event of system failure or re-engineering. The case studies presented in this paper assume that the payload is developed along with the core bus subsystems and not customer-held. The communications subsystem includes the uplink and downlink power requirements for receiving engineering data from and transmitting scientific data to a ground station, respectively.

Table II shows the power budget analysis of highly adaptive small satellites system engineering for a meteorology mission in LEO. Assume that the payload equipment for the meteorology mission will utilize 15, 10, 1, and 0.5 W for the representative highly adaptive microsatellite (HAM), nanosatellite, picosatellite, and femtosatellite, respectively [1].

TABLE II
HASS POWER BUDGET ANALYSIS FOR A METEOROLOGY MISSION [1]

Satellite Category: **Highly Adaptive Microsatellite (HAM) (18.4 kg)**	
In-orbit Total Power Summary	
Parameter	Value (W)
Maximum available payload power in LEO	18.02
Maximum available core bus power in LEO	16.75
Required payload power	15.00
Calculated payload power	14.42
Payload power margin	3.60
Calculated core bus power	13.40
Core bus power margin	3.35
Total HAM power required	31.75
Power savings	1.67
Maximum power of a 18.4-kg HAM in LEO	34.77
Max. available HAM power margin in LEO	6.95

TABLE III
HASS MASS BUDGET ANALYSIS FOR A METEOROLOGY MISSION

Satellite Category: **Highly Adaptive Microsatellite (HAM)**	
Conventional on-orbit dry mass (kg): 20	
Subsystem mass reduction (kg) = 1.6	
Equivalent on-orbit dry mass of a HAM = 18.4	
Total subsystem mass for allocation (kg) = (18.72/1.25) = 14.72	
HAM Mass Allocation Summary	
Parameter	Value (kg)
Subsystem budget total	14.72
Mass margin	3.68
Mass-saving	1.6
Maximum on-orbit dry mass	18.4
Launch cost-saving ($)	16,000.00

The power estimations for the various subsystems are utilized to develop the link budget and the operational times [8] of the payload subsystem. The payload-based PER P_t used to derive the total METSAT power requirements P_T is given by [3]

$$P_t = 1.96P_{\mathrm{pl}}. \quad (20)$$

The system engineering design parameters for the meteorology mission are summarized as: payload holder: spacecraft design team; $C_{\mathrm{MF}} = 8\%$; orbit: LEO; design phase: conceptual design; power contingency factor (C_f) = mass contingency factor $(C_f) = 25\%$ [3]; class of design = 2 (next generation) [3]; cable loss factor $C_{\mathrm{lf}} = 1.6\%$ [3].

Table III presents the mass budget analysis of HASSs for a meteorology mission. It shows that an intelligent parametric system engineering design process can achieve mass savings and the elimination of undue system oversizing. It indicates the operational and business implications of the mission for satisfying and qualifying end users, technology platforms, and service delivery components. The subsystem mass allocation for the meteorology mission is given in Fig. 1.

At the conceptual design stage, Tables II and III enable the system engineer to allocate spacecraft resources to the various components and subsystems of the functional modules of the spacecraft.

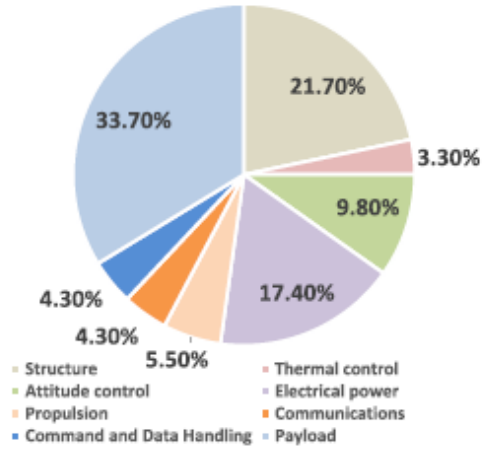

Fig. 1. Core bus subsystem mass allocation for the METSAT.

TABLE IV
HASS POWER BUDGET ANALYSIS FOR A COMMUNICATION MISSION

Satellite Category: **Highly Adaptive Microsatellite (HAM) (97 kg)**		
Core Bus Subsystem Power Allocation		
Core Bus Subsystem	Allocation (%)	Power (W)
Thermal control	30.5	18.08
Attitude control	28.5	16.89
Electrical power	14.6	8.65
Command and data handling	19.3	11.44
Communications	0	0
Propulsion	7.1	4.21
Mechanics	0	0
In-orbit Total Power Summary		
Parameter		Value (W)
Maximum available payload power in LEO		42.74
Maximum available core bus power in LEO		74.09
Required payload power		35.00
Calculated payload power		34.19
Payload power margin		7.74
Calculated core bus power		59.27
Core bus power margin		14.82
Total HAM subsystems power required		94.27
Power savings		3.13
Maximum power of a 97-kg HAM in LEO		116.83
Max. available HAM power margin in LEO		23.37

B. Communication Mission

Based on the database of past spacecraft missions, the communication and planetary spacecraft would require at least 56 and 122 W, respectively, for an appreciable mission accomplishment [1]. From (11), the total in-orbit PERs of capability-based microsatellites for communication missions in LEO are similar to the case studies 1 and 2 in (12) and (13).

Table IV shows the HASS power budget analysis for a communication mission. The SE design analysis for the 97-kg HAM gives a calculated payload power of 34.19 W with a corresponding power margin of 8.55 W relative to the maximum available payload power in LEO. Assume that the actual payload subsystem consumes 35 W, the calculated power margin of the payload would be 7.74 W (i.e., reduced by approximately 9.5%). The calculated payload power margin is approximately 22% of the actual payload power and well above the minimum power contingency (10%) required for the subsystem at liftoff [3]. The HASS power budget analysis for the case study communication satellite in LEO (see Table IV) shows that the power generation capability of the 97-kg HAM (i.e., 116.83 W) is sufficient for it. Hence, given the payload power requirement, no deployable solar reflectors would be required. However, to boost the payload power and enable more mission functions, deployable solar reflectors can be integrated into the four-panel array of the HAM. The reflectors would increase the solar intensity of the solar panels by approximately 51%. The payload-based PER P_t is given by [3]

$$P_t = 1.1568P_{pl} + 55.497. \tag{21}$$

The total communication satellite system power requirements P_T is obtained from (21). Hence, the total PER for the communication mission P_T is adjusted to account for the extra power generation from the solar reflectors as follows:

$$P_T = 0.522M_{\text{HAM}} + 0.5P_t(1 + C_f)(1 - C_{lf}) + 7.78 + NP_{\text{reflector}}. \tag{22}$$

Similarly, the mass estimating relationship for the communication mission is adjusted to account for the extra weight of the solar reflectors as follows:

$$M_{\text{HASS}} = M_{\text{CODM}}(1 - C_{\text{MF}}) + NM_{\text{reflector}}. \tag{23}$$

The system engineering design parameters [3] for the communication mission are summarized thus: payload holder: spacecraft design team; $C_{\text{MF}} = 3\%$; number of solar of reflectors, $N = 4$; mass of solar reflector $M_{\text{reflector}} = 0.16$ kg; generated power per reflector $P_{\text{reflector}} = 15$ W; orbit: LEO; design phase: conceptual design; power contingency factor $(C_f) =$ mass contingency factor $(C_f) = 25\%$; class of design $= 2$ (next generation); cable loss factor $C_{\text{lf}} = 1.7\%$; conventional on-orbit dry mass (kg) $= 100$; subsystem mass reduction (kg) $= 3$; equivalent on-orbit dry mass of an HAM (kg) $= 97$; total subsystem mass for allocation (kg) $= (97/1.25) = 77.6$.

Table V shows the mass budget for the communication mission; the corresponding power budget is stated in Table V. For the conceptual design and development phase, the mass contingency of 0.25 is chosen (i.e., next-generation class of design). This yields a mass of 77.6 kg for allocation to the subsystems of the 97-kg communication spacecraft. Compared with the subsystems mass allocation for a conventional microsatellite [3] developed for the same mission, a mass-saving of 2.4 kg is realized. A 7-year communication mission utilizing the presented 97-kg HAM would require an end-of-life (EOL) power of 96.11 W [1], [3]. This gives the design point for the mission and can be easily accommodated based on the power generation capability of the spacecraft and the total power requirement of the subsystems for the mission (see Table IV). Furthermore, the HAM system can adapt its mission capabilities to lengthen the design lifetime

TABLE V
HASS MASS BUDGET ANALYSIS FOR A COMMUNICATION MISSION

Satellite Category: **Highly Adaptive Microsatellite (HAM)**		
Subsystem Mass Allocation		
Subsystem	Allocation (%)	Allocated mass (kg)
Structure	21.6	16.76
Thermal control	4.1	3.18
Attitude control	7.2	5.59
Electrical power	26.8	20.80
Propulsion	7.2	5.59
Communications	-	-
CDH	4.1	3.18
Payload	29.0	22.50
HAM Mass Allocation Summary		
Parameter	Value (kg)	
Subsystem budget total	77.6	
Mass margin	19.4	
Mass-saving	3.0	
Max. on-orbit dry mass	97.0	
Launch cost-saving ($)	30,000	

of the spacecraft thereby prolonging the mission or enabling a postmission reuse.

C. Planetary Mission

From (11), the total in-orbit PERs of capability-based microsatellites for planetary missions in LEO are similar to the estimating relationships presented in case studies 1 and 2 in (12) and (13).

The cost of scientific satellites for planetary exploration and astronomical observation is prohibitively high. Hence, the current researches in the space community focus on achieving advanced capabilities for scientific and other missions using small payload subsystems and advanced small spacecraft technologies. For instance, a 72-kg Japan's innovative technology demonstration experiment (INDEX) satellite was launched to test the functionalities of modern sensor, processor, semiconductor, and battery technologies in a nearly sun-synchronous LEO at 655-km altitude [9]. The INDEX is a scientific microsatellite with a size of $72 \times 62 \times 62\ \text{cm}^3$. The solar panel capability of the INDEX satellite was 150 W at launch time; 120 W could be generated using two solar-concentrator paddles each weighing 1.3 kg. Two thin-film reflectors with a total mass of 0.32 kg were also integrated into the two paddles. The reflectors improved the solar intensity on the deployed solar panels by 25%. Hence, the power generation capability of the solar array was increased by 30 W yielding a specific power of about 94 W/kg for the two reflectors. As a scientific satellite for the observation of aurora and demonstration of advanced spacecraft technologies, the INDEX carried space-qualified field programmable gates array devices within its sensors and actuators. It also had an integrated control unit that performed command and data-handling, thermal control, and attitude determination and control; the conventional satellite design would have these subsystems mounted separately onboard the spacecraft [7]. This implementation is supported onboard the HASS systems through the adaptive multifunctional architecture design. A 66.88-kg HAM with four thin-film solar reflectors each weighing 160 g can sustain the scientific requirements of the INDEX satellite mission. The power budget of the HAM system indicates that it would have a power generation capability of at least 145 W and it enhances its solar intensity by a factor of 1.71. This results in a mass saving of 7.1% relative to the mass of the INDEX satellite. The payload subsystem of the HAM for the planetary mission is designed based on advanced sensor technologies such as miniature cameras. For instance, the imaging and mapping of the moon's surface (lunar mission) can be accomplished by developing integrated adaptive and/or reconfigurable payload sensors along the core bus subsystem. Cameras such as star tracker (for wide-field coverage, long-wave infrared, near-infrared/shortwave-infrared) and ultraviolet visible can be deployed onboard a HASS system for lunar surface mapping and earth observation missions. The Clementine spacecraft, launched to image and map the moon surface, utilized two star trackers (each 4.5 W and 0.29 kg), an integrated laser ranger and high-resolution imager (9.5 W, 1.12 kg), long-wave infrared imager (13 W, 2.1 kg), near-infrared imager (11 W, 1.92 kg), and ultraviolet-visible imager (4.5 W, 0.41 kg). The system engineering design parameters [3], [8] for the planetary mission are summarized as: payload holder: spacecraft design team; $C_{\text{MF}} = 7\%$; number of solar of reflectors $N = 4$; mass of solar reflector $M_{\text{reflector}} = 0.16$ kg; generated power per reflector $P_{\text{reflector}} = 15$ W; orbit: LEO; design phase: conceptual design; power contingency factor (C_f) = mass contingency factor $(C_f) = 25\%$; class of design = 2 (next generation); cable loss factor $C_{\text{lf}} = 2.7\%$; required payload power = 25 W; conventional on-orbit dry mass (kg) = 108.17; subsystem mass reduction (kg) = 7.53; equivalent on-orbit dry mass of an HAM (kg) = 100.64; total subsystem mass for allocation (kg) = (100.64/1.25) = 80.51.

The payload-based PER P_t, which is used to derive the total planetary satellite system power requirements P_T, is given by [3]

$$P_t = 1.13P_{\text{pl}} + 122. \tag{24}$$

The total power (P_T) and mass (M_{HASS}) estimating relationships for the planetary mission are as obtained in (22) and (23), respectively.

The Clementine spacecraft was deployed in the lunar orbit and had an on-orbit dry mass of 228 kg [9]. From Table VI, it is evident that the mass of the HAM system is approximately 44.14% of the mass of the Clementine spacecraft. Furthermore, the payload module of the HAM system can accommodate the payload sensors of the Clementine spacecraft for the lunar mission with a mass contingency of 3.37 kg (see Table VII). Depending on the image resolution and/or detail level required, the adaptive architecture of the HAM can be reconfigured to combine the sensors for accomplishing the mission. Each sensor enables a unique field-of-view (FOV). The near-infrared ($160 \times 160\ \text{km}^2$ FOV), ultraviolet-visible ($160 \times 125\ \text{km}^2$ FOV), long-wave infrared ($25 \times 25\ \text{km}^2$ FOV), and high-resolution imagers ($7.5 \times 9\ \text{km}^2$ FOV) can be aligned together to capture the same background. Various configurations of this arrangement can be achieved within the power budget of the payload module onboard the HAM system. For the charge-coupled device (CCD)

TABLE VI
HASS POWER BUDGET ANALYSIS FOR A PLANETARY MISSION

Satellite Category: **Highly Adaptive Microsatellite (HAM) (100.64 kg)**		
Core Bus Subsystem Power Allocation		
Core Bus Subsystem	Allocation (%)	Power (W)
Thermal control	28.8	34.85
Attitude control	20.6	24.93
Electrical power	7.5	9.07
Command and data handling	17.5	21.17
Communications (UL and DL)	23.6	28.55
Propulsion	1	1.21
Mechanics	1	1.21
In-orbit Total Power Summary		
Parameter		Power (W)
Maximum available payload power in LEO		28.72
Maximum available core bus power in LEO		151.24
Required payload power		25.00
Calculated payload power		22.98
Payload power margin		5.74
Calculated core bus power		120.99
Core bus power margin		30.25
Total HAM subsystems power required		145.99
Power savings		7.86
Maximum power of a 100.64-kg HAM deploying four solar reflectors in LEO		179.96
Maximum available HAM power margin in LEO		35.99

TABLE VII
HAM MASS BUDGET ANALYSIS FOR A PLANETARY MISSION

Satellite Category: **Highly Adaptive Microsatellite (HAM)**		
Subsystem Mass Allocation		
Subsystem	Allocation (%)	Allocated mass (kg)
Structure	27.8	22.38
Thermal control	3.3	2.67
Attitude control	9.7	7.81
Electrical power	20.4	16.42
Propulsion	14.0	11.27
Communications	6.5	5.23
Command and data handling	6.5	5.23
Payload	11.8	9.50
HAM Mass Allocation Summary		
Parameter		Value (kg)
Subsystem budget total		80.51
Mass margin		20.13
Mass-saving		7.53
Maximum on-orbit dry mass		100.64
Launch cost-saving ($)		75,300

based cameras and/or sensors, the HASS architecture presents a power-efficient payload integration platform for a cost-effective mission. Moreover, the operational power generation and over-power modes (such as power-storing, processing, uplink, and downlink) of the HAM can be reconfigured to allow for the desired configuration of the payload sensors to be implemented.

D. Quality and Reliability Analyses of CSS Systems

This section presents the analyses of the quality and reliability of HASS systems. The development of space systems is informed by the market segment they are expected to serve. For instance, space products manufactured for the civilians are influenced by the level of innovation built into it whereas those developed for the governments have their emphasis on the system quality and reliability [8], [14]. A high reliability is required for space-borne equipment due to the prohibitive cost of in-orbit maintenance and the returns-on-investment expected. The quality factor of a space system is assessed and determined by the part quality Q_p and the number of components n constituting the product [8], [14]. The value of Q_p is raised to the exponent n to obtain the overall system quality factor Q_s. Assume that the quality value for a part Q_p is 0.995 (i.e., 99.5% of unit pass) and a 140 such parts comprise a system. The overall quality factor of the system is approximately 50% of system units pass.

Due to the existence of subsystem boundaries, conventional spacecraft reliability calculations are subsystem based. For the purpose of comparing the conventional spacecraft and capability-based satellite architectures, each bus subsystem is assigned a reliability of 0.9999. The payload subsystem is assumed to contain a solid-state power amplifier ($R = 0.9994$) and an antenna ($R = 1$). Based on the published reliability parameters [9], a conventional nanosatellite has a system-level reliability of 93.74% at the end of the 30th day of operation. The absence of the subsystem boundaries (at the functional subsystem-level only) enables a baseline HASS system architecture to achieve a reliability of 99.88%. The system-level reliability of the spacecraft decreases with the increase in the number of components constituting the modules and subsystems. The absence of subsystem boundaries in a capability-based system translates the reliability calculation to a functional module-based one. Assume each adaptive multifunctional structural unit-borne functional module has a reliability factor of 0.9999. The advanced mass-producible manufacturing process [9] envisaged for the capability-based system architecture provides a feasible platform for obtaining multifunctional modules with reliability values close to unity. Since the reliability parameter is functionally determined, the combined core bus subsystems reliability $R_{\mathrm{CBM}} = R_{\mathrm{payload}} = 0.9999$. Substituting these values into $R_{\mathrm{HASS}} = R_{\mathrm{payload}} R_{\mathrm{CBM}}$ yields a system-level reliability of 99.98% for the HASS system. It can be concluded that to obtain a space-borne equipment with a desired reliability and quality, the unit pass reliability and quality values of its constituent components must be appreciably much higher. Furthermore, the objective would be to reduce the number of component footprints and integrate subsystems onto a common multifunctional module.

III. POSTMISSION SATELLITE APPLICATIONS

Integrated pre- and postmission system engineering analyses are important for a holistic understanding of the feasible mission applications and operations that capability-based spacecraft architectures can enable.

A. Postmission Analysis and Applications

Given that a HASS design lifetime (in years) is T_{life} and postmission reapplication years T_{pm}, its conceptual system engineering design would require a system parameters estimate for T_{HASS} given by

$$T_{\mathrm{HASS}} = 2\sqrt{T_{\mathrm{life}} T_{\mathrm{pm}}} \tag{25}$$

where T_{HASS} is the overall mission and postmission reapplication lifetime of the HASS system in years.

According to (25) and for a three-year postmission reuse, the maximum capability-based design lifetime (CDL) for an initial five-year HAN mission is approximately seven years eight months. Hence, the postmission system engineering task would involve remotely reengineering functional system parameters with appropriate trade-offs to support the emergent postmission program. At this stage, the postmission function could be such that demands less from the ADC and propulsion subsystems. This is especially so for conserving premium resources such as power which is technically being reduced to the EOL value. Following a judicious estimation of the postmission lifetime, the overall SE design process follows the same procedure as the initial mission, and conceptual design techniques.

IV. Capability-Based Small Satellite Link Budget

A. Communication Link Design Parameters

To assess the parametric SE design process with recourse to the communication uplinks and downlinks, a link budget analysis is required. A link design involves the development of a comprehensive budget based on the parameters that characterize a given satellite communication system network. The following parameters define a satellite communication link: data rate, maximum bit error rate, frequency, modulation and coding, symbol rate, transmitter, antenna gains, system gains and losses, and receiver noise for achieving a given spacecraft mission's required link margin [13]. Carrier link margin and data link margin constitute the two main satellite links margins that characterize the uplink and downlink performances of spacecraft communication system networks [13].

B. Link Budget Analysis

This paper presents a link budget analysis for a microsatellite deployed for meteorology, communication, and planetary missions at altitudes-frequencies pairs of 4 GHz, 700 km; 2 GHz, 750 km; and 1.5 GHz, 800 km, respectively. The power budget analysis procedure in [1] will be utilized for these three generic space satellite missions. Fig. 2 shows the path loss values as a function of the elevation angle above the horizon at different frequencies and altitudes for each case study spacecraft mission. Though the elevation angle ranges from 0° to 180°, the practicable range for an LEO satellite mission is approximately 160° (and spans from about 10° to 170°). The practicable highest path losses for the meteorology, communication, and planetary missions are 107.0, 114.2, and 106.3 dB, respectively.

For the meteorology mission (see Table II), the calculated core bus power is 13.4 W and 15.2% (i.e., 33.10 dBm) is allocated for the communication subsystem for uplink and downlink data transmission. The calculated core bus power and allocated communication subsystem percentage for the communication mission are 59.27 W and 19.3% (i.e., 40.58 dBm), respectively (see Table IV). The planetary mission (see Table VI) has calculated core bus power and communication subsystem allocations of 120.99 W and 23.6% (i.e., 44.56 dBm), respectively.

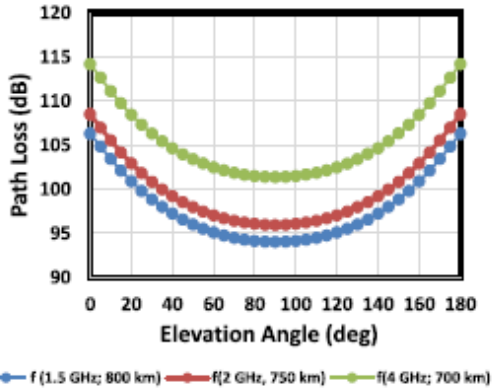

Fig. 2. Path loss for the case study generic spacecraft missions.

To assess the signal-to-noise ratio (SNR) performance of the link, the following assumptions are made for each microsatellite and the ground station: omnidirectional antennas with gains of 0 dBi are installed; and a receiver noise floor of −90 dBm. This design yields SNRs of 16.1, 16.38, and 28.26 dB for the meteorology, communication, and planetary microsatellites missions, respectively. Practical measurements of fiber-integrated satellite reception system revealed modulation error ratio of 16.1, 16.8, and 16.5 dB at 10.905, 10.906, and 11.126 GHz, respectively. These values agree with the SNR thresholds of the link analysis in this paper. It should be noted that the SNR will vary with the transmission due to a variable path loss. A constant SNR at the ground station receiver would imply that the microsatellites perform dynamic reconfiguration of their transmit powers to accommodate the radio link and range of the ground station. Maintaining a constant SNR would ensure that a minimum power is transmitted resulting in equipment downsizing and onboard microsatellite battery longevity. This further supports the need for adaptive multifunctional architectures onboard capability-based satellites that can utilize trajectory data to adapt power transmission following an established radio communication link. An onboard data processing is sustained for low-cost link profiling and critical and noncritical information transmission.

The operational times of the satellites can be estimated based on the prevailing power modes [9], [11]. Given the power consumption of the maximized power mode P_{max} the corresponding maximized operational time t_{max} is obtained as

$$t_{\max} = \frac{E_o + P_s\left(\sum_{i=1}^{N-2} t_i + t_e - \tau_o\right) - \left(\sum_{i=1}^{N-2} P_i t_i\right)}{P_{\max} - P_s} \tag{26}$$

where E_o is the total energy produced by the spacecraft's solar panels (J); P_s is the power-storing mode power consumption (W); τo is the orbital period of a satellite (s); t_e is the eclipse time of a satellite (s); P_i is the ith power mode's power consumption (W); and t_i is the operational time (s).

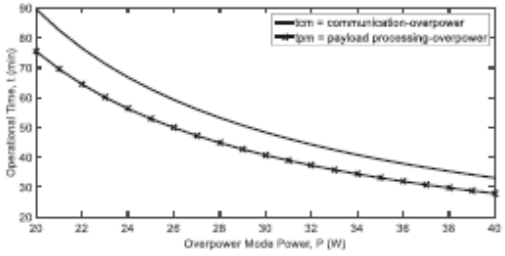

Fig. 3. CSS operational times versus overpower modes.

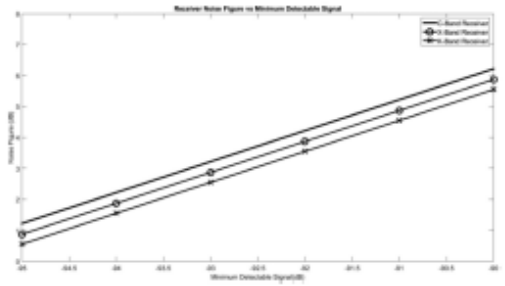

Fig. 4. Receiver noise figure versus minimum detectable signal.

Fig. 3 shows the plots of the payload processing-overpower and the communication-overpower modes for a METSAT mission. The orbital, payload, and power modes parameters are obtained from [8]. The data communication downlink duration/temporal window is assumed to be 10 min [8], [9]. The satellite altitude is 800 km at 180° inclination [8]. For the Sanyo CCD camera module payload [8] under consideration, the calculated communication-overpower mode power consumption is 25.29 W. The payload operational time in Fig. 3 considers three power modes: power-storing, payload processing-overpower, and communication-overpower. Similarly, the communication operational time considers power-storing and communication-overpower modes. It is obvious from the "operational time-power consumption decay" plots that the higher the required power for an overpower mode operation, the lower the operational time the satellite can sustain it to accomplish the mission's task (see Fig. 4). Alternatively, the higher the available power for an overpower mode operation, the lower the operational time that satellite would utilize to accomplish the mission; communication data uplinks and downlinks can be achieved directly and/or via intersatellite links. Hence, the C-SWaP limitations of small satellite systems imply that advanced, sustainable, and low-power consumption components are required for cost-effective missions. Moreover, for the same power consumption per an overpower mode of operation, the higher the number of modes, the higher the operational time required to accomplish the mission tasks. Assuming a communication-overpower and payload processing-overpower modes powers of 25 W, respectively, the corresponding operational times are approximately 62.8 and 52.9 min.

To enable the payload subsystem operate for a longer period of time, advanced low-power subsystems (see Table I) (including reconfigurable digitized analog components) must be utilized in its design (see Fig. 3). Hence, premium onboard resources [15], [16] can be judiciously adapted for sustainable, optimal, reliable, high-performing, and cost-effective satellite programs.

A further analysis of the receiver sensitivity of CSS for mission and postmission applications reveals that at bandwidths of 60, 65, and 70 MHz for the *C*-, *X*-, and *K*-bands, the noise figure decreases by 5 dB for a −5 dBm improvement in the minimum detectable signal (see Fig. 4). This holds a great promise for reconfigurable low-noise amplifier architectures that can offer in-orbit device-level reconfiguration for mission optimization [13]. This is applicable in distributed satellite networks (including satellite constellation, formation flying spacecraft, fractionated spacecraft, and swarms/clusters) [17], [18] with adaptive broadband beamforming [19], [20] capabilities. Most of the published works on distributed satellite systems emphasize formal representation and analysis [17] without the physical layer design constraints and enhancements. This paper proactively considers small satellite size, mass, cost, and power budgets in developing the functional estimating relationships that are applicable to past and future spacecraft missions with embedded innovative concept designs.

A prevailing novelty of this paper is the development of parametric estimating relationships for capability-based small satellite designs that satisfy past and future mission requirements. With the presented mathematical models, the mass, power, size, and cost of small satellites can be reliably and sustainably estimated with recourse to the enabling and emerging space subsystems technologies. Another prevailing novelty of this paper is that inputs from the concurrent engineering design techniques [4] can be integrated at the subsystem- and system-levels to optimize the deliverables of the mission and conceptual design objectives.

V. Conclusion

This paper presents parametric models for a holistic system engineering design analysis of capability-based small satellite programs. The presented case study design yields SNRs of 16.1, 16.38, and 28.26 dB for the meteorology, communication, and planetary microsatellites missions, respectively. These results agree with practical satellite downlink systems that utilize the fiber-integrated reception system technology. Furthermore, for a 30-W power utilization for the communication-overpower and two-power mode mission, the achieved operational time is 48.3 min. For the same power consumption level, the payload processing-overpower mode for a three-power mode mission would only operate for 40.7 min. The presented satellite system models functions can be integrated seamlessly with popular electronic design automation tools for sustainable, optimized, secure, and advanced space-borne systems development.

The presented small satellite SE design process addresses high-level system requirements with recourse to the historical and emerging subsystems technologies. Hence, interconnected device, subsystem and system models can be accurately designed and characterized using the appropriate adapted parameter estimating relationship. My future work will investigate the optimal subsystems operational times assignments for integrated reconfigurable real-time earth-space communication systems operations.

REFERENCES

[1] S. C. Ekpo and D. George, "A system engineering analysis of highly adaptive small satellites," *IEEE Syst. J.*, vol. 7, no. 4, pp. 642–648, Dec. 2013.

[2] S. Sepahban, J. Aguilar, A. Dawdy, S. Paige, and J. Sercel, "Modeling and simulation in conceptual design," in *Space Modeling and Simulation: Roles and Applications Throughout the System Life Cycle*, L. B. Rainey, Ed. El Segundo, CA, USA: The Aerospace Press, 2004, pp. 197–223.

[3] C. Brown, *Elements of Spacecraft Design*. Reston, VA, USA: AIAA, 2002.

[4] R. Stevens, "Concurrent engineering methods and models for satellite concept design," in *Proc. IEEE Aerosp. Conf.*, 2015, pp. 1–15.

[5] S. Ekpo and D. George, "A system-based design methodology and architecture for highly adaptive small satellites," in *Proc. IEEE Int. Syst. Conf.*, 2010, pp. 516–519.

[6] B. Jackson and K. Epstein, "A reconfigurable multifunctional architecture approach for next generation nanosatellite design," in *Proc. IEEE Aerosp. Conf.*, 2000, pp. 185–188.

[7] D. Barnhart, T. Vladimirova, and M. Sweeting, "Very-small-satellite design for distributed space missions," *J. Spacecraft Rockets*, vol. 44, no. 6, pp. 244–257, 2007.

[8] S. Ekpo, D. George, and B. Adebisi, "A multicriteria optimisation design of SPSE for adaptive LEO satellites missions using the PSI method," in *Proc. Amer. Inst. Aeronaut. Astronaut. Space Conf. Expo.*, 2013, pp. 1–19.

[9] H. Helvajian and S. W. Janson, *Small Satellites: Past, Present, and Future*. Reston, VA, USA: AIAA, 2008.

[10] M. Waseem and M. U. Sadiq, "Application of model-based systems engineering in small satellite conceptual design-A SysML approach," *IEEE Aerosp. Electron. Syst. Mag.*, vol. 33, no. 4, pp. 24–34, Apr. 2018.

[11] S. Ekpo, B. Adebisi, G. Danielle, R. Kharel, and M. Uko, "System-level multicriteria modelling of payload operational times for communications satellites missions in LEO," *Recent Prog. Space Technol.*, vol. 4, no. 1, pp. 67–77, 2014.

[12] W. J. Larson and J. R. Wertz, *Space Mission Analysis and Design*. Torrance, CA, USA: Microcosm, Inc., 1992.

[13] S. C. Ekpo and D. George, "Impact of noise figure on a satellite link performance," *IEEE Commun. Lett.*, vol. 15, no. 9, pp. 977–979, Sep. 2011.

[14] R. Hassan and W. Crossley, "Spacecraft reliability-based design optimization under uncertainty including discrete variables," *J. Spacecr. Rockets*, vol. 45, pp. 394–405, 2008.

[15] S. Ekpo and D. George, "4–8 GHz LNA design for a highly adaptive small satellite transponder using InGaAs pHEMT technology," in *Proc. IEEE 11th Annu. Wireless Microw. Technol. Conf.*, 2010, pp. 1–4.

[16] P. Hershey, B. Wolpe, J. Klein, and C. Dekeyrel, "System for small satellite onboard processing," in *Proc. Annu. IEEE Int. Syst. Conf.*, 2017, pp. 1–6.

[17] W. Edmonson and E. Al, "Systems engineering of intersatellite communications for distributed systems of small satellites," in *Proc. Annu. IEEE Syst. Conf.*, 2015, pp. 705–710.

[18] F. Dong, X. Li, Q. Yao, Y. He, and J. Wang, "Topology structure design and performance analysis on distributed satellite cluster networks," in *Proc. 4th Int. Conf. Comput. Sci. Netw. Technol*, 2015, pp. 881–884.

[19] S. C. Ekpo, B. Adebisi, and A. Wells, "Regulated-element frost beam former for vehicular multimedia sound enhancement and noise reduction applications," *IEEE Access*, vol. 5, pp. 27254–27262.

[20] Q. Yu, W. Meng, M. Yang, L. Zheng, and Z. Zhang, "Virtual multibeam forming for distributed satellite clusters in space information networks," in *Proc. IEEE Wireless Commun.*, 2016, pp. 95–101.

Sunday Cookey Ekpo (M'08) received the M.Sc. degree in communication engineering and the Ph.D. degree in electrical and electronic engineering with specialty in highly adaptive satellite system design; multiphysics design and modeling of radio frequency (RF), microwave, millimeter-wave, and optical transceivers; Internet of things sensors characterization; multiobjective system engineering; and complex systems optimization from the University of Manchester, Manchester, U.K., in 2008 and 2011, respectively.

He is a Lecturer of Electrical and Electronic Engineering with the Manchester Metropolitan University, Manchester, U.K. He is a Chartered Engineer.

Dr. Ekpo is a Fellow of the Higher Education Academy, U.K. He is a member of the Institution of Engineering and Technology, U.K., and the American Institute of Aeronautics and Astronautics, USA.

3.2.2 Paper 2 [SE2]

Thermal Subsystem Operational Times Analysis for Ubiquitous Small Satellites Relay in LEO, *International Review of Aerospace Engineering*, pp. 48–57, Vol. 11, No. 2, April 2018.

DOI: https://doi.org/10.15866/irease.v11i2.13663.

Sunday Cookey Ekpo
Department of Engineering, Manchester Metropolitan University, UK

This subsection is an exact copy of Paper 2.

Praise Worthy Prize

This paper is available online at www.praiseworthyprize.org
International Review of Aerospace Engineering (I.RE.AS.E), Vol. 11, N. 2
ISSN 1973-7459 April 2018

Thermal Subsystem Operational Times Analysis for Ubiquitous Small Satellites Relay in LEO

Sunday C. Ekpo

Abstract – *The success of the satellite subsystems engineering depends on the optimal design, modeling, simulation, and validation of the deliverables of the conceptual and mission design objectives. This paper presents the operational times analysis of the thermal control subsystem onboard a 97-kg microsatellite in low-Earth orbit during an eclipse period. Power-storing, communication downlink and uplink, payload processing, and thermal control overpower modes were implemented for a communication mission under worst-case orbital patterns. An embedded digital temperature and lighting controller circuitry was designed and practically validated to effect a desired logic. For an average eclipse period of 34.4 mins, the operational times of the thermal subsystem at altitudes of 400 km, 500 km, and 600 km are 38.6 mins, 38.1 mins, and 37.7 mins respectively. Moreover, the thermal control subsystem simulation reveals that reducing the operational times of non-thermal control subsystems during the eclipse period by 50 % can result in an operational factor of safety of over 1.5. At least 10 dB data link transmission margin can be achieved. The reported findings show that the operational times of spacecraft subsystems overpower modes can be reconfigured in orbit to reliably sustain the operating conditions of the capability-based satellite components for ubiquitous communication.* **Copyright © 2018 The Authors.**

Published by Praise Worthy Prize S.r.l. This article is open access published under the CC BY-NC-ND license (http://creativecommons.org/licenses/by-nc-nd/3.0/).

Keywords: *Adaptive Device, Onboard Electronics, Operational Times, Reconfigurable, Satellite Communication, Temperature Control*

Nomenclature

CFP	Customer-furnished payload
CO	Communication overpower mode
CO	Communication overpower
ComSat	Communication satellite
E_o	Round-trip energy generated by the solar arrays, J
E_s	The energy consumptions in the power-storing
E_{ss}	Subsystem processing-overpower
f_e	Eclipse fraction
FPGA	Field programmable gate array
HAM	Highly adaptive microsatellite
HASS	Highly adaptive small satellite
H_{sat}	Altitude of the satellite, km
JTAG	Joint test action group
LCC	Light controller circuit
LEO	Low-earth orbit
LNA	Low-noise amplifier
MetSat	Meteorology satellite
OM	Overpower mode
P_i	The ith power mode's power consumption, W
PlaSat	Planetary satellite
P_{max}	Maximized power mode, W
P_n	*n* subsystem overpower, W
PPO	Payload processing overpower mode
PPO	Payload processing overpower
PSM	Power-storing mode
PSO	Power-storing overpower
PSO	Power-storing overpower mode
P_{sp}	Sunlit power generation of the solar array, W
P_{ss}	Subsystem processing-overpower, W
P_u	Uplink-overpower, W
R	The radius ratio, R_{eq}/R_{sat}
R_{eq}	Mean equatorial radius of the Earth, 6378 km
R_{sat}	Geocentric radius of the satellite, km
SE	System engineering
SoC	System-on-a-chip
STP	Spacecraft team's payload
SWaP	Size, weight and power
TCC	Temperature controller circuit
TCO	Thermal control overpower mode
TCO	Thermal control overpower
t_i	*i*th power mode's operational time, s
t_{max}	Maximized operational time, s
t_n	*n* subsystem overpower time, s
TSOT	Thermal subsystem operational times
t_{ss}	Operational time of the subsystem processing OM
t_u	Uplink overpower time, s
ULO	Uplink overpower mode
ULO	Uplink overpower

Copyright © 2018 The Authors. Published by Praise Worthy Prize S.r.l.
This article is open access published under the CC BY-NC-ND license (http://creativecommons.org/licenses/by-nc-nd/3.0/)
Available online by April 30th, 2018 https://doi.org/10.15866/irease.v11i2.13663

β Sun-orbit-plane angle, °
μ Gravitational constant of the Earth, km^3/s^2
τ_o Orbital period of the satellite, s

I. Introduction

The range of the incident angle of the sunlight on the solar panel is a function of the inclination between the ecliptic and equatorial planes. For an inclination of 23.45°, the incident angle of the sunlight on the solar panel ranges from 66.55 to 90°. On equinox days (vernal and autumnal equinoxes), the satellite experiences the longest eclipse once a day due to the blocking of the illuminating sunlight by the Earth. When the Earth shadows a satellite, a two-fold immediate impact unfolds thus: the solar array power generation stops and the satellite temperature decreases abruptly. Thus, the ability to predict the eclipse as well as deploy reliable and fast real-time devices for the thermal and lighting control subsystems is vital for the spacecraft electrical power system design. The satellite system can experience total eclipse (umbra period lasting for 69.4 mins) or partial and total (penumbra period, lasting for 73.7 mins). Spacecraft systems engineers utilize the penumbra (eclipse) duration to design the electrical power subsystem. In order to meet the mission operation requirements, sustainable, reliable, reconfigurable and low-cost radiation-hardened digital circuits are vigorously being investigated and designed for space-borne assets and integrated seamless communication networks. Every spacecraft contains sensors for measuring the amount of thermal radiation (infra-red), visible light and other radiations that arrive from the EM spectrum.

The thermal control subsystem of a space satellite maintains the right temperature margins of all onboard equipment during normal and abnormal mission operations. Passive and active modes of cooling are provided via this subsystem. It typically consists of thermostats, thermistors (temperature sensors), control electronics, multilayer blankets, louvers, fixed radiators, control electronic, coatings, tapes and heaters.

The existing system engineering analysis (SEA) margins are insufficient to sustainably address the conceptual design and mission objectives of capability-based small satellite missions [1] operating in the low-Earth orbit (LEO). Current space missions have heavily depended upon commercial-of-the-shelf (COTS) components and subsystems for their development to provide an economical platform for emerging technology demonstrations, scientific mission investigations, and constellations/clusters for advanced mission concepts [2].

An intelligent conceptual characterisation of the optimal operational times for the satellite subsystems is one of the critical design considerations that spacecraft engineers must qualify prior to launch [1], [3], [4]. The passive, active and adaptive components onboard a satellite operate under static and dynamic power regimes that must be estimated [4]–[6]. A balanced energy budget is established following a subsystems-level analysis of the satellite's operational times margins [7]. In-orbit performance metrics are determined by the available cost-effective and energy-efficient multiple power modes a spacecraft can accommodate [7]. In terms of a round-trip data communication, the eclipse period presents a critical regime for the onboard electronics resources. The feasibility of fulfilling premium operational margins by small satellites is determined by their size, weight and power (SWaP) limitations. To obviate this constraint, an innovative design of embedded digitized analog RF circuits with very low power consumptions and small components footprints is required [3]. Deploying highly adaptive functional architectures would enable onboard mission data processing, and handling to be reliably performed during the eclipse duration [8]. This would lead to ubiquitous high data rate, sustainable link margin, bandwidth availability, and reliable communication subsystem.

For a given satellite mission, at least two basic power modes are feasible: a power-storing and an overpower modes. The satellite's subsystems consume more power in the overpower mode (OM) (during which the sunlit solar power generation/production for the spacecraft is less than the spacecraft's power consumption) than in the power-storing mode (PSM) (during which the illuminated solar power generation/production for the spacecraft is less than the spacecraft's power consumption). The spacecraft utilizes the PSM regime to store energy on the onboard batteries; this is utilized to sustain the mission capabilities during the OM regime. Typical overpower-mode spacecraft applications include engineering and scientific data transmission [9], onboard payload processing [10], and thermal control during eclipse periods.

II. Small Satellite Thermal Subsystem

In this section, the thermal subsystem engineering and the associated components are explained. The satellite system definition requirements for the thermal subsystem design, characterization, deployment and operation are presented.

II.1. Thermal Subsystem Engineering

The thermal control and management subsystem is responsible for maintaining the acceptable temperature ranges of the different components onboard a spacecraft. The radiated heat experienced by a satellite comes from the onboard electronic components, Sun and reflections from off the Earth. This radiated heat must be lost to the spacecraft environment to enable it cool down and perform optimally. Once the orbital patterns and eclipse time of a satellite are known, the radiative heat sources and sink can be estimated with an appreciable degree of accuracy.

To understand and validate the operational times of components, subsystems, and modules of a spacecraft, a

Copyright © 2018 The Authors. Published by Praise Worthy Prize S.r.l.

careful investigation and analysis of the subsystems power requirements and thermal dissipation (based on the orbital patterns) must be carried out. Table I gives the core bus subsystems power allocation for the thermal subsystem of capability-based small satellite missions (including communication (ComSat); planetary (PlaSat); meteorology (MetSat); and other satellites). The two generic case studies considered are based on a customer-furnished payload (CFP) and a payload developed along with the core bus subsystems (i.e., spacecraft team's payload (STP). The thermal subsystem engineering is aimed at qualifying the different heat sources and sinks within the spacecraft environment.

TABLE I
CORE BUS SUBSYSTEMS POWER ALLOCATION FOR SMALL SATELLITES

	Percentage of Total Core Bus Subsystems Power Allocation (%)							
	ComSat		PlaSat		MetSat		Other	
Subsystem	STP	CFP	STP	CFP	STP	CFP	STP	CFP
Thermal	30.5	30.5	28.8	28.8	48.8	48.8	33.2	30.1

A comprehensive system engineering analysis and design process for capability-based small satellites [1], [3] and conventional [4], [11] missions can be found in references. The next section explains a FPGA-based real-time digital thermal and lighting control subsystem design and analysis for investigating the operational times of small satellites in LEO.

II.2. Real-time Thermal and Lighting Control Subcystem

For the purpose of analyzing the system engineering implication(s) of using FPGA-based adaptive devices in satellite missions [1], [12], [13], two mission applications were considered thus:

1) A light controller circuit (LCC) for a small satellte in LEO:
   - The output signal controls the electrical lighting system of the satellite (especially during the eclipse period); and
   - The input signal(s) is from radiation sensors (including visible light and thermal radiation) that sense the ambient lighting condition of the satellite system.
2) A temperature controller circuit (TCC) for a small satellte in LEO:
   - The input signal(s) is from a sensor (such as a thermistor) that senses the environmental condition parameter (i.e., temperature, especially during the eclipse period) onboard the satellite; and
   - The output signal(s) from the digital hardware is used for enabling the controlling device (e.g., a thermostat) with recourse to the desired ambient temperature of the satellite system.

The FPGA device was utilized to design the thermal and lighting controller circuits for the small satellites missions in LEO presented in this paper. Altera's Quartus II software and Cyclone IV E EP4CE115F29C7 FPGA device family were utilized for the implementation of the circuit. The digital component development adopted for this work involved a schematic circuit design; timing constraint and clocking analysis; functional and timing simulation; and FPGA device programming and configuration (to implement the designed digital circuit(s)).

FPGA devices support both functional and timing simulations. For n number of inputs, there is a corresponding 2^n number of test vectors to be generated and used for the system simulation. The reported designed digital circuits were simulated using the Quartus II Simulator; the ModelSim application can also be utilized for the simulation of the presented FPGA designs. In a functional simulation, it is assumed that the logic blocks/elements and interconnects within the FPGA fabric are perfect with no signal propagation delays. It is mostly used to ascertain the functional integrity of a circuit at the design stage. It has a low latency since the simulation uses the logic expressions that characterise the digital circuit. The timing simulation takes the signal propagation through the circuit into consideration; it tests the fitter circuit to authenticate its functional correctness and timing. The timing analysis enables the embedded system designer to estimate the expected performance of the digital circuit with recourse to the results of the propagation delays across the several paths in the fitted actual FPGA circuit and/or chip. Following the designed circuit simulation, a physical FPGA chip is utilized to implement it. This is done by programming the configuration controls (switches) that configure the logic elements (LEs) and create the desired wiring connections. Altera's DE-series boards permits the FPGA configuration to be carried out in Joint Test Action Group (JTAG) and Active Serial (AS) modes. The JTAG mode retains its configuration information as long as the FPGA chip is powered on and loses it when it is turned off.

The AS mode uses a configuration device that employs flash memory to store the configuration data. During power-up or reconfiguration, the data is loaded onto the FPGA chip. This obviates the need to reprogram and/or reconfigure the device when the power is turned-on. This can be implemented on small satellites to sustain the optimal energy balance for a given mission.

II.3. Thermal and Lighting Controller Circuit Design

The satellite digital lighting controller circuit is shown in Fig. 1. The digital circuit can be used to provide a reliable two-way control of the spacecraft light (where logic value 0 represents an open switch); it involves the Exclusive-OR function of the two input signals. The functional and timing simulation waveforms that implement the truth table in Table II are explained in section IV.

The Altera's cyclone IV E FPGA device was used for these two simulations.

Copyright © 2018 The Authors. Published by Praise Worthy Prize S.r.l.

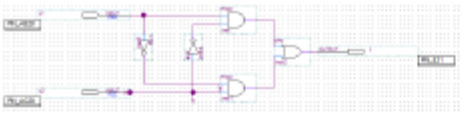

Fig. 1. A schematic design of the small satellite's LCC

TABLE II
TRUTH TABLE FOR THE DIGITAL LCC

x_1	x_2	f
0	0	0
0	1	1
1	0	1
1	1	0

The digital TCC (Fig. 2) is an automatic temperature controller onboard a small satellite in LEO. It can be equally used for the spacecraft's lighting control. The heater and/or light should be "On" only when a shadow is detected (i.e., when the satellite is in the Earth's shadow (during eclipse)) or when a ground station (engineering data) command activates a switch (such as the freezing/colliding button or due to any other abnormal conditions of operation) to turn the heaters on. The heaters should only operate if they have been "Off." The logic sequence is described below:

- output: $y = 1$ (Turn On Heater/Light)
- inputs:
  - $x_3 = 1$ (Earth's Shadow Detected);
  - $x_1 = 1$ (Turn Holding the Heater and/or Light On/Open); and
  - $x_2 = 0$ (Heater Off/Shutdown)
- the Heater/Light should be turned on when:
  - the heater/light is shutdown and Earth is passing between the satellite and the Sun ($x_2 = 0$; $x_3 = 1$);
  - the Earth's shadow is detected; heater/light is Off and the switch is set to hold it open ($x_3 = 1$; $x_2 = 0$; $x_1 = 1$); and
  - the temperature of the onboard electronics is below a threshold value ($x_1 = 1$; $x_2 = 0$; $x_3 = 0$).

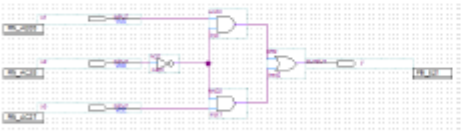

Fig. 2. A schematic design of the small satellite's TCC

TABLE III
TRUTH TABLE FOR THE DIGITAL TCC

x_1	x_2	x_3	y
0	0	0	0
0	0	1	1
0	1	0	0
0	1	1	0
1	0	0	1
1	0	1	1
1	1	0	0
1	1	1	0

The functional and timing simulation waveforms that implement the truth table in Table III are explained in section IV. Multiple deployments of the digital TCC can be carried out depending on the subsystem requirements definitions to satisfy the mission objectives.

III. Thermal Subsystem Operational Times Analysis

The operational times of the thermal subsystem of a core bus module of a small satellite is a function of the instantaneous in-orbit power modes. Each power mode is in turn affected by the prevailing orbital patterns experienced by the satellite. The thermal subsystem operational times analysis presented in this paper will consider the worst-case scenarios for the ubiquitous data relay of capability-based small satellites.

III.1. Orbital Patterns Analysis

A typical satellite system engineering considers subsystems' design variables with recourse to the orbital patterns to ensure a successful mission (and post-mission) program(s). The LEO is suitable for short-term and low-cost missions up to 2000 km. The orbital pattern parameters form the system design variables used to qualify the operational and power generation margins of spacecraft [14]. The orbital patterns are characterized by the inclination (i.e., the angular orbital sweep of a spacecraft around the Earth relative to the equator) and eccentricity (i.e., the deviation of the orbit from an Earth-referenced two-dimensional plane round-trip circle) of a spacecraft orbit.

Satellites operating non-sun-synchronous orbits experience the Earth's eclipse for a given duration during their orbital period. Hence, the eclipse period reduces the solar power generation capability of the satellite. Mathematically, the eclipse time, t_e, of a satellite is given by:

$$t_e = \frac{\tau_o}{\pi}\left(\cos^{-1}\left(\frac{\sqrt{1-R^2}}{\cos\beta}\right)\right) \quad (1)$$

where:
R = the radius ratio = R_{eq}/R_{sat};
R_{eq} = mean equatorial radius of the Earth = 6378 km;
R_{sat} = geocentric radius of the satellite, km = $R_{eq} + H_{sat}$;
H_{sat} = altitude of the satellite, km;
β = Sun-orbit-plane angle, °;
τ_o = orbital period of the satellite, s;
μ = gravitational constant of the Earth = 398,600.4418 km^3/s^2.

The eclipse fraction, f_e, is obtained from (1) as follows:

$$f_e = \frac{1}{\pi}\left(\cos^{-1}\left(\frac{\sqrt{H_{sat}^{\ 2} + 2R_{eq}H_{sat}}}{(R_{eq}+H_{sat})\cos\beta}\right)\right) \quad (2)$$

The orbital period of the satellite, τ_o is given by:

Copyright © 2018 The Authors. Published by Praise Worthy Prize S.r.l.

$$\tau_o = 2\pi\sqrt{R_{sat}^{\ 3}/\mu} \quad (3)$$

The energy generation of the solar panels is 0 W during the eclipse period, and the satellite maintains the system functionalities using the onboard storage batteries. The worst-case sun-orbit plane angle, β, occurs at 0° when the satellite experiences the maximum Earth's eclipse; the best-case β occurs at ±90° when the orbit never enters the Earth's eclipse.

III.2. Operational Modes of a Small Satellite

For a N-power mode system involving several power modes for single and multiple missions and post-mission applications, the following power consumptions are feasible:

1) Power-storing;
2) Communication (downlink and uplink)-overpower, P_{dw}, with a corresponding time, t_{dw};
3) Uplink-overpower, P_u, with a corresponding time, t_u;
4) Subsystem processing-overpower, P_{ss}, with a corresponding time, t_{ss}; and
5) Other overpower modes, P_n, with a corresponding time, t_n, where $n = 1, 2, \ldots$.

The prevailing modes of the various subsystems of a small satellite can be accommodated and adapted to fulfil the conceptual design and mission objectives.

III.3. Thermal Subsystem Operational Times Analysis

The eclipse period is a fraction of a satellite's orbital period and affects the total energy reserve of the satellite. The round-trip total energy generated by the satellite's solar arrays, E_o, is given by:

$$E_o = P_{sp}(\tau_o - t_e) \quad (4)$$

where P_{sp} is the average sunlit power generation (in Watts) of the solar array in a given orbit.

The power consumptions for a two-power mode system can be modelled by considering the following:

1) Power-storing, P_s; and
2) Subsystem processing-overpower, P_{ss}.

From (4), the total generated energy of the satellite during a round-trip for a two-power mode system can be obtained thus:

$$E_o = P_s t_s + P_{ss} t_{ss} \quad (5)$$

where
t_s = the operational times of the power-storing in second;
t_{ss} = subsystem overpower modes in second.

Equation (5) represents the energy consumptions in the power-storing, $E_s = P_s t_s$, and subsystem processing-overpower, $E_{ss} = P_{ss} t_{ss}$, modes. The operational time of the subsystem processing-overpower mode, t_{ss}, is a function of the orbital period and eclipse time and obtained as:

$$t_{ss} = \tau_o - (t_s + t_e) \quad (6)$$

For a two-power mode system, the operational time of the subsystem processing-overpower mode is derived from (4) to (6) as follows:

$$t_{ss} = \frac{E_o - P_s(\tau_o - t_e)}{P_{ss} - P_s} \quad (7)$$

The in-orbit mission's energy budget balance is obtained as a sum of the energy requirements of the satellite's subsystems and given by:

$$E_o = E_s + E_{dw} + E_u + E_{ss} + E_1 + E_2 + \ldots + E_N \quad (8)$$

The overall operational time of the subsystem processing-overpower mode is a function of the power-storing time, eclipse time, downlink time, uplink time and other prevailing times of N-power modes. This can be obtained mathematically as:

$$t_{ss} = \tau_o - (t_s + t_e + t_{dw} + t_u + t_1 + t_2 + \ldots + t_N) \quad (9)$$

From (8) and (9), the overall in-orbit operational time of the subsystem processing-overpower mode, t_{ss}, is derived as:

$$t_{ss} = \frac{E_o - P_s(\tau_o - (t_e + t_{dw} + t_u + t_1 + t_2 + \ldots + t_N))}{P_{ss} - P_s} + \frac{-(P_1 t_1 + P_2 t_2 + \ldots + P_N t_N)}{P_{ss} - P_s} \quad (10)$$

Equation (10) can be re-written thus:

$$t_{ss} = \frac{E_o + P_s\left(\sum_{i=1}^{N-2} t_i + t_e - \tau_o\right) - \left(\sum_{i=1}^{N-2} P_i t_i\right)}{P_{ss} - P_s} \quad (11)$$

where P_i and t_i represent the ith power mode's power consumption and operational time respectively. The summations in (8) are implemented respecting all the overpower modes except the power-storing and the particular subsystem processing-overpower mode. A comprehensive temporal enumeration of the power consumptions and corresponding operational times of the power modes of interest must be estimated in order to obtain the t_{ss} for the satellite mission. The correct estimates of the power consumptions of the power-storing mode and the power mode whose operational time are required to compute the t_{ss}.

In spacecraft missions, it is vital to maximize the operational time of a power mode. Hence, (11) is adjusted to obtain the maximized power mode, P_{max}. The corresponding maximized operational time, t_{max}, is given by:

Copyright © 2018 The Authors. Published by Praise Worthy Prize S.r.l.

$$t_{max} = \frac{E_o + P_s\left(\sum_{i=1}^{N-2} t_i + t_e - \tau_o\right) - \left(\sum_{i=1}^{N-2} P_i t_i\right)}{P_{max} - P_s} \quad (12)$$

Equation (12) enables the modeling of the operational times of the subsystems and modules of a spacecraft based on the systems definition requirements, conceptual objectives, and mission design variables.

IV. TSOT Simulation Parameters

To simulate the behavior of the digital circuit, a sufficient number of input valuations would be applied to observe the expected output values. For a large circuit, a relatively small and representative values of the huge input valuations are chosen. For the designed small satellite's LCC, the desired functional and timing simulations were set to run from 0 to 200 ns. The four test vectors were applied using four 50-ns time intervals. The logic states timings were set as follows: x_1 [0: 0 to 100 ns; 1: 100 to 200 ns]; x_2 [1:50 to 100 ns; 1:150 to 200 ns].

A similar procedure was followed for the FPGA-based digital TCC for a small satellite mission. The TCC is shown in Fig. 2. For the designed small satellite's TCC, the desired functional and timing simulations were set to run from 0 to 400 ns. The eight test vectors were applied using four 50-ns time intervals. The logic states timings were set as follows: x_1 [0: 0 to 200 ns; 1: 200 to 400 ns]; x_2 [1: 100 to 200 ns; 1: 300 to 400 ns]; x_3 [1: 50 to 100 ns; 1: 150 to 200 ns; 1: 250 to 300 ns; 1: 350 to 400 ns]. The operational times of the thermal control processing overpower, payload processing overpower and communication-overpower modes for a candidate communication mission are obtained with recourse to the orbital pattern parameters (Table IV).

Table V presents the orbital patterns for the TSOT analysis of the case study communication mission in LEO.

From the system engineering analysis of highly adaptive microsatellites (HAM) in LEO [14] and (13) and (14), an altitude of 500 km is chosen for the case study communication mission using a microsatellite with an on-orbit dry mass of 97 kg. For a Class 2 design (i.e., next-generation spacecraft), a contingency factor of 25 % is chosen for the microsatellite mass and power margins. Assuming that four solar panels are deployed by the microsatellite in orbit, the maximum generated electrical power is 116.83 W [1]. The calculated corresponding core bus power is 59.27 W. Hence, the power allocation for the thermal subsystem is 18.08 W. During the eclipse period, the thermal subsystem would need more than this power value to maintain the right operating temperature range for the different electronic components onboard the microsatellite. The prevailing orbital pattern limits how much power can be generated and hence, the thermal control subsystem must enter the "overpower" operational mode.

TABLE IV
DESIGN PARAMETERS FOR SATELLITE TSOT MODELLING

Parameter	Description	Value
Spacecraft mass (kg)	Microsatellite	$95 \leq M \leq 100$
TSOT (mins)	Payload processing	$t_p > 0$
	Communication	$t_{DL} > 0$; $t_{UL} > 0$
	Thermal control	$t_h > 0$
Power-storing power, P_s (W)	Power is generated; no payload processing and communication	$P_s > 0$
Max. eclipse time, t_e (mins)	Payload processing; communication and thermal control; no power is generated.	$t_e \geq 35.0$
β range (°)	Sun-orbit-plane angle	0
Orbital period, τ_o (mins)	Power is generated; Payload processing and Communication.	$90 \leq \tau_o \leq 100$
Inclination (°)	Closed orbit; Elliptical	$22.5 \leq I_{inc} \leq 157.5$
RAAN (°)	Right ascension of the ascending node.	$0 \leq RAAN \leq 90$
Altitude (km)	LEO	$400 \leq H_{alt} \leq 2500$

TABLE V
ORBITAL PATTERNS FOR THE COMSAT MISSION IN LEO

Orbit	Altitude, H_{alt} (km)	Inclination (°)	RAAN (°)
Inclination	400	22.5	30
Inclination	500	45	60
Inclination	600	67.5	90
Inclination	400	112.5	30
Inclination	500	135	0
Inclination	600	157.5	0

Table VI contains the power-storing overpower (PSO), communication overpower (CO), uplink overpower (ULO), payload processing overpower (PPO) and thermal control overpower (TCO) modes for the case study microsatellite. For the purpose of modelling the impact of implementing five power modes during the eclipse period, an operational time of 10 minutes is assumed for the communication overpower, uplink overpower and payload processing overpower modes.

TABLE VI
ENERGY RESERVE BUDGET FOR THE COMSAT MISSION IN LEO

Subsystem	Power Mode's Power Consumption (W)				
	PSO	CO	ULO	TCO	PPO
ADC	2	5	5	5	5
C&DH	3	15	15	15	10
Uplink	3	23	20	15	15
Downlink	5	30	30	15	24
Payload	0	23	23	15	40
Board	1	2	2	5	5
Thermal	0	10	10	40	10
EPS	5	10	10	15	10
Propulsion	1	0	5	5	5
Mechanics	0	0	0	0	0
Total	20	118	120	130	124

V. Results and Discussion

The functional (Fig. 3) and timing (Fig. 4) simulations are similar with no noticeable delay in producing a change in the signal f from the time when the input signals, x_1 and x_2, change their values. For a cyclone II device, there is a delay of about 6 ns in producing a change in the signal f from the time when the input signals, x_1 and x_2, change their values. This delay is due

Copyright © 2018 The Authors. Published by Praise Worthy Prize S.r.l.

to the propagation delays in the logic element and the wires in the FPGA device.

The designed digital LCC was implemented on an actual FPGA chip (Fig. 5) to realize the truth table shown in Table II. The JTAG mode was utilized for the programming/configuration setting. The hardware setup for downloading the configuration data involved adding a USB Blaster (USB-0) interface for the data link between the PC and the FPGA board. The FPGA-based digital circuit was tested by changing the switch positions on the DE2-115 prototyping board (with recourse to the four test vectors) to predict its performance during an actual spacecraft mission.

Fig. 3. Functional Simulation Result of the Digital LCC

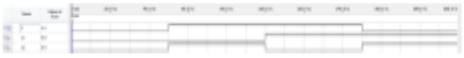

Fig. 4. Timing Simulation Result of the Digital LCC

Both the functional (Fig. 6) and the timing (Fig. 7) simulations confirm the correctness of the digital circuit aimed at implementing the desired control performance while onboard a small satellite in LEO. The output at each temporal resolution is a function of the logic states combination of the three inputs.

The designed digital TCC was implemented on an actual FPGA chip (Fig. 8) to realize the truth table shown in Table III.

Fig. 9 shows the measured power consumption profiles of the Cyclone IV E FPGA device during the TCC implementation. The pre-configuration power of the FPGA board increased abruptly from approximately 1.2 W to approximately 3.7 W in 8 secs when the board was turned on. It then decreased to about 3.5 W before settling at 3.6 W during the programming and configuration of the FPGA device.

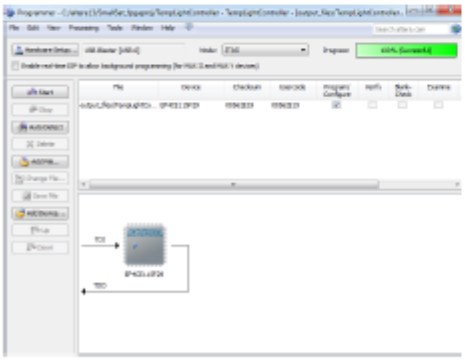

Fig. 5. Programming and configuring the FPGA device for the digital LCC

Fig. 6. Functional simulation waveform of the digital TCC

Fig. 7. Timing simulation waveform of the digital TCC

As in most space systems designs, the temperature onboard a spacecraft might vary at different locations within the system due to directional and/or selective impacts of space radiations. This can cause the various subsystems onboard a small satellite to be exposed to different temperature profiles at different times of the day and season. This kind of scenario would benefit from a real-time, high-speed reconfigurable device such as a differential digital TCC feeder.

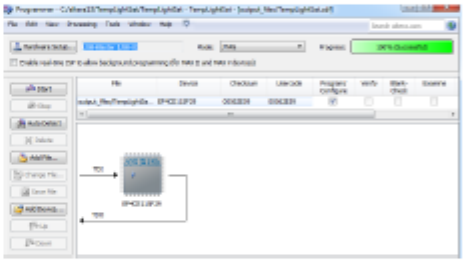

Fig. 8. Programming and configuring the FPGA device for the digital TCC

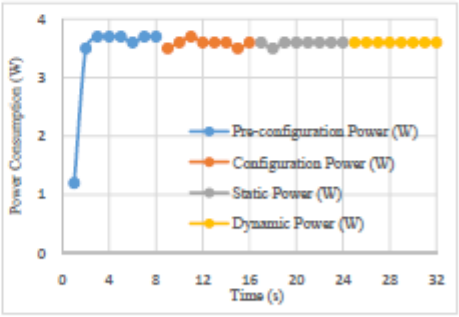

Fig. 9. Measured power consumption of the FPGA device for the digital TCC

An important information of great interest to a digital hardware designer is the speed at which a given circuit implements its logic functions. The maximum frequency, f_{max} for clocking the digital circuit is a good measure of

Copyright © 2018 The Authors. Published by Praise Worthy Prize S.r.l.

the speed of implementation. f_{max} depends on the longest delay experienced along any path between two concurrently-clocked registers. A timing analysis to determine the performance of the differential TCC was carried out using the Quartus® II software. The f_{max} summary for multiple models of analysis under different operating conditions were done. The Slow 1100 mV 85C Model shows that the maximum frequency for the differential TCC implemented on the Cyclone IV E FPGA chip is 274.05 MHz. Timing constraints were created and analyzed for the differential TCC to operate at a clock frequency of 300 MHz. This was carried out using Altera's Quartus® II TimeQuest Timing Analyzer tool. The analysis yielded a maximum clock frequency of 275.56 MHz.

With the advances in adaptive devices technologies, embedded FPGAs can be implemented to address the SWaP limitations of capability-based small satellites. An embedded FPGA is an IP block that allows a complete FPGA to be incorporated in a system-on-a-chip (SoC) module or any kind of integrated electronic circuit (including digitized analog RF). Embedded FPGAs support customization. Hence, a small footprint of reprogrammable logic on the peripheral bus can be implemented to program the serial interface register transfer language (RTL). This would enable any serial-interface protocol to be deployed on-demand. Moreover, an embedded FPGA enables in-system reprogrammability.

It allows a chip, and the electronic system it resides in, to be reprogrammed to handle new/emergent communication standards that did not exist when the chip was designed. Battery life in short-term space mission applications is critical due to the SWaP limitations of capability-based small satellites. Most battery usage is attributed to the frequent, repetitive, low-level tasks, rather than the infrequent more complex operations. Several low-level digital signal processing functions could be processed by a small block of embedded FPGAs as fast or faster than a competing microprocessor, but using 2× to 5× less energy.

The embedded FPGA offloads the repetitive, low-level tasks at lower energy and the microprocessor is only engaged when it is time for a more complex task. This helps to extend the battery life onboard the small satellite for successful mission applications and possible post-mission reuse.

Table VII reports the orbital period, maximum eclipse time, and the operational times of the thermal control subsystem with recourse to the orbital patterns in Table V and the modelling parameters.

TABLE VII
TSOT ANALYSIS FOR THE COMSAT MISSION IN LEO

Altitude, H_{sat} (km)	Orbital Period, τ_o (min.)	Max. eclipse time, t_{emax} (min.)	TSOT, t_{tc} (min.)
400	92.6	36.1	24.8
500	94.6	35.7	24.4
600	96.7	35.5	24.0

It is obvious from Table VII that the corresponding operational time of the thermal subsystem decreases as the altitude of deployment increases. The same pattern is also observed with the orbital period and the eclipse time of the satellite.

Though the maximum eclipse time for the case study mission is 35.7 mins, the operational time of the thermal control during the eclipse period is approximately 24.4 mins when the operational times of the communication, uplink and payload processing overpower modes are set to 10 mins. This result presents two challenges. Firstly, the thermal control and management of the satellite can be constrained to cover the eclipse period through power rationing.

Alternatively, the operational times of the communication, uplink and payload processing overpower modes can be reduced to allow for more power to be reserved for the optimal control of the temperature range of the different components onboard the microsatellite during the eclipse period. If the second option is implemented and the operational times of the other three power modes are 50 % less, the operational times of the thermal subsystem at 400 km, 500 km, and 600 km are 38.6 min, 38.1 mins, and 37.7 mins respectively. This implementation shows that the thermal control subsystem can reliably sustain the operating conditions of the satellite components over the eclipse period by a factor of safety of approximately 1.6.

A further novelty of the presented spacecraft subsystems operational times analysis is in using the technique to optimize communication link margins. For a capability-based spacecraft with different multiple transponder subsystems, achieving a good signal-to-noise ratio (SNR) for LEO mission applications is challenging. With the developed and reported operational times modeling technique, multi-band, multi-standards radio communication channel links performance metrics can be enhanced.

Fig. 10 shows the SNRs for a radio frequency communication receiver operating at C- (4–8 GHz), X- (8–12 GHz) and K-(18–21.6 GHz) bands with sensitivities of -96.51 dBm, -94.51 dBm and -96.01 dBm respectively. Each low-noise amplifier (LNA) can be configured in-orbit for a real-time round-trip data reception and processing over the same communication range.

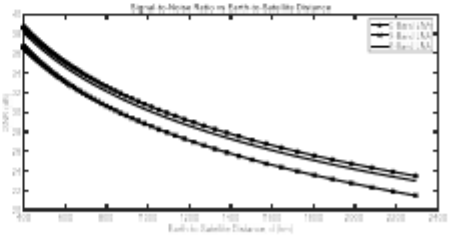

Fig. 10. Signal-to-noise ratios of a satellite receiver subsystem at C-, X- and K-bands in LEO

Copyright © 2018 The Authors. Published by Praise Worthy Prize S.r.l.

It is evident from Fig. 10 that the C- and K-bands LNAs outperform the X-band LNA due to their achieving lower minimum detectable signals at those bands by adjusting their operational times constraints. Thermal noise increases the noise figure of LNAs. Hence, providing the right temperature control for onboard electronics enhances the operational margins required for a given mission application. Furthermore, space-borne resource allocation within a distributed satellite cluster network [15], [16] can be improved through implementing optimal subsystems operational times regimes.

Multi-beamforming that operates with the conventional architecture with a limited noise floor level has been proposed for distributed satellite relay clusters [15]. With advanced residual noise extraction techniques employed within an adaptive broadband beamformer [18], subsystems operational times can be optimized for a high throughput and seamless inter-satellite beamforming links for distributed satellite networks. As these have not been carried out and/or reported in the literature, this work promises to enable future spacecraft systems perform real-time in-orbit subsystem-level adjustments to deliver optimal operational margins.

VI. Conclusion

This paper presents a thermal subsystem operational times for ubiquitous small satellites relay. Five power modes were analyzed and utilized to develop an operational time model for the thermal control subsystem of a microsatellite under different orbital patterns. The findings indicate that the operational times vary for different orbital and eclipse periods. A case study communication mission at an altitude of 500 km was considered.

For an operational time of 10 minutes for each of the communication overpower, uplink overpower and payload overpower modes, the operational time of the thermal control during the eclipse period is approximately 24.4 mins. The research reveals that the lower the operational times of non-critical overpower modes, the higher the operational factor of safety for the mission during the eclipse period. Furthermore, embedded field programmable gate array devices can be utilized as an IP block to achieve in-orbit in-system reprogrammability, customization and extended onboard battery life for seamless airborne communication application. High data rate communication links can be configured on-demand for critical data transmissions in real-time. Thus, selective subsystems operations can be implemented onboard the spacecraft for cost-effective and optimal data relay margins.

This paper utilized measured parametric data of capability-based small satellite subsystems to derive the power estimating relationships and operational times models. Hence, they are limited to adaptive small satellite system engineering design. However, the presented design parameters have considered enabling and emerging technologies and so can be extended and scaled-up to address the mission definitions requirements of medium and large spacecraft.

Acknowledgements

The author wishes to thank the Akwa Ibom State Government of Nigeria for sponsoring this research at The University of Manchester, UK, and the Engineering & Materials Science Research Centre, Manchester Metropolitan University, UK for sponsoring extra research equipment through its open bid scheme.

References

[1] S. Ekpo, D. George, A System Engineering analysis of highly adaptive small Satellites, *IEEE Systems Journal*, 7 (2013), 642–648.

[2] L. B. Rainey, *Space Modeling and Simulation: Roles and Applications Throughout the System Life Cycle*. (California: The Aerospace Press, 2004).

[3] S. Ekpo, D. George, A Deterministic Multifunctional Architecture Design for Highly Adaptive Small Satellites, *International Journal of Satellite Communication Policy and Management*, 1 (2012), 174–194.

[4] C. Brown, *Elements of Spacecraft Design*. (Reston, VA: AIAA, 2002, pp. 1–43).

[5] S. Ekpo, D. George, A System-based Design Methodology and Architecture for Highly Adaptive Small Satellites, *The 4th Annual IEEE Int. Systems Conference*, 516–519 (2010).

[6] H. Helvajian, S. W. Janson, *Small Satellites: Past, Present, and Future*. Reston (VA: AIAA, 2008, pp. 559–569, 773).

[7] S. Ekpo, D. George, B. Adebisi, A Multicriteria Optimisation Design of SPSE for Adaptive LEO Satellites Missions Using the PSI Method, *The AIAA Space Conference & Exposition*, 1–19 (2013).

[8] R. Hassan, W. Crossley, Spacecraft reliability-based design optimization under uncertainty including discrete variables, *J. Spacecraft Rockets*, 45 (2008), 394–405.

[9] S. Ekpo, D. George, Impact of Noise Figure on a Satellite Link Performance, *IEEE Communications Letters*, 15 (2011), 977–979.

[10] S. Ekpo, D. George, 4–8 GHz LNA design for an adaptive small Satellite Transponder using InGaAs PHEMT Technology, *The 11th IEEE Wireless & Microwave Conference Proc.*, 1–4 (2010).

[11] W. J. Larson, J. R. Wertz, *Space Mission Analysis and Design*, second ed. (Torrance, CA: Microcosm, Inc. and Kluwer Academic Publishers, 1992).

[12] H. Schmitz, Application Examples: How to Use FPGAs in Satellite Systems, *Actel Corporation Publication, California*, 1–7 (2010).

[13] H. Helvajian, S. W. Janson, *Small Satellites: Past, Present, and Future*. (AIAA, Inc., Virginia, 2008, pp. 771–810).

[14] S. C. Ekpo, et al., A system-level multicriteria modelling of payload operational times for communication satellite missions in LEO, *Recent Progress in Space Technology*, 4 (2014), 67–77.

[15] X. Zhong et al., Joint Downlink Power and Time-Slot Allocation for Distributed Satellite Cluster Network Based on Pareto Optimization, *IEEE Access Journal*, 5 (2017), 25081-25094.

[16] F. H. Dong, et al., Topology structure design and performance analysis on distributed satellite cluster networks, *Proc. 4th ICCSINT*, 881–884, (2015).

[17] Q.Y. Yu et al., Virtual multi-beamforming for distributed satellite clusters in space information networks, *IEEE Wireless Commun.*, 23 (2016) 95–101.

[18] S. Ekpo, B. Adebisi,A. Wells, Regulated-element Frost Beamformer for Vehicular Multimedia Sound Enhancement and Noise Reduction Applications, *IEEE Access Journal*, 5 (2017) 27254–27262.

Copyright © 2018 The Authors. Published by Praise Worthy Prize S.r.l.

Authors' information

Dept. of Electrical & Electronic Engineering,
School of Engineering, Manchester Metropolitan University,
Manchester, M1 5GD, United Kingdom.
E-mails: scekpo@ieee.org
S.Ekpo@mmu.ac.uk

Sunday C. Ekpo obtained the M.Sc. degree in communication engineering from the University of Manchester, Manchester, U.K. in 2008 and completed his Ph.D. degree in electrical and electronic Engineering at the same institution in 2011. He is a lecturer in electrical and electronic engineering at the Manchester Metropolitan University, UK.

He has published over 40 peer-reviewed and refereed technical papers in communication and space systems engineering. His specialty spans adaptive satellite system design; multiphysics characterization of RF and optical transceivers; multi-objective system engineering analysis; intelligent sensors design; and internet of things implementations.

Dr Ekpo is a member of the IET (UK), the AIAA (USA), and the Applied Computational Electromagnetics Society (USA) and a Fellow of the Higher Education Academy (UK).

Copyright © 2018 The Authors. Published by Praise Worthy Prize S.r.l.

3.2.3 Paper 3 [SE3]

Regulated-element Frost Beamformer for Vehicular Multimedia Sound Enhancement and Noise Reduction Applications, *IEEE Access Journal*, Vol. 5, pp. 27254–27262, Dec 2017.

DOI: https://doi.org/10.1109/ACCESS.2017.2775707.

Sunday Ekpo[1], Bamidele Adebisi[1] and Andrew wells[2]

[1]Department of Engineering, Manchester Metropolitan University, UK

[2]Department of Research & Development Engineering, Jaguar Land Rover PLC, UK

This subsection is an exact copy of Paper 3.

IEEE Access

Received October 21, 2017, accepted November 16, 2017, date of publication November 20, 2017, date of current version December 22, 2017.

Digital Object Identifier 10.1109/ACCESS.2017.2775707

Regulated-Element Frost Beamformer for Vehicular Multimedia Sound Enhancement and Noise Reduction Applications

SUNDAY C. EKPO[1], (Member, IEEE), BAMIDELE ADEBISI[1], (Senior Member, IEEE), AND ANDREW WELLS[2]

[1]Department of Electrical and Electronic Engineering, Manchester Metropolitan University, Manchester M1 5GD, U.K.
[2]Department of Research and Development Engineering, Jaguar Land Rover PLC, Warwick CV35 0RR, U.K.

Corresponding author: Sunday C. Ekpo (scekpo@theiet.org)

This work was supported by the Engineering and Materials Science Research Centre, Manchester Metropolitan University, U.K. through the Open Bid Scheme.

ABSTRACT A key requirement of an adaptive sensor array involves the ability to deterministically adjust the directional response of the array to reduce noise and reverberations, null interferences, and enhance the gain and recognition of the desired signal. This paper presents a low-carbon adaptive broadband beamforming algorithm called the regulated-element Frost beamformer. It enhances the desired signal based on the noise conditions of the individual omnidirectional sensors deployed in a complex dynamic environment that is prone to steering errors. The investigation of this algorithm was carried out in an interference-dominant, noisy automobile environment characterized by diffuse noise conditions. An embedded system measurement of real-time signals was carried out using omnidirectional acoustic sensors mounted in a model convertible F-Type car driven at speed limits of 20 to 50 mph. The simulation results indicate an array gain enhancement of 2 dB higher than the conventional Frost beamformer and it requires less sensors and filter taps for real-time reconfigurable implementations. The experimental results reveal that the average array gain of the regulated-element beamformer is 2.9 dB higher than the conventional Frost beamformer response. The minimum floor array gain of the regulated-element beamformer is 5 dB, representing 70% noise reduction than the conventional adaptive beamformers.

INDEX TERMS Acoustics applications, adaptive beamformer, multimedia infotainment, noise reduction, physical acoustics layer, vehicular noise control.

I. INTRODUCTION

The reception, recognition and enhancement of acoustic signals in a dynamic complex environment (such as a moving vehicle with multimedia broadband infotainment provisioning) pose a great challenge due to the time-varying nature of the noise sources, reverberations, and interferences impinging on a uniform linear microphone array (ULMA). The literature is replete with system noise evaluation studies spanning handheld cellular devices to space-borne assets involved in data and information communication. Adaptive broadband beamformers have been developed for signal detection and estimation using sensors arrays for numerous applications involving multimedia infotainment, acoustics, communications systems, radar, sonar, seismology, and radio astronomy [1]–[5]. However, the gain enhancement performance of the conventional adaptive broadband beamformers deteriorates when there is a steering error in the array deployment [6]–[8].

The single-frequency array theories and algorithms are insufficient to address the multimedia acoustic system requirements for wideband operations. The technical challenge relates to designing, developing and deploying the sensor array for a broadband reception of sounds in the presence of uncorrelated noise sources, interferences, and jammers within a moving vehicle [3], [8]–[10]. A number of array-processing applications have been carried out and most of the works assume a farfield source [5] with the signal arriving at the microphone array as plane waves. Furthermore, most practical microphones deployed for in-vehicle multimedia infotainment applications have their

2169-3536 © 2017 IEEE. Translations and content mining are permitted for academic research only.
Personal use is also permitted, but republication/redistribution requires IEEE permission.
See http://www.ieee.org/publications_standards/publications/rights/index.html for more information.

excitation sources situated well within the nearfield [6]. This presents a serious technical constraint in validating the classical farfield assumptions for the beamformer design and has the potential to severely deteriorate the beampattern. The aerodynamic noise dominates at cruising and higher speeds and the system noise characterization usually occurs in the car interior and exterior [1], [3]. At different speed and environmental (such as temperature) conditions, the aerodynamic noise of moving vehicles influences the level of passenger comfort experienced [5], [8]. Hard- and soft-constrained iterative optimization methods have been investigated and proposed for the deterministic and non-deterministic (stochastic) signal processing applications. The majority of the studies have revolved around long and short data runs and the susceptibility of the constrained iterative optimization techniques to cumulative roundoff errors [6]–[11].

To obviate the above problems, we propose the adaptation of the elements of the array for gain computation based on the noise field conditions of individual sensors. The Frost beamformer is a constrained least mean square (LMS) method which is designed to eliminate error accumulation while maintaining a hard constraint. The regulated-element Frost beamforming algorithm (REFBA) adapts noisy sensors to the array performance in real-time (RT) and selectively optimizes the finite impulse response filter taps until the array gain saturates [3]. Furthermore, the REF technique can be implemented as an embedded system with recourse to hardware/software co-design. It constrains array elements with undesirable and corrupting noise, jamming, and interference contents to be screened for the array gain computation. An exclusion principle is applied and accepted after comparing the performance of the array gains involving all the deployed sensors with the array response without the noisy elements. This novel integrated electro-acoustic signal processing technique enables the REF beamformer to have low electronic and acoustic components footprints, resulting in very reliable and cost-effective multimedia infotainment systems manufacturing and implementations.

This paper is organized as follows. Section II provides the system architecture, algorithm, and model analyses of the REFBA. Section III explains the hybrid REF beamformer. Section IV examines the acoustic noise characterization procedure using the REF technique. It states the REF noise model and covers the parameters of the acoustic array system utilized in the aerodynamic noise characterization for a moving vehicle. Beamforming simulations and experiment are explained in section V. Section VI reports the simulation and experimental analysis of the REF noise models for vehicles. Section VII concludes the paper.

II. REF BEAMFORMER ARCHITECTURE AND MODEL ANALYSIS

A. SYSTEM ARCHITECTURE

Data-dependent or adaptive beamforming techniques constantly and continuously update their data parameters with

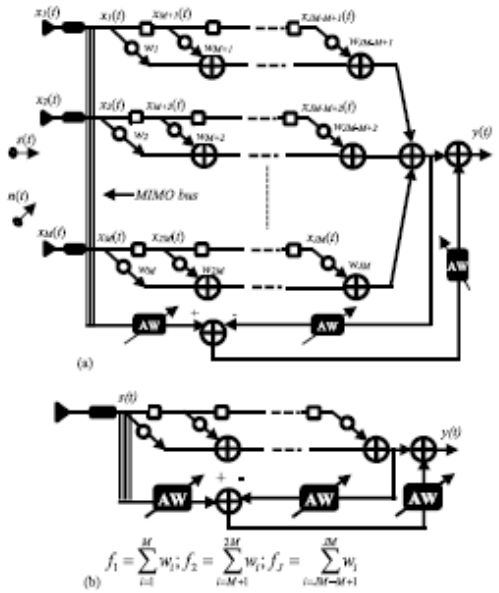

FIGURE 1. System Model Architecture of the REF Beamformer (a) Expanded version (b) Condensed version.

recourse to the received (input) signals. The generic architecture of an adaptive broadband array comprises an array of sensors in tandem with tapped-delay lines and finite impulse response filter networks [13].

The REF beamformer comprises an array of sensors followed by a network of tapped-delay lines, transversal finite impulse response (FIR) filter, and an adjustable element-dependent feedback system. Depending on the noise condition of each sensor, a portion of the received input signal is selectively added to the sum of the filter outputs to yield the feedback outputs. The beamformer output is the sum of the filter and the feedback outputs. The REF beamformer architecture (Fig. 1) contains a multiple-input-multiple-output (MIMO) bus system for selectively adapting the dynamic system noise to the optimal performance requirement of the overall linear array. The REF architecture lends credence to a deterministic tracking of the noise source behavior and parameters for a reliable system-level characterization. Hence, field programmable gates arrays (FPGAs) can be utilized to implement its FIR filter network [3].

B. SYSTEM MODEL ANALYSIS

The problem formulation of adaptive beamforming methods is a constrained optimization function of the form defined by:

$$\text{minimize } w^T R_{xx} w \quad (1)$$

$$\text{subject to } C^T w = f \quad (2)$$

where C is the constraint matrix, f, the constrained system impulse response, and R_{XX}, the autocorrelation matrix. The sum of the FIR filter outputs gives the output of the Frost beamformer, $y(t) = w^T x(t)$. The optimum weight vector, w_{opt}, for a stationary signal that minimises the expected output power of the array at the time of nth sample (i.e., $E[y^2(n)] = w(n)^T E\{x(n)x^T(n)\}w(n) = w^T E\{x(n)x^T(n)\}w = w^T R_{xx} w$), and satisfies the constraint $C^T w = f$, has to be derived. This is termed the Wiener solution [12] and the method of Lagrange multiplier is utilised to obtain it as follows:

$$w_{opt} = R_{xx}^{-} C \left(C^T R_{xx}^{-1} C\right)^{-1} f \tag{3}$$

where the initial weight vector, $w[0] = f$. The corresponding system impulse response vector, f_{ir}, is given by:

$$f_{ir} = C \left(C^T C\right)^{-1} f \tag{4}$$

The regulated-element Frost beamforming algorithm (REFBA) chooses weights to minimise the mean square error between the Frost beamformer output and the reference signal based on an adaptive detection of the received signal at each sensor. Due to the regulated feedback system of the REF beamformer for an optimal noise reduction, the required FIR filter taps is reduced by a factor of two for a 6-dB array gain increase compared with the Frost method. The constraint functions of the REF beamformer can be represented in a matrix form as:

$$W \begin{bmatrix} 1 \\ 1 \\ \cdot \\ \cdot \\ \cdot \\ 1 \end{bmatrix} = \begin{bmatrix} f_1 \\ f_2 \\ \cdot \\ \cdot \\ \cdot \\ f_J \end{bmatrix} \tag{5}$$

where the weight matrix, W, is given by:

$$W = \begin{bmatrix} w_1 & w_2 & \cdot & \cdot & \cdot & w_M \\ w_{M+1} & w_{M+2} & \cdot & \cdot & \cdot & w_{2M} \\ \cdot & \cdot & & & & \\ \cdot & \cdot & & & & \\ \cdot & \cdot & & & & \\ w_{JM-M+1} & w_{JM-M+2} & & & & w_{JM} \end{bmatrix} \tag{6}$$

and the system impulse response, f, is obtained as a J-dimensional vector thus:

$$f = [f_1, f_2, \ldots, f_J]^T \tag{7}$$

where $f_1 = \sum_{i=1}^{M} w_i, f_2 = \sum_{i=M+1}^{2M} w_i, f_J = \sum_{i=JM-M+1}^{JM} w_i$.

The noisy signals on taps and the weight vector are represented by $x(n)$ and w respectively. The constrained system impulse response, f, and the matrix of JM column vectors, C, are utilized for the constraint formulation. These parameters are represented as follows:

$$\begin{aligned} x^T(n) &= \begin{bmatrix} x_1(n) & x_2(n) & \cdot & \cdot & \cdot & x_{JM}(n) \end{bmatrix}, \\ w^T &= \begin{bmatrix} w_1 & w_2 & \cdot & \cdot & \cdot & w_{JM} \end{bmatrix}, \\ f_{ir}^T &= \begin{bmatrix} f_1 & f_2 & \cdot & \cdot & \cdot & f_{JM} \end{bmatrix}, \\ C &= \begin{bmatrix} c_1, & c_2, & \cdot & \cdot & \cdot, & c_J \end{bmatrix}. \end{aligned}$$

For J FIR filter coefficients and M sensors, the entries, c_i, of the constraint matrix, C, are the column vectors of length JM with $(i-1)M$ zeros followed by M ones and $(J-i)M$ zeros. For a 2-element ULMA system deploying 4 FIR filter taps, the constraint matrix, C, is given by:

$$C = [c_1, c_2, c_3, c_4]$$

where the entries (c_1, c_2,c_3, andc_4) are obtained as:

$$\begin{aligned} c_1 &= [1 \quad 1 \quad 0 \quad 0 \quad 0 \quad 0 \quad 0 \quad 0] \\ c_2 &= [0 \quad 0 \quad 1 \quad 1 \quad 0 \quad 0 \quad 0 \quad 0] \\ c_3 &= [0 \quad 0 \quad 0 \quad 0 \quad 1 \quad 1 \quad 0 \quad 0] \\ c_4 &= [0 \quad 0 \quad 0 \quad 0 \quad 0 \quad 0 \quad 1 \quad 1] \end{aligned}$$

The expected beamformer output of the individually adaptive regulated-element algorithm can be formulated. The received signal vector, $S_r(t)$, for the entire uniform linear array (ULMA) (Fig. 1) is given by:

$$S_r(t) = \sum_{i=1}^{M} x_i(t) \tag{8}$$

where the received signal at each sensor, $x_i(t)$, is given as a function of the received desired signal, $s_i(t)$, and dynamic system noise, $n_i(t)$, thus:

$$x_i(t) = s_i(t) + n_i(t) \tag{9}$$

The residual noise, n_o', is estimated based on the expected (mean average) output signal of the Frost array, $E[y^2(n)]$, the received signal at the time of nth sample, $S_r(n)$, and the number of sensors as follows:

$$n_o'(n) = \frac{S_r(n)}{M^M} - ME[y^2(n)] \tag{10}$$

The output of the REF algorithm is obtained by applying sensor-dependent adjustable weight (AW) vectors to the adaptive linear-constrained least mean square architecture output. This is based on the incoming data statistics at each sensor. Mathematically, the array output gain, $REF_o(n)$, is obtained (with recourse to Fig. 1) from (1), and (8) to (10) as:

$$REF_o(n) = w^T E[S_r(n) S_r(n)^T] w + \frac{\frac{S_r(n)}{M^M} - M\left(w^T E[S_r(n) S_r(n)^T] w\right)}{M^M} \tag{11}$$

From (11), the REF output at the time of *nth* sample can be computed using the following relationship thus:

$$REF_o(n) = \frac{1}{M^{2M}}\left(M^{M+1}\left(M^{M-1}-1\right)w^T E[S_r(n)S_r(n)^T]\, w + \sum_{i=1}^{M} x_i(n)\right)$$

or

$$REF_o(n) = \frac{1}{M^{2M}}\left(M^{M+1}\left(M^{M-1}-1\right)w^T R_{xx} w + \sum_{i=1}^{M} x_i(n)\right) \quad (12)$$

Equation (12) yields a high array gain for an appreciable residual noise reduction. However, the cumulative array signal gain reduces by M^{-2M} as the number of sensors increases beyond a threshold number. This results in array compression as the active elements are enabled beyond the threshold number. To overcome this challenge, a hybrid regulated-element Frost (HREF) beamformer that improves the residual noise with a corresponding cumulative array gain is discussed in the next section.

III. HYBRID REF BEAMFORMER

The REF beamformer adjusts the array gain output based on the noise condition of each sensor and its algorithm for the acoustic array system noise modelling has been formulated in the last section by considering the noise properties of individual sensors. The hybrid REF algorithm is derived with the individual array elements enabled for a M^{-2} feedback threshold factor at the time of the received nth sample, $S_r(n)$.

Given that the expected (mean average) output power of the array is $E[y^2(n)]$, the residual noise of the *HREF* beamformer, n'_r, is estimated with recourse to Fig 1 and (8) to (10) thus:

$$n'_r(n) = \frac{\sum_{i=1}^{M}(x_{ri}(n))}{M} - E[y^2(n)] \quad (13)$$

The overall output of the HREF beamformer is obtained by applying element-dependent adjustable weight (AW) vectors based on the incoming data statistics at each ULMA sensor. The output signal is a function of the number sensors and the residual noise extraction estimate for a system noise characterisation. Hence, the HREF beamformer output, $HREF_o(n)$, is given by:

$$HREF_o(n) = E\left(y^2[n]\right) + \frac{n'_r}{M} \quad (14)$$

or

$$HREF_o(n) = \frac{1}{M^2}\left(M\,(M-1)\,E\left(y^2[n]\right) + \sum_{i=1}^{M}(x_{ri}(n))\right) \quad (15)$$

To incorporate the autocorrelation function and weight vectors into the functional relationship of the array gain, Eq. (6) is modified to compute the *HREF* beamformer output as follows:

$$HREF_o(n) = \frac{1}{M^2}\left(M\,(M-1)\,w^T E[S_r(n)S_r(n)^T]w + \sum_{i=1}^{M}(x_{ri}(n))\right)$$

or

$$HREF_o(n) = \frac{1}{M^2}\left(M\,(M-1)\,w^T R_{xx} w + \sum_{i=1}^{M}(x_{ri}(n))\right) \quad (16)$$

Equations (10) and (13) represent the residual noise extraction functions for the REF and HREF beamformers respectively. The following section explores the procedure that both noise estimating relationships adopt to improve the signal-to-noise ratio of array sensors.

IV. ACOUSTIC NOISE CHARACTERIZATION

A. REF NOISE MODELING

An acoustic noise characterization (ANC) in a dynamic system starts with the identification of the noise field condition(s) of individual sensors constituting an acoustic array. In a vehicular environment, the diffuse noise field (DNF) prevails.

Figures 2 and 3 show the adaptive noise cancellation architecture and the acoustic noise modeling flow chart for the REF beamformer respectively.

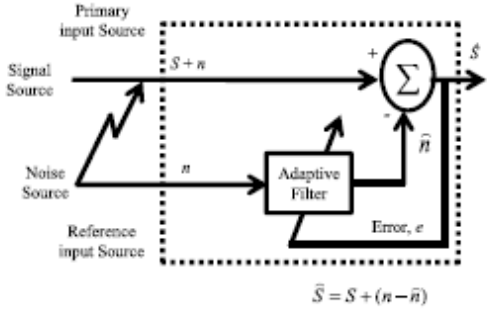

FIGURE 2. Adaptive noise cancellation architecture.

The engine transmission speed and the interaction between the tyre and the road surface generate a noise intensity level that is proportional to the magnitude of the resultant vibration. This translates into a vehicle acoustical discomfort that affects the driver and the passenger in the automobile cabin. Adaptive filters are capable of adjusting their impulse response to filter out the correlated signal in the input. They require no a priori knowledge of the correlated signal in the input [12], [15]. Figure 2 can be implemented to suppress noise contributions in an acoustic array signal processing. The main energy of a car noise pattern is estimated to fall

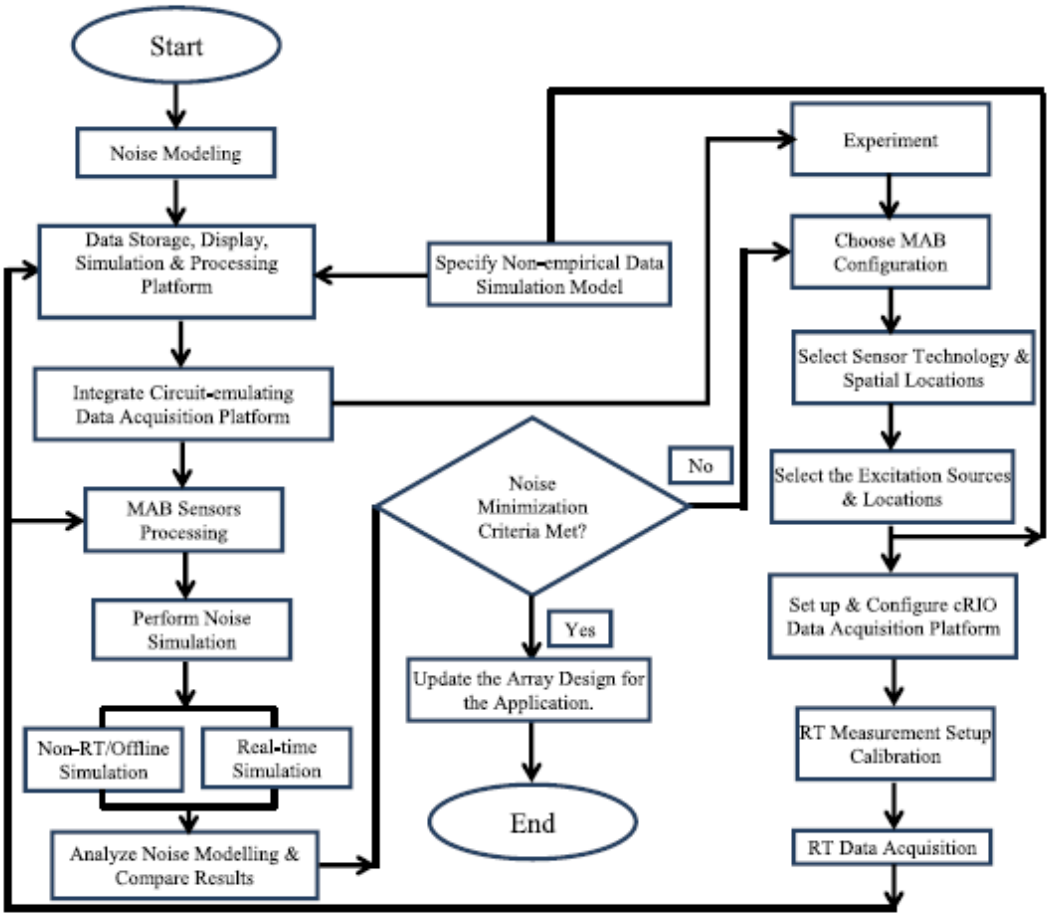

FIGURE 3. Acoustic noise modeling flow chart.

within the frequency range of 5 kHz and below. A number of key factors limit real-time acoustic measurements of moving vehicles. These include background noise, variable vehicle speed (deceleration and acceleration), uncertain vehicle direction, RF/EM interferences, multipath reflections, complicated traffic flow density, sensor differences, and hardware compatibility constraints. Vehicle speed and changes in direction determine the frequency component shift in the moving object signal. The REF beamformer considers these real-time sound validation constraints while implementing the residual noise extraction algorithm on the complex dynamic system.

B. REF NOISE CHARACTERIZATION PROCEDURE

The noise characterisation procedure of the REF beamformer comprises two paths: the non-emperical and the emperical validations. The non-emperical ANC procedure path involves a system model simulation based on a historical database. Similarly, the emperical ANC procedure path entails an experimental measurement based on a real-time data acquisition. The noise modelling procedure is illustrated in Fig. 3. The simulation process path is meant for a non-RT, offline and hypothetical data-generation validation of the system noise model. The development computer runs the appropriate software packages including a real-time operating system for a compact real-time input/output (cRIO), CAD programs and graphical, object-oriented and technical simulation/computing softwares. A system noise estimating relationship (SNER) based on the non-empirical data acquired is obtained from a statistical analysis and curve-fitting implementation.

V. BEAMFORMING SIMULATION AND EXPERIMENT

A. ANALYSES OF TIME DELAY, FROST AND REF BEAMFORMERS

The simulations and experimental investigation of the time delay, Frost, and REF beamformers were carried out to

extract desired speech signals in an interference-dominant, noisy environment such as the one found in an automobile characterized by diffuse noise conditions. The routes were carefully mapped to enable the noise signals to be obtained at the worst traffic conditions. Noise waveforms and spectra at car speed limits of 20 mph, 30 mph, 40 mph, and 50 mph were measured using omnidirectional MEMS acoustic sensors mounted inside a closed-roof car. Multichannel signals received by the microphone array were simulated by loading two recorded speeches, vehicle noise recordings at the considered speed limits, and one laughter recording; the laughter audio segment was loaded as an interference signal arriving at 20° azimuth and 0° elevation angles. The sampling frequency of the acoustic signals was set to 8 kHz. The incident azimuth and elevation directions of the first speech signal were maintained at ±90°. The direction of the second speech signal was at −10° azimuth, and 10 elevation angles. The signal-to-interference-and-noise ratio (SINR) gain for the ULMA system was determined for the Frost and REF methods. Table 1 shows a summary of the array performance results for the time delay, Frost, and REF beamformers. It is obvious that the FBA is outperformed by the REFBA by over 1.6 W output power (2 dB gain). The hybrid REF indicates approximately 1.8 W received power (2.5 dB gain) better than the Frost beamformer. The REFBA reveals a signal-to-noise ratio (SNR)-based steering gain enhancement of over 3 W received power (5 dB) more than the FBA output in the incident angle (-30, 0) direction. The REF technique responses also indicate the capability of the algorithm to perform real-time reconfiguration of audio processing and correct system-level hardware anomalies in the presence of steering errors.

TABLE 1. Array performance results for the case study beamformers.

No. of Acoustic Sensors:	2			
	Microphone Spacing (m)			
	0.05	0.10	0.15	0.20
MAB Technique	Array Gain (dB)			
TD	1.49	3.76	5.78	5.26
Frost	8.23	8.85	8.52	7.93
REF	10.28	10.79	10.89	10.96

Sensor Spacing (m)	0.05				0.10			
	Number of Microphones							
	2	4	6	8	2	4	6	8
MAB Technique	Array Gain (dB)							
TD	1.49	4.34	7.07	8.50	3.76	8.17	10.06	11.36
Frost	8.23	10.37	12.08	13.61	8.85	12.11	14.72	16.29
REF	10.28	10.50	12.08	13.61	10.79	12.23	14.72	16.29

The REF and Frost beamformers have been utilized to investigate the array gain enhancement and speech recognition profile of a moving vehicle at different speeds. The dominant noise components at different vehical speeds include motor noise, acceleration, and tyre/road noise. Table 2 states the minimum and maximum acoustic array gains of a moving vehicle for the Frost, REF and HREF beamformers. With reference to a 1-W input power, the Frost beamformer gives an average minimum array signal power output of approximately 1.1 W compared with the REF's 2.6 W, and hybrid

TABLE 2. Array gain at different vehicle speeds.

Speed (mph)	LimitArray Gain (dB)					
	Frost		REF		Hybrid REF	
	Min	Max	Min	Max	Min	Max
20	18.4	23.2	22.3	26.4	23.5	27.2
30	18.5	24.1	22.5	27.0	23.9	28.2
40	17.5	21.4	21.5	24.9	23.0	26.3
50	19.0	27.3	23.0	29.3	24.3	29.6

REF's 3.8 W. Similarly, the average maximum array signal powers for the Frost, REF, and hybrid REF are approximately 8 W (Fig. 4), 12 W (Fig. 5), and 13 W (Fig. 6) respectively over the case study speed limits. The array gain difference is approximately 3 dB at any given moving vehicle speed.

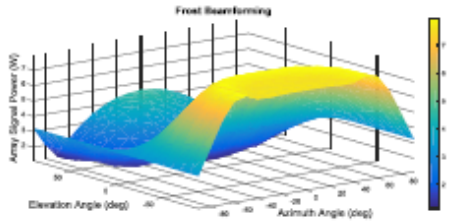

FIGURE 4. FBA (d = 10 cm; 2-element ULMA; FIRL = 5).

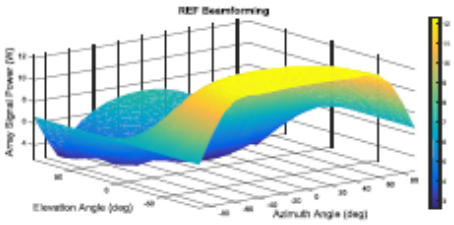

FIGURE 5. REFBA (d = 10 cm; 2-element ULMA; FIRL = 5).

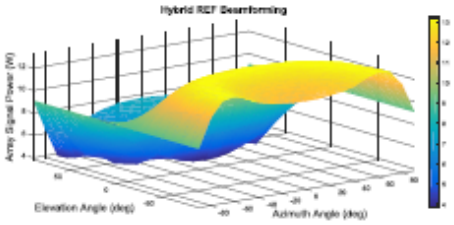

FIGURE 6. Hybrid REFBA (d = 10 cm; 2-element ULMA; FIRL = 5).

VI. REF NOISE SIMULATION AND EXPERIMENTAL ANALYSIS

A simulation of the noise extraction of the REF noise model was carried out with recourse to the signal sources, noise field

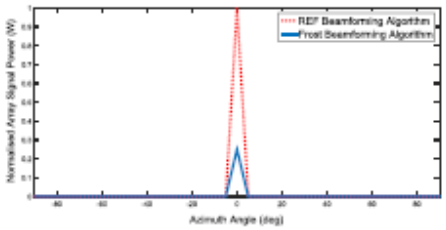

FIGURE 7. Broadside Array Signal Power for the ULMA ($N = 2$; $d = 10$ cm; Filter Length = 2).

condition(s), number of sensors, upper frequency aliasing threshold (which sets the element spacing), and the filter taps required. In the experimental investigation of the REF noise model for vehicles, we considered the prevailing automobile speed limits in the UK. The routes were carefully mapped to enable the noise signals at car speed limits of 20 mph, 30 mph, 40 mph and 50 mph to be measured using omnidirectional MEMS acoustic sensors.

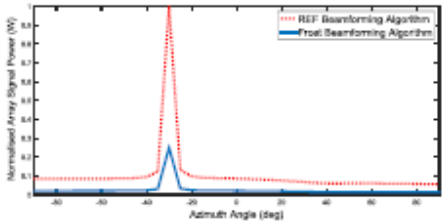

FIGURE 8. SNR-based Steering Signal Power for the FBA and REFBA ($N = 2$; $d = 10$ cm; Filter Length = 2).

A. RESULTS AND DISCUSSION

In Fig. 7, the REF achieves a broadside array signal power enhancement of approximately four times better than the Frost algorithm. Furthermore, the SNR-based steering gain (Fig. 8) for the REFBA ULMA reveals a gain enhancement of over 5 dB more than the FBA output in the incident angle (-30, 0) direction. The normalised broadside system selectivity response for the REFBA (Incident Angle = (0, 0)) is approximately 5 dB better than the FBA response. The SNR-based dynamic system selectivity gains of the ULMA based on the residual noise extraction technique was also investigated; the REF outperforms the conventional Frost beamformer by 3 dB. The results indicate that fewer filter taps are required for the REFBA compared with the FBA resulting in a lower computational cost than the latter. Since one needs to invert a 4-by-2 matrix, the REFBA offers a less expensive real-time processing using a field programmable gates array (FPGA)-based embedded signal conditioning system. Table 3 shows an analysis of the Doppler noise power of a moving vehicle at different source excitation frequencies and car speeds. The REF algorithm analysis shows that the reported

TABLE 3. Doppler noise power at different vehicle speeds.

Source Frequency (Hz)	Vehicle Speed (mph)						
	20	30	40	50	60	70	80
	Doppler Noise Power (dBm)						
3000	-139.10	-139.04	-138.99	-138.94	-138.88	-138.83	-138.78
2000	-140.86	-140.80	-140.75	-140.70	-140.64	-140.59	-140.54
1500	-142.11	-142.05	-142.00	-141.95	-141.89	-141.84	-141.79
1000	-143.87	-143.81	-143.76	-143.71	-143.65	-143.60	-143.55
500	-146.88	-146.82	-146.77	-146.72	-146.66	-146.61	-146.56
440	-147.43	-147.38	-147.32	-147.27	-147.22	-147.17	-147.12

adaptive beamformer can accurately estimate the Doppler frequency for applications involving satellite navigation system receivers of vehicles under varying environmental conditions.

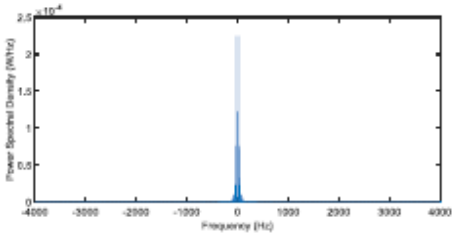

FIGURE 9. Periodogram Power Spectral Density of a Car Noise at 20 mph.

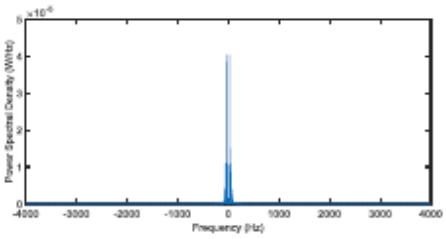

FIGURE 10. Periodogram Power Spectral Density of a Car Noise at 30 mph.

Figures 9 and 10 depict the double-sided periodogram noise power spectrum estimates of the case study moving car at the speed limits of 20 mph, 30 mph, 40 mph, and 50 mph respectively. The average noise power for the considered speed limits is approximately −60 dB from about 0.2 to 3 kHz. At a speed limit of 20 mph, the noise power shows a more compact frequency response with a maximum value of −40 dB at close to DC level and about −120 dB at 4 kHz. A similar response is observed at 30 mph, 40 mph, and 50 mph except for the obvious lower noise power (<−140 dB) at the 1.5 to 2.5 kHz spectral contents.

Table 4 shows the measured noise power and signal-to-noise ratio (SNR) of a moving vehicle at different speed limits. The SNR of the Frost beamforming technique trails

TABLE 4. Measured noise power and SNR at different vehicle speeds.

Speed Limit (mph)	Noise Power (dB)		SNR (dB)	
	1.715 kHz	Total	Frost	REF
20	-142.8	-30.27	63.78	66.10
30	-135.0	-34.45	67.96	72.19
40	-125.9	-28.81	61.40	64.40
50	-128.5	-36.64	70.06	75.01

behind the REF algorithm by approximately 3-dB and 4-dB margins for even and odd speed limits respectively. The total system noise is nonlinear with 40 mph giving the highest noise power and 50 mph, the lowest noise power. This is due to the dynamics of the system where the acoustic sensors are deployed at the time. The extracted residual noise power (ERNP) for both acoustic sensors averages at approximately 31 W (i.e., 15 dBW). Table 5 shows that the prevailing noise field condition affects the amount of residual noise that can be extracted within a complex dynamic system. Moreover, by using an acoustic array design, the moving vehicle system noise can be characterised accurately and reduced systematically for a predetermined passenger comfort.

TABLE 5. Extracted residual noise power at different vehicle speeds.

Speed Limit (mph)	ERNP (dB)	
	Sensor 1	Sensor 2
20	15.2013	15.2014
30	15.1688	15.1688
40	14.6923	14.6908
50	15.0752	15.0760

B. POTENTIAL APPLICATIONS OF THE REF BEAMFORMER

The expanding city-wide traffic congestion problem can be improved through an intelligent deployment of REF beamformer sensors for an event-driven vehicular access control strategy implementation. The current trend is that of an increasing number of vehicular communication sensors and onboard compute power to process the received big data [13]. The REF beamformer also has the potential to enhance passive cooperative collision warning [14] for reliable vehicular safety messaging via electro-vibro-acoustic emissions. This is utilised to achieve a highly reliable real-time collision avoidance system. Due to the steerable nature of the REF beamformer sensors array, different channel models, vehicular densities, transmission frequencies, and predictive handovers can be implemented concurrently [14]. Another potential application for the REF beamformer is in capability-based small satellite [19] data transmission. The REF beamformer has the capability to enable low computational burden by global navigation satellite system receivers [15]–[17] that require the implementation of low-complexity algorithms for on-demand real-time and sensor array signal processing. Given the size, weight and power limitations of small satellites, the REF technique would provide a cost-effective and low-power solution to onboard signal processing for high data link margins and space-borne smart earth observation applications. Furthermore, hidden parametric and non-parametric sound quality agreement can be reliably assessed using adaptive beamforming techniques. The experimental measurements and simulation models presented in this paper show that at even speed limits (including 20 mph and 40 mph), the corresponding SNR of the REF beamformer averages at 65 dB. This result shows an appreciable agreement with the acoustic noise response of electric powertrains modeled using the boundary element method [18] over the same operating frequencies at vehicular speed limits. Hence, this indicates a potential application for the multiphysics modeling of electric powertrains [19], [20]. The proposed REF technique for the sound enhancement and noise characterization of complex dynamic system uses fewer computational resources than the state-of-the-art beamformers. Hence, this promises a low-power, low-component footprint and cost-effective electro-acoustic system characterization.

VII. CONCLUSION

The regulated-element Frost beamformer is an adaptive algorithm that selectively enhances the desired signal based on the noise field conditions in a dynamic complex environment. This algorithm was utilized to investigate the effect of different vehicle speeds on an acoustic array gain in real-time. The dynamic system selectivity gains of the array based on the residual noise extraction technique revealed that the regulated-element Frost outperforms the conventional Frost beamformer by 3 dB. The broadside signal-to-noise ratio-based array gain for the regulated-element Frost beamformer is at least four times the value of the conventional Frost beamformer for each threshold frequency. The steering error-correcting capability of the algorithm makes it suitable for real-time recognition and enhancement of signals without a priori knowledge of their properties. The REF algorithm requires fewer finite impulse response filters (FIR) than the traditional adaptive beamforming techniques. Thus, the algorithm has a low complexity and converges faster than its competing methods.

Moreover, various electronic communication applications can be implemented with the presented adaptive beamformer (including advanced smart sensors signaling and internet of things networking; predictive collision warning; adaptive moving vehicle high-speed wireless handover; inter-vehicle trustworthiness estimation; efficient wireless power transfer; and reconfigurable inter-satellite data transmission).

REFERENCES

[1] I. Tashev, M. Seltzer, Y.-C. Ju, Y. Wang, and A. Acero, "Commute UX: Voice enabled in-car infotainment system," in *Proc. Mobile HCI*, 2009, pp. 1–7.

[2] S. Ekpo, B. Adebisi, A. Sabagh, and A. Wells, "Gain enhancement of acoustic beamforming arrays in complex dynamic systems," in *Proc. 30th Annu. Rev. Prog. Appl. Comput. Electromagn.*, Jacksonville, FL, USA, Mar. 2014, pp. 720–725.

[3] M. Omolgo, "Front-end processing of a distant-talking speech interface for control of an interactive TV system," *J. Acoust. Soc. Amer.*, vol. 123, no. 5, p. 3181, 2008.

[4] B. Adebisi, S. Ekpo, A. Sabagh, and A. Wells, "Acoustic noise characterisation in dynamic systems using an embedded measurement platform," in *Proc. 30th Annu. Rev. Progr. ACES*, Jacksonville, FL, USA, 2014, pp. 726–731.
[5] M. Strupl and P. Sovka, "Analysis and simulation of Frost's beamformer," *Radioengineering*, vol. 12, no. 2, pp. 1–9, 2003.
[6] S.-J. Chern and C.-Y. Sung, "The hybrid Frost's beamforming algorithm for multiple jammers suppression," *Signal Process.*, vol. 43, no. 2, pp. 113–127, 1995.
[7] B. Adebisi, S. C. Ekpo, A. Sabagh, and A. Wells, "Acoustic signal gain enhancement and speech recognition improvement in smartphones using the REF beamforming algorithm," in *Proc. 9th IEEE/IET Int. Symp. Commun. Syst., Netw. Digit. Signal Process.*, Manchester, U.K., Jul. 2014, pp. 472–477.
[8] S. Doclo and M. Moonen, "Superdirective beamforming robust against microphone mismatch," *IEEE Trans. Audio, Speech, Language Process.*, vol. 15, no. 2, pp. 617–631, Feb. 2007.
[9] J. Meyer and G. W. Elko, "Exploring spherical microphone arrays for room acoustic analysis," *J. Acoust. Soc. Amer.*, vol. 131, no. 4, p. 3208, 2012.
[10] Y. Sun, J. Zhang, and X. Yang, "Design of experimental adaptive beamforming system utilizing microphone array," in *Proc. IET Int. Radar Conf.*, Xi'an, China, Apr. 2013, pp. 1–5.
[11] H. Duan, B. P. Ng, C. M. S. See, and J. Fang, "Broadband beamforming using TDL-form IIR filters," *IEEE Trans. Signal Process.*, vol. 55, no. 3, pp. 990–1001, Mar. 2007.
[12] J. Benesty, J. Chen, and Y. A. Huang, "Study of the widely linear Wiener filter for noise reduction," in *Proc. IEEE Int. Conf. Acoust. Speech Signal Process. (ICASSP)*, Mar. 2010, pp. 205–208.
[13] R. Florin and S. Olariu, "A survey of vehicular communications for traffic signal optimization," *Veh. Commun.*, vol. 2, no. 2, pp. 70–79, 2015.
[14] N. Jaber, W. G. Cassidy, K. E. Tepe, and E. Abdel-Raheem, "Passive cooperative collision warning (PCCW) MAC designs for reliable vehicular safety messaging," *Veh. Commun.*, vol. 2, no. 2, pp. 95–109, 2015.
[15] S. C. Ekpo and D. George, "A system engineering analysis of highly adaptive small satellites," *IEEE Syst. J.*, vol. 7, no. 4, pp. 642–648, Dec. 2013.
[16] N. Linty and L. L. Presti, "Doppler frequency estimation in GNSS receivers based on double FFT," *IEEE Trans. Veh. Technol.*, vol. 65, no. 2, pp. 509–523, Feb. 2016.
[17] S. C. Ekpo and D. George, "Impact of noise figure on a satellite link performance," *IEEE Commun. Lett.*, vol. 15, no. 9, pp. 977–979, Sep. 2011.
[18] C. Ma, Q. Li, L. Deng, C. Chen, Q. Liu, and H. Gao, "A novel sound quality evaluation method of the diagnosis of abnormal noise in interior permanent-magnet synchronous motors for electric vehicles," *IEEE Trans. Ind. Electron.*, vol. 64, no. 5, pp. 3883–3891, May 2017.
[19] Y. Fang and T. Zhang, "Sound quality investigation and improvement of an electric powertrain for electric vehicles," *IEEE Trans. Ind. Electron.*, to be published, doi: 10.1109/TIE.2017.2736481.
[20] J. Le Besnerais *et al.*, "Multiphysics modeling: Electro-vibro-acoustics and heat transfer of PWM-fed induction machines," *IEEE Trans. Ind. Electron.*, vol. 57, no. 4, pp. 1279–1287, Apr. 2010.

SUNDAY C. EKPO (M'08) received the M.Sc. degree in communication engineering and the Ph.D. degree in electrical and electronic engineering from the University of Manchester, Manchester, U.K., in 2008 and 2011, respectively. He is currently a Lecturer in electrical and electronic engineering with the Manchester Metropolitan University, U.K. His specialty spans adaptive satellite system design, multiphysics characterization of RF and optical transceivers, multiobjective system engineering, intelligent sensors design, and Internet of Things implementations. He is a member of the IET, U.K., the AIAA, USA, and the Applied Computational Electromagnetics Society, USA and a fellow of the Higher Education Academy, U.K.

BAMIDELE ADEBISI (SM'06–M'09–SM'15) received the bachelor's degree in electrical engineering from Ahmadu Bello University, Zaria, Nigeria, in 1999, and the master's degree in advanced mobile communication engineering, and the Ph.D. degree in communication systems from Lancaster University, U.K., in 2003 and 2009, respectively. He was a Senior Research Associate with the School of Computing and Communication, Lancaster University, from 2005 to 2012. He joined Metropolitan University, Manchester, in 2012, where he is currently a Reader with Communication Systems and the Director of the EMS Research Centre. He is currently a Chartered Engineer, a member of the IET. He is particularly interested in research and development of communication technologies for electrical energy monitoring/management, transport, water, critical infrastructures protection, home automation, Internet of Things, and Cyber Physical Systems. He has several publications in the research area of data communications over power line networks and smart grid.

ANDREW WELLS received the master's degree in mobile communications and the Ph.D. degree in communications system and computer science from Lancaster University, U.K., in 2007 and 2010, respectively. In 2011, he joined the Advanced Electrical Research Department with Jaguar Land Rover (JLR) involved in several projects focusing on the development of future infotainment and vehicle connectivity. He joined the Electrical and Electronic Software Engineering Department, JLR and is currently the Technical Lead for JLRs cross carline next generation audio platform. He is particularly interested in the research and development of communications technologies for vehicle communications (V-X), Internet of Things, autonomous vehicles, and automotive security.

3.2.4 Paper 4 [SE4]

System Engineering Analysis of Highly Adaptive Small Satellites, *IEEE Systems Journal*, Vol. 7, No. 4, pp. 642–648, September 2013.

DOI: https://doi.org/10.1109/JSYST.2012.2198138.

Sunday Ekpo[1] and Danielle George[2]

[1]Department of Engineering, Manchester Metropolitan University, UK

[2]School of Electrical & Electronic Engineering, The University of Manchester, UK

This subsection is an exact copy of Paper 4.

642 IEEE SYSTEMS JOURNAL, VOL. 7, NO. 4, DECEMBER 2013

A System Engineering Analysis of Highly Adaptive Small Satellites

Sunday C. Ekpo, *Member, IEEE,* and Danielle George, *Member, IEEE*

***Abstract*—Spacecraft systems have undergone tremendous system-level transformations following advances in subsubsystems, subsystems, and systems designs and technologies. Furthermore, the ever expanding space applications and entrants necessitate a holistic review of current spacecraft system engineering (SE) margins. This paper seeks to examine contemporary space systems engineering procedures and develop a corresponding SE analysis tool for next-generation small satellites. Mass and power budgets are the considered SE margins. Case studies of highly adaptive small satellites (HASS) for a meteorology mission in low earth orbit are presented. HASS have demonstrated mass-, power-, and cost-savings with advanced capabilities than the conventional ones. The presented SE procedure can be extended to any spacecraft category and mission. As a capability-based SE analysis tool, it will enable the design and development of lightweight, reliable, adaptive, optimal, multifunctional, and economical satellites. This will enhance the provision of space systems that have postmission reapplications capability.**

***Index Terms*—Adaptive systems, satellites, system engineering (SE), system-level design.**

I. Introduction

THE INCREASE in the number of spacecraft launched each year has necessitated a reassessment of the system engineering (SE) margins, governing their design, production, and operation. Technical and environmental constraints have also prompted a review of existing SE procedures used for spacecraft programs. For instance, the majority of artificial and communication satellites are placed in the low earth orbit (LEO); this has an altitude span of 160–2000 km. As a nongeostationary orbit, LEO contains satellites that form a constellation to provide continuous coverage. They experience atmospheric drag (due to gases in the thermosphere) and harsh radiation environment. Cosmic rays and heavy charged particles streaming out from the sun in the solar wind react with gases in the upper atmosphere to produce high-energy neutrons. These neutrons impact the onboard semiconductor devices to produce unpredictable in-orbit failures. As a result of this, the space systems in LEO have potential replacement timeframe of 10 years. This translates into a huge investment cost that could be avoided through a judicious system-level reengineering. Furthermore, limited frequency spectrum and spatial capacity (orbital slots), high equipment costs, increased space debris, and expanding global broadband connectivity require adaptive, reconfigurable, and multifunctional space systems [1]–[6].

The development of the highly adaptive small satellite (HASS) seeks to overcome the enormous technological and operational challenges of space programs cost-effectively. A HASS is a reconfigurable, multifunctional, and deterministic small space satellite that has capabilities for dynamic space applications and operations while retaining its designed optimal performance [3]. Existing SE procedures are insufficient to give a complete analysis of this type of space system; hence, the need to review the existing SE with respect to the emerging satellite designs technology(s) and applications.

This paper is organized as follows. Section II explains the SE margins and project reviews that characterize the design of satellites. Small satellite categories covered span femtosatellites, picosatellites, nanosatellites, and microsatellites. The conventional payload-based mission-related power estimating relationships (PERs) and mass budgets are covered here. A discussion of developed mass-based PERs in LEO is also presented in this section. Adaptive technology implementation and the SE of a HASS system are stated in Section III. A case study of the SE of four categories of HASS for a meteorology mission is given in Section IV. The considered SE margins are mass and power budgets; the pertinent results and analysis are presented as well. Section V features the conclusion bordering on this paper.

II. SE of Spacecraft

System engineering of spacecraft involves the functional development of the detailed engineering tasks in a spacecraft design. It begins with the complete requirements that should characterize the satellite system together with the choice of key aspects that satisfy those requirements. In satellite SE, key performance parameters are tracked and assessed based on the observed system-level changes. Subsystem failures and/or issues revealed during final system integration are redressed by simulation/modeling. Vital technical adjustments are then carried out to ascertain the desired system-level functional margins. The overall procedure leans credence to the steps outlined in the SIMILAR process for SE by the International Council of Systems Engineering (INCOSE) [1].

The customer's requirement drives the choice of technology(s) to meet it. The major elements of the spacecraft SE

Manuscript received May 24, 2011; revised October 2, 2011 and January 8, 2012; accepted April 22, 2012. Date of publication May 30, 2012; date of current version September 25, 2013.

The authors are with the Department of Electrical and Electronic Engineering, University of Manchester, Manchester M60 1QD, U.K. (e-mail: cookey_sunday@ieee.org; danielle.george@manchester.ac.uk).

Digital Object Identifier 10.1109/JSYST.2012.2198138

1932-8184 © 2012 IEEE

TABLE I
SPACECRAFT SE PROCEDURE

Requirements definition
Resource budgeting
System-level trade studies
System integration
Operational margins
Post-mission reapplication assessment

TABLE II
SPACECRAFT PROJECT REVIEWS

Conceptual design review
Preliminary design review
Critical design review
Preshipment readiness review
Flight readiness review
Assembly, test, and launch operations
Mission operations
Completion of mission
Post-mission capability review

TABLE III
CORE BUS SUBSYSTEMS OF A SPACECRAFT

Structure
Propulsion
Power
Thermal control
Command and data handling
Attitude determination and control
Communication

procedure are given in Table I [1], [2]. This design routine implements the phases of a spacecraft system design. A reviewed spacecraft project has the lifecycle route shown in Table II [2]. These are the major formal customer reviews that must be conducted in the course of a mission development. Each phase of the SE entails a detailed review of the technological basements of the subsubsystems and subsystems that constitute the spacecraft system. Hence, the system-level SE follows the subsubsystem-level and subsystem-level SEs. In this paper, the two major spacecraft resources to be considered are power and mass. Detailed analyses of the mass and power properties of a spacecraft for the launch, cruise, and mission modes are vital for understanding its system reliability.

The spacecraft subsystems that will be analyzed are stated in Table III. The stated subsystems form the core bus functional module of a spacecraft. Each subsystem contains subsubsystems integrated on a common design and/or production platform.

A. Mass Budget Analysis

The development of a mass budget for a spacecraft requires the specification of the following: design phase, class of design, launch weight capability, and propellant mass required. These parameters are used to determine the on-orbit dry mass of a spacecraft and the corresponding mass margin. Mathematically, the spacecraft on-orbit dry mass is given by

$$M_{\mathrm{ODM}} = M_{\mathrm{LVC}} - M_{\mathrm{LVA}} - M_P \tag{1}$$

where M_{ODM} is the on-orbit dry mass (kg), M_{LVC} is the launch vehicle mass capability (kg), M_{LVA} is the launch vehicle adapter mass (kg), and M_P is the propellant mass (kg).

The launch vehicle adapter is a function of the launch vehicle mass. Based on the past spacecraft analysis, this is given by

$$M_{\mathrm{LVA}} = 0.076 M_{\mathrm{LVM}} + 50. \tag{2}$$

From the AIAA guidelines [2], the mass margin is given by

$$M_{\mathrm{margin}} = \frac{C_f M_{\mathrm{ODM}}}{1 + C_f} \tag{3}$$

where M_{margin} is the mass margin in kg and C_f, the mass contingency factor.

Equation (3) holds true if the payload is developed along with other core bus subsystems. In the event that the customer provides the payload subsystem, (3) becomes

$$M_{\mathrm{margin}} = \frac{C_f (M_{\mathrm{ODM}} - M_{\mathrm{pl}})}{(1 + C_f)} \tag{4}$$

where M_{pl} is the payload mass in kg. The corresponding core bus subsystems mass, M_{CBS}, in kg is thus

$$M_{\mathrm{CBS}} = \frac{M_{\mathrm{ODM}} - M_{\mathrm{pl}}}{1 + C_f}. \tag{5}$$

The next step in the spacecraft subsystem mass budget analysis is the mass allocation to the individual subsystems. This is calculated as a percentage of the total core bus subsystems mass as provided by the AIAA guidelines for the various spacecraft missions [2].

B. Power Budget Analysis

The next SE consideration in the design of a spacecraft is power requirement. Based on past missions, the total spacecraft power depends largely on the payload power requirement [1], [2]. This can be used during the conceptual SE analysis to estimate the initial spacecraft power budget. Moreover, in LEO, power–mass ratios (PMRs) of past missions have been reported [8]. This reveals that the total small satellite power can be modeled as a function of its mass. In this paper, total spacecraft PERs for a meteorology mission have been modeled as a function of mass and payload. This serves to enhance the SE analysis of small satellites in the congested and challenging LEO environment. Table IV states the small satellite categories investigated and reported in this paper.

Equations (6)–(9) show the PMRs or specific power of small satellites in LEO. The plots of the total spacecraft and maximum subsystem powers as functions of the small satellite mass are shown in Figs. 1–4. The figures are obtained based on a statistical analysis of past small satellites in LEO. The prevailing meteorology mission payload-based PER that satisfies Figs. 1–4 is given in (10) [2]

$$PMR_{\mathrm{MICRO}} = 10^{-5}\left(0.01M^4 - 4M^3\right) + 0.0035M^2 - 0.1475M + 3.6945 \tag{6}$$

TABLE IV
SMALL SPACECRAFT CATEGORIES

Satellite Category	Mass (kg)
Microsatellite	10–100
Nanosatellite	1–10
Picosatellites	0.1–1
Femtosatellites	0.01–0.1

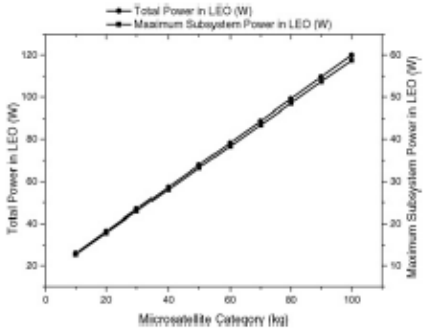

Fig. 1. Power profile of microsatellites in LEO.

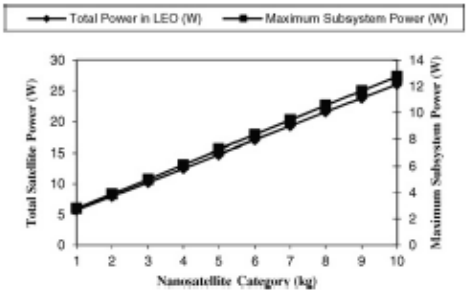

Fig. 2. Power profile of nanosatellites in LEO.

$$PMR_{\mathrm{NANO}} = 10^{-3}\left(3.2M^4 - 83.8M^3\right) + 0.8057M^2 - 3.4063M + 8.3292 \quad (7)$$

$$PMR_{\mathrm{PICO}} = 64.656M^4 171.33M^3 + 164.6M^2 - 69.525M + 17.367 \quad (8)$$

$$PMR_{\mathrm{FEMTO}} = 2 * 10^6 M^4 - 454\,115M^3 + 42\,683M^2 - 1750.2M^{40.309} \quad (9)$$

$$P_l = 1.96P_{\mathrm{pl}} \quad (10)$$

where PMR_{MICRO} is the PMR of microsatellites in LEO (W/kg), PMR_{NANO} is the PMR of nanosatellites in LEO (W/kg), PMR_{PICO} is the PMR of picosatellites in LEO (W/kg), PMR_{FEMTO} is the PMR of femtosatellites in LEO (W/kg), M is the small satellite mass (kg), P_l is the total payload-based spacecraft power (W), and P_{pl} is the payload power (W).

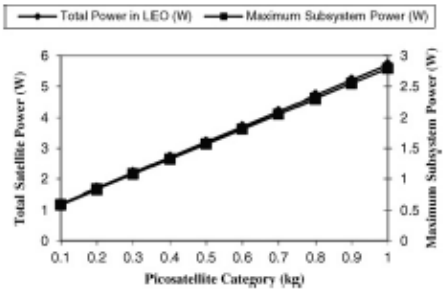

Fig. 3. Power profile of picosatellites in LEO.

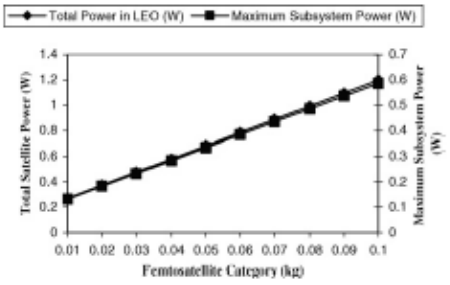

Fig. 4. Power profile of femtosatellites in LEO.

For the purpose of spacecraft SE analysis, the maximum payload power in LEO can be deduced from (6) to (9) for each category of small satellites.

The total in-orbit spacecraft power in watt, P_T, for a space mission is given by [1], [2]

$$P_T = P_{\mathrm{pl}} + P_{\mathrm{bus}} + P_{\mathrm{margin}} \quad (11)$$

where P_{margin} is the power margin or contingency in W and P_{bus}, the core bus subsystems power in W.

Based on a statistical analysis of past spacecraft [2], [7], (11) can be rewritten as follows:

$$P_T = 1.13M + 0.98P_{\mathrm{pl}} + C_f P_{\mathrm{bus}} + 1.72 \quad (12)$$

where C_f is the contingency factor based on the design stage and category.

Equation (12) represents a more generic power estimating function for carrying out a reliable analysis of modern spacecraft power budgets. The total in-orbit spacecraft power is expressed as a function of its payload power, PMR, core bus power, and power contingency factor. With (12), undue electrical power system redundancy and equipment oversizing can be avoided. In a typical HASS design and depending on the adaptive device technology utilized, (12) is modified and modeled to account for in-orbit dynamic system operations.

TABLE V
HASS POWER BUDGET ANALYSIS

HASS SE		
Analysis: power budget		
Mission: meteorology, P_t(W) = 1.96P_{pl} [2]		
Orbit: LEO, design phase: conceptual design		
Power contingency (C_f): 25% [2]		
Class of design: 2 (next-generation) [2]		
Satellite category: highly adaptive microsatellite (HAM) (20 kg)		
Core bus subsystem power allocation [2], [3], [8]		
Core Bus Subsystem	Allocation (%)	Power (W)
Thermal control	53	6.87
Attitude control	21	2.72
Electrical power	6	0.78
Command and data handling	15	1.94
Communications	5	0.65
Propulsion	0	0
Mechanics	0	0
In-Orbit Total Power Summary		
Parameter		Power (W)
Maximum available payload power in LEO		18.60
Required payload power		15.00
Maximum core bus power		17.85
Calculated core bus power		12.96
Power margin		3.24
Total required power		31.2
Power-savings		1.80
Max. power of a 20 kg microsat in LEO		36.45
Max. available core bus power in LEO		14.28
Max. available power margin in LEO		3.57
Satellite category: highly adaptive nanosatellite (HAN) (10 kg)		
Core bus subsystem power allocation		
Core Bus Subsystem	Allocation (%)	Power (W)
Thermal control	53	4.58
Attitude control	21	1.81
Electrical power	6	0.52
Command and data handling	15	1.30
Communications	5	0.43
Propulsion	0	0
Mechanics	0	0
In-Orbit Total Power Summary		
Parameter		Power (W)
Maximum available payload power in LEO		13.30
Required payload power		10.00
Maximum core bus power		12.74
Calculated core bus power		8.64
Power margin		2.16
Total required power		20.8
Power-savings		1.20
Max. power of a 10 kg nanosat in LEO		26.04
Max. available core bus power in LEO		13.3
Max. available power margin in LEO		2.55
Satellite category: highly adaptive picosatellite (HAP) (1 kg)		
Core bus subsystem power allocation		
Core Bus Subsystem	Allocation (%)	Power (W)
Thermal control	53	0.458
Attitude control	21	0.181
Electrical power	6	0.052
Command and data handling	15	0.130
Communications	5	0.043
Propulsion	0	0
Mechanics	0	0

TABLE V
(CONTINUED)

In-Orbit Total Power Summary		
Parameter		Power (W)
Maximum available payload power in LEO		2.910
Required payload power		1.000
Maximum core bus power		2.790
Calculated core bus power		0.864
Power margin		0.216
Total required power		2.080
Power-savings		0.120
Max. power of a 1 kg picosat in LEO		5.700
Max. available core bus power in LEO		2.230
Max. available power margin in LEO		0.560
Satellite category: highly adaptive femtosatellite (HAF) (0.1 kg)		
Core bus subsystem power allocation		
Core Bus Subsystem	Allocation (%)	Power (W)
Thermal control	53	0.311
Attitude control	21	0.123
Electrical power	6	0.035
Command and data handling	15	0.088
Communications	5	0.030
Propulsion	0	0
Mechanics	0	0
In-Orbit Total Power Summary		
Parameter		Power (W)
Maximum available payload power in LEO		0.611
Required payload power		0.500
Maximum core bus power		0.587
Calculated core bus power		0.432
Power margin		0.108
Total required power		1.04
Power-savings		0.06
Max. power of a 0.1 kg femtosat in LEO		1.198
Max. available core bus power in LEO		0.470
Max. available power margin in LEO		0.117

III. SE OF HIGHLY ADAPTIVE SMALL SATELLITES

A HASS is a reconfigurable, multifunctional and deterministic small space satellite that has capabilities for dynamic space applications and operations while retaining its designed robust and/or optimal performance [3], [4]. The HASS architecture is designed to eliminate wire harnesses and enable subsubsystem-, subsystem-, and system-levels adaptability and reconfiguration. As a complex system of systems (SoSs), the HASS exhibits the foundational attributes of SoSs [1]–[4]. Although it retains the conventional functional modules of conventional spacecraft, a HASS system is devoid of subsystem boundaries at the system level. Hence, it presents a unique platform for reliable and robust space mission applications and postmission reapplications.

A HASS employs the deterministic multifunctional architecture concept in its system design [3], [8]. Due to the elimination of wire harnesses and subsystem boundaries, a HASS system is a capability-based small satellite design that offers unprecedented application possibilities [3], [4], [8]. Consequently, the mass budgets of a HASS system decrease by about 3%, 8%, and 7% for communication, meteorology, and planetary missions, respectively [2]. Furthermore, there is

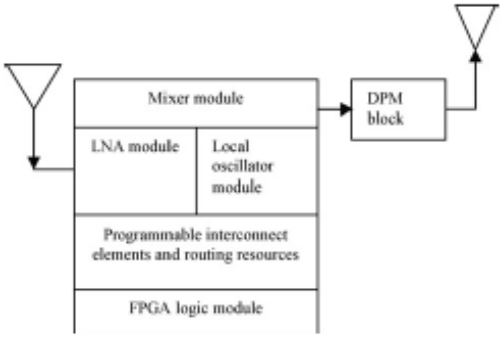

Fig. 5. AWT architecture.

about 15% reduction in the power budget of a HASS compared with a conventional small satellite [1]–[4], [7], [8]. A small satellites SE case study for a meteorology mission in LEO is presented in Section IV.

A typical HASS transponder architecture is shown in Fig. 5. The adaptive wideband transponder (AWT) subsubsystem is a component of the core bus module of the HASS system. Each unit of the AWT can be remotely accessed and deterministically reconfigured depending on the current and/or emergent mission requirements. The duplexer, power gain, and multiplexer interfaces the adaptive receiver and mixer units with the transmit antenna. In this novel design, interface bandwidth constraints, circuit parasitics, and coupling issues can be modeled with ease in realtime. The architecture of Fig. 5 is adaptive at the device, module, and system level; this supports remote in-orbit partial reconfiguration of the spacecraft.

IV. Case Study of a Meteorology Mission

Table V shows HASS SE for a meteorology mission in LEO. The core bus power of a HASS for a meteorology mission is reduced by 10% [1]–[4], [7], [8]. The governing equation for the analysis in Table V is (12). The categories considered include microsatellites, nanosatellites, picosatellites, and femtosatellites [1]–[14]. Conventional small satellites and HASSs are analyzed. The mass-savings and power-savings recorded with the HASS compared with the traditional small satellite systems make HASSs the obvious choice for future spacecraft missions. Assume that the payload equipment for each of microsatellites, nanosatellites, picosatellites, and femtosatellites requires 15 W, 10 W, 1 W, and 0.5 W, respectively, for the meteorology mission. The payload and core bus modules of the mission are developed together. Hence, the stated subsystem mass allocation margins must reflect lower percentages compared with a government-funded payload according to the AIAA guidelines. It is worth stating that the mass and power allocation percentages of the propulsion subsystem follow past spacecraft programs. In this paper, a miniaturized cold gas thruster system is considered for the mission. Low-power miniature cold gas thruster (MCGT) provides full attitude control capabilities in a package weighing only 50 g. MCGT is an innovative solenoid valve design requiring less than 0.4 W continuous operation power throughout its operational pressure and temperature ranges. For the case study meteorology mission using HAMs and HANs, this is accommodated in the attitude determination and control power and mass budgets.

A good SE analysis reveals the design margins that can be sustained in the event of system failure or reengineering. In the case study meteorology mission, each HASS system has inbuilt power and mass margins satisfied within the subsystems. Hence, mission assurance and reliability are further guaranteed through the judicious inclusion of a system-level margin. For instance, the HAN system payload requires 10 W, but its electrical power system can sustain up to 13.3 W. This is very useful for adaptive transponder subsystems that would perform dynamic mission requirements.

Table VI gives the mass budget analysis of HASS. Each HASS generation has a candidate mass category selected for the analysis; it can be extended to higher categories of spacecraft. The analysis reveals that mass-savings and consequently elimination of undue system oversizing can be realized through a careful SE treatment. Tables V and VI give the complete summaries of the budgets of two key resources of spacecraft. A careful study of the respective budgets helps in defining the problem as the first step in INCOSE's SIMILAR process [1]. Furthermore, the choice of solar panels for meeting current and emergent mission objectives would be greatly enhanced. The presented SE reveals the operational and business implications of the mission. Thus, the end users, technology platforms, and service delivery components are easily satisfied and qualified following a judicious SE analysis.

Moreover, and as a first approximation, the cost of a satellite is usually viewed as being directly related to its mass. Though heavier satellites cost more than their preceding generations, other factors have a direct impact on costs also. These include payload complexity, maturity of the design, lifecycles, premission and postmission objectives, and schedules [2], [9], [10], [13], [14]. Based on past space missions, a particular satellite cost estimating relationship comprises recurring and nonrecurring costs [10], [14]. Spacecraft has cost-per-unit weight of the order of $70 000/kg [14]. Though specific costs are insufficient for predicting the actual cost of spacecraft, HAM, HAN, HAP, and HAF have cost-savings of $89 600, $44 800, $4480, and $448, respectively, over their conventional counterparts [1], [2], [9], [10], [13], [14]. Furthermore, launch costs have obvious influence on a spacecraft's cost to initial operating capability and cost per operational day [10], [14]. For an LEO nanosatellite, the specific cost to orbit for both the United States and European launchers is about $10 000/kg [14]. As shown in Table VI, this results in appreciable cost-savings for all classes of HASSs compared with their conventional counterparts.

The allocation of a flat 5% mass and no power to the propulsion subsystem of the meteorology mission follows past historical database and is based on the AIAA guidelines [2]. This is also supported by current space technology breakthroughs in subsystem design and integration. Spacecraft propulsion functions span two major tasks: translational and rotational velocity changes. Small satellites propulsion options range

TABLE VI
HASS MASS BUDGET ANALYSIS

HASS SE		
Analysis: mass budget, mission: meteorology, orbit: LEO		
Design phase: conceptual design, mass contingency: 25% [2]		
Class of design: 2 (next-generation)		
Cabling mass factor, C_{mf}: 8% [2]		
Small satellite category: HAM		
Conventional on-orbit dry mass (kg): 20		
Subsystem mass reduction (kg) = 1.28		
Equivalent on-orbit dry mass of a HAM = 18.72		
Total subsystem mass for allocation (kg) = (18.72/1.25) = 14.976		
Subsystem Mass Allocation		
Subsystem	Allocation (%)	Allocated Mass (kg)
Structure	20	2.995
Thermal control	3	0.449
Attitude control	9	1.348
Power	16	2.396
Propulsion	5	0.749
Telecom	4	0.599
CDS	4	0.599
Payload	39	5.841
HAM Mass Allocation Summary		
Parameter		Value (kg)
Subsystem budget total		14.976
Mass margin		3.7440
Mass-savings		1.28
Maximum on-orbit dry mass		18.72
Launch cost-savings ($)		12800.00
Small satellite category: HAN		
Conventional on-orbit dry mass (kg): 10		
Subsystem mass reduction (kg) = 0.64		
Equivalent on-orbit dry mass of a HAN (kg) = 9.36		
Total subsystem mass for allocation (kg) = (9.36/1.25) = 7.488		
Subsystem Mass Allocation		
Subsystem	Allocation (%)	Allocated Mass (kg)
Structure	20	1.498
Thermal control	3	0.224
Attitude control	9	0.674
Power	16	1.198
Propulsion	5	0.374
Telecom	4	0.300
CDS	4	0.300
Payload	39	2.920
HAN Mass Allocation Summary		
Parameter		Value (kg)
Subsystem budget total		7.488
Mass margin		1.872
Mass-savings		0.640
Maximum on-orbit dry mass		9.360
Launch cost-savings ($)		6400.00
Small satellite category: HAP		
Conventional on-orbit dry mass (kg): 1		
Subsystem mass reduction (kg) = 0.064		
Equivalent on-orbit dry mass of a HAP (kg) = 0.936		
Total subsystem mass for allocation (kg) = 0.7488		

TABLE VI
(CONTINUED)

Subsystem Mass Allocation		
Subsystem	Allocation (%)	Allocated mass (kg)
Structure	20	0.1498
Thermal control	3	0.0224
Attitude control	9	0.0674
Power	16	0.1198
Propulsion	5	0.0374
Telecom	4	0.0300
CDS	4	0.0300
Payload	39	0.2920
HAP Mass Allocation Summary		
Parameter		Value (kg)
Subsystem budget total		0.7488
Mass margin		0.1872
Mass-savings		0.064
Maximum on-orbit dry mass		0.936
Launch cost-savings ($)		640.00
Small satellite category: HAF		
Conventional on-orbit dry mass (kg): 0.1		
Subsystem mass reduction (kg) = 0.0064		
Equivalent on-orbit dry mass of a HAM = 0.0936		
Total subsystem mass for allocation (kg) = 0.07488		
Subsystem Mass Allocation		
Subsystem	Allocation (%)	Allocated Mass (kg)
Structure	20	0.01498
Thermal control	3	0.00224
Attitude control	9	0.00674
Power	16	0.01198
Propulsion	5	0.00374
Telecom	4	0.00300
CDS	4	0.00300
Payload	39	0.02920
HAF Mass Allocation Summary		
Parameter		Value (kg)
Subsystem budget total		0.07488
Mass-savings		0.00640
Mass margin		0.01872
Maximum on-orbit dry mass		0.0936
Launch cost-savings ($)		64.00

from miniaturized thrusters based on traditional chemical engines to MEMS-based thruster systems. Moreover, the case study meteorology mission does not require many propulsive mission requirements. A 34 m/s velocity increment using micropropulsion is sufficient for the necessary manoeuvring and/or orbit changing. For a typical LEO mission, a 30 m/s ΔV would easily meet the propulsion requirements. An integrated 500 g, 9.1 cm^2 cold-gas micropropulsion subsystem has been developed by VACCO industries [7]. This has been fabricated for the MEMS-based picosatellite inspector program. Furthermore, a cold-gas thruster system has been developed for a 1 kg co-orbiting satellite assistant mission [7]. According to the rocket equation, this can accommodate the case study meteorology mission using HASS systems. The stated allocation margins are for the initial mass and power estimations during the conceptual design stage of the spacecraft development program. Where desired propulsive missions are required, the propulsion technology and associated mass and power margins would be modified to reflect the mission requirements.

Once the mass and power properties of a spacecraft are estimated, the functional modules are allocated their respective margins. At the conceptual design stage, Tables V and VI help the spacecraft system engineer to allocate resources to the various subsystems of its functional modules.

V. CONCLUSION

A SE analysis of HASS was presented in this paper. Appropriate power and mass estimating relationships were derived and explained for small satellite missions in LEO.

Mass and power-savings were recorded by implementing the HASS missions rather than the traditional small satellite

systems. Furthermore, appreciable cost-savings were realized for the initial specific and launch costs of HASS.

The derived PMRs are inversely proportional to the satellite mass in each category. In LEO, a 100 g femtosatellite has a PMR of 11.7 W/kg, while a 10 g femtosatellite has a PMR of 27 W/kg. Similarly, the heavier the satellite mass, the more the cost-savings, hence, the economies of scale.

The analysis can be applied to study any spacecraft mission with an established past history/database. The reported SE promises to enhance a holistic design and development of next-generation satellite missions and constellations in LEO. This paper can be extended to provide a ready spacecraft SE reference handbook for the space community.

REFERENCES

[1] B. R. Elbert, *Introduction to Satellite Communication*, 3rd ed. London, U.K.: Artech House, 2008, pp. 195–205, 389–393.

[2] C. Brown, *Elements of Spacecraft Design*. Reston, VA: AIAA, 2002, pp. 1–43.

[3] S. Ekpo and D. George, "A system-based design methodology and architecture for highly adaptive small satellites," in *Proc. 4th Annu. IEEE Int. Syst. Conf.*, Apr. 2010, pp. 516–519.

[4] S. Ekpo and D. George, "4–8 GHz LNA design for a highly adaptive small satellite transponder using InGaAs pHEMT technology," in *Proc. 11th IEEE Wirel. Microw. Conf.*, Apr. 2010, pp. 1–4.

[5] H. Schmitz, *Application Examples: How to Use FPGAs in Satellite Systems*. Mountain View, CA: Actel Corporation, 2010, pp. 1–7.

[6] *Radiation-Hardened FPGAs*, Ver. 3.1, Actel Corporation, Mountain View, CA, 2005.

[7] H. Helvajian and S. W. Janson, *Small Satellites: Past, Present, and Future*. Reston, VA: AIAA, 2008, pp. 559–569, 773.

[8] B. Jackson and K. Epstein, "A reconfigurable multifunctional architecture approach for next generation nanosatellite design," in *Proc. IEEE Aerospace Conf.*, vol. 7. Mar. 2000, pp. 185–188.

[9] R. Hassan and W. Crossley, "Spacecraft reliability-based design optimization under uncertainty including discrete variables," *J. Spacecraft Rockets*, vol. 45, pp. 394–405, Mar.–Apr. 2008.

[10] J. Saleh, "Flawed metrics: Satellite cost per transponder and cost per day," *IEEE Trans. Aerospace Electron. Syst.*, vol. 44, no. 1, pp. 147–156, Jan. 2008.

[11] H. M. Quinn, P. S. Graham, M. J. Wirthlin, B. Pratt, K. S. Morgan, M. P. Caffrey, and J. B. Krone, "A test methodology for determining space readiness of Xilinx SRAM-based FPGA devices and designs," *IEEE Trans. Instrum. Meas.*, vol. 58, no. 10, pp. 3380–3395, Oct. 2009.

[12] T. Vladimirova and C. Bridges, "Dual core system-on-a-chip design to support intersatellite communications," in *Proc. NASA/ESA Conf. Adaptive Hardw. Syst.*, 2008, pp. 191–197.

[13] D. Barnhart, T. Vladimirova, and M. Sweeting, "Very-small-satellite design for distributed space missions," *J. Spacecraft Rockets*, vol. 44, no. 6, pp. 244–257, Nov.–Dec. 2007.

[14] J. Saleh, D. Hastings, and D. Newman, "Spacecraft design lifetime," *J. Spacecraft Rockets*, vol. 39, no. 2, pp. 244–257, Mar.–Apr. 2002.

Sunday C. Ekpo (M'08) received the B.Eng. (hons.) degree in electrical and electronic engineering from the Federal University of Uyo, Uyo, Nigeria, in 2001, and the M.Sc. degree in communication engineering from the University of Manchester, Manchester, U.K., in 2008. He is currently pursuing the Ph.D. degree in electrical and electronic engineering with the Department of Electrical and Electronic Engineering, University of Manchester, with specialty in low noise amplifier design for satellite transponders, adaptive intelligent satellite constellations control, and highly adaptive small satellite design for space applications.

Mr. Ekpo is a member of the Institution of Engineering and Technology, the American Institute of Aeronautics and Astronautics, and the Society of Satellite Professionals International.

Danielle George (M'00) is currently a Senior Lecturer with the Department of Electrical and Electronic Engineering, University of Manchester, Manchester, U.K. She is the U.K. Lead Academic in the field of low-noise amplifier research and has worked on radio astronomy telescope projects, including the Square Kilometer Array and the EU-Funded FARADAY One Centimeter Radio 100-Beam Array Program. She was part of the technical team that developed the low-frequency instrument for the successfully launched PLANCK space telescope. Her research collaborations include Rolls Royce, European Space Agency, Indian Space Research Organization, and Chinese Academy of Sciences for Space Studies.

3.2.5 Paper 5 [SE5]

Reconfigurable Cooperative Intelligent Control Design for Space Missions, *Recent Patents on Space Technology*, Vol. 2, No. 1, pp. 2–11, April 2012.

DOI: https://doi.org/10.2174/1877611611202010002.

Sunday Ekpo[1] and Danielle George[2]

[1]Department of Engineering, Manchester Metropolitan University, UK

[2]School of Electrical & Electronic Engineering, The University of Manchester, UK

This subsection is an exact copy of Paper 5.

2 *Recent Patents on Space Technology, 2012, 2, 2-11*

Reconfigurable Cooperative Intelligent Control Design for Space Missions

Sunday C. Ekpo* and Danielle George

Microwave & Communications Systems Research Group, School of Electrical & Electronic Engineering, The University of Manchester, M60 1QD, UK

Received: 12 July 2011; Revised: 02 September 2011; Accepted: 18 October 2011

Abstract: Space satellite network design and operation have become more challenging following emerging advanced applications and the increased number of satellites launched into the Earth orbit each year. This has also occasioned an obvious concern for space situational awareness management, interplanetary communications, post-launch reengineering and post-mission reapplications of spacecraft; these all require adaptive, reconfigurable and multifunctional space systems and networks. Enormous advances aimed at making spacecraft systems reconfigurable, reliable, broadband, and multifunctional have been patented. Consequently, recent space technology patents in reconfigurable and autonomous system designs and architectures have been studied and qualified. This paper presents a reconfigurable space satellite network design that uses cooperative space-borne systems to complement ground-based enhancements. Each network node employs the deterministic multifunctional architecture with packet router interface switch matrix platforms. The reconfigurable cooperative intelligent control (RCIC) design exploits the deterministic and reconfigurable property of field programmable gate array to offer in-situ autonomous control. Four reliable and adaptive space control capability modes have been identified for a robust space satellite network. Furthermore, the control capability has been analysed with recourse to satellite generations. Consequently, a case study reconfigurable space network covering femtosatellites to minisatellites has been designed. The analysis presented in this work promises to enhance small satellite formation and constellations designs and applications. It also enables real-time space surveillance and provides platforms for the reuse of decommissioned satellite systems.

Keywords: Formation flying, highly adaptive small satellite, intelligent control, space mission.

1. INTRODUCTION

The last decade has witnessed an unprecedented increase in the number of satellites deployed in multiple planes and orbits. These satellite systems have been made possible through the advancements in monolithic microwave integrated circuits, microtechnology, nanotechnology and allied atomic-scale technologies. As the wireless technologies evolve, the computing and processing resources correspondingly revolutionise the in-orbit control of geosynchronous and non-geosynchronous satellite missions. These technologies mix enables the design, development and production of small satellite that, amongst other benefits, are economical with greater intelligence transmission capabilities. Over 42 % of the current space satellites fall below the 500 Kg mass. This unceasing and ever-expanding drive for small satellites is occasioned by the advances in micro-technology, nanotechnology/microelectronics, microwave monolithic integrated circuit and allied technologies. Hence, almost every nation can now feel the space. However, a key issue is the design of the control mode of the constellations to enhance security and reliability. Fig. (1) shows the global space budget from years 2005 to 2009 and Fig. (2), the commercial satellites and launch demand from 2009 to 2018. The earth orbit is currently crowded with objects including fragmentation debris, spacecraft, mission-related objects and rocket bodies [1-20].

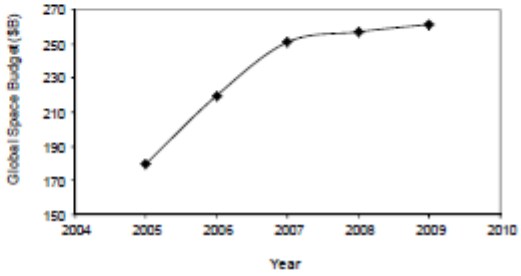

Fig. (1). International space budget growth.

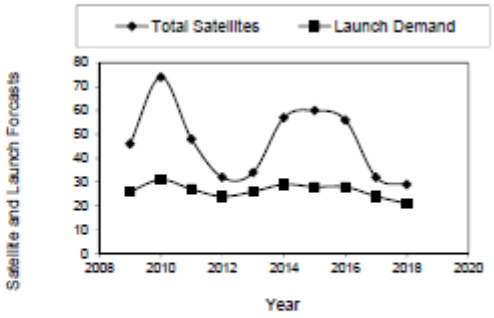

Fig. (2). Commercial space satellite and launch forecasts.

*Address correspondence to this author at the 79 Beresford Street, Manchester, M14 4RZ, UK; Tel: 4479 5047 8245;
E-mails: Sunday.Ekpo@postgrad.manchester.ac.uk,
Danielle.George@manchester.ac.uk

1877-6116/12 $100.00+.00

© 2012 Bentham Science Publishers

Table 1. Number of Objects in Earth Orbit from Years 2004 to 2010

Object Type	Number of Objects in Earth Orbit in Years 2004, 2006, 2008 and 2010			
	2004	2006	2008	2010
Fragmentation Debris	3990	4000	7000	8500
Spacecraft	2900	2950	3100	3250
Mission-related objects	1540	1550	1600	1650
Rocket bodies	1500	1530	1550	1600

The obvious conclusion from Figs. (**1**, **2**) is that the global space activity is gathering an unprecedented momentum with attendant technical and operational challenges. Table **1** reveals the steady increase in the yearly number of objects in earth orbit from years 2004 to 2010 [7].

This paper presents a reconfigurable design model that integrates the different emerging satellite generations (SatGens) and technologies together to achieve robust, ad-hoc, adaptive and proactive intersatellite connectivity and surveillance. It is organized as follows. Section II reviews the satellite generations, intelligent mode configurations and the enabling technologies and implementation challenges necessitating a new design approach. The adaptive reconfigurable multifunctional architecture (ARMA) network for sustaining and operating the adaptive multifunctional structural units (AMSUs) of HASSs is explained here. Section III presents the developed reconfigurable intelligent control modes for distributed small satellites formation flying and constellations. The satellite category- and network-based control capability factors (CCFs) of each chosen case study satellite generation are also given in this section. The RCIC network design and analysis are reported in section IV. Section V concludes the findings of this paper and the benefits of the reported emerging satellite network control for future space missions. The current and future developments are also featured here.

2. SPACECRAFT MISSIONS AND TECHNOLOGIES FOR RECONFIGURABLE COOPERATIVE INTELLIGENT CONTROL DESIGN

Each year, for the past 20 years, satellites, probes, capsules, space shuttle missions and international space station (ISS) assembly hardware across the globe are computed to ascertain the future space payloads and operations. This yearly Worldwide Mission Model (WMM) forecasts the payload market the next decade ahead. It has been found that a steady growth of space payloads would be the case for the next 20 years. The WMM for 2011 reveals that 2,315 spacecraft payloads and piggyback satellite payloads have been documented for the period 2011 to 2030 based on announcement and/or proposed missions [4]; these span all categories of satellites and deployed across various orbits. This represents a 4% increase over the 2010 WMM result. The majority of the launches would probably come from the increased global focus on small satellites developments. For instance, a total of 351 and 397 payloads have been proposed for manufacturing and launching in 2011 and 2012 respectively. The LEO will house additional 246 payloads to be launched in 2011; 268 more payloads will be deployed in LEO in 2012. Commercial payloads take the largest chunk of the total proposed space programmes for the next 20 years; it accounts for 38% while the civil, military and others account for 35%, 20% and 7% respectively. By orbital deployment, the low Earth orbit (LEO) accounts for 63%, geostationary orbit (GEO), 23%, medium Earth orbit (MEO), 8%, deep space, 5% and elliptical orbit, 1%. This suggests that the mobile communication satellites will dominate the space activities in LEO for commercial purposes including fresh launching and replenishment satellites (currently underway for launch in the next 4 to 5 years) programmes; this application has dominated the LEO space programmes in the last two decades. The Globalstar, Iridium and Orbcomm are the three major constellations currently occupying this orbit. Furthermore, the LEO orbit is known for cosmic radiation effects and impacts on semiconductor subsubsystems. Going by the WWM report, it is now the most targeted orbit for satellite missions spanning commercial, civil, military, science and planetary applications. These activities suggest increasing and congested orbital operations that will pose obvious operational and environmental challenges. Hence, the need for a satellite communication network that offers adaptability, multifunctionality and reliability at the hardware and software levels. The end result is the ever-expanding and enlarging demand for space situational awareness and optimal, reliable, and economical management of space resources. This has orchestrated the development of the RCIC to address issues bordering on inter- and intra-mission reengineering, post-mission reapplication and post-launch and emergent mission(s) capabilities [4].

Though enabling space technologies have greatly advanced the design, development, deployment, operation and servicing of space systems, the attendant reliability, flexibility, deterministic performance realization, cost-effectiveness and post-mission reapplication have continued to reveal the need for appreciable/optimal margins attainment. This has prompted the design and development of the highly adaptive small satellites (HASSs) for dynamic, sustainable and reliable space programmes and operations [2, 3]. Based on satellite classification by mass, the various satellite generations that can benefit from the RCIC concept are shown in Table **2** [1].

The design of the RCIC model for space missions starts with the space elements that constitute the network infrastructure. The HASS system architecture is made up of building blocks that contain adaptive and reconfigurable multifunctional subsubsystems and subsystems. These span data processing, communications, power control,

attitude/navigation, payload and associated spacecraft equipment. Implementing and deploying adaptive multifunctional structural unit-based space systems in an adaptive reconfigurable multifunctional architecture network helps to increase network reliability and performance [2, 3, 17, 20-27].

Table 2. Satellite Classifications by Mass

Satellite Category	Mass (kg)
Large satellite	> 1000
Medium satellite	500-1000
Minisatellite (minisat)	100-500
Microsatellite (microsat)	10-100
Nanosatellite (nanosat)	1-10
Picosatellite (picosat)	0.1-1
Femtosatellite (femtosat)	<0.1

Gate-level adaptive and reconfigurable computing devices (such as FPGAs) can be coupled with high interconnection bandwidth, radio frequency (RF)/microwave and microtechnology devices with relatively high data transfer bandwidths and minimal wiring to provide dynamic, reliable and sustainable mission operations. Furthermore, AMSUs characterise the ARMA network of space communications; this can connect other spacecraft devices to implement the RCIC capability function. These computing and input/output devices include, but not limited to, analog/digital converters, digital/analog converters, RF transceivers and distribution system and sensor/transducer interfaces. Moreover, the internet, compute nodes and wired network, wireless network, bus and human interfaces are also supported.

The ARMA system may use embedded serial I/O devices such as embedded multi-gigabit serial transceiver (MGT) to maintain the input/output (I/O) connections of multiple FPGAs. Consequently, a duplex data communication link is maintained between a MGT of a packet router interface switch matrix (PRISM) of a FPGA and another MGT of a PRISM of another FPGA. This is deployed in a manner that decreases on-card I/O counts and large numbers of termination components. To boost the data routing capability of the ARMA, the various FPGAs and other computing devices implement packet routing either on a single AMSU or across AMSUs through one or more switch fabrics such as crossbar switches. This has the advantage of minimising switch-constrained packet transfer latency times while maintaining a dynamic node-to-node access within and between spacecraft. The presented adaptive architecture enables emergent independent or loosely-coupled processes in parallel [2, 3, 9, 10, 13, 25-32].

An adaptive multifunctional structural unit design for a HASS system is shown in Fig. (**3**). It is an adaptive form of the architecture of the integrated circuit package system for stackable devices [22]. The surface and inter- and intra-substrates components are reprogrammable. It is made up of a base substrate, a lower interposer substrate (LIS), an upper interposer substrate (UIS), interposer connectors (programmable interconnects and routing resources), surface conductors, stack connectors, dice or chips and external devices. Each chip has active surface areas. These are connected to the exposed conductors of the lower and upper interposer substrates *via* stack connectors. The exposed conductors are located on the lower inward and upper inward surfaces of the LIS and UIS respectively. The chips form clusters of adaptive, active solid-state fast input/output and microcontroller subsubsystems. The embedded electronic subsystem and FPGA module are integrated on the same substrate as the analog RF/microwave subsystem. This solution greatly enhances system-level real-time response with almost zero latency and dedicated data bandwidth availability [2, 3, 22, 23]. With this architecture, interface bandwidth constraints are obviated.

Fig. (**3**) only shows a 2-D AMSU unit. Solar absorptance and emittance are influenced by the surface material and orbital parameters of the spacecraft. Depending on whether active or passive thermal control subsystem architecture is used, Fig. (**4**) addresses this in the system-level integration of subsubsystems and subsystems. Each AMSU is designed in such a way that heat sources are intrinsically identified and heat transfer occurs between all satellite components. Consequently, heat rejection is achieved dynamically so that different spacecraft components stay within their operating temperature margins.

Fig. (**4**) shows an adaptive multifunctional structural units implementation onboard a HASS system. It is made up of various AMSU blocks integrated together to form a deterministic multifunctional architecture that has an inherent dynamic redundancy. Furthermore, different device technologies can be supported by the proposed RCIC underlying system hardware architecture.

The top deck of Fig. (**4**) allows for satellite separation from the launch vehicle and provides a mounting surface for multibeam/multiband antennas, cameras and solar arrays.

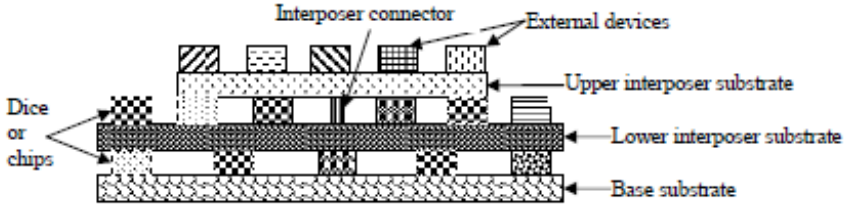

Fig. (3). Adaptive multifunctional structural unit design for a HASS system.

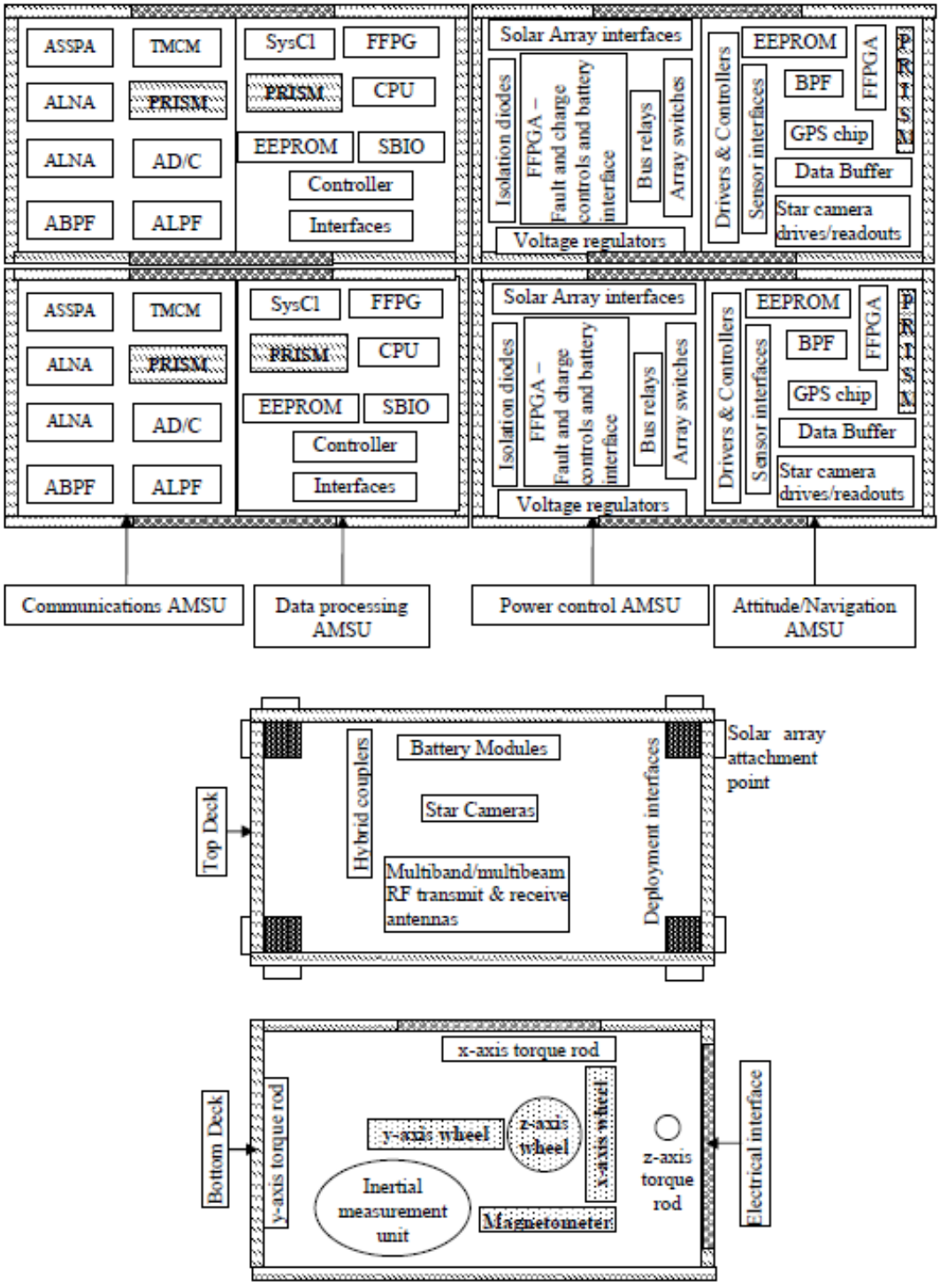

Fig. (4). Adaptive multifunctional structural units implementation onboard a HASS system.

This design incorporates the battery modules on the top deck to eliminate undue power generation loss between the solar arrays and the battery bank. A further advantage of this is that the moment of inertia of the satellite system can be uniformly distributed/balanced between the top deck components and the bulkier discrete components mounted on the bottom deck (torque rods, reaction wheels, magnetometer). The power control AMSU implements solar array string isolation, string switching, voltage regulation, battery interface and charge control, fault control and power bus distribution. The attitude/navigation AMSU processes the input from various attitude sensors to determine the satellite's attitude. Raw global positioning system (GPS) data from an onboard GPS chip subsubsystem are used to adaptively compute the position of the satellite; this can also be done post-pass on the ground. Command processing, telemetry conditioning and multiplexing, timing, emergency mode control, data storage and processing are performed within the data processing AMSU. The communications AMSU contains adaptive transponder multichip module, solid-state power amplifier, packet router interface switch matrix device for high bandwidth duplex data transfer and adaptive RF/microwave components.

The benefits of the AMSU implementation onboard a HASS system includes, but not limited to, the elimination of black boxes, bulky wire harnesses and connectors, increased system-level reliability, fast design reengineering, streamlined subsystem integration and test process and cost-effective mass production. The associated savings include, but not limited to, satellite mass, power and cost [2, 19, 17-21, 28].

3. RECONFIGURABLE COOPERATIVE INTELLIGENT CONTROL MODES AND PROTOCOLS

Some intelligent control modes have been identified for a small satellite formation flying (SSFF) regime of a satellite generation. The mode configurations are master-slave, cooperative and single satellite failure [5]. The advancements and progressive complexity of the space and terrestrial distributed and networked platforms require a more proactive, reactive and adaptive control scenario [1-5]. Field programmable gates arrays (FPGAs) and agent-based systems have revolutionised control systems and large scale computing respectively [7-13]. These are employed to realise a resilient and secure cross-SatGen control algorithms/modes for real-time intelligent detection and surveillance.

From the foregoing analysis, several kinds of geosynchronous and non-geosynchronous orbits satellite RCIC modes have been realised. These are depicted in Table **3**. A, B, C, D, and E are the minisats, microsats, nanosats, picosats and femtosats respectively to be controlled. While enhanced control capabilities are possible with preceding satellite generations, the attendant benefits of data and signal acquisition and processing and surveillance platforms they provide the succeeding generations are incredible.

The RCIC capability function for small satellites is developed based on the satellite generation and mass category [1]. Mathematically, this is given by:

$$CF_{HASS} \propto \frac{\sum_{i\in n}^{n} M_i}{\sum_{i\in N}^{N} M_i} \quad (1)$$

where M_i is the combined in-orbit mass of the controlling spacecraft; n, the number of controlling spacecraft; M_i, the total in-orbit mass of the controlled spacecraft; N, the total number of controlled spacecraft (including the n number of controlling spacecraft).

Table 3. RCIC Modes

Small Satellite Category	Control Capability
Minisat: A	A, B, C, D & E
Microsat: B	B, C, D & E
Nanosat: C	C, D & E
Picosat: D	D, E
Femtosat: E	E

The reconfigurable cooperative intelligent control (RCIC) design model exploits the deterministic and reconfigurable property of FPGA to offer insitu autonomous control. The more the satellites to control, the larger the FPGA size required [10]. Hence, instead of changing a SSFF generation, a candidate from a higher generation, say, microsat is chosen to offer a quasi-cooperative mode intelligent control to, say, a nanosats constellation. This quasi-master-slaves configuration becomes possible because the FPGA size of the microsat is larger and so can handle more on-board data processing tasks. Furthermore, the microsat runs Agent systems to offer proactive and reactive responses to the constellation environment and assigned tasks. The corresponding ground stations run Agent-based systems and multicore FPGAs to cope with the large scale computing tasks downlinked from space in real-time. This RCIC model based on cross-SatGen control enhances advanced application of inverse synthetic aperture radar for a real-time insitu space surveillance. Hence, the microsat in our example can cooperatively probe as many space objects as possible and relay to an earth station while intelligibly steering the endangered nanosat(s) away from the danger and/or disaster.

A case study of one number of each satellite category is presented in this paper. Fig. (**5**) shows the small satellite control capability factor computation as a function of its mass. It is obvious from the plot that satellites greater than 100 Kg can reliably control lower generation satellites with about 80% success without recourse to the groundstation support. This is called network-based control capability. On the other hand, the category-based control capability factor (CCF) plot reveals that controlling only satellites within and below a given satellite generation yields higher CCFs for fewer nodes (Fig. **5**). The ability to maintain an in-orbit autonomous operation and management of space systems is enabled by the advanced emerging signal processing and transponder technologies onboard the satellite system [11].

A combination of satellite generations for robust and reliable control scenarios can be realised within a constellation design. This is particularly important for distributed small satellite missions where the satellites are expected to operate within a controlled range and cooperatively work together to perform the mission such as space-based sensor networks and earth observation [20].

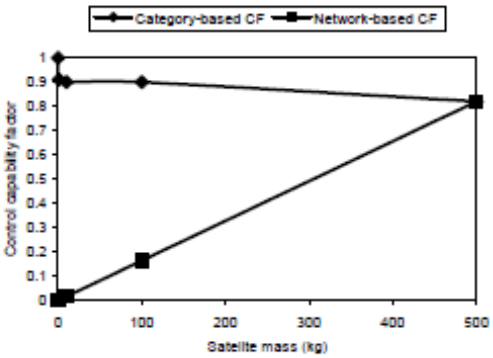

Fig. (5). Small satellite mass versus control capability factor.

A key aspect of the proposed RCIC for highly adaptive small satellites is spacecraft connectivity. The metrics for assessment beacons on network communication link reliability, availability, quality of service (QoS) and cost-benefits. A number of network protocols have been developed and proposed for interplanetary communications which support autonomic operation and reconfiguration [32]. These include, but not limited to, the Bundled Protocol, Licklider Transmission Protocol (LTP) and Context-Aware Broker (CAB). These advanced protocol suites seek to enable swarms of networked components achieve scientific feats "on-the-fly" within constrained networks without recourse to ground resources. For instance, the CAB aims at enabling adaptive signal transmission at the basest cost without compromising the QoS level expected for the environment-constrained application. It has been proposed for Delay Tolerant Networks (DTNs) characterising deep-space communications systems. The CAB implementation transfers spacecraft mission-control on Earth to the spacecraft thereby enhancing operational efficiency, eliminating long round-trip latencies and optimising network lifetimes. This suits well with the RCIC network where the hardware platform is adaptive, multifunctional and reconfigurable [32].

The increase in the number of payloads that can be deployed with reduced costs has been orchestrated by the concept of "hosted hardware." This concept refers to the use of a parent spacecraft "host" platform to enable the "hosted payload" have access to space. The hosted payload may be a collection of sensors, transponder modules, waveguide or a small satellite. The two major ways of realising this objective are integrating the payload into the parent satellite or integrating the payload onto the parent satellite. In the former, the payload hardware is "significantly-integrated or installed" during the manufacturing of the parent spacecraft. The hosted units are mounted extrinsically on the internal equipment panels of the primary (or parent) spacecraft. This requires redesigning the parent spacecraft subsystems to accommodate the unique features and capabilities of the hosted hardware. For non-HASS systems, the hosted flight hardware must be available in time for the assembly and test of the primary spacecraft and the non-recurring costs are high due to the spacecraft reengineering which must be done. Furthermore, the hosted hardware is constrained to fly on the parent satellite; this utilises the parent satellite bus resources including power, thermal control and orbital maintenance. Onboard HASS systems, this integration approach can be implemented by adaptive subsubsystem-, subsystem- and system-levels reconfigurations and without undue non-recurring expenses. The system engineering analysis of a HASS takes emergent mission and post-launch capabilities/requirements into consideration. The technique of mounting a secondary payload onto the primary spacecraft allows for little non-recurring work and costs; the hosted hardware (e.g., a small satellite) can arrive later in the mission development and reconfiguration/integration is easier. A hosted payload can also be interchanged or deactivated for another rapidly and easily. The HASS system also supports this approach. The RCIC design accommodates the piggyback satellite payload system in that spacecraft with multiple payload adapters (MPAs) can use existing unused launch vehicles to deploy several small satellites from a parent satellite [25-33].

4. RECONFIGURABLE COOPERATIVE INTELLIGENT CONTROL NETWORK DESIGN

The RCIC network is used to sustain highly adaptive small satellites constellations. Each network node and/or interface implements the adaptive reconfigurable architecture (ARMA) and run the CAB algorithm at the transport layer of its protocol stack.

Fig. (**6**) shows a reconfigurable cooperative intelligent control network hierarchy design for the various small satellite generations. It is evident from the design that as the satellite mass increases (with a corresponding increasing control capability), the number of satellites per generation decreases. Though this has an obvious recourse to the cost implication and volume production and launch, the processing power and capabilities of space satellites generally scale directly with their in-orbit weight. Hence, to achieve a previous satellite generation control capabilities, more swarms of the current generation would be required. This lends credence to and justifies the support for distributed formation flying small satellites and constellations being the current focused research area. Each of the satellites represented in Fig. (**6**) implements the adaptive reconfigurable multifunctional architecture onboard it.

The presence of hybrid FPGA and packet router interface switch matrix enables each HASS system to maintain a deterministic and seamless communication link with the rest of the satellite network nodes. The preceding satellite generation deploys more adaptive components and computing devices than the succeeding one. This enables each HASS system to dynamically access every other satellite and/or groundstation within and beyond the adaptive reconfigurable multifunctional architecture network in real-time.

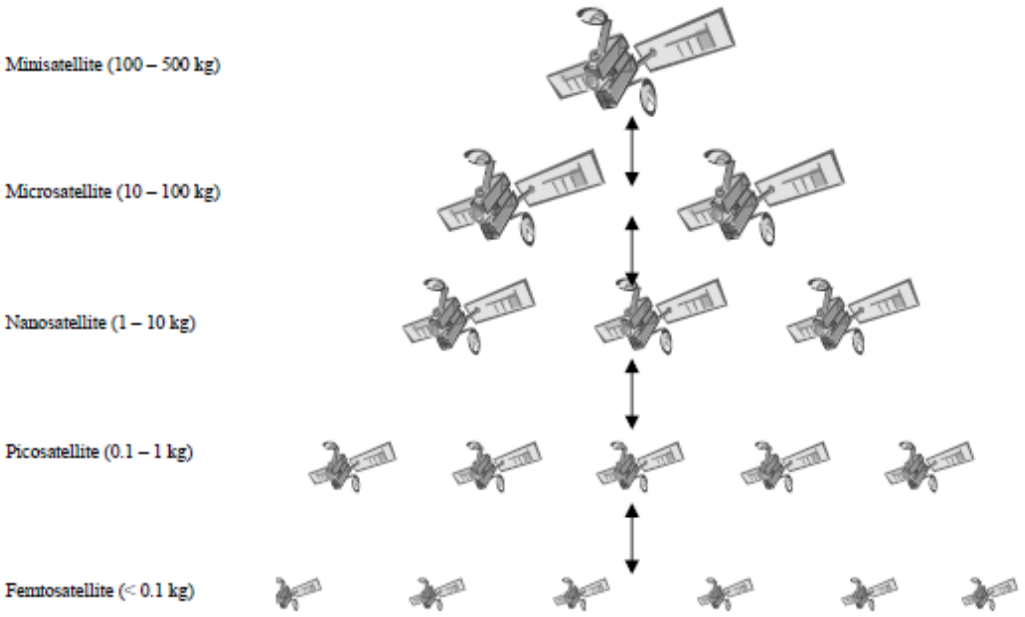

Fig. (6). Satellite generations and control capabilities.

The presented RCIC network optimises network utility by ensuring that the local constraints on the mission, node operation definition, protocol and transmission configurations and system-level multifunctional adaptability occur autonomically using resources onboard the spacecraft. This minimises failure risks and improve recovery/response time to emergent mission requirements and conditions. Consequently, the expense associated with remote mission management is substantially reduced.

The RCIC network establishes and maintains a RF link with a groundstation for relaying communication, engineering and scientific data. Fig. (**7**) shows a typical data and signal distribution and communication network for a RCIC application. The four RCIC control regimes can realise several intelligent control states. For instance, Fig. (**7**) shows five satellites launched into space thus: LEO orbit (nanosat, picosat and femtosat), MEO (microsat) and GEO (minisat). A higher generation satellite within an orbit maintains network attribute information for the satellites within its orbit and those in lower orbit(s). For instance, the GEO satellite can initiate data collection regarding the environment (propagation delay between satellites), network (link health and bandwidth availability) and application (required bit error rate and latency) for the satellites in MEO and LEO.

The minisatellite can act as the parent satellite for up to six nanosatellites (piggyback satellite payloads) using standardised MPAs. Each femtosatellite can then be deployed in their respect orbits at different times or at once. Furthermore, the minisatellite can offer post-deployment services such as data storage, processing and transmission for the secondary satellite payloads.

The nanosat maintains a reconfigurable cooperative intelligent control mode with the picosat and femtosat. Signals and data from the picosat and femtosat are processed onboard the nanosat and transmitted to and from the groundstation. Though the picosat and femtosat can receive direct engineering data from the groundstation, their scientific and control data are processed and managed onboard the higher-capacity nanosat [11]. Due to the deterministic architecture that characterises the nanosat system, adaptive and reconfigurable capabilities incomparable with the groundstation response can be reliably and cost-effectively realised. The groundstation maintains an interruptible RF link with the nanosat. In event of a loss in connectivity by and failure of the nanosat, the microsat can be elected to serve a master-slaves mode with the LEO orbit satellites. The adaptive architecture of the nanosat enhances the ability of the microsat to retrieve data from the nanosat to continue the RCIC operation.

The pass information for the modelled satellites-ComSat, ComSat2, ComSat3, ComSat4 and ComSat5-were studied and qualified based on the orbital constraints set. Fig. (**8**) shows the modelled communication satellites using the satellite tool kit (STK) software. Four communication satellites placed in circular orbits above 500 km were considered for the RCIC case study. The communication network (Fig. **8**) links were designed to ensure that each satellite maintained an uninterruptible communication with its neighbour(s) and/or a groundstation. Furthermore, the terrestrial facilities were strategically positioned to remain

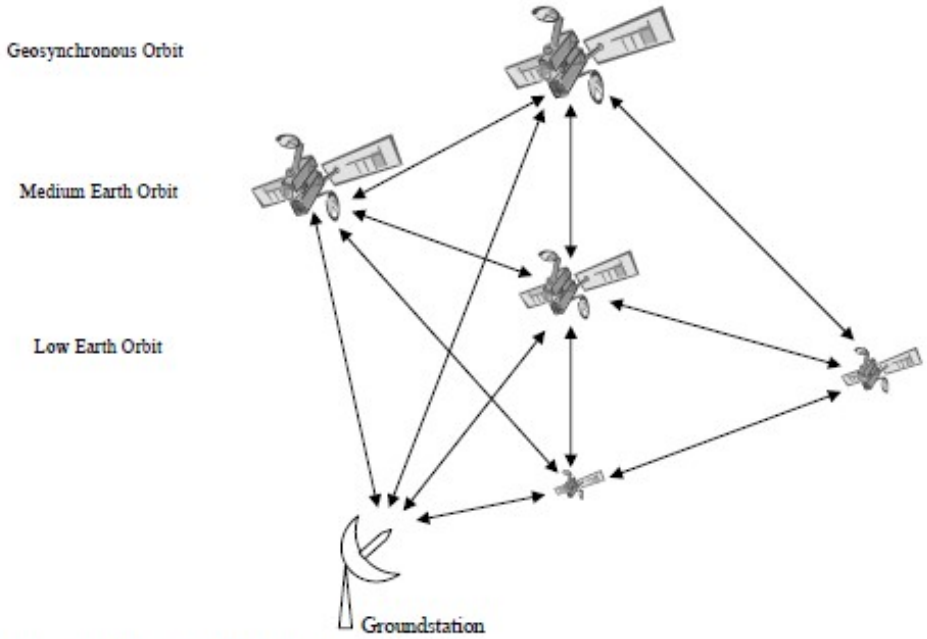

Fig. (7). RCIC signal and data communication network.

within the footprints of the satellites for adaptive and reconfigurable operations. The longitude, latitude and altitude assignments ensured 100% connectivity and lighting. The radial, in-track and cross-track (RIC) coordinates of the modelled communication satellites were modelled to ensure each satellite maintains a footprint with its neighbour and/or the groundstation. With the RCIC network configuration, the health and availability of each node can be remotely and adaptively monitored in real-time by the parent satellite for the constellation.

The RCIC network nodes maintain proactive intersatellite connectivity and surveillance information

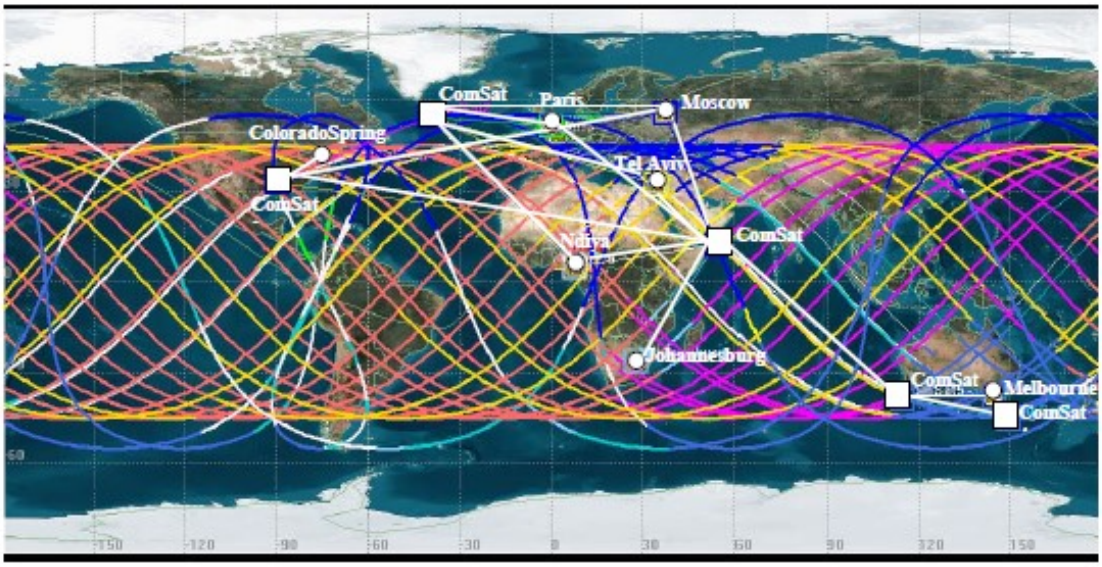

Fig. (8). STK modelling of the RCIC communication network.

through the cooperative intelligent algorithms deployed onboard each system and updated by each neighbouring satellite. Since each satellite bears the AMSU architecture, data and/or information concerning the network state and situational awareness can be shared without undue processing and storage overheads. For instance, if a single node gets the network surveillance data, this is shared amongst the neighbouring satellites pending when a network change occurs or new update is received. Engineering and scientific data can be received, processed, stored and retrieved within the network without any recourse to the ground facility(s). Intersatellite communication links data are also maintained in turn be each node. For instance, given a 24-hour operation involving 8 formation flying satellites, each can be assigned a 6-hour surveillance period with 3 hours per node for dynamic redundancy using two satellites at a time. In this case, each satellite shares network information with its neighbour and can offer in-orbit cooperative achievement of mission's objective. Table 4 describes a typical proactive intersatellite pairing that can be realised within the RCIC network.

Table 4. Satellite Assignment for Proactive Surveillance within a RCIC Network

Surveillance Time (Hours)	Satellite Number	
	Main Controller	Backup
3	1	2
3	2	1
3	3	4
3	4	3
3	5	6
3	6	5
3	7	8
3	8	7

The presented RCIC design has a great potential for integrating technologies for multifunctional operations and applications. For instance, consider adapting each HASS system to operate in both radar and communications modes. The block circuitry of Fig. (**9**) shows an adaptive transponder system that has an active electronically scanned array (AESA) radar capability. The presented communication/ radar subsystem is a transmit/receive module that can be replicated and/populated as a monolithic microwave integrated circuit (MMIC) or multichip module (MCM) and stacked together within the AMSU architecture. The end result is the adaptive realisation of in-orbit multifunctional applications reconfiguration. The FFPGA logic module interfaces with an appropriate beamforming signal circuitry. Each of the adaptive transponder subsystem units can be accessed remotely *via* the programmable interconnect elements and routing interface. Variable gain amplifier and variable phase shifting networks are implemented on the same substrate layer as the FFPGA. The high power amplifier (HPA) serves to generate the right pulse level. The circulator restricts an incoming reflected signal from a target (during a radar mode) from raveling down the HPA path. During a communications mode, the transponder system relays a received signal/data to another spacecraft and/or groundstation after performing an appropriate signal processing (including duplexing, amplification and multiplexing into the relevant channels). The possible communications/radar band designations include L- (1-2 GHz), S- (2-4 GHz), C- (4-8GHz), X- (8-12.4 GHz) Ku- (12.4-18 GHz) and K- (18-27 GHz) bands. The implementable applications include space-based radar, synthetic aperture radar (SAR) and long-range surveillance (LRS) (L-band); airborne-weather radar (AWR) and air surveillance/tracking (S-band); SAR, AS, WR (C-band); LRS and AWR (X); atmospheric research, small-range surveillance and space debris detection (Ku/K).

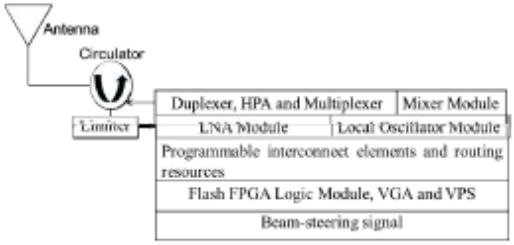

Fig. (9). An adaptive transponder subsystem with an AESA radar capability.

5. CURRENT AND FUTURE DEVELOPMENTS

A new network control concept has been presented in this paper. It is called reconfigurable cooperative intelligent control. The reported analysis shows that the network control capability factor for minisat is about 0.8, microsat, 0.2 and Nanosat, 0.02. Picosat and femtosat have network capability control factors less than 0.01. The category-based control capability factors are higher for each satellite generation with the femtosats recording about 99%. Hence, the design of distributed small satellite formation flying and constellation requires an inclusion of a higher generation satellite(s), at least a nanosat, for a robust and reliable space-based network in-orbit autonomous control. Furthermore, four reconfigurable cooperative intelligent control regimes have been identified. These regimes are classified based on the satellite generation and category and leverages on the higher adaptive technology capacity of higher satellite generations. The network can autonomously adjust and adapt itself to respond to environmental and mission changes that may ensue following a launch.

Reconfigurable network control protocols such as Context-Aware Broker algorithm has been studied and found to be suitable for implementation onboard a highly adaptive small satellite. The HASS system houses a hardware architecture that offers adaptability, reliability and multifunctionality for achieving optimal quality of service and signal transmission. Issues bordering with interface bandwidth and parasitics constraints are addressed through an intelligent design of the RCIC hardwares.

The benefits of the reported findings are fast network node response, reliable and available line-of-sight

communication link, improved signal integrity, reduced network control overhead, adaptive surveillance, reliable and robust in-orbit distributed small satellite formation flying and constellation missions, ease of mission operations and economical space segment maintenance amongst others.

The next stage in this work involves integrating the Context-Aware Broker algorithm with the deterministic multifunctional architecture concept to assess the cost-benefits that would result following possible trade-offs and operational scenarios. This will be extended to cover failure-free seamless communication infrastructure analysis for the network protocols that would be the candidate for optimally operating highly adaptive small satellite missions. Post-mission models will also be studied and qualified for various orbits, applications and environmental constraints. The core functionalities of CAB-reliability and sustainability optimisation-will be tested in a reconfigurable cooperative intelligent control network where spacecraft systems employing the adaptive multifunctional structural units are deployed.

REFERENCES

[1] C. Brown, Elements of Spacecraft Design. Virginia: AIAA, Inc. 2002, pp. 1-43.

[2] S. Ekpo, and D. George, "A System-based Design Methodology and Architecture for Highly Adaptive Small Satellites," in *Proceedings of the 4th Annual IEEE International Systems Conference*. San Diego CA, USA, April 2010, pp. 516-519.

[3] S. Ekpo, and D. George, "4-8 GHz LNA Design for a Highly Adaptive Small Satellite Transponder using InGaAs pHEMT Technology," in *Proceedings of the 11th IEEE Wireless & Microwave Conference*. Melbourne FL, USA, April 2010, pp. 1-4.

[4] M. Caceres, "Mission Model Offers Snapshot of Space Payloads," *Aerospace Magazine*, AIAA, pp. 24-27, June 2011.

[5] L. Bin, Y. Zheng, Z. Chenguang, Z. Xiaomin, "Design and Experiment on Small Satellite Formation Flying Simulation Platform," in *Proceedings of the IEEE Aerospace Conference*, 2005.

[6] D. Barnhart, T. Vladimirova, and M. Sweeting, "Very-Small-Satellite Design for Distributed Space Missions," *Journal of Spacecraft and Rockets*, vol. 44, pp. 244-257, November-December 2007.

[7] J. L. Valero, "Space Situational Awareness at the European Union Satellite Centre," in *Proceedings of the Near Space Security Conference*, Amsterdam, March 2010.

[8] P. Mario, "*Study of a Cube-Sat Mission*," M.S. Thesis, Karl Franzens University of Graz, Graz, Austria, Spring 2005.

[9] Actel Corporation, "Radiation-Hardened FPGAs," Ver. 3.1, 2005. Available from www.actel.com (Accessed: Jan.18, 2010).

[10] National Instruments, "Introduction to FPGA Technology: Top Five Benefits," *National Instruments conference and exhibition*, London, United Kingdom, 2009.

[11] M. Wittig, "Satellite Onboard Processing for Multimedia Applications," *IEEE Communications Magazine*, pp. 135, 2000.

[12] T. Vladimirova, and C. Bridges, "Dual Core System-on-a-Chip Design to Support Intersatellite Communications," in *Proceedings of the NASA/ESA Conference on Adaptive Hardware and Systems*, 2008.

[13] H. Schmitz, "Application Examples: How to Use FPGAs in Satellite Systems," *Actel Corporation, California*, 2010.

[14] S. Ekpo, and D. George, "Mm-wave LNAs Design for Adaptive Small Satellite Applications," in *Proceedings of the Joint ESA Workshop on Millimetre Wave and 31st ESA Antenna Workshop*, Noordwijk, Netherlands, May 2009, pp. 843-837.

[15] L. Xuwen, L. Li, L. Huawang, C. Yinjian, S. Dexin, and Y. Genqing, "Silicon Solid-state Small Satellite Design Based on IC and MEMS," in *Proceedings* of the *Solid-State and Integrated Circuit Technology*, 1998, pp. 932-935.

[16] S. R. Cvetkovic, and G. J. Robertson, "Spacecraft Design Considerations for Small Satellite Remote Sensing," *IEEE Trans. on Aerospace and Electronic Systems*, vol. 23, pp. 391-403, 1993.

[17] R. Hassan, and W. Crossley, "Spacecraft Reliability-Based Design Optimization under Uncertainty Including Discrete Variables," *Journal of Spacecraft and Rockets*, vol. 45, pp. 394-405, March-April 2008.

[18] J. Saleh, "Flawed metrics: Satellite Cost per Transponder and Cost per Day," *IEEE Trans. on Aerospace and Electronic System*, vol. 44, 147-56, 2008.

[19] D. Barnhart, T. Vladimirova, and M. Sweeting, "Satellite Miniaturization Techniques for Space Sensor Networks," *Journal of Spacecraft and Rockets*, vol. 46, pp. 469-472, March-April 2009.

[20] B. Jackson, and K. Epstein, "A Reconfigurable Multifunctional Architecture Approach for Next Generation Nanosatellite Design," in *Proceedings of the IEEE Aerospace Conference*, 2000.

[21] T. James, and D. Shah, "*Transponder Tuning and Mapping*," U.S. 7950038, May 2011.

[22] D. Moon, and S. Song, "*Integrated Circuit Package System for Stackable Devices*," U.S. 7919871, April 2011.

[23] J. Yancey, and Y. Kuo, "*Reconfigurable Communications Infrastructure for ASIC Networks*," U.S. 7921323, April 2011.

[24] Z. Camacho, J. Caparas, and A. Trasporto, "*Integrated Circuit Packaging System with Circuitry Stacking and Method of Manufacture Thereof*," U.S. 7919360, April 2011.

[25] L. Tay, H. Bathan, and Z. Camacho, "*Integrated Circuit Package with Improved Connections*," U.S. 7911040, March 2011.

[26] C. De Lair, C. Owan, J. Sowers, D. Budisalich, M. Castor, and M. Francis, "Lightweight Deployment System and Method," U.S. 7908973, March 2011.

[27] P. Karabinis, and R. Singh, "*Integrated or Autonomous System and Method of Satellite-Terrestrial Frequency Reuse using Signal Attenuation and/or Blockage, Dynamic Assignment of Frequencies and/or Hysteresis*," U.S. 7907893, March 2011.

[28] S. Rao, and D. Bressler, "*Multibeam and Multiband Antenna System for Communication Satellites*," U.S. 7868840, January 2011.

[29] A. Wang, "*System and Method for Continuous Broadcast Service from Non-geostationary Orbits*," U.S. 7877089, January 2011.

[30] B. Benedict, "*Satellite Payload Arrangement, a Device for and Method of attaching a Piggyback Satellite Payload and Adapter to be used for a Payload Arrangement for launching the Piggyback Satellite*," U.S 7,866,607, January 2011.

[31] F. Panzani, and K. Pierre, "*Satellite Telecommunication System*," U.S. 7835733, November 2010.

[32] C. Peoples, G. Parr, B. Scotney, A. Moore, "Autonomic Context-Aware Management in Interplanetary Communications Systems," *IEEE Aerospace and Electronic Systems Magazine*, vol. 26, pp. 26-33, 2011.

[33] J. Saleh, D. Hastings, and D. Newman, "Spacecraft Design Lifetime," *Journal of Spacecraft and Rockets*, vol. 39, pp. 244-257. March-April 2002.

3.2.6 Paper 6 [SE6]

Impact of Noise Figure on a Satellite Link Performance, *IEEE Communications Letters*, Vol. 15, No. 9, pp. 977–979, June 2011.

DOI: https://doi.org/10.1109/LCOMM.2011.11.111073.

Sunday Ekpo[1] and Danielle George[2]

[1]Department of Engineering, Manchester Metropolitan University, UK

[2]School of Electrical & Electronic Engineering, The University of Manchester, UK

This subsection is an exact copy of Paper.

IEEE COMMUNICATIONS LETTERS, VOL. 15, NO. 9, SEPTEMBER 2011

Impact of Noise Figure on a Satellite Link Performance

Sunday C. Ekpo, *Member, IEEE*, and Danielle George, *Member, IEEE*

Abstract—**Small satellite link performance analysis is critical for assessing the adequacy of a transmitter to successfully transfer data at the desired rate. This is especially obvious when considering highly adaptive small satellite systems that exhibit static and active/dynamic power requirements. This paper presents the impact of noise figure on the carrier and data links performances of a highly adaptive small satellite application. The noise figures of a MMIC LNA, designed using GaAs technology operating within the C- and X-bands, were used to study the link performance of a planetary mission. An existing Magellan spacecraft link performance was considered in this study. The analysis reveals that designing a broadband LNA to have a ripple of less than 0.1 dB within its operating bandwidth is essential for a less than 2 dB drop in the carrier and data links margins. This fixes a 6.8 K receiver noise temperature swing margin for reliable, dynamic, broadband and adaptive space operations.**

Index Terms—**Carrier, data, highly adaptive small satellite, link performance, noise figure, satellite application.**

I. Introduction

THE need for a reliable, stable, dynamic and robust satellite link has numerous side effects including larger and heavier satellites. This extra satellite weight and size in turn shoots the overhead cost of the satellite procurement program. A link design is inevitable for ascertaining that the operational transmitted power is sufficient to successfully relay information at the desired data rate. Existing satellite links performances are qualified after a judicious and systematic analysis of subsubsystem-, subsystem- and system-levels gains and losses. The result of this evaluation reveals the transmitted power required for a given symbol rate, range and losses. For a small space satellite, power is at a premium. This is occasioned by the stringent requirement of radio frequency (RF) power generation and amplification amongst other factors. There is therefore a need for achieving an adaptive satellite link performance that meets the mission and post-mission objectives through a careful and objective selection of satellite system parameters.

Implementing a satellite design architecture that incorporates an adaptive low noise amplifier(s) (LNA) reveals huge economies of scale whilst enabling the achievement of a stable, reliable, dynamic, robust and optimal satellite link performance. Receiver noise temperature (RNT) and frequency of operation are amongst the critical parameters that a link designer must give due attention for possible post-launch changing mission requirements and post-mission reapplications. Antenna gain, line losses and noise figure of the front-end receivers LNA are the factors that determine the receiver noise temperature. Moreover, the degradation of solar arrays and associated electronics and reliability/redundancy issues decrease the satellite link performance [1, 2]. This paper will explore the various components of the satellite link performance indices as they affect the desired link margins. Second, the receiver front-end architecture of a highly adaptive small satellite (HASS) system will be presented. The impact of the noise figure and broadband operation on the carrier and data links performances is investigated. Furthermore, a case study of a space planetary mission is presented and the issues bordering on the satellite link performance discussed.

Manuscript received May 20, 2011. The associate editor coordinating the review of this letter and approving it for publication was C. Sacchi.

The authors are with the School of Electrical & Electronic Engineering, The University of Manchester, Manchester, M60 1QD United Kingdom (e-mail: Sunday.Ekpo@postgrad.manchester.ac.uk, Danielle.George@manchester.ac.uk).

Digital Object Identifier 10.1109/LCOMM.2011.072011.111073

II. Space Satellite Communication Links

Carrier link margin (CLM) and data link margin (DLM) are the two major satellite links margins that characterise the uplink and downlink performances of spacecraft communication. A CLM refers to the difference between the carrier signal-to-noise power achieved and the carrier signal-to-noise power required by a satellite network link. A DLM defines the difference between the data signal-to-noise power achieved to the data signal-to-noise power required by a satellite network link. The evaluation of these links in turn reveals the link margins available for a safe and reliable transmission of intelligence between the space and terrestrial communication networks. A link design involves the development of a comprehensive budget based on the subsubsystem, subsystem and system parameters that characterise a given satellite communication network. A typical satellite communication link table states the data rate, maximum bit error rate, frequency, modulation and coding, symbol rate, transmitter, antenna gains, system gains and losses and receiver noise for achieving a given spacecraft mission's required link margin [1]. The next section contains the architecture of the receiver front-end of a HASS system.

III. The Receiver Front-End of a HASS System

The concept of highly adaptive small satellites (HASS) [2, 3] for space applications promises boundless applications for all frontiers of the space world [1–4]. A HASS is a reconfigurable, multifunctional and deterministic small space satellite that has capabilities for dynamic space applications and operations while retaining its designed optimal performance [2, 3]. It is envisaged as the key to realizing reliable and optimal structural and functional reconfigurations for cost-effective small satellites [1–8]. Traditional small satellites design concepts with reconfigurable platforms lack the subsystem adaptability. Hence, the HASS architecture exploits this shortcoming of conventional small satellites design approaches

1089-7798/11$25.00 © 2011 IEEE

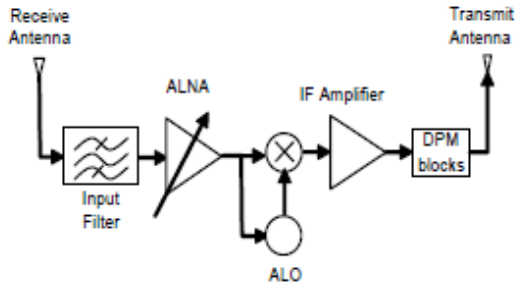

Fig. 1. An adaptive small satellite transponder.

by utilizing the functional design concept to adaptively reconfigure its subsystems. In this way, a new mission requirement can be realized even after a HASS system might have been launched for a different mission. The system noise temperature of a space satellite receiver consists of the effective antenna noise temperature, the effective cable noise temperature and the effective receiver noise temperature. Mathematically, this is given in (1) by: [1, 2]

$$T_s = \frac{T_a}{L_c} + T_t\left(\frac{L_c - 1}{L_c}\right) + T_o(F - 1) \quad (1)$$

where,
T_s = effective system noise temperature, K
T_a = effective antenna temperature including all external noise, K
T_t = thermodynamic temperature of the cable, K
T_o = standard reference temperature, 290 K
L_c = input cable loss factor
F = noise figure for the receiver defined at the terminal as a linear ratio

The adaptive transponder of the HASS system carries an adaptive wideband receiver that sits between the receive antenna and the input demultiplexer [2]. For a 500 MHz bandwidth, 20 MHz guard band and centre frequencies covering the entire C-band, a total of 120 transponder channels (TCs) are available [2]. Hence, 24 TCs per C-band frequency for either a downlink or an uplink transmission can be realized. An adaptive mapping of the 24 TCs partitions them into uplink and downlink transmission frequencies; the uplink uses the higher frequency range for each adaptively assigned C-band frequency. Fig. 1 shows an adaptive small satellite transponder system. The complete equipment channel consists of receive antenna, input filter (bandpass), adaptive low noise amplifier (ALNA), adaptive local oscillator (ALO), intermediate frequency (IF) amplifier, DPM (demultiplexer, power gain and multiplexer) blocks and transmit antenna [2]. The adaptive low noise amplifier (ALNA) can be adaptively reconfigured to yield a link margin of interest at the corresponding frequency. A portion of its signal is sent to the adaptive local oscillator to generate a corresponding constant oscillator frequency for the mixer network. In-orbit partial reconfiguration is possible [2].

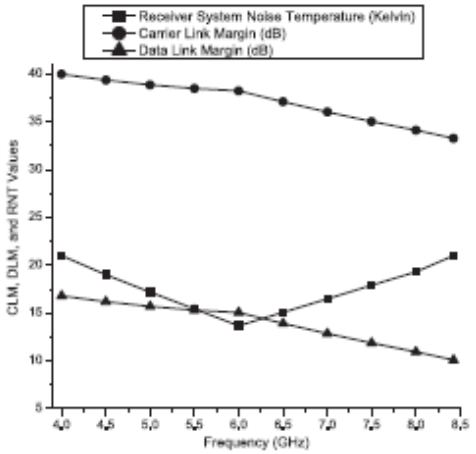

Fig. 2. Link margins and noise temperatures versus operating frequencies.

IV. Case Study and Applications

The case study done involved an analysis of the high-rate downlink table for the Magellan spacecraft launched for a planetary mission [1]. The link equation of a satellite network is given in (2) by:

$$E_b/N_o = P_t + \sum G - \sum L + 228.6 - 10\log T_s - 10\log R_s \quad (2)$$

where
E_b/N_o = signal-to-noise ratio, dB
P_t = power input to transmitting antenna, dB
G = gains of the receiving and transmitting antennas, dB
L = path and cable losses, dB
T_s = effective system noise temperature, K
R_s = symbol rate, symbol/second or sps

A HASS architecture is designed to eliminate interface bandwidth issues and wire harnesses [3, 6, 8]. From (1), this results in a negligible cable noise contribution. Similarly, the waveguide loss in (2) would be approximated by the free space path loss. With Ts and L greatly reduced, Eb/No improves. Hence, a HASS can easily achieve Shannon's requirement for an error-free communication in realtime [1, 5]. Furthermore, a HASS has an ALNA onboard it. Consequently, (1) and (2) reveal that it can remotely improve its in-orbit Ts and hence CLMs and DLMs for an exceptionally low bit error rate [1]. Equation (2) shows that a HASS can verify a link margin by varying its onboard subsubsystems parameters while in orbit. The carrier and data links margins of the Magellan spacecraft were studied and qualified based on link design parameters used for the actual satellite system. The findings are shown in Figs. 2 and 3. At a given receiver system noise temperature, the carrier and data links margins decrease with increase in the operating frequency. Switching from 8 to 8. 2459 GHz (at 13.67 K) resulted in an average of 0.5 dB loss in both the CLM and DLM of the Magellan spacecraft (Figs. 2 and 3).

Furthermore, the change in the receiver noise temperature at a given frequency was found to exert a considerable influence

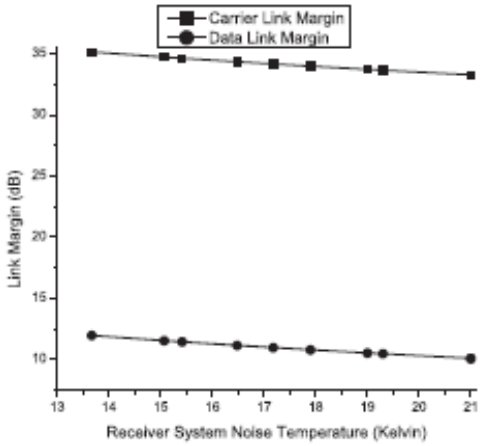

Fig. 3. Link margins versus noise temperatures at 8.4259 GHz.

on the carrier and data links performances of the spacecraft under study (Fig. 3). The link design analysis yielded an average of 1.9 dB loss in the CLM and DLM for a noise figure increase of 0.1 dB over the operating bandwidth. This finding has interesting benefits including the use of adaptive LNAs to remotely adjust the link performance of space-based systems employing the deterministic multifunctional architecture concept [3]. Non-HASS systems (current state-of-the art spacecraft) lack in-orbit adaptability and exhibit loss of data and information due to an electronic component failure onboard the satellite [1, 4–10]. These occur often where the satellite experiences cosmic rays (from outside the solar system) and charged particles (streaming out from the Sun in the solar wind) and the onboard components are not radiation-tolerant [7].

V. Conclusion

This paper has presented a case study of the impact of noise figure swing on a satellite link performance. Carrier and data links of a Magellan planetary spacecraft were considered. The link margins of each link operating from 4 to 8.2459 GHz were analyzed. The overall downlink result shows a 0.5 dB loss in both the carrier and data links margins of the case study spacecraft when hopping from 8 to 8.2459 GHz. The study further unraveled a 1.9 dB loss in both the carrier and data links margins when the receiver noise figure changes by 0.1 dB. This report reveals the need for adopting the highly adaptive small satellite system architecture in future small satellite programs. It can also be extended to larger satellites tailored for specific space missions. The end result is the realization of reliable, high performance and economical small satellites for sustainable space missions and operations.

References

[1] C. Brown, *Elements of Spacecraft Design*, pp. 1–43. AIAA, Inc., 2002.

[2] S. Ekpo and D. George, "4—8 GHz LNA design for a highly adaptive small satellite transponder using InGaAs pHEMT technology," in *Proc. 11th IEEE Wireless & Microwave Conference*, 2010, pp. 1–4.

[3] S. Ekpo and D. George, "System-based design methodology and architecture for highly adaptive small satellites," in *Proc. 4th Annual IEEE International Systems Conference*, 2010, pp. 516–519.

[4] L. Castillo, et al, "Flexible electronic assemblies for space applications," *IEEE Aerospace and Electronic Systems Mag.*, vol. 25, no. 6, pp. 25–29, June 2010.

[5] M. Wittig, "Satellite onboard processing for multimedia applications," *IEEE Commun. Mag.*, pp. 135, June 2000.

[6] T. Vladimirova and C. Bridges, "Dual core system-on-a-chip design to support intersatellite communications," in *Proc. NASA/ESA Conference on Adaptive Hardware and Systems*, 2008, pp. 191–195.

[7] H. Schmitz, "Application examples: how to use FPGAs in satellite systems," Actel Corporation, CA, 2010, pp. 1–7.

[8] B. Jackson and K. Epstein, "Reconfigurable multifunctional architecture approach for next generation nanosatellite design," in *Proc. IEEE Aerospace Conference*, 2000, vol. 7, pp. 185–188.

[9] J. Saleh, D. Hastings, and D. Newman, "Spacecraft design lifetime," *J. Spacecraft and Rockets*, vol. 39, no. 2, pp. 244–257, Mar.-Apr. 2002.

[10] D. Barnhart, T. Vladimirova, and M. Sweeting, "Very-small-satellite design for distributed space missions," *J. Spacecraft and Rockets*, vol. 44, no. 6, pp. 1294–1304, Nov.-Dec. 2007.

3.2.7 Paper 7 [SE7]

Multicriteria Optimisation Design of SPSE for Adaptive LEO Satellites Missions Using the PSI Method, *AIAA Space 2013 Conference & Exposition*, San Diego CA, USA, 10–12 September 2013, pp. 1–19.

DOI: http://arc.aiaa.org/doi/pdf/10.2514/6.2013-5470.

Sunday Ekpo[1], Danielle George[2] and Bamidele Adebisi[1]
[1]Department of Engineering, Manchester Metropolitan University, UK
[2]School of Electrical & Electronic Engineering, The University of Manchester, UK

This subsection is an exact copy of Paper 7.

AIAA SPACE 2013 Conference and Exposition
September 10-12, 2013, San Diego, CA

AIAA 2013-5470

A Multicriteria Optimisation Design of SPSE for Adaptive LEO Satellites Missions Using the PSI Method

Sunday C. Ekpo[1]
Manchester Metropolitan University, Manchester, Greater Manchester, M1 5GD, United Kingdom

Danielle George[2]
The University of Manchester, Manchester, Greater Manchester, M60 1QD, United Kingdom

and

Bamidele Adebisi[3]
Manchester Metropolitan University, Manchester, Greater Manchester, M1 5GD, United Kingdom

Downloaded by Sunday Ekpo on September 18, 2013 | http://arc.aiaa.org | DOI: 10.2514/6.2013-5470

The spacecraft power system engineering (SPSE) analysis for the radiation-prone space environment is a major critical satellite engineering definition for realising successful mission and post-mission capabilities. The dynamic operations and post-mission applications of capability-based small satellites require an adaptive architecture(s) which exhibits an enormous conceptual system engineering design task in terms of the trade space – which can be too large to explore, study, analyse and qualify – for a reliable and sustainable mission. This paper involves a multicriteria optimisation design of the SPSE subsystems for adaptive LEO satellites missions using the parameter space investigation (PSI) method. A three-axis stabilised 10-kg nanosatellite is considered for a meteorological spacecraft (METSAT) mission at 800 km altitude. The initial case study SE parameters considered include the required payload power and spacecraft power and mass contingencies. The PSI method allows for a large-scale multicriteria optimisation of dynamic engineering systems. This was implemented in the multicriteria optimisation and vector investigation (MOVI) software. Specific power profiles for LEO satellites were used for the mathematical modelling of the highly adaptive nanosatellite (HAN) system in LEO. In the multicriteria optimisation process, 2765 design vectors entered the test table out of which 2762 formed the feasible solutions set. The PSI was conservatively designed to yield 10 pareto optimal solutions; a pareto optimal solution of 12.36 W for the payload subsystem yielded HAN mass and power margins of 1.84 kg and 2.37 W respectively. From the analysis, the solar array capability was found to deliver 24.23 W for the mission; this forms the beginning-of-life design point. The actual on-orbit mass of the HAN system (with enhanced capabilities including post-mission reuse) was found to be 9.2 kg as opposed to a conventional 10-kg nanosat implementation. The findings serve to eliminate undue space-borne equipment oversizing and advance the state-of-the-art in the conceptual design of future-generations spacecraft at the subsystem and system levels. Adaptive space systems promise to enable capability-based, dynamic, cost-effective, reliable, multifunctional, multipurpose and optimal-performing space systems with recourse to post-mission re-applications. Furthermore, the PSI-MO results show that HASS architectures can be extended to implement higher satellite generation missions with economies of scale.

[1] Research Associate, Electrical & Electronic Engineering, RM 313a, JD Building (East), *MAIAA*.
[2] Reader, Electrical & Electronic Engineering, RM 13b, Sackville Street Building.
[3] Lecturer, Electrical & Electronic Engineering, RM 331 JD Building (East).

Copyright © 2013 by the American Institute of Aeronautics and Astronautics, Inc. All rights reserved.

Nomenclature

β	=	Sun-orbit-plane angle, ^{o}
C_f	=	contingency factor
E_o	=	the energy production of the solar panel during an orbital period, J
H_{sat}	=	altitude of the satellite, km
M	=	mass of a spacecraft, kg
P_{cb}	=	power consumption of the core bus module, W
P_{margin}	=	power margin or contingency for the spacecraft mission, W
P_p	=	power consumption of the payload processing-overpower mode, W
P_{pl}	=	power consumption of the payload module, W
P_s	=	power consumption of the power-storing mode, W
P_{sp}	=	sunlit power generation of solar panels, W
P_T	=	total power consumption of the spacecraft in orbit, W
R	=	the radius ratio
R_{eq}	=	mean equatorial radius of the Earth, km
R_{sat}	=	geocentric radius of the satellite, km
t_e	=	eclipse time of spacecraft, s
τ_o	=	orbital period of the satellite, s
μ	=	gravitational constant of the Earth, km^3/s^2

I. Introduction

THE increasing adoption and development of adaptive space systems for reconfigurable and real-time applications in space missions have necessitated the corresponding design, development and validation of the critical mission resources. Power and/or energy generation for spacecraft in orbits is based on the subsystem requirements. For highly adaptive small spacecraft (HASS)[1–3] and the conventional small satellites, the electrical power is at a premium.[4–12] Due to the size (volume), weight, shape and power limitations imposed on small satellites, it is vital for spacecraft system engineers to understand and appropriate the relevant power budget model that would guarantee a mission's success cost-effectively.

Adaptive Small satellite missions operating in the low Earth orbit (LEO) have been the bane of current global interest and hence, the existing system engineering margins are insufficient to objectively address the missions' options. CubeSats in the 1U (one unit; 10 cm x 10 cm x 10 cm; 1 kg), 2U (two unit; 10 cm x 10 cm x 20 cm; 2 kg) and 3U (three unit; 10 cm x 10 cm x 10 cm; 3 kg) categories have attracted unprecedented research interests amongst the academia, spin-off companies, space research organisations and nations with partially-funded space programmes.[1,6,7] Appropriate SE procedures that validate the mission capabilities with recourse to post-mission reuse are required. Current missions have heavily depended upon commercial-of-the-shelf (COTS) subsubsystems and subsystems for their prototyping, development construction. The low-cost benefits of using these devices are often outweighed by the inherent reliability concerns and failures of the components in space. The space environment presents a unique challenge to mission's success in that it is radiation-prone and this impacts onboard electronics and consequently the power generation, operation and design lifetime of the spacecraft.

Achieving a maximum operational and processing time by the payload module onboard a satellite is one of the critical design considerations spacecraft designers must validate prior to launch. Hence, the static and dynamic power requirements of the passive, active and adaptive components and subsystems onboard a satellite must be estimated. Furthermore, a knowledge of their respective operational times would enable a judicious development of a balanced energy budget for the current and emergent missions.

Orbital patterns[4–6] influence the power generation probability of solar panels and hence, the batteries' stored energy reserve. This usually translates into enabling the spacecraft to operate in different cost-effective and energy-efficient multiple power modes with recourse to performance trade-offs during an orbital period.

Space-based payload data capturing and processing, mission data downlink and engineering data uplink represent the major spacecraft's in-orbit operation phases the spacecraft systems engineer must carefully and objectively qualify and quantify.[1,4,13–15] For adaptive space subsystems and components, the static power consumption is less than its dynamic counterpart. A payload module that utilises field programmable gates array (FPGA) in its architecture experiences various power consumption regimes based on the prevailing power mode(s) in the course of the spacecraft mission.[7–9] This is also true for a command and data handling subsystem that processes mission data using FPGA-based processors. For small satellites in LEO, accomplishing the mission largely depends on the energy generation capacity and reserve margin possible during a single orbital period and/or

Copyright © 2013 by the American Institute of Aeronautics and Astronautics, Inc. All rights reserved.

Downloaded by Sunday Ekpo on September 18, 2013 | http://arc.aiaa.org | DOI: 10.2514/6.2013-5470

round-trip. The increase in the use of radiation-hardened FPGAs in space missions has been occasioned by its circuit-emulating hardware functionalities and/or software implementation of reconfigurable custom hardware architectures in real-time. Moreover, onboard mission data processing and handling are performed to reduce the subsystem and functional requirements of the communication subsystem. Transmitting unprocessed data to a ground station usually demands more communication subsubsystem and subsystem resources which may not be feasible for small satellites by virtue of their limited size, weight and power. The implementation of high-speed data processing using adaptive device architectures would greatly enhance the data rate, bandwidth, availability and reliability of the communication subsystem. For instance, current medium and large satellites utilise FPGAs for computationally-intensive data processing spanning hyperspectral image, audio/sound and video processings. Traditional microprocessors have been outperformed by FPGAs in implementing data processing algorithms. A Virtex-4 SX35 FPGA device has implemented a hyperspectral imaging data processing algorithm within 15x less than the time required by a PowerPC 7455 microprocessor.[6]

In an actual satellite mission, at least two basic power modes[6] are feasible: a power-storing and an overpower modes. The total satellite system's power requirement is greater in the overpower mode (OM) than in the power-storing mode (PSM). In the OM, the sunlit solar power generation/production for the spacecraft is less than the spacecraft's power consumption and vice versa in the PSM. Energy is stored on the onboard batteries during the PSM and utilised to leverage the mission capabilities during the OM.

The integration of adaptive space subsubsystems and subsystems with other traditional active and passive devices onboard spacecraft for various mission functionalities and/or capabilities has necessitated the re-examination of existing SPSE design procedures. Consequently, an objective investigation of promising spacecraft technologies and the development of a suitable SPSE validation tool that addresses dynamic mission requirements with recourse to post-mission reapplication of space systems are inevitable.

This paper focuses on the design parameters that spacecraft systems engineers can utilise to qualify highly adaptive space systems' capacity, performance and operational time during the pre-launch, mission and post-mission phases. Section II establishes a spacecraft power and energy balance budget for space missions. The multicriteria optimisation of a spacecraft power system with recourse to the METSAT mission is presented in section III. The results and pertinent discussions are stated in section IV. Section V concludes the paper.

II. Spacecraft Power and Energy Budgets

A. Spacecraft Power Estimating Relationships

The design of spacecraft power and energy budgets starts with the identification and qualification of the power consumption requirements of the spacecraft modules of subsystems. The spacecraft power system engineering (SPSE) establishes the power regimes of the various core bus and payload subsystems. Past spacecraft missions have revealed an overwhelming dependency of the total space satellite power on the power consumption requirement of the payload subsystem. Mathematically, the generic total in-orbit power, P_T, of a spacecraft is given by:[1-4]

$$P_T = P_{pl} + P_{cb}(1 + C_f) \tag{1}$$

where P_{pl} is the payload power consumption (W) P_{cb}, the core bus power consumption (W) and C_f, the power contingency factor. The power margin, P_{margin}, for the spacecraft mission is given by:[1-4]

$$P_{margin} = C_f P_{cb} \tag{2}$$

For a HASS system with dynamic functional and structural in-orbit operations, Eq. (1) is modified to reflect the varying power requirements that characterise the prevailing respective power modes of the mission. The power mode adjustment takes into account the differential power consumption, δP, occasioned by the dynamic operation and in-orbit onboard processing of a HASS system. The corresponding power margin constraint on Eq. (1) is $P_{margin} \le P'_{margin} \le (P_{margin} + \delta P)$.[1] The adaptive power margin function, P'_{margin}, is determined respecting the deterministic and dynamic capability-based mission applications. The total in-orbit power requirement of a HASS system is accurately modelled by:[1-3]

Copyright © 2013 by the American Institute of Aeronautics and Astronautics, Inc. All rights reserved.

Downloaded by Sunday Ekpo on September 18, 2013 | http://arc.aiaa.org | DOI: 10.2514/6.2013-5470

$$P_T = P_{pl} + P_{cb}(1 + C_f) + \delta P \tag{3}$$

While Eq. (1) defines the total power consumption of the spacecraft subsystems for a minimum payload capability utilisation, Eq. (3) takes into account the maximum capacity and/or data capturing and processing capability of the payload subsystem. Hence, in Eq. (3), the full capacity of the payload module for the designed and emergent missions is envisaged. The differential power variable builds up the satellite power requirement from the static (no-payload or only core bus subsystems utilisation) value to the dynamic (full-capacity payload subsystem) operation level.

Table 1 gives a summary of the mass-based spacecraft power estimating relationships (PERs) for the various categories of small satellites in LEO[2]. Table 2 shows the PERs of the meteorological spacecraft (METSAT) mission. For a 9.2-kg HAN, Table 1 gives the total in-orbit electrical power requirement, P_T, as 24.2 W. This represents the total sunlit solar power (P_{SP}) production of a four-panel solar array. Hence, from Table 2, the minimum power consumption of the payload subsystem for the mission is 12.3 W and the corresponding core bus module's power requirement is 11.9 W.

Downloaded by Sunday Ekpo on September 18, 2013 | http://arc.aiaa.org | DOI: 10.2514/6.2013-5470

Table 1. Mass-based spacecraft power estimating relationships in LEO[2]

Satellite category, kg	Power estimating relationship, W
Microsatellite (10 – 100)	$P_T = 1.044M + 15.56$
Nanosatellite (1 – 10)	$P_T = 2.26M + 3.44$
Picosatellites (0.1 – 1)	$P_T = 5M + 0.7$
Femtosatellites (0.01 – 0.1)	$P_T = 10.3M + 0.167$

Table 2. Meteorology spacecraft power estimating relationships in LEO[3]

Satellite category, kg	Power estimating relationship, W
Microsatellite (10 – 100)	$P_T = 0.522M + 0.98P_{pl} + 7.78$
Nanosatellite (1 – 10)	$P_T = 1.13M + 0.98P_{pl} + 1.72$
Picosatellites (0.1 – 1)	$P_T = 2.5M + 0.98P_{pl} + 0.35$
Femtosatellites (0.01 – 0.1)	$P_T = 5.15M + 0.98P_{pl} + 0.0835$

For a C_f of 0.25 and using the nanosatellite's PER in Table 1, we derived the core bus power for a HAN in LEO to be given by:

$$P_{cb} = 1.808M - 0.8P_{pl} + 2.752 \tag{4}$$

The corresponding power margin from Eq. (2) is given by:

$$P_{margin} = 0.452M - 0.2P_{pl} + 0.688 \tag{5}$$

B. Core Bus and Payload Power Consumptions Analysis

For the METSAT mission, four payload subsystems[1,7] are considered; the payloads are paired (P1, P2) and (P3, P4) and their corresponding features are shown in Tables 3 and 4 respectively. The Mitsubishi's camera module[7] features two charged couple chip devices (CCDs) and yields an output image size of 2304 pixel x 1728 pixel.

The total power consumptions for payloads P1, P2, P3 and P4 are 387.6 mW, 717.6 mW, 257.6 mW and 537.6 mW respectively. The spatial resolution of the camera technology; the higher the spatial resolution, the more the

Copyright © 2013 by the American Institute of Aeronautics and Astronautics, Inc. All rights reserved.

power consumed/required during a mission operation. The size (volume) of the satellite represents a key design parameter for realising the area available for solar panels in the case of a spin-stabilised spacecraft system; for deployable solar panels (in a three-axis stabilised case), the small satellite size mostly dictates the available space for component mounting and integration. Given the common density of 1000 kg/m^3 for the CubeSats, approximately 21cm x 21 cm x 21 cm size is required for the case study 9.2-kg HAN; in an actual mission implementation, these nonconservative size and weight of HAN would be less than the stated values due to the very high level subsubsystems integration (VHLSI).[10,16-19]

Table 3. Payloads 1 and 2 subsystems requirements for the METSAT mission in LEO

Feature	Payload 1 (P1)	Payload 2 (P2)
Sensor technology	OmniVision 2655 CMOS image camera	Mitsubichi's CCD camera module
Sensor power Consumption, mW	250	580
FPGA device	Spartan-3 XC3A400T	Spartan-3 XC3A400T
FPGA power consumption, mW	137.6	137.6
Spatial resolution, pixel	2 x 1024 x 1024	1152 x 864 x 2
Spectral resolution, bit	3 x 8	3 x 8

Table 4. Payloads 3 and 4 subsystems requirements for the METSAT mission in LEO

Feature	Payload 3 (P3)	Payload 4 (P4)
Sensor technology	Sanyo's CCD camera module	Sharp's LZ0P373F CCD camera module
Sensor power Consumption, mW	120	400
FPGA device	Spartan-3 XC3A400T	Spartan-3 XC3A400T
FPGA power consumption, mW	137.6	137.6
Spatial resolution, pixel	1 x 1024 x 1024	1632 x 1224
Spectral resolution, bit	3 x 8	3 x 8

Table 5. Power budget of payload modules for the METSAT mission in LEO

Design Parameter	Payload module			
	P1	P2	P3	P4
Payload module power, W	14.010	14.340	13.880	14.160
Core bus power, W	8.180	7.910	8.280	8.060
Power margin, W	2.040	1.980	2.070	2.010

In this paper, four payload case studies are considered for the METSAT mission. Table 5 is determined based on the maximum individual power consumptions of the subsubsystems (camera and FPGA devices) integrated onto each payload module.

Tables 6 to 9 state the power and/or energy budget of the payloads under consideration. Table 6 reveals that the power margin for each case study payload can be obtained from the range $1.98 \leq P_{margin} \leq 2.04$ W. A 1.2-W Superstar GPS receiver[7] subsubsystem can be integrated onto the HAN system's ADC subsystem for an accurate tracking of at least twelve satellites in its neighbourhood. This promises to enhance a cooperative data relay network thereby virtually increasing the real-time operational times of the downlink and payload processing power modes. Satellites with an accurate neighbour's position can still transmit unfinished transmitted data via a constellation node that has its footprint coverage on the desired ground station. This would enable an energy budget refinement onboard the

Copyright © 2013 by the American Institute of Aeronautics and Astronautics, Inc. All rights reserved.

Downloaded by Sunday Ekpo on September 18, 2013 | http://arc.aiaa.org | DOI: 10.2514/6.2013-5470

satellite system to accommodate the critical data transmission needs outside the temporal window of the communication-overpower (downlink) power mode.

Table 6. Power budget for the METSAT mission in LEO using Payload P1

Subsystem	Power Mode's Power Consumption (W)			
	Power-storing	Communication-overpower	Uplink-overpower	Payload processing-overpower
ADC	0	0	0	0
C&DH	2.500	2.500	2.500	2.500
Uplink	0.750	0.750	0.750	0.750
Downlink	4.580	16.500	16.300	8.300
Payload (camera+FPGAs)	0	5.066	5.066	14.010
Board	0.350	0.350	0.350	0.350
Thermal control	0	0	0	0
Propulsion	0	0	0	0
Mechanics	0	0	0	0
Total	8.180	25.166	24.966	25.910

Table 7. Power budget for the METSAT mission in LEO using payload P2

Subsystem	Power Mode's Power Consumption (W)			
	Power-storing	Communication-overpower	Uplink-overpower	Payload processing-overpower
ADC	0	0	0	0
C&DH	2.500	2.500	2.500	2.500
Uplink	0.750	0.750	0.750	0.750
Downlink	4.310	16.500	16.300	8.300
Payload (camera+FPGAs)	0	5.396	5.396	14.340
Board	0.350	0.350	0.350	0.350
Thermal control	0	0	0	0
Propulsion	0	0	0	0
Mechanics	0	0	0	0
Total	7.910	25.496	25.296	26.240

Downloaded by Stanley Rigo on September 18, 2013 | http://arc.aiaa.org | DOI: 10.2514/6.2013-5470

Copyright © 2013 by the American Institute of Aeronautics and Astronautics, Inc. All rights reserved.

Table 8. Power budget for the METSAT mission in LEO using payload P3

Subsystem	Power Mode's Power Consumption (W)			
	Power-storing	Communication-overpower	Uplink-overpower	Payload processing-overpower
ADC	0	0	0	0
C&DH	2.500	2.500	2.500	2.500
Uplink	0.750	0.750	0.750	0.750
Downlink	4.682	16.500	16.300	8.300
Payload (camera+FPGAs)	0	4.936	4.936	13.880
Board	0.350	0.350	0.350	0.350
Thermal control	0	0	0	0
Propulsion	0	0	0	0
Mechanics	0	0	0	0
Total	8.282	24.286	24.836	25.780

Table 9. Power budget for the METSAT Mission in LEO using payload P4

Subsystem	Power Mode's Power Consumption (W)			
	Power-storing	Communication-overpower	Uplink-overpower	Payload processing-overpower
ADC	0	0	0	0
C&DH	2.500	2.500	2.500	2.500
Uplink	0.750	0.750	0.750	0.750
Downlink	4.460	16.500	16.300	8.300
Payload (camera+FPGAs)	0	5.216	5.216	14.160
Board	0.350	0.350	0.350	0.350
Thermal control	0	0	0	0
Propulsion	0	0	0	0
Mechanics	0	0	0	0
Total	8.060	25.316	25.116	26.060

C. Orbital Patterns and Operational Time of Spacecraft

Orbital patterns determine the amount of solar power that a satellite captures for the mission. Hence, mission design must incorporate a holistic and objective analysis of the mission requirements vis-à-vis the orbit of deployment. The LEO favours short-term and low-cost missions and most of the small satellite missions have concentrated in the orbit altitude spanning 160 to 2000 km. The inclination and eccentricity of a satellite orbit define the orbital patterns; the inclination defines the angular orbital sweep of a satellite around the Earth relative to the equator while the eccentricity states the orbit's deviation from an Earth-referenced two-dimensional plane round-trip

Copyright © 2013 by the American Institute of Aeronautics and Astronautics, Inc. All rights reserved.

Downloaded by Sandy Elgo on September 18, 2013 | http://arc.aiaa.org | DOI: 10.2514/6.2013-5470

circle. The orbital pattern parameters form the design variables used to assess the operational and illumination margins and/or regimes of satellites in space. The inclination defines the spatial location of an orbiting satellite relative to the Earth and its range is 0° (orbit heading for eastward flight) to180° (orbit heading for westward flight). On the other hand, the eccentricity partitions the orbits into closed (circular and elliptical orbits) and open (hyperbolic and parabolic orbits); open-orbit satellites orbit the Earth once while closed-orbit satellites orbit the Earth periodically along the same path. The METSAT mission reported in this paper will be assessed with recourse to closed orbits.

Small satellites require a nearly constant illumination from the sun for their missions. Sun-synchronous (usually circular and retrograde) orbits spanning 600 to 800 km at 98° inclination have been utilised for satellite missions[7]; the satellites experience a nearly constant surface sunlight (illumination) and the daily satellite's ascents and descents over a particular Earth geographic location/latitude occurs at the same local mean time. A sun-synchronous orbit satellite might ascend the Earth ten times a day each time passing over an Earth location at approximately the same local mean solar time. The METSAT images the Earth's landscape in visible or infrared wavelengths and therefore require a constant sunlight for their payload's primary mission function and satellite energy supply.

Satellites operating in orbits other than the sun-synchronous experience the Earth's eclipse for a given amount of time during their round-trip. This decreases the available solar energy for the satellite. Mathematically, the eclipse time, t_e, of a satellite is given by:[6]

$$t_e = \frac{\tau_o}{\pi}\left(\cos^{-1}\left(\frac{\sqrt{1-R^2}}{\cos\beta}\right)\right) \tag{6}$$

where,

R = the radius ratio = R_{eq}/R_{sat}

R_{eq} = mean equatorial radius of the Earth = 6378 km

R_{sat} = geocentric radius of the satellite, km = $R_{eq}+H_{sat}$

H_{sat} = altitude of the satellite, km

β = Sun-orbit-plane angle, °

τ_o = orbital period of the satellite, s

μ = gravitational constant of the Earth = 398,600.4418 km^3/s^2

The worst-case β occurs at 0° when the satellite experiences the maximum Earth's eclipse and the best-case occurs at ±90° when the orbit never enters the Earth's eclipse. The orbital period of the satellite is given by:[6]

$$\tau_o = 2\pi\sqrt{R_{sat}^3/\mu} \tag{7}$$

During the Earth's eclipse, the satellite depends on the onboard storage batteries to maintain system functionalities; the power generation of the solar panels is 0 W while the satellite is eclipsed. Hence, the total energy reserve of the satellite is reduced per an orbital period due to the absence of the Sun's illumination during the eclipse period. The total energy produced by the spacecraft's solar panels, E_o, during a round-trip is given by:

$$E_o = P_{sp}(\tau_o - t_e) \tag{8}$$

where P_{sp} is the solar panel's average sunlit power generation in a given orbit. This information can be obtained from the datasheets provided by the solar panel manufacturers; a direct practical test of the panels (with recourse to the prevailing space environmental conditions) can also be done. Table 1 provides a summary of the mass-based PER for small satellites utilising a four-panel array in LEO.[1–3,5] The PERs take into consideration the impact of space radiation and other prevailing orbital dynamics that affect the sunlit power generation of solar panels onboard spacecraft in a given orbit.

The sunlit power generation capacity of solar panels is used to develop the electrical energy production of spacecraft in orbits. For a two-power mode system, the following power modes' power consumptions are feasible:

1) Power-storing, P_{ss}; and
2) Payload processing-overpower, P_p.

Copyright © 2013 by the American Institute of Aeronautics and Astronautics, Inc. All rights reserved.

Downloaded by Sunday Ekpo on September 18, 2013 | http://arc.aiaa.org | DOI: 10.2514/6.2013-5470

The total energy of the spacecraft during a single orbital period for a two-power mode system is given by:

$$E_o = E_s + E_p \tag{9}$$

where E_s and E_p are the energy consumptions in the power-storing and payload processing-overpower modes respectively. The operational time of the payload processing-overpower mode, t_p, is given by:

$$t_p = \tau_o - (t_s + t_e) \tag{10}$$

where t_s is the operational time of the power-storing mode.

From Eqs. (8) and (9), we obtained the operational time of the payload processing-overpower mode for a two-power mode system as:

$$t_p = \frac{E_o - P_s(\tau_o - t_e)}{P_p - P_s} \tag{11}$$

Downloaded by Sunday Ekpo on September 18, 2013 | http://arc.aiaa.org | DOI: 10.2514/6.2013-5470

Equation (11) can be extended to accommodate several power modes for multiple mission and post-mission applications. For a *N*-power mode system, the following power consumptions are feasible:

1) Power-storing;
2) Communication (downlink and uplink)-overpower, P_{du}, with a corresponding time, t_{du};
3) Uplink-overpower, P_u, with a corresponding time, t_u;
4) Payload processing-overpower; and
5) Other overpower modes, P_n, with a corresponding time, t_n, where n = 1, 2, …

The energy budget balance for the above in-orbit mission applications is obtained thus:

$$E_o = E_s + E_{du} + E_u + E_p + E_1 + E_2 + \ldots + E_N \tag{12}$$

The corresponding operational time of the payload processing-overpower mode is given by:

$$t_p = \tau_o - (t_s + t_e + t_{du} + t_u + t_1 + t_2 + \ldots + t_N) \tag{13}$$

Hence, we derived the in-orbit operational time of the payload processing-overpower mode, t_p, using Eqs. (12) and (13) as:

$$t_p = \frac{E_o - P_s(\tau_o - (t_e + t_{du} + t_u + t_1 + t_2 + \ldots + t_N)) - (P_1 t_1 + P_2 t_2 + \ldots + P_N t_N)}{P_p - P_s} \tag{14}$$

Equation (14) can be re-written thus:

$$t_p = \frac{E_o + P_s(\sum_{i=1}^{N-2} t_i + t_e - \tau_o) - (\sum_{i=1}^{N-2} P_i t_i)}{P_p - P_s} \tag{15}$$

where P_i and t_i represent the *i*th power mode's power consumption and operational time respectively; the summations in Eq. (15) consider all the power modes except the power-storing and the payload processing-overpower mode. In the case of calculating the operational time of a power mode other than the payload processing-overpower mode's, the latter is held constant and included in the summations while the considered power mode is excluded. The various power modes' power consumptions and their corresponding operational times must be

Copyright © 2013 by the American Institute of Aeronautics and Astronautics, Inc. All rights reserved.

estimated in order to obtain the t_p for the spacecraft mission. Furthermore, the power consumptions of the power-storing mode and the power mode whose operational time is being calculated must be estimated as well.

To maximise the operational time of a power mode, Eq. (15) is adjusted to reflect the maximised power mode. Given the power consumption of the maximised power mode, P_{max}, the corresponding maximised operational time, t_{max}, is obtained from Eq. (15) as:

$$t_{max} = \frac{E_o + P_s(\sum_{i=1}^{N-2} t_i + t_e - \tau_o) - (\sum_{i=1}^{N-2} P_i t_i)}{P_{max} - P_s} \tag{16}$$

Equation (16) is very useful for the multiobjective optimisation of the mission design variables in an integrated design environment. Hence, the operational time of any power mode can be modelled and optimised for a reliable, cost-effective and optimal-performing mission.

Downloaded by Sunday Ekpo on September 18, 2013 | http://arc.aiaa.org | DOI: 10.2514/6.2013-5470

III. Multicriteria Optimisation of a Spacecraft Power System

A. Parameter Space Investigation Method

Complex engineering systems such as space-borne equipment require optimised system architectures for their reliability and mission accomplishment. The investigation for optimal solutions generically poses an enormous task of objective locational and procedural searches. The accurate statement of the optimisation problem for the mission and conceptual design objectives enables the feasible solution set and the optimal solutions to be obtained for the space equipment. The parameter space investigation (PSI) method[20] has been created and developed to enable the construction of the feasible solution set for complex engineering systems such as space shuttle, unmanned vehicles, aeroplane, automobiles, ships, control systems, communication network nodes, metallurgical systems, robots and large-scale electrical energy generation systems. The PSI systematically investigates a multidimensional domain space and generates multidimensional points with each point representing a design prototype for the system under development. The PSI method is implemented in the multicriteria optimisation and vector identification (MOVI) software. The integrated PSI-MOVI platform depends on the correct development of the mathematical model governing the complex engineering system under investigation. An approximate model of any engineering system is also supported by the PSI-MOVI application. The tools for constructing and analysing the feasible solution set of a multicriteria optimisation problem are provided by the PSI method and the MOVI system.[20]

The PSI method enables the identification, optimisation and analysis of constraints on design variables, functional dependencies and multicriteria; these constitute the feasible solution set of the optimisation problem. The method comprises three major stages: compilation of test tables, selection of criterion constraints and verification of the solvability of the optimisation problem.[20]

B. Multicriteria Design of Spacecraft Power System

In this paper, we applied the PSI method in the multicriteria design of the spacecraft power system engineering for small satellites in LEO. The mathematical model of the electrical power requirement of the spacecraft modules was developed based on past missions and emerging space systems technology. We placed an objective emphasis on the spacecraft design variables that occasion dynamic, cost-effective and reliable operations with recourse to post-mission applications. A METSAT mission in LEO was chosen as the candidate small satellite mission. We limited the scale of the optimisation problem to three design variables: the payload power, P_{pl}, total spacecraft power, P_T and mass contingencies, M. We developed four functional constraints and six criteria parameters respecting the candidate METSAT mission. The functional and criteria constraints were set to minimise the total power consumptions of the HAN and its payload. The in-orbit dry mass was also minimised in the optimisation problem. The results of the multicriteria optimisation of the SPSE design are stated in section IV.

IV. Results and Discussions

A. Orbital and Operational Times

Table 10 shows the orbital patterns[6] that we utilised to investigate the appropriateness of payloads P1 to P4 for the METSAT mission with recourse to the in-orbit power budget and operational times. The orbit, inclination and

Copyright © 2013 by the American Institute of Aeronautics and Astronautics, Inc. All rights reserved.

altitude were chosen according to reflect the typical prevailing operational orbital margins of small satellite missions in LEO.[5–7] The suitability of each orbit for the mission was also considered based on the average energy production per orbital period and the desired data rates for the downlink communication. For the METSAT mission, we evaluated the power and energy budget by setting the uplink and downlink operational times to 10 minutes respectively. The communication-overpower mode utilizes 10 minutes for both the communication-downlink-overpower and communication-uplink-overpower modes. Tables 11 to 14 show the operational times for the payloads P1 to P4; the analyses were done using Tables 5 to 10 and Eq. (15). The operational times of the payload processing-overpower mode, t_{pp1} to t_{pp4}, for each candidate payload were obtained with recourse to the average eclipse time per orbit and altitude of deployment (Table 10).

Table 10. Orbital patterns for the METSAT Mission in LEO

Orbit	H_{sat}, km	β range, °	τ_o, mins	t_{eavgp}, min
Equatorial	300	-23:23	90.5	36.2
Inclination 22.5	400	-43:45	92.6	35.2
Inclination 45	500	-61:65	94.6	32.7
Inclination 67.5	600	-88:85	96.7	26.1
Inclination 90 (polar)	300	36:60	90.5	32.3
Inclination 112.5	400	-88:88	92.6	29.7
Inclination 135	500	-67:63	94.6	32.6
Inclination 157.5	600	-46:46	96.7	34.3
Inclination 180	800	-23:23	100.9	34.4
Sun-synchronous (polar) 90	300	71:79	100.9	0
Sun-synchronous (nonpolar) 98	400	-75:82	92.6	0

Table 11. Operational times of the candidate payloads for the METSAT Mission in LEO

Orbit	H_{sat}, km	t_{pp1}, min	t_{pp2}, min	t_{pp3}, min	t_{pp4}, min
Equatorial	300	30.02	28.49	30.79	29.63
Inclination 22.5	400	32.82	31.18	33.61	32.41
Inclination 45	500	36.88	35.09	37.70	36.44
Inclination 67.5	600	44.74	42.64	45.62	44.24
Inclination 90 (polar)	300	33.54	31.87	34.34	33.12
Inclination 112.5	400	37.79	35.95	38.61	37.33
Inclination 135	500	36.97	35.17	37.80	36.53
Inclination 157.5	600	37.33	35.52	38.16	36.89
Inclination 180	800	41.04	39.08	41.89	40.57
Sun-synchronous (polar) 90	300	72.12	68.96	73.18	71.41
Sun-synchronous (nonpolar) 98	400	64.62	61.75	65.63	63.97

Table 10 shows that the orbital period of as spacecraft is largely dependent upon the orbital pattern chosen for the mission. Sun-synchronous orbits favour the small satellite missions for its near-constant sunlight and relatively

Copyright © 2013 by the American Institute of Aeronautics and Astronautics, Inc. All rights reserved.

Downloaded by Sunday Ekpo on September 18, 2013 | http://arc.aiaa.org | DOI: 10.2514/6.2013-5470

high round-trip duration for the 90 ° polar orbit; an orbital spacecraft experiences no eclipse. At an altitude of 800 km and inclination of 180 °, the HAN system would experience an average eclipse time of 34.4 minutes.

Table 12. Excess energy storage for the METSAT Mission in LEO

Orbit	H_{sat},	E_{ep1}, Wh	E_{ep2}, Wh	E_{ep3}, Wh	E_{ep4}, Wh
Equatorial	300	1.73	2.35	1.42	1.88
Inclination 22.5	400	1.85	2.51	1.53	2.01
Inclination 45	500	2.02	2.75	1.69	2.20
Inclination 67.5	600	2.36	3.21	2.01	2.56
Inclination 90 (polar)	300	1.88	2.55	1.56	2.05
Inclination 112.5	400	2.06	2.80	1.73	2.24
Inclination 135	500	2.03	2.75	1.70	2.21
Inclination 157.5	600	2.04	2.77	1.71	2.22
Inclination 180	800	2.20	2.99	1.86	2.39
Sun-synchronous (polar) 90	300	3.54	4.81	3.11	3.83
Sun-synchronous (nonpolar) 98	400	3.22	4.38	2.81	3.48

Downloaded by Sunday Ekpo on September 18, 2013 | http://arc.aiaa.org | DOI: 10.2514/6.2013-5470

While the sun-synchronous orbits remain the favoured for the METSAT mission, Table 11 reveals that at 800 km altitude and 180 ° inclination, an average of 40 minutes for the operational times of the candidate payloads under investigation is obtained. This leaves the choice of the appropriate payload to be considered based on the desired data quality and integrity and the expected system performance. In a typical spacecraft mission, more operational time is required for the payload subsystem. Table 12 states the excess energy stored during as the spacecraft orbits around the Earth. As expected, the sun-synchronous orbits store the most energy for each payload configuration. At 180 km altitude and 180 ° inclination, the HAN system stores an average of 2.4 Wh. Thus, the energy budget balance reveals that a polymer Li-ion battery with a capacity of 3.99 Wh can store the round-trip excess energy for an increased operational time for the payload processing-overpower mode. During the eclipse time, the payload and an active thermal subsystem can be accommodated. Furthermore, the analysis indicates that a low-cost three-axis momentum wheel with an accuracy of <0.01 ° can be integrated with a moderate difficulty; this would utilise attitude sensors which can be conveniently supported by the HAN system.

The excess energy stored, E_{ep} on the batteries per orbital period and based on the operational times of the individual payloads are summarised in Table 12. The minimum storable excess energy is 1.42 Wh and the maximum, 4.81 for the considered candidate payloads. Including two polymer Li-ion batteries in the electrical power subsystem of the HAN, each with a capacity of 3.89 Wh, would enable secondary payloads and more operational times for a power mode of interest to be accomplished for the METSAT mission.

B. Data Transmission

Data transmission from a spacecraft to a ground station is inevitable for any given space mission. The operational times of the communication-overpower mode and the data rate of the downlink greatly influence the data delivery to a ground station. For a 9600 bps data rate and downlink time of 10 minutes, 720 kB of data can be transmitted to a ground station. If this is increased to 19200 bps, 1440 kB of data can be downlinked. The challenge lies in the spatial and spectral resolutions of the payload module onboard the spacecraft and the data quality expected by the end-user. A payload with a sensor (camera) of 2-Mpixel spatial resolution and 3 x 8 bits spectral resolution would generate a data size of approximately 6.3 MB. If the HAN system transmits at 9600 bps, only about 11.4 % of the payload data would be transmitted within 10 minutes of its contact with a ground station. The 19200 bps data rate allows the HAN system to downlink 22.9 % of its payload data to a ground station within its footprint. Increasing the data rate to 100 kbps enables the HAN system to downlink approximately 7.5 MB to a 4-m diameter ground station antenna during its 10 minutes pass. This would completely transmit the data generated by payloads P1, P3 and P4 and about 60 % of the data generated by payload P2. A second approach would be to implement a JPEG (joint pictures expert group) compression algorithm on the onboard signal processing devices such as FPGAs. This would allow the payload data to be transmitted to the ground station at the expense of some

Copyright © 2013 by the American Institute of Aeronautics and Astronautics, Inc. All rights reserved.

information. The JPEG algorithm scales the data to be transmitted to fit the allowable maximum data size of the downlink (data link) margin. For a 4-Mpixel image, the unprocessed data size is 12.58 MB. The corresponding compression ratio at 100 kbps downlink margin is 1: 1.68. This is well below the allowable maximum compression ratio of 1:10.[7] Hence, the HAN system can still process its payload data within its payload's operational time of 40 minutes and downlink a good quality data to a ground station within 10 minutes.

C. Multicriteria Optimisation of the HAN Power System Engineering

The results of the multicriteria optimisation of the HAN power system engineering is shown in Figures 1 to 5. The design variables for the SPSE optimisation problem were the mass of HAN, the payload power consumption and the power contingency. Figure 1 states the optimisation vectors of the HAN system's SPSE design. The pareto optimal solution concentrates around 9.2 kg for the METSAT mission implementation. It shows the histogram of the feasible and pareto optimal solutions for the first design variable (mass of HAN) for the METSAT mission.

Figure 2 shows the optimisation design vectors that represent the histogram of the feasible and pareto solutions set for the second design variable (payload power) for the METSAT mission. The pareto optimal solution for the baseline power consumption of HAN's payload module is indicated by the green dots. These power consumptions are the minimum that can sustain the METSAT mission given the mission and conceptual design objectives. The optimisation result yielded 12.36 W as the best (minimum) baseline payload module power consumption for the mission. The corresponding core bus power consumption and power margin for the mission were obtained from the multicriteria optimisation as 9.5 W and 2.37 W respectively.

Figures 3 and 4 indicate that the optimised payload power consumption for the METSAT mission is 12.36 W. This forms the design point in the choice of the components of the payload module for the mission. The stated power is based on the minimum acceptable data capturing, processing and transmission quality for the mission. In Fig. 3, the total payload power consumption is compared with the HAN category that can satisfy the mission and conceptual design objectives. Figure 4 reports the entire optimisation solutions set for the total HAN power requirement and the corresponding payload power consumption. The histogram of the feasible and pareto optimal solutions for the third design variable (contingency factor) are given in Fig. 5. The power margin versus contingency factor graph is shown in Fig. 6. The pareto optimal solutions for the HAN system yielded a power margin of 2.37 W; this is approximately 10 % of the total spacecraft power and satisfies the stipulated mission's conceptual design requirement.[4] It is required for the mission to have enough power margin for emergent capabilities and operational uncertainties; Figs. 5 and 6 were obtained for a minimised power margin design to enable the threshold power margin for the mission to be determined. The performances of the design variables are further explained in the optimisation criteria for the METSAT mission (Fig. 7). Six criteria were considered by the authors and the results indicate the worst and best results realisable for the METSAT mission.

Downloaded by Sunday Ekpo on September 18, 2013 | http://arc.aiaa.org | DOI: 10.2514/6.2013-5470

Copyright © 2013 by the American Institute of Aeronautics and Astronautics, Inc. All rights reserved.

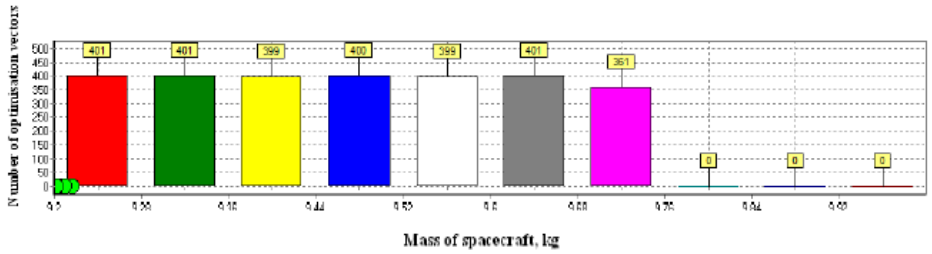

Figure 1. Optimisation vectors versus mass of spacecraft for the METSAT mission

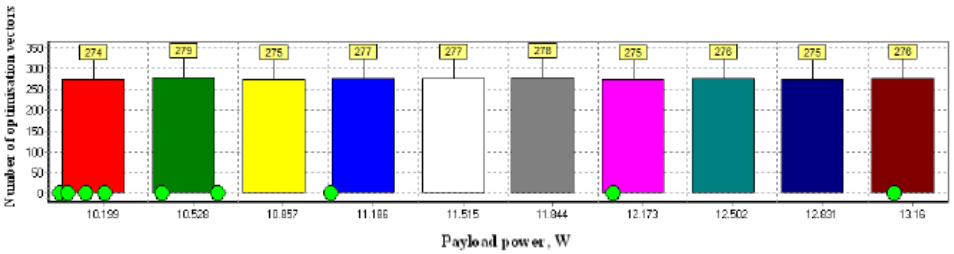

Figure 2. Optimisation vectors versus payload power for the METSAT mission

Copyright © 2013 by the American Institute of Aeronautics and Astronautics, Inc. All rights reserved.

Downloaded by Sunday Ekpo on September 18, 2013 | http://arc.aiaa.org | DOI: 10.2514/6.2013-5470

Downloaded by Sunday Ekpo on September 18, 2013 | http://arc.aiaa.org | DOI: 10.2514/6.2013-5470

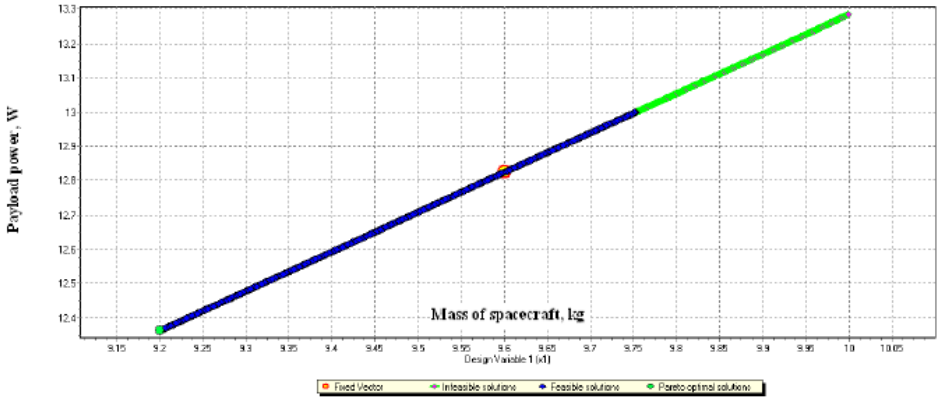

Figure 3. Optimised payload power versus mass of spacecraft for the METSAT mission

Copyright © 2013 by the American Institute of Aeronautics and Astronautics, Inc. All rights reserved.

Downloaded by Sunday Ekpo on September 18, 2013 | http://arc.aiaa.org | DOI: 10.2514/6.2013-5470

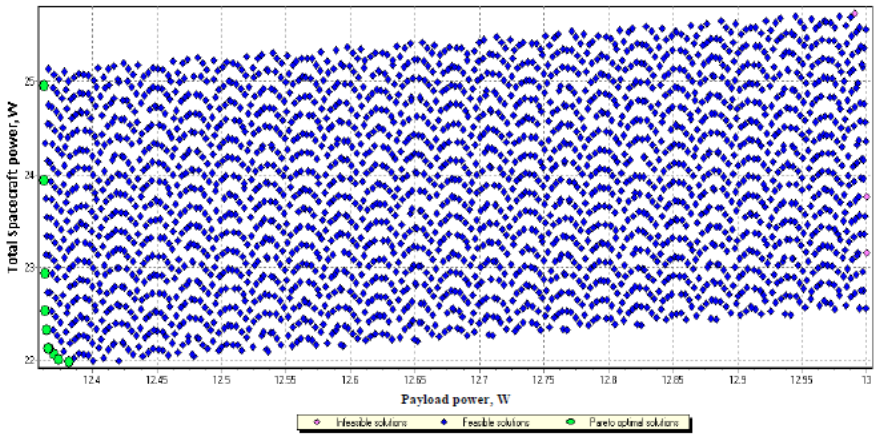

Figure 4. Optimisation solutions set of the total spacecraft and payload power consumptions

Copyright © 2013 by the American Institute of Aeronautics and Astronautics, Inc. All rights reserved.

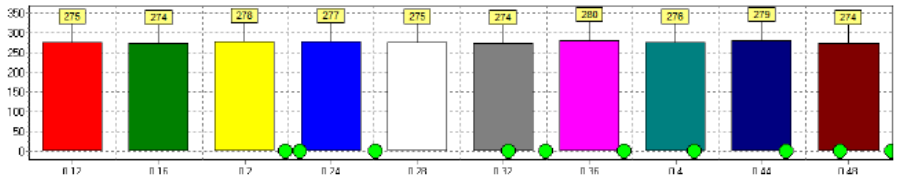

Figure 5. Optimisation vectors versus power contingency for the METSAT mission

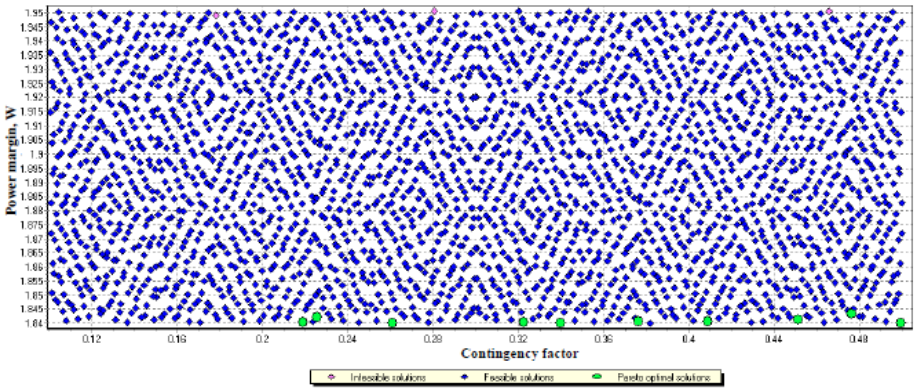

Figure 6. Optimisation solutions set of the power margin and contingency factor

Copyright © 2013 by the American Institute of Aeronautics and Astronautics, Inc. All rights reserved.

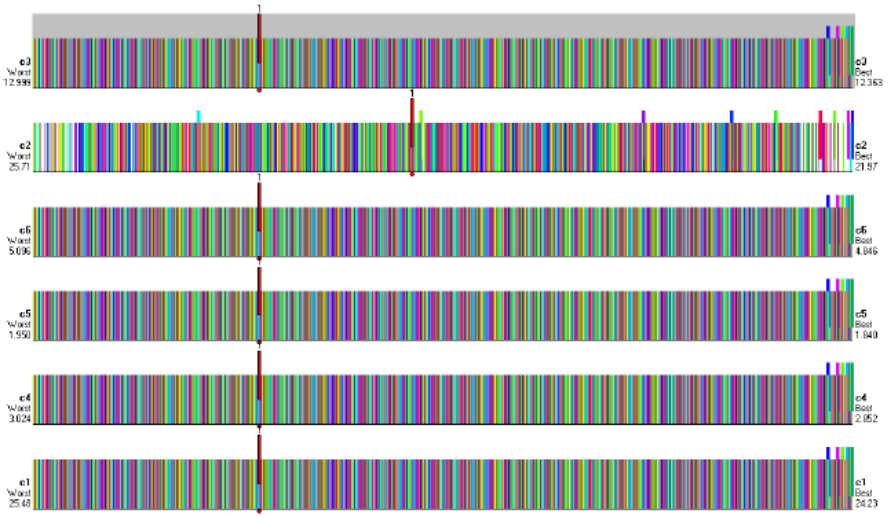

Figure 7. Optimisation criteria for the METSAT mission's design variables

Copyright © 2013 by the American Institute of Aeronautics and Astronautics, Inc. All rights reserved.

V. Conclusion

A multicriteria optimisation of a highly adaptive nanosatellite system has been investigated and reported in this paper. Four candidate payload modules, each containing a camera and an FPGA device, were chosen for a meteorology mission. The multicriteria optimisation yielded a 9.2-kg HAN for the METSAT mission. We carried out an analysis of the orbital patterns and the operational times of the 9.2-kg HAN. Furthermore, the authors calculated the total energy production of the HAN system at an altitude of 800 km and inclination of 180 ^{o} as 26.82 Wh. The operational time of 40 minutes for the payload processing-overpower model and downlink time of 10 minutes are well suited for the mission. The HAN system also received uplink engineering data for 10 minutes during its orbital period. The reported power and energy balance budget for the METSAT mission using a highly adaptive small satellite promises to enable spacecraft systems engineers objectively and reliably design, validate and develop spacecraft mission assets with economies of scale.

Acknowledgments

S. C. Ekpo specially thanks the AKSU/AKUTECH for the sponsorship of this research project. The authors express their appreciation to The University of Manchester, UK for the use of the institution's research facilities to achieve the technical findings that have been reported by them in this paper.

Downloaded by Stanley Ekpo on September 18, 2013 | http://arc.aiaa.org | DOI: 10.2514/6.2013-5470

References

[1]Ekpo, S., and George, D., "A System Engineering Analysis of Highly Adaptive Small Satellites," *IEEE Systems Journal*, Vol. PP, No. 99, 2012, pp. 1–8.

[2]Ekpo, S., and George, D., "A Power Budget Model for Highly Adaptive Small Satellites," *Recent Patents on Space Technology*, Vol. 3, No. 2, 2013, pp. 1–9.

[3]Ekpo, S., and George, D., "A System Engineering Consideration for Future-Generations Small Satellites Design," *Proceedings of the First IEEE European Satellite Telecommunications Conference*, Rome, 2012, pp. 1–4.

[4]Brown, C., *Elements of Spacecraft Design*, AIAA, Inc., Virginia, 2002, pp. 1–43.

[5]Janson, S. W., "The Future of Small Satellites," *Small Satellites: Past, Present, and Future*, edited by Helvajian, H., and Janson, S. W., AIAA, Inc., Virginia. pp. 771–810, 2008.

[6]Arnold, S. S., Nuzzaci, R., and Gordon-Ross, A., "Energy Budgeting for CubeSats with an Integrated FPGA," *IEEE Aerospace Conference*, Big Sky, Montana, 2012, pp. 1–14.

[7]P. Mario, "Study of a Cube-Sat Mission," University of Karl Franzens University of Graz, Austria, 2005, pp. 56–82.

[8]Ekpo, S., and George, D., "A System-based Design Methodology and Architecture for Adaptive Small Satellites," *Proceedings of the 4th Annual IEEE International Systems Conference*, San Diego, CA, 2010, pp. 516–519.

[9]H.Schmitz , "Application Examples: How to Use FPGAs in Satellite Systems," *Actel Corporation, California*, 2010, pp. 1–7.

[10]Ekpo, S., and George, D., "A Deterministic Multifunctional Architecture Design for Highly Adaptive Small Satellites," *International Journal of Satellite Communication Policy and Management*, Vol.1, No.2/3, 2012, pp. 174–194.

[11]J. Saleh, D. Hastings, and D. Newman, "Spacecraft Design Lifetime," *Journal of Spacecraft and Rockets*, Vol. 39, No. 2, 2002, pp. 244–257.

[12]Vladimirova, T. and Barnhart, D. J., "Towards Space-based Wireless Sensor Networks," *Small Satellites: Past, Present, and Future*, edited by Helvajian, H., and Janson, S. W., AIAA, Inc., Virginia. pp. 595–629, 2008.

[13]Ekpo, S., and George, D., "Impact of Noise Figure on a Satellite Link Performance," *IEEE Communications Letters*, Vol. 15, No. 9, 2011, pp. 1–3.

[14]Ekpo, S., and George, D., "4–8 GHz LNA design for an adaptive small Satellite Transponder using InGaAs PHEMT Technology," *Proceedings of the 11th IEEE Wireless & Microwave Conference*, Melbourne, FL, 2010, pp. 1–4.

[15]Ekpo, S., and Kettle, D., "Mm-wave LNAs design for adaptive small Satellite applications," *Proceedings of the Joint 5th ESA Workshop on Millimetre Wave and 31st ESA Antenna Workshop*, Noordwijk, Netherlands, 2009, pp. 843–847.

[16]Barnhart, D., Vladimirova, T., and M. Sweeting, "Very-Small-Satellite Design for Distributed Space Missions," *Journal of Spacecraft and Rockets*, Vol. 44, No. 6, 2007, pp. 244–257.

[17]Ekpo, S., and George, D., "Reconfigurable Cooperative Intelligent Control Design for Space Missions," *Recent Patents on Space Technology*, Vol. 2, No. 1, 2012, pp. 2–11.

[18]B. Jackson and K. Epstein, "A Reconfigurable Multifunctional Architecture Approach for Next Generation Nanosatellite Design," *Proceedings of the IEEE Aerospace Conference*, Vol.7, *2000*, pp. 185–188.

[19]Ekpo, S., and George, D., "A Highly Adaptive Small Satellites Experiment for Space Missions Modelling," *International Journal of Satellite Communication Policy and Management*, Vol. 2, 2013, pp. 1–18.

[20]Statnikov, R., and Statnikov, A., "The Parameter space Investigation Method," Artech House Publishers, Inc., London, 2011, pp. 13–94.

Copyright © 2013 by the American Institute of Aeronautics and Astronautics, Inc. All rights reserved.

3.2.8 Paper 8 [SE8]

4–8 GHz LNA Design for an Adaptive Small Satellite Transponder using InGaAs pHEMT Technology, *in Proc. 11th IEEE Wireless & Microwave Conference*, Melbourne FL, USA, April 2010, pp. 1–4.

DOI: https://doi.org/10.1109/WAMICON.2010.5461877.

Sunday Ekpo[1] and Danielle George[2]

[1]Department of Engineering, Manchester Metropolitan University, UK

[2]School of Electrical & Electronic Engineering, The University of Manchester, UK

This subsection is an exact copy of Paper 8

4 – 8 GHz LNA Design for a Highly Adaptive Small Satellite Transponder Using InGaAs pHEMT Technology

Sunday Ekpo[*1] and Danielle George[*2]
[*]Microwave & Communication Systems Research Group, School of Electrical & Electronic Eng.,
The University of Manchester, Manchester, M60 1QD, United Kingdom
[1]Sunday.Ekpo@postgrad.manchester.ac.uk; [2]Danielle.George@manchester.ac.uk

Abstract – **The ever increasing global space activity is characterised by emerging space systems, operation and applications challenges. Hence, reliable RF and microwave receivers for in-orbit highly adaptive small satellites are needed to support reconfigurable multimedia/broadband applications in real-time with optimal performance. Though other parameters of the small satellite communication system may be critical, the noise level of the receiver determines the viability, reliability and deliverability of the project. Thus, a good design that delivers low noise performance, high gain and low power consumption for multipurpose space missions is inevitable. This paper describes a 0.15µm InGaAs pseudomorphic high electron mobility transistor amplifier with low noise and high gain in the frequency band 4 – 8 GHz. The monolithic microwave integrated circuit LNA design presented here shows the best performance known using this technology; noise figure of 0.5 dB and gain of 37 ± 1 dB over the characterised bandwidth.**

Index terms – **Highly adaptive small satellite, linear gain, low-noise amplifiers, noise temperature, pHEMT, satellite transponder.**

I. Introduction

Space communications applications have greatly advanced following advances in systems and subsystems materials and technologies and systems architectures. A highly adaptive small satellite system (HASS) is a reconfigurable, multifunctional and deterministic small space satellite that has capabilities for dynamic space applications and operations while retaining its designed optimal performance. It is a new concept that has attracted considerable interest in the space community owing to its obvious benefits including reliability, reconfigurability, multifunctionality, dynamic redundancy and real-time optimal performance amongst others. Adaptive payload systems require wideband receivers which are critical to all space transponders. These receivers provide the low-noise amplification needed to maintain an optimal signal-to-noise ratio (SNR) for space satellite communications. Consequently, multimedia and broadband small satellite receivers are required to have very low noise and high gain over the operating bandwidth. A key component in all space satellite wideband receivers is the low noise amplifier (LNA); it sits at the front-end of the receiver. As space applications become more challenging, low noise amplifiers for HASSs receivers are increasingly expected to be unconditionally stable at any load and source conditions, and at any frequency value within the useable bandwidth. Active device (III – IV) technologies (GaAs and InP) have been the drivers for space LNAs designs in the last three decades. A key concern for space satellite communication systems is designing a high performance LNA with a low power dissipation. This is especially demanding for HASS architectures where deterministic service and/or operation swings are required and inevitable. In this paper, the small satellite LNA design using InGaAs structures grown pseudomorphically on GaAs substrates is described. C-band (4 – 8 GHz) designs with metamorphic high electron mobility transistor (mHEMT) and MESFET have been reported [1, 2]. The mHEMT technology was based on the 0.15 µm GaAs Foundry service; it reported a MMIC LNA design with noise figure of 0.53 dB and gain of 30 dB at 6 GHz [1]. The MESFET LNA reported a noise figure of 0.88 dB and gain of 23 dB at 6 GHz [2].

This paper reports a monolithic microwave integrated circuit (MMIC) LNA based on a 0.15µm gate length InGaAs pseudomorphic HEMT GaAs Foundry technology. The pseudomorphic high electron mobility transistor (pHEMT) model used shows the active device has a minimum noise figure of 0.3 dB and gain of 17 dB at 6 GHz. In this paper, a three-stage broadband MMIC LNA design that covers a wide range of space applications is presented. The first stage of the amplifier was matched for optimal noise performance while the subsequent stages were matched for gain compensation. Source inductive feedback (for overall LNA stability) and parallel feedback (for LNA gain enhancement and flatness) were used at the second and third stages respectively.

II. Broadband Space LNA Design

A single-ended three-stage low noise amplifier in the C-band was designed using Agilent's ADS circuit simulation software. The baseline MMIC configuration [1, 3] was used in the single chip design. Each of the three stages employed a 4 x 75µm HEMT. The first stage of the three-stage C-band MMIC LNA was matched for noise while the second and third stages were matched for maximum stable gain (MSG). The first stage of the MMIC LNA was designed to

978-1-4244-6689-0/10/$26.00 ©2010 Crown

present the optimum match, Γ_{opt}, over the operating frequency, to the gate of the first HEMT when the MMIC input is terminated in 50 Ω. Optimum impedance was presented to the device to achieve the minimum noise figure for the first stage. The gain of the first stage renders the noise contribution from the second stage negligible according to Frii's noise factor formula:

$$F = F_1 + \frac{F_2 - 1}{G_1} + \frac{F_3 - 1}{G_1 G_2} + \frac{F_4 - 1}{G_1 G_2 G_3} \quad (1)$$

where F_n is the noise factor and G_n is the power gain of component n in the chain. The noise figure of the first stage is the most critical according to (1); noise contributions from the proceeding stages are reduced by the gain of the preceding stages.

The MMIC LNA chip was 1.5 x 0.8 mm and its circuit layout is shown in Fig. 1.

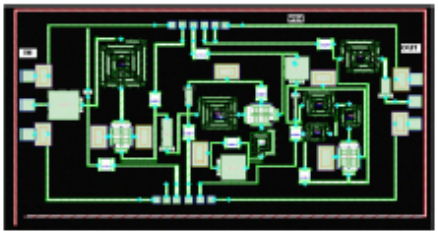

Fig. 1. The layout of the C-band MMIC LNA chip

Hybrid technology is the first-pass option for high performance LNAs in the microwave frequency range [1, 3]. However, the circuit topology used in this baseline MMIC configuration outperforms the available hybrid results [1]. Furthermore, the 1.5 x 0.8 mm GaAs chip area corresponds to about 58 % reduction in the chip area used by the hybrid mHEMT reported in [1].

III. Simulations And Results

A scalable EEHEMT large signal model was used in the simulation. The S-parameters and noise figure simulated for the baseline MMIC LNA are shown in Figs. 2 – 4. Fig. 2 shows the simulated amplifier gain to be 37 ± 1 dB between 4 – 8 GHz. The input and output reflection coefficients are better than -15 dB at the centre-design frequency (Fig. 3). The noise figure is almost constant over the characterised frequency range with a value of 0.5 dB at 6 GHz. The total DC power consumption for the MMIC LNA is about 119 mW. On the average, the power consumption per stage is less than competing designs by 67 % [1].

A most important design criterion in MMIC LNA design for space applications is unconditional stability at any load and source conditions over any frequency range. This is obtained by computing the Rollet stability factor, K, of the two-port active network. The simulation results show that the amplifier is unconditionally stable up to the cut-off frequency of 95 GHz; the minimum K factor is 2.

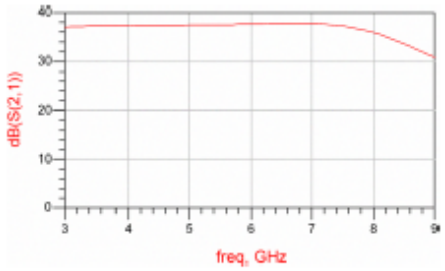

Fig. 2. The simulated gain for the MMIC LNA.

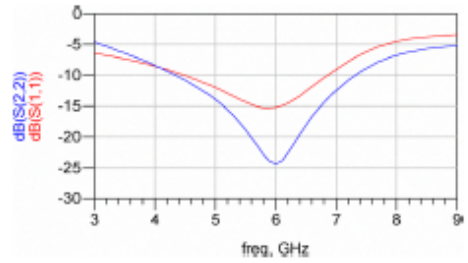

Fig. 3. The simulated input and output reflection coefficients for the MMIC LNA.

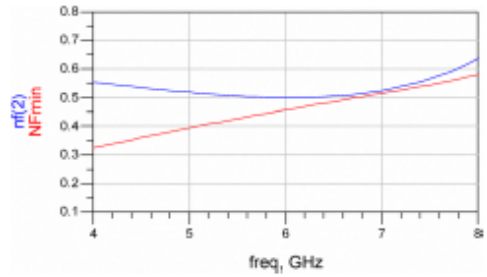

Fig. 4. Simulated noise figure (dB).

Furthermore, a figure of merit (FOM) [5] for MMIC LNA designs helps to give an indication of the amplifier performance given the overall design criteria. The higher the value of FOM for a given MMIC LNA design the better. The input and output FOMs for a MMIC LNA are respectively given by (2) and (3) as: [5]

$$FOM_{IN} = 10 \log ((S_{21}/S_{11})^{1/NF})BW/(D^2 f_c)$$

or

$$FOM_{IN} = ((S_{21})_{dB} - (S_{11})_{dB})BW/(D^2 f_c\, NF) \quad (2)$$

$$FOM_{OUT} = \frac{10 \log ((S_{21}/S_{22})\,((K + P1dB_{out})/P_{diss})BW}{(D^2 f_c)}$$

or

$$FOM_{OUT} = \frac{(S_{21})_{dB} - (S_{22})_{dB}(K + P1dB_{out})BW}{P_{diss}(D^2 f_c)} \quad (3)$$

where
FOM_{IN} = input FOM for the LNA
FOM_{OUT} = output FOM for the LNA
S_{21} = forward transmission gain (dB)
S_{11} = input reflection coefficient (dB)
S_{22} = output reflection coefficient (dB)
BW = characterised bandwidth of the LNA (GHz)
f_c = central design frequency of the LNA (GHz)
NF = noise figure of the LNA (dB)
P_{diss} = power consumption in milli-watt
$P1dB_{out}$ = output power at P1 dB compression point (dBm)
D = Size of the MMIC LNA in mm^2
K = 25 (a constant to eliminate negative FOM values).

All the parameters in (2) and (3) should have the average value within the operating bandwidth.

The FOM for the MMIC LNA reported in this paper was calculated and compared with those of existing designs. The input FOM yielded 23; this is about thrice the best available competing simulated design [1]. The MMIC LNA gave an output FOM of 4; at a 0 dBm P1 dB output power reference, this is 94 % higher than the best available competing simulated design [1].

TABLE I
SUMMARY OF SIMULATED C-BAND MMIC LNA RESULTS

Parameter	Existing Design [1]	Reported Design
Frequency band (GHz)	4 – 8	4 – 8
LNA stages	3	3
Noise figure (dB)	0.53	0.5
Linear gain (dB)	30±1	37±1
Power consumption (mW)	360	119
Size (mm^2)	1.9 x 1.5	1.5 x 0.8
Figure of merit	FOM_{IN} = 7 FOM_{OUT} = 0.2	FOM_{IN} = 23 FOM_{OUT} = 4
Technology	mHEMT	pHEMT

Table 1 summarises the key design and response parameters of comparison between the MMIC LNA design reported in this paper and the best available competing simulated design.

IV. MMIC LNA APPLICATIONS IN A HASS TRANSPONDER DESIGN

A satellite transponder consists of some units that are common to all transponder channels and others that are channel-specific. This equipment channel traverses the satellite system and connects the receive antenna with the transmit antenna. Within the HASS transponder system, the wideband receiver sits between the receive antenna and the input demultiplexer [4]. For a 500 MHz bandwidth, 20 MHz guard band and centre frequencies covering the entire C-band, a total of 120 transponder channels (TCs) are available with the MMIC LNA reported in this paper [4]. This implies 24 TCs per C-band frequency for either a downlink or an uplink transmission. Each set of 24 TCs can be adaptively mapped to form uplink and downlink transmission frequencies. The uplink uses the higher frequency range for each adaptively assigned C-band frequency. For the purpose of fequency reuse, polarisation techniqiues are applied to the adjacent TCs. Different polarisations prevent interference from occurring in the overlapped transponder bandwidths. Fig. 5 shows a C-band adaptive small satellite transponder system. The entire equipment channel consists of receive antenna, input filter (bandpass), low noise amplifier, adaptive local oscillator (ALO), intermediate frequency (IF) amplifier, DPM (demultiplexer, power gain and multiplexer) blocks and transmit antenna. The input signal from the receive antenna passes through the input bandpass filter before it is detected by the low noise amplifier. A portion of it is sent to the adaptive local oscillator to generate a corresponding constant oscillator frequency for the mixer network. The output of the mixer goes through an IF amplifier to the DPM blocks where it is demultiplexed, amplified and multiplexed. The multiplexed output signal is then transmitted at the appropriate downlink frequency and polarisation.

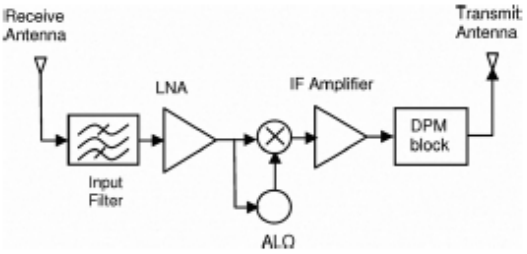

Fig. 5. C-band adaptive small satellite transponder.

V. Conclusion

A three-stage C-band (4 – 8 GHz) MMIC LNA (for a satellite transponder network) has been designed using InGaAs pseudomorphic HEMT. The latest broadband design presented in this paper uses the 0.15µm gate length LN InGaAs pHEMT technology. It has a linear gain of 37 ± 1 dB and noise figure of 0.5 ± 0.1 dB. Compared with available C-band designs, the power consumption per stage is less by 67 %. Also, the chip geometry corresponds to about 58 % reduction. This is very promising for an adaptive small satellite receiver system; the transponder can accommodate up to 120 channels multiplexed for various missions with no RF interference.

Further work involves the comparison of the noise temperature and gain measurement of the presented MMIC LNA design with the simulated responses.

Acknowledgement

The authors wish to thank Miss Mousumi Roy for her help in the preparation of this technical paper.

References

[1] M. Kelly, I. Angelov, J. P. Starski, N. Wadefalk, and H. Zirath, "4 – 8 GHz low noise amplifiers using metamorphic HEMT technology," in *Proc. 2006 European Microwave Integrated Circuits Conference*, pp. 118 – 121.

[2] Y. Wang, Y. Fu, W. Cui and W. Ma, "A broadband low noise amplifier design," in *Proc. 2008 Progress in Electromagnetics Research Symposium*, Hangzou, China, pp. 99 – 102.

[3] S. Ekpo and D. Kettle, "Mm-wave LNAs design for adaptive small satellite applications," in *Proc. 2009 Joint 5th ESA Workshop on Millimetre Wave and 31st ESA Antenna Workshop*, Noordwijk, Netherlands, pp. 843 – 847.

[4] D. Roddy and J. Coolen, *Electronic Communications*, Fourth Edition, New Jersey: Prentice-Hall, Inc., pp. 730 – 733, 1995.

[5] S. Bhaumik and D. Kettle, "Broadband X-Band LNA based on 70 nm GaAs mHEMT technology for deep space and satellite communication networks and oscillation issues," *Journal of IET Microwaves, Antennas & Propagation*, accepted for publication, June 2010.

3.2.9 Paper 9 [SE9]

A System-level Multicriteria Modelling of Payload Operational Times for Communication Satellite Missions in LEO, *Recent Progress in Space Technology*, Vol. 4, No. 1, pp. 67–77, June 2014.

DOI: https://doi.org/10.2174/2210687104666140620221119.

Sunday C. Ekpo[1] and Bamidele Adebisi[1], Danielle George[2], Rupak Kharel[1] and MfonObong Uko[1]

[1]Department of Engineering, Manchester Metropolitan University, UK

[2]School of Electrical & Electronic Engineering, The University of Manchester, UK

This subsection is an exact copy of Paper 9

Send Orders for Reprints to reprints@benthamscience.net

Recent Progress in Space Technology, 2014, 4, 000-000 1

System-Level Multicriteria Modelling of Payload Operational Times for Communication Satellite Missions in LEO

Sunday C. Ekpo[*,1,2], Bamidele Adebisi[1], Danielle George[2], Rupak Kharel[1] and Mfon Uko[2]

[1]Department of Electrical & Electronic Engineering, School of Engineering, Manchester Metropolitan University, Manchester, M1 5GD, UK

[2]Microwave & Communications Systems Research Group, School of Electrical & Electronic Engineering, The University of Manchester, Manchester, M60 1QD, UK

Received: 28 February 2014; Revised: 19 May 2014; Accepted: 19 May 2014

Abstract: The spacecraft payload operational time (SPOT) is amongst the main critical design considerations that must be optimised and validated during the system engineering analysis of a spacecraft mission. This requirement becomes more demanding for a communication satellite mission that relies on the functionality of the payload for its operation and service delivery. The design principles and performance budgets of the payload module are based on the subsubsystems and subsystems that enable the mission to be accomplished. The SPOT constraint is tied to the spacecraft size, weight and power (SWAP) limitations, operational modes of the subsystems and orbital patterns where the system is being deployed. This paper presents a system-level multicriteria optimisation of POTs for communication satellite (ComSat) missions in low-Earth orbit (LEO). The parameter space investigation (PSI) method was utilised to accomplish the multicriteria optimisation of the payload power and spacecraft mass. In the multicriteria optimisation and vector investigation (MOVI) process, 2048 tests were performed and the PSI was conservatively designed to yield 658 pareto optimal solutions vectors; a pareto optimal solution of 37.119 W for the payload module yielded highly adaptive microsatellite (HAM) mass and power margin of 97.021 kg and 23.366 W respectively. The required maximum subsystem power consumption for the power-storing mode is 25.703 W. From the analysis, the solar array capability was calculated to deliver 116.828 W for the mission; this forms the beginning-of-life design point. The prototype design for the ComSat mission yielded a maximum POT of approximately 494 minutes for the onboard payload processing and communication (downlink and uplink). The findings promise to enhance the design of a reliable and capability-based payload module for real-time digital video and broadband media, mobile services, interactive data transfer and voice communication.

Keywords: Adaptive small satellite, communication satellite, downlink, modelling, multicriteria, operational times, payload module, power budget, power contingency, power modes, space mission, system engineering, uplink.

I. INTRODUCTION

The spacecraft represent artificial man-made systems that operate in space and are utilised for wireless communication [1-5], navigation [1, 3, 5-9], remote sensing [3, 5, 10-14], space reconnaissance [3, 5, 15], weather forecasting [3, 5, 16-18], scientific investigations [3, 5, 13-16] and global security [17-20]. Communication satellites account for over 50% of the current operational satellites in space [5]. They complement the terrestrial telecommunication infrastructure in enabling data, video/motion pictures and voice exchange across different geographical locations on the Earth [1, 3-5, 12-16]. The large coverage of ComSats footprints makes them ideal for mobile applications anywhere including air, land and water.

A communication satellite consists of the core bus (or service) and the payload modules. The core bus module (CBM) of a ComSat encompasses the generic standard (CBM) of a ComSat encompasses the generic standard onboard elements which support the spacecraft missions. The CBM of a ComSat includes the electrical power, telemetry, tracking and command (TT&C), structural, attitude determination and control, thermal and propulsion subsystems [21, 22]. The payload module of a ComSat comprises the mission-specific RF/microwave communication repeater module as well as receiving and transmitting antennas [13-17, 20]. Fig. (**1**) shows the subsystems of a communication satellite. The primary structure provides the framework/skeleton for the rigidity of the spacecraft especially during launch; the secondary structure serves as the mounting surface for the satellite equipment. The solar array panels [23-25] utilise photovoltaic cells to generate electricity for the spacecraft; this is folded at launch and deployed when the satellite is in orbit [15, 26, 27]. The batteries supply the spacecraft's power needs at launch phase and during the period the solar array is in the Earth's shadow [28, 29]; this eclipse period can be up to 72 minutes depending on the satellite's orbit [5]. Avionics comprises the electronic equipment of the CBM that enable mission service functions such as power control and distribution, attitude and orbit control, TT&C, data handling and flight software management *via* the onboard

*Address correspondence to this author at the Department of Electrical & Electronic Engineering, School of Engineering, Manchester Metropolitan University, Manchester, M1 5GD, UK; Tel: +4479 5047 8245;
E-mail: cookey_sunday@ieee.org

2210-6871/14 $100.00+.00 © 2014 Bentham Science Publishers

computer. The propulsion subsystem enables pre-deployment orbit-raising (for energy efficiency) and attitude control; the service life of propulsive missions utilising chemical propellants is limited to approximately between 3 and 15 years. New propulsion technologies based on solar electric propulsion (SEP) (such as plasma and ionic propulsion systems) have been developed. Fig. (2) illustrates the building blocks of a communication satellite system; the international space station (ISS) is part of the space segment.

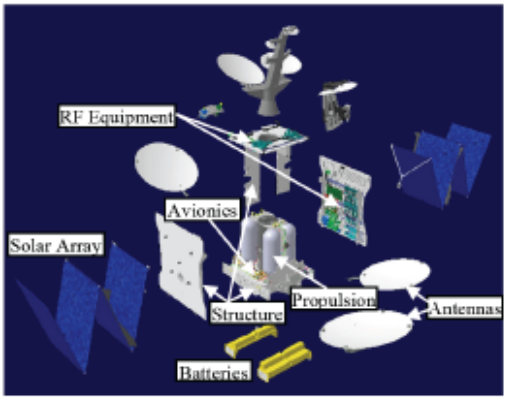

Fig. (1). Communication satellite subsystems [15].

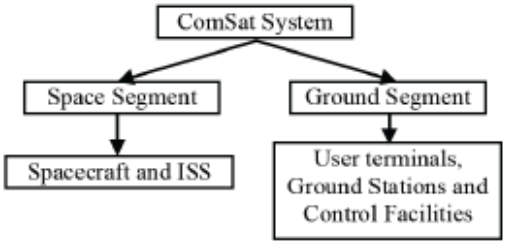

Fig. (2). Communication satellite system.

This paper is organised as follows. Section II explains the components and architectures of a communication spacecraft payload module. The operational times of spacecraft subsystems and modules are derived with recourse to the orbital patterns and mission power modes in section III. The multicriteria modelling of spacecraft payload operational times is reported in section IV. This section also outlines the key design parameters that are indispensable for studying the operational regimes of highly adaptive small satellites (HASSs). The results of the system-level multicriteria modelling of SPOT in LEO and the pertinent discussion are presented in section V. Both power/energy and mass budgets are covered for the candidate highly adaptive spacecraft (HAS). The considered payload provisioning case studies involve customer-furnished payload (CFP) and spacecraft team's payload (STP). Section VI concludes the paper.

II. SPACECRAFT COMMUNICATION PAYLOAD MODULE

A communications spacecraft payload receives signals from the Earth and other neighbouring spacecraft and transmits same to them *via* the onboard receive and transmit antennas respectively. The repeater subsystem represents the transponder and other mission-specific equipment deployed to translate the communication frequencies and perform filtering, demultiplexing, amplification and multiplexing of the signals carried by individual channels prior to routing to the correct space-based and/or Earth-based address.

Information-carrying electromagnetic (EM) waves are prone to distortion and interferences as the transmitted signals traverse the space links. Consequently, uplink signals (from the ground station to a satellite) and downlink signals (from a satellite to a ground station) are usually allocated non-overlapping frequency bands to enable non-interfering two-way communication. Furthermore, intersatellite or cross links also occur between neighbouring satellites in space. As promising as wireless communications *via* spacecraft may be, channel effects due to the weakening and distorting of the propagated signals occur. Depending on the channel conditions and the extent of signal degradation, the received signals approximate the transmitted information and/or data. Hence, payload signal enhancement and processing onboard the ComSat are carried out to curtail the channel effects. This has a system-level impact on the operational times of the payload processing and communications (uplinks and downlinks). Transparent (i.e., non-regenerative or "bent-pipe") repeaters typically amplify the uplink signals without processing it while regenerative repeaters effect an onboard processing of the received signals. Onboard antennas interface the transmitted and received signals with the communication payload (transmitters, payload-based signal conditioning avionics and receivers).

A bent-pipe payload architecture (BPP) (Fig. 3) only translates the transmitted uplink carrier frequency to another carrier frequency for downlink transmission and performs amplification without demodulating the received signal [25]. The BPP requires complex ground infrastructure to support the routing functions. The frequency conversion block is made up of a low noise amplifier (LNA), local oscillator (LO), mixer, travelling wave tube amplifier (TWTA) or solid state power amplifier (SSPA) and filter. Received waveforms channelisation is accomplished within the transponder subsystem using heavy weight and high power-consuming analog components. This usually results in a relatively poor overall system bit error rate (BER) since the uplink signal corruption is transferred to the downlink unchecked.

A full-processing payload (FPP) architecture allows for the uplink signal to be demodulated, decoded, re-encoded and re-modulated for downlink transmission (Fig. 4) [25]. With payload processing, flexible channelisation and routing schemes can be accomplished using digital devices for a sustainable system performance improvement. The probable complexity of the full-processing payload architecture is

traded-off with the capability(s) afforded by the digital components with recourse to the small footprint, reduced cost, light weight and low power consumption of the subsystems.

In between the bent-pipe and full-processing payload architectures is the partial-processing payload module (PPP). The PPP (Fig. 5) enables the uplink signal to be demodulated, beam-switched and re-modulated for the downlink transmission [25]. This module capability does not support received signal decoding onboard the ComSat. Moreover, the PPP suffers from end-to-end BER performance compared with the FPP due to the absence of uplink coding gain enhancement.

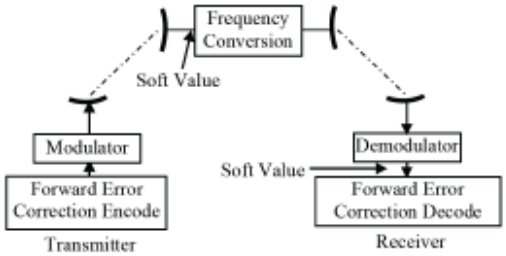

Fig. (3). A Bent-pipe payload architecture.

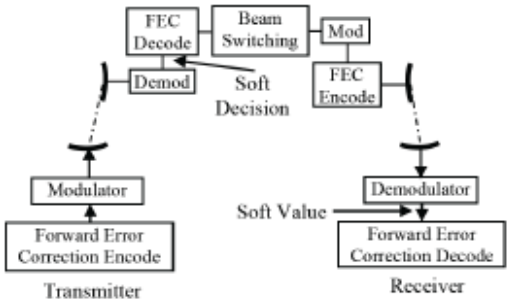

Fig. (4). A Full-processing payload architecture.

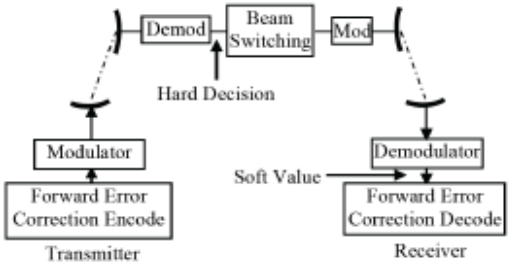

Fig. (5). A Partial-processing payload architecture.

The system-level architecture of highly adaptive spacecraft (HAS) employs adaptive multifunctional structural units (AMSUs) to achieve flexibility and functional and structural transformations during mission operations. Each AMSU carries embedded RF/microwave semiconductors and adaptive devices (such as field programmable gate arrays (FPGAs)) [1-4, 26-38]. Hence, the BPP, PPP and FPP can be functionally implemented onboard a HAS system depending on the mission requirements and the criticality of the communication applications. This level of modular system operation scaling, multicomponent-level customisation and capability-based deployment of the relevant payload architecture lend credence to the improved operational times and data transmission throughput.

III. PAYLOAD OPERATIONAL TIMES ANALYSIS

The total energy reserve of the spacecraft is reduced per an orbital period due to the eclipse period. The total energy produced by the spacecraft's solar panels, E_o, during a round-trip [4, 6] is given by:

$$E_o = P_{sp}(\tau_o - t_e) \quad (1)$$

where P_{sp} is the solar panel's average sunlit power generation in a given orbit. The sunlit power generation capacity of solar panels is used to develop the electrical energy production of spacecraft in orbits. For a two-power mode system, the following power modes' power consumptions are feasible: [4, 6]

1) Power-storing, P_s; and
2) Payload processing-overpower, P_p.

The total energy of the spacecraft during a single orbital period for a two-power mode system is given by: [4]

$$E_o = P_s t_s + P_p t_p \quad (2)$$

where E_s and E_p are the energy consumptions in the power-storing and payload processing-overpower modes respectively. The operational time of the payload processing-overpower mode, t_p, is given by: [4]

$$t_p = \tau_o - (t_s + t_e) \quad (3)$$

where t_s is the operational time of the power-storing mode.

From Eqns. 1 to 3, the operational time of the payload processing-overpower mode for a two-power mode system is obtained thus: [4]

$$t_p = \frac{E_o - P_s(\tau_o - t_e)}{P_p - P_s} \quad (4)$$

For a N-power mode system involving several power modes for single and multiple missions and post-mission applications, the following power consumptions are feasible [4]:

1. Power-storing;
2. Communication (downlink and uplink)-overpower, P_{dn}, with a corresponding time, t_{dn};
3. Uplink-overpower, P_u, with a corresponding time, t_u;
4. Payload processing-overpower; and
5. Other overpower modes, P_n, with a corresponding time, t_n, where n = 1, 2, ...

The energy budget balance for the above in-orbit mission applications is obtained thus: [4]

$$E_o = E_s + E_{du} + E_u + E_p + E_1 + E_2 + ... + E_N \quad (5)$$

The corresponding operational time of the payload processing-overpower mode is given by: [4]

$$t_p = \tau_o - (t_s + t_e + t_{du} + t_u + t_1 + t_2 + ... + t_N) \quad (6)$$

Hence, the in-orbit operational time of the payload processing-overpower mode, t_p, is derived using Eqns. 5 and 6 as: [4]

$$t_p = \frac{E_o - P_s(\tau_o - (t_s + t_{du} + t_u + t_1 + t_2 + ... + t_N)) - (P_1 t_1 + P_2 t_2 + ... + P_N t_N)}{P_p - P_s} \quad (7)$$

Equation 7 can be re-written thus: [4]

$$t_p = \frac{E_o + P_s(\sum_{i=1}^{N-2} t_i + t_e - \tau_o) - (\sum_{i=1}^{N-2} P_i t_i)}{P_p - P_s} \quad (8)$$

where P_i and t_i represent the ith power mode's power consumption and operational time respectively; the summations in Eqn. 8 consider all the power modes except the power-storing and the payload processing-overpower mode. In the case of calculating the operational time of a power mode other than the payload processing-overpower mode's, the latter is held constant and included in the summations while the considered power mode is excluded [4]. The various power modes' power consumptions and their corresponding operational times must be estimated in order to obtain the t_p for the spacecraft mission [4]. Furthermore, the power consumptions of the power-storing mode and the power mode whose operational time is being calculated must be estimated as well [4].

To maximise the operational time of a power mode, Eqn. 8 is adjusted to reflect the maximised power mode. Given the power consumption of the maximised power mode, P_{max}, the corresponding maximised operational time, t_{max}, is obtained as: [4]

$$t_{max} = \frac{E_o + P_s(\sum_{i=1}^{N-2} t_i + t_e - \tau_o) - (\sum_{i=1}^{N-2} P_i t_i)}{P_{max} - P_s} \quad (9)$$

Equation 9 is very useful for the multiobjective optimisation of the mission design variables in an integrated design environment. Hence, the operational time of any power mode can be modelled and optimised for a reliable, cost-effective and optimal-performing mission [4].

To understand and validate the operational times of spacecraft modules, subsystems and subsubsystems, a careful investigation and analysis of power estimating relationships (PERs) based on the orbital patterns must be carried out [39- 51]. Table **1** provides a summary of the PERs for communication satellites utilising a four-panel array in LEO [1-5].

Table **2** gives the core bus subsystems power allocation for HASS missions [1-3, 8-10, 21]. The two generic case studies considered are based on a customer-furnished payload (CFP) and a payload developed along with the core bus subsystems (i.e., spacecraft team's payload (STP).

The generic total in-orbit spacecraft power, P_T, of a spacecraft for a CFP is given by: [1-4, 21].

$$P_T = P_{pl} + P_{cb}(1 + C_f) \quad (10)$$

where P_{pl} is the payload power consumption (W) P_{cb}, the core bus power consumption (W) and C_f, the power contingency factor. The in-orbit power margin, P_{margin}, for the spacecraft mission is given by: [1-4, 21]

$$P_{margin} = \left(\frac{C_f}{1 + C_f}\right) P_T \quad (11)$$

For a HASS system with dynamic functional and structural in-orbit operations, Eqn. 10 is modified to reflect the varying power requirements that characterise the prevailing respective power modes of the mission. The power mode adjustment takes into account the differential power consumption, δP, occasioned by the dynamic operation and in-orbit onboard processing of a HASS system. The corresponding power margin constraint on Eqn. 11 is $P_{margin} \le P'_{margin} \le (P_{margin} + \delta P)$. The adaptive power margin function, P'_{margin}, is determined respecting the deterministic and dynamic capability-based mission applications. The total in-orbit power requirement of a HASS system for a CFP is accurately modelled by: [1-4]

$$P_T = P_{pl} + P_{cb}(1 + C_f)(1 - C_{lf}) + \delta P \quad (12)$$

For a STP, Eqn. 12 becomes: [1-4]

$$P_T = (P_{pl} + P_{cb})(1 + C_f)(1 - C_{lf}) + \delta P \quad (13)$$

where C_{lf} is the cable loss factor used to estimate the level of spacecraft subsystems integration. From Eqn. 13, the payload power margin is given by:

$$P_{plmargin} = P_{pl} C_f \quad (14)$$

Equation 14 is utilised to determine how much power margin is built into the payload module for the mission of

Table 1. Communication spacecraft PERs in LEO.

Satellite Mission	Communication
Satellite Category	Microsatellite
Case Study	Power Estimating Relationship
1	$P_T = 0.522 M_{HAM} + (1 + C_f)(1 - C_{lf})(0.0784 P_{pl} + 27.7485) + 0.5 P_{pl} + 7.78$
2	$P_T = 0.522 M_{HAM} + (1 + C_f)(1 - C_{lf})(0.5784 P_{pl} + 27.7485) + 7.78$

Cable loss factor: $0 < C_{lf} < 1$; Contingency factor: $0 < C_f < 1$; Case study: (1) Customer-held payload; (2) Payload developed along with the core bus subsystems.

Table 2. Core bus subsystems power allocation for HASS missions.

Subsystem	Percentage of Total Core Bus Subsystems Power Allocation (%)							
	Communication		Planetary		Meteorology		Other	
	STP	CFP	STP	CFP	STP	CFP	STP	CFP
Thermal	30.5	30.5	28.8	28.8	48.8	48.8	33.2	30.1
ADC	28.5	28.5	20.6	20.6	19.3	19.3	11.1	11.1
EPS	14.6	14.6	7.5	7.5	3.5	3.5	1.5	1.6
CDH	19.3	19.3	17.5	17.5	13.2	13.2	15.1	15.1
Coms	0	0	23.6	23.6	15.2	15.2	30.1	30.1
Propulsion	7.1	7.1	1	1	0	0	4.0	4.0
Mechanism	0	0	1	1	0	0	5.0	5.0

interest. In the case of a ComSat, the value of P_{plmargin} would vary depending on the payload technology adopted. Moreover, the operational times of the payload processing is influenced by the payload type, power mode(s) of the mission, spacecraft energy budget and the generated solar energy. The in-orbit solar power produced is dependent upon the orbital pattern(s) the communication spacecraft will be exposed to.

IV. MULTICRITERIA OPTIMISATION MODELLING OF SPOT

The operational times of the payload processing-overpower and communication-overpower modes for a candidate ComSat's payload technology is obtained with recourse to the average eclipse time per orbit and altitude of deployment (Table *3*).

Communication satellite systems require optimised system architectures for their reliability and mission accomplishment. The design of such complex engineering systems generally demands objective locational and procedural searches for optimal solutions. The optimisation problem statement for the ComSat mission and conceptual design objectives enables the feasible solution set and the optimal solutions to be obtained for the space equipment [4]. The parameter space investigation (PSI) method [52] has been created and developed to enable the construction of the feasible solution set for complex engineering systems such as space shuttle, unmanned vehicles, aeroplane, automobiles, ships, control systems, communication network nodes, metallurgical systems, robots and large-scale electrical energy generation systems. The PSI systematically investigates a multidimensional domain space and generates multidimensional points with each point representing a design prototype for the system under development [4, 52]. The integrated parameter space investigation-multicriteria optimisation and vector identification (PSI-MOVI) platform depends on the accurate development of the mathematical model governing the complex engineering system under investigation [4, 52].

The PSI method enables the identification, optimisation and analysis of constraints on design variables, functional dependencies and multicriteria. These parameters constitute the feasible solution set of the optimisation problem. The method comprises three major stages: compilation of test tables, selection of criterion constraints and verification of the solvability of the optimisation problem [4, 52].

In this paper, we applied the PSI method in the multicriteria design of the spacecraft payload operational times for highly adaptive communication spacecraft (HACS) missions in LEO. The mathematical model of the electrical power requirement of the payload module was developed based on past missions and emerging space systems technologies. We placed an objective emphasis on the HACS and its payload design variables that occasion dynamic, cost-effective and reliable operations with recourse to post-

Table 3. Design parameters for a communication satellite POT modelling.

Parameter	Description	Value
Spacecraft mass (kg)	Microsatellite	$95 \leq M \leq 100$
SPOT (mins)	Processing	$t_p > 0$
	Communication	$t_{DL} > 0$; $t_{UL} > 0$
Power-storing power, P_{ps} (W)	Power is generated; no payload processing and communication	$P_{ps} > 0$
Eclipse time, t_e (mins)	Payload processing and communication; no power is generated.	32.7
Orbital period, t_o (mins)	Power is generated; Payload processing and Communication.	94.6
Inclination (°)	Closed orbit; Elliptical	45
Altitude (km)	LEO	500

mission applications. We limited the scale of the optimisation problem to three design variables: the payload power, P_{pl}, total spacecraft power consumption during power-storing mode, P_S and mass of the communication satellite, M. We developed six functional constraints and eight criteria parameters respecting the candidate HACS mission. The functional and criteria constraints were set to minimise the total power consumptions of the HACS and its payload while maximising its operational times and power margins. The in-orbit dry mass and core bus power consumption during power-storing mode operation were also minimised in the optimisation problem. The results and discussion of the system-level multicriteria optimisation of the SPOT are stated in section V.

V. RESULTS AND DISCUSSION

In the multicriteria optimisation and vector investigation (MOVI) process, 2048 tests were performed and the PSI was conservatively designed to yield 658 pareto optimal solutions vectors. A pareto optimal solution of 37.119 W for the payload module yielded highly adaptive microsatellite (HAM) mass and power margin of 97.021 kg and 23.366 W respectively. The required maximum subsystem power consumption for the power-storing mode is 25.703 W. From the system-level analysis, the solar array capability was calculated to deliver 116.828 W for the mission and this forms the beginning-of-life design point. The prototype design for the HACS mission yielded a POT of approximately 483 minutes for the onboard payload processing and communication (downlink and uplink).

The results of the multicriteria optimisation of the SPOTs using a HAM are shown in Figs. (**6-11**). Fig. (**6**) illustrates the POT versus the mass of the communication satellite (HAM system) required. The POTs that satisfy the required payload power (35 W) and operational margins yield spacecraft mass of approximately 97 kg for the payload processing-overpower mode. Fig. (**7**) states the optimisation vectors histogram for the HAM system's mass requirement. The pareto optimal solution spans 95 kg to 100 kg to meet the business needs of the highly adaptive communication satellite mission implementation. It shows the histogram of the feasible and pareto optimal solutions for the first design variable (mass of HAM) for the HACS mission.

Fig. (**8**) shows the optimisation design vectors that represent the histogram of the feasible and pareto solutions set for the second design variable (payload power requirement) for the highly adaptive ComSat mission. The pareto optimal solution for the baseline power consumption of HAM's payload module is indicated by the green dots. These power consumptions are the minimum that can sustain the mission given the mission and conceptual design objectives. The optimisation result yielded 37.119 W as the best (minimum) baseline payload module power consumption for the mission. Fig. (**9**) presents the POTs versus the payload power requirement. To meet the business needs of the highly adaptive ComSat mission, the pareto optimal solution reveals a realistic POT of approximately 480 minutes.

Figs. (**10**, **11**) give the optimisation vectors histogram and POTs for the HAM power requirement during the power-storing mode operation (i.e., the third design variable). The maximum service bus power during the power-storing mode is 25.703 W. This core bus power is based on the minimum acceptable data capturing/reception, processing and transmission quality for the mission. In some cases, no payload processing is carried out and the aim is to enable the onboard batteries to be fully charged. This forms the SE design point in the choice of the components of the core bus module for the various mission modes [4, 6, 21, 53-54]. It is required for the mission to have enough power margin for emergent capabilities and operational uncertainties [4].

Table 4. Power budget analysis for a communication spacecraft mission.

System Engineering Technology & Architecture: HASS Analysis: Power Budget; Mission: Communication Payload holder: Spacecraft design team $P_S(\mathrm{W}) = 1.1568P_{pl} + 55.497$ $C_{MP} = 3\%$ %; $N = 4$; $M_{reflector} = 0.16$ kg; $P_{reflector} = 15$ W $M_{HAM} = M_{COTS}(1 - C_{MP}) + NM_{reflector}$ $P_T = 0.522M_{HAM} + 0.5P_S(1 + C_f)(1 - C_g) + 7.78 + NP_{reflector}$ Required payload power = 35 W Orbit: LEO; Design Phase: Conceptual Design Power contingency (C_f): 25% Class of Design: 2 (Next-generation) Cable loss factor, C_g: 0.017		
Satellite Category: Highly Adaptive Microsatellite (HAM) (97 kg)		
Core Bus Subsystem Power Allocation		
Core Bus Subsystem	**Allocation (%)**	**Power (W)**
Thermal control	30.5	18.08
Attitude control	28.5	16.89
Electrical power	14.6	8.65
Command and data handling	19.3	11.44
Communications	0	0
Propulsion	7.1	4.21
Mechanics	0	0
In-orbit Total Power Summary		
Parameter		Value (W)
Maximum available payload power in LEO		42.74
Maximum available core bus power in LEO		74.09
Required payload power		35.00
Calculated payload power		34.19
Payload power margin		7.74
Calculated core bus power		59.27
Core bus power margin		14.82
Total HAM subsystems power required		94.27
Power savings		3.13
Maximum power of a 97-kg HAM in LEO		116.83
Maximum available HAM power margin in LEO		23.37

Table 5. Mass budget analysis for a communication spacecraft mission.

System Engineering Technology & Architecture: HASS Analysis: Mass Budget; Mission: Communication Orbit: LEO; Payload holder: Spacecraft design team Design Phase: Conceptual Design; Mass contingency (C_f): 25% Class of Design: 2 (Next-generation); Cabling mass factor, C_{MF}: 3%		
Small Satellite Category: Highly Adaptive Microsatellite (HAM) Conventional on-orbit dry mass (kg): 100 Subsystem mass reduction (kg) = 3 Equivalent on-orbit dry mass of a HAM (kg) = 97 Total subsystem mass for allocation (kg) = (97/1.25) = 77.6		
Subsystem Mass Allocation		
Subsystem	Allocation (%)	Allocated mass (kg)
Structure	21.6	16.76
Thermal control	4.1	3.18
Attitude control	7.2	5.59
Electrical power	26.8	20.80
Propulsion	7.2	5.59
Communications	-	-
Command and data handling	4.1	3.18
Payload	29.0	22.50
HAM Mass Allocation Summary		
Parameter	Value (kg)	
Subsystem budget total	77.6	
Mass margin	19.4	
Mass-saving	3.0	
Maximum on-orbit dry mass	97.0	
Launch cost-saving ($)	30,000	

Table 4 shows the HASS power budget analysis for a communication mission based on the multicriteria optimisation outcomes. The SE analysis for the candidate LEO-deployed 97-kg HAM gives a payload power of 34.19 W with a corresponding payload power margin of 8.55 W. Assume that the payload subsystem consumes 35 W, the power margin of the payload would be reduced by approximately 9.5%. This payload power contingency is approximately 22% of the actual payload power and well above the 10% minimum power contingency required for the subsystem at lift-off [21]. The HASS power budget analysis for the case study communication satellite in LEO (Table 4) shows that the power generation capability of the 97-kg HAM is sufficient for it. Hence, given the payload power requirement, no deployable solar reflectors would be required. However, to boost the payload power and enable more mission functions and operational times, deployable solar reflectors can be integrated into the four-panel array of the HAM. The reflectors would increase the solar intensity of the solar panels by approximately 51%. The communications satellite services that can benefit from capability-based adaptive operational times include, but are not limited to, broadcasting satellite service (L-, S- and Ku-bands), mobile satellite service (L-, S-, Ku- and Ka-bands) and fixed satellite service (S-, C-, Ku- and Ka-bands). Regulating the operational times of the ComSat payload can enhance network flexibility, capacity and performance through shedding-off non-critical routine operations. The adaptive SPOT algorithm can also be implemented with payload technologies such as digital channelisation, multi-beam antenna, steerable beam antenna, space-based inflatable reflector antenna and space-based internet routers to achieve a sustainable and reliable space mission.

The functionalities of the power modes are mission-dependent. In the power-storing mode, only the command and data handling (CD&H) subsystem is kept active to enable the ComSat switch between power modes. The switching capability can be internally regulated or externally triggered (e.g., during flight into eclipse). The communications-overpower mode activates the downlink and uplink subsystems to transmit and receive data

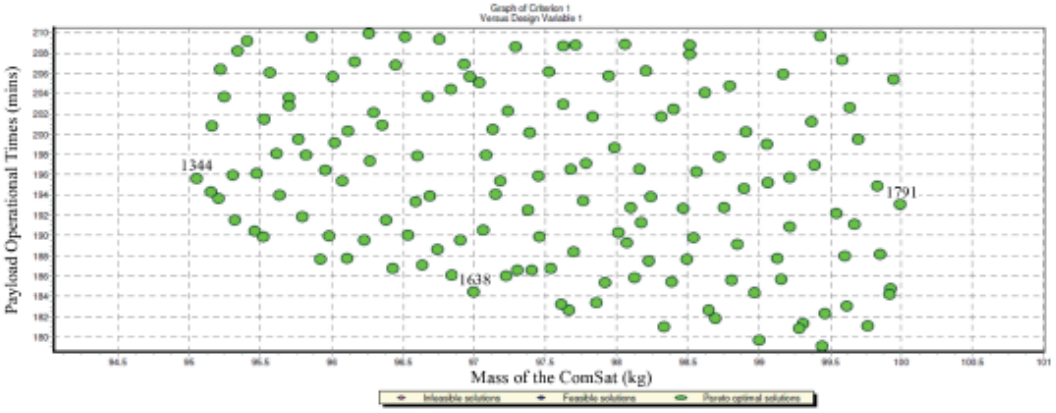

Fig. (6). Payload operational times versus mass of the communication satellite.

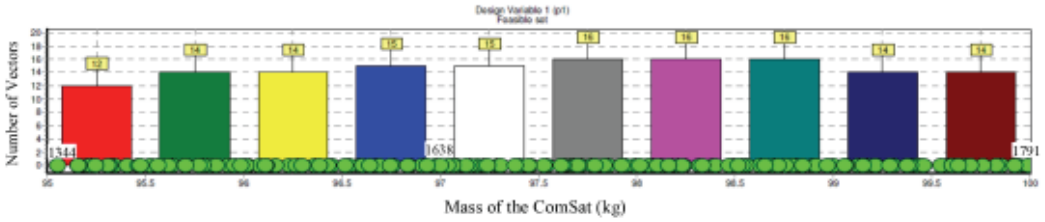

Fig. (7). Optimisation vectors versus mass of the communication satellite.

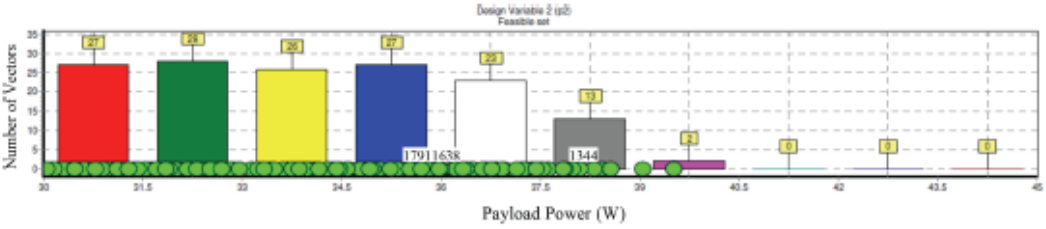

Fig. (8). Optimisation vectors versus the payload power requirement.

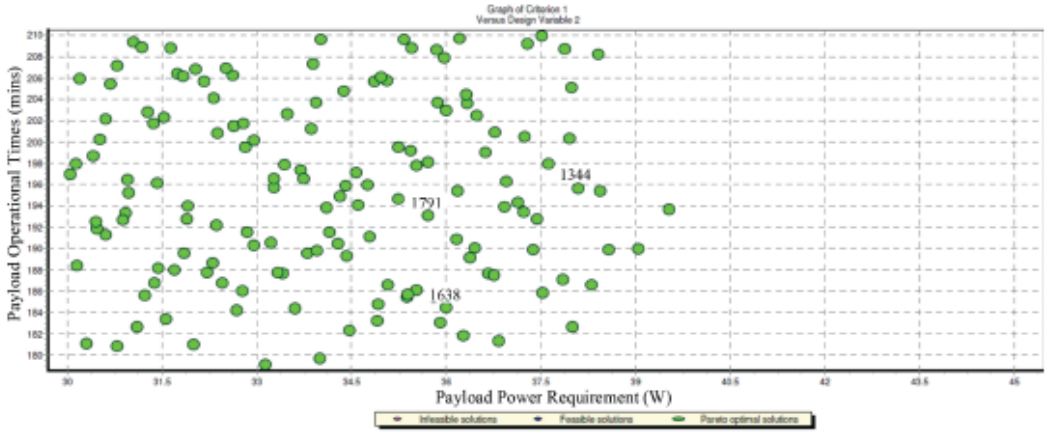

Fig. (9). Payload operational times versus the payload power requirement.

respectively. Similarly, during the processing-overpower mode, the communication subsystems (transmitters and receivers) are deactivated and the spacecraft assigns power and operational times to the CD&H and the FPP components concerned with onboard data processing only.

From Eqn. 4, the operational time of the processing-overpower mode can be negative for some orbits and hence, disqualifying such orbits for the ComSat mission requirements. Moreover, the negative operational times signify the excess power consumption of competing power modes. A case scenario might involve too much power consumption by the uplink and/or downlink subsystems during the communication over-power mode resulting in an ineffective mission sustenance by that orbital pattern. In Fig. (**11**), the multicriteria optimisation results show that the higher the power consumption of the service module during the ComSat's power-storing mode operation, the higher the operational time that the payload would require to complete its full data processing operation. This agrees with Eqn. 4 in that more power would have to be generated and/or reserved to meet the needs of the payload. While the power consumption of the core bus module may be relaxed by shutting down certain non-critical subsystems, the basic functionalities of the ComSat and its payload must be preserved. The AMSU architecture [10] permits component-level switching and hence, the ability to enable or disable power modes for an optimal operational time configuration. For instance, for a 26-W power-storing mode's power consumption in a single (round-trip) orbit, a 37-W, 40-W, 90-W and 100-W HAM payload module would require the

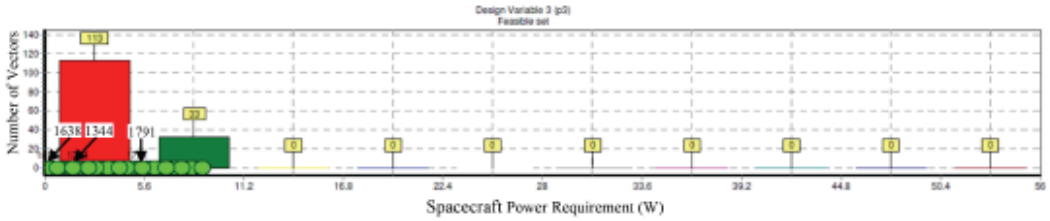

Fig. (10). Optimisation vectors versus the spacecraft power requirement (power-storing mode).

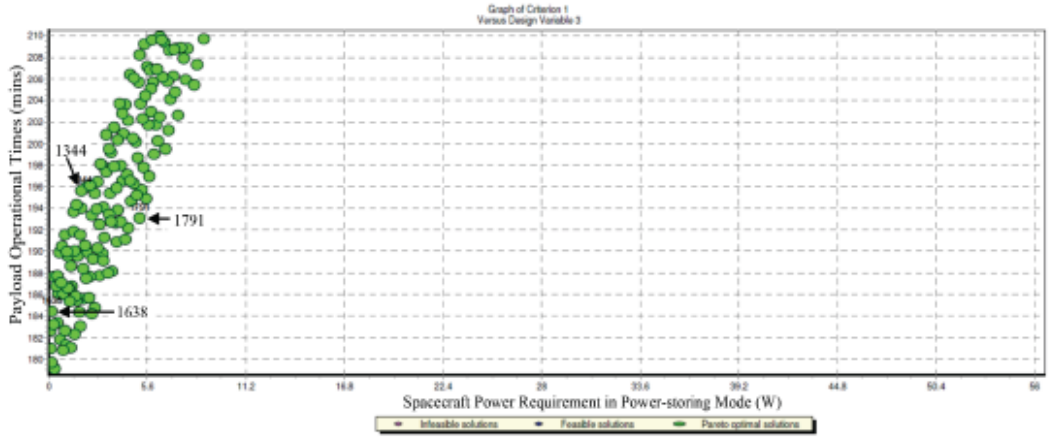

Fig. (11). Payload operational times versus the spacecraft power requirement (power-storing mode).

maximum operational times of approximately 494 minutes, 394 minutes, 88 minutes and 76 minutes respectively. The spacecraft mission designer can revise this energy reserve budget to allow for better orbital patterns to be utilised or modify the spacecraft subsystems to enable sustainable orbital patterns to be explored. Another option would be to review and modify the mission requirements by decreasing the required POTs or power consumptions of the power modes. The payload subsystems can be completely replaced or redesigned as the case may be. Thus, an adaptive spacecraft architecture (such as a HASS system) [1, 8, 10] which is flexible and easily amenable to this kind of critical mission objective(s) is required.

For a two-power mode, the minimum operational time occurs when the payload power approximates the in-orbit generated power. Hence, the intelligent switching network must be designed to ensure that the ComSat system does not overload itself and/or operate beyond its designed contingencies. The pareto optimal design vectors in Figs. (**6-11**) reveal a trade-off of the ComSat's in-orbit dry mass, size, power margins and modes, payload operational times, cost and performance metrics. The candidate pareto optimal vectors (POVs) for the SPOT analysis are 1344 (minimum mass), 1638 (medium mass) and 1791 (maximum mass). Each vector represents a unique performance requirement with recourse to the mission and conceptual design objectives. For instance, the POVs 1344, 1638 and 1791 correspond to the SPOTs of approximately 196 minutes, 193 minutes and 184 minutes respectively. The in-orbit spacecraft mass, payload power requirement and power-storing mode's power consumption of the CBM are respectively given thus: vector 1344 (95.051 kg, 38.093 W, 1.832 W); vector 1638 (97.000 kg, 36.000 W, 0.1367 W); and vector 1791 (99.988 kg, 35.706 W, 5.168 W). It is obvious from the optimisation results that the less the number of power-consuming components that operate during the power-storing mode of the satellite, the more the energy stored during a round-trip flight. Moreover, the SPOT is reduced as more power is committed to sustaining the onboard payload processing operation. The ratio of the available payload power to the power-storing mode's power consumption is approximately 310 for the POV 1638 and 25 for the POVs 1344 and 1791.

The operational times of the payload processing-overpower mode decreases as the payload power consumption increases for a constant power-storing mode's power consumption. For instance, given a communication-overpower mode (10-minute downlink consuming 100 W) and an uplink-overpower mode (10-minute uplink consuming 20 W), the maximum operational time available for a 100-W payload processing-overpower mode is 64 minutes; a 90-W payload would have a maximum of 74 minutes. This energy budget analysis is useful for the objective conceptual design of payload architectures and reconfigurable intelligent space-borne subsystems aimed at realising capability-based missions.

VI. CONCLUSION

This paper has presented a system-level multicriteria optimisation of spacecraft payload operational times for highly adaptive communication satellites in LEO. The business needs and operational constraints drive the payload technology and architecture deployed to achieve the required operational times. The power modes and orbital patterns of the mission also affect the operational times. The payload processing-overpower and data communications (uplinks and downlinks)-overpower modes are further delimited in their temporal assignments/slots by the power-storing mode's power consumption constraint.

In this research, three payload architectures were considered in the multicriteria optimisation process; bent-pipe, partial-processing and full-processing. With the highly adaptive spacecraft architecture, the real-time functional requirements of the communication satellite can be flexibly accomplished while in orbit. Furthermore, intelligent remote switching of payload power modes and subsystems reconfiguration are key to adapting the payload architecture to the dynamic mission requirements. The current business needs of the communication satellite mission limit the mass category to at least the upper end of microsatellites. The presented analysis can be extended to investigate the operational times of hybrid missions requiring capability-based system architectures.

Furthermore, the highly adaptive satellite system can adapt its mission capabilities to lengthen the design lifetime of the spacecraft thereby prolonging the mission and/or enabling a post-mission reuse.

CONFLICT OF INTEREST

The authors declare that there is no conflict of interest.

ACKNOWLEDGEMENTS

S.C. Ekpo and D. George specially thank the Akwa Ibom State University of Technology (AKSU/AKUTECH) and the Akwa Ibom State Government of Nigeria for the sponsorship of this research project. The authors express their appreciation to The University of Manchester, UK for the use of the institution's research facilities to achieve the technical findings that have been reported by them in this paper.

REFERENCES

[1] S. Ekpo, and D. George, "A system engineering analysis of highly adaptive small satellites," *IEEE Systems Journal*, vol. 7, no. 4, pp. 642-648, September 2013.

[2] S. Ekpo, and D. George, "A power budget model for highly adaptive small satellites," *Recent Patents on Space Technology*, vol. 3, no. 2, pp. 118-127, 2013.

[3] S. Ekpo, and D. George, "A system engineering consideration for future-generations small satellites design," *in Proc. IEEE First European Satellite Telecommunications Conference*, Rome, Italy, October 2012, pp. 1-6.

[4] S. Ekpo, D. George, and B. Adebisi, "A multicriteria optimisation design of spse for adaptive leo satellites missions using the psi method," *AIAA Space 2013 Conference & Exposition*, San Diego CA, USA, September 2013, pp. 1-19.

[5] S. W. Janson, "The future of small satellites," in *Small Satellites: Past, Present, and Future*, H. Helvajian, and S. W. Janson, Ed. Virginia: AIAA, Inc., pp. 771-810, 2008.

[6] S. S. Arnold, R. Nuzzaci, and A. Gordon-Ross, "energy budgeting for cubesats with an integrated FPGA," *IEEE Aerospace Conference*, Big Sky, Montana, March 2012, pp. 1-14.

[7] P. Mario, "Study of a cube-sat mission," University of Karl Franzens University of Graz, Austria, 2005, pp. 56-82.

[8] S. Ekpo, and D. George, "A system-based design methodology and architecture for adaptive small satellites," *in Proceedings of the 4th Annual IEEE International Systems Conference*, San Diego, CA, 2010, pp. 516-519.

[9] H. Schmitz, "Application examples: how to use fpgas in satellite systems," *Actel Corporation, California*, 2010, pp. 1-7.

[10] S. Ekpo, and D. George, "A Deterministic Multifunctional Architecture Design for Highly Adaptive Small Satellites," *International Journal of Satellite Communication Policy and Management*, vol. 1, no.2/3, pp. 174-194, August 2012.

[11] J. Saleh, D. Hastings, and D. Newman, "Spacecraft design lifetime," *Journal of Spacecraft and Rockets*, vol. 39, no. 2, pp. 244-257, 2002.

[12] T. Vladimirova, and D. J. Barnhart, "Towards space-based wireless sensor networks," *in Small Satellites: Past, Present, and Future*, H. Helvajian, and S. W. Janson, Ed. Virginia: AIAA, Inc., pp. 595-629, 2008.

[13] S. Ekpo, and D. George "Impact of noise figure on a satellite link performance," *IEEE Communications Letters*, vol. 15, no. 9, pp. 977-979, September 2011.

[14] S. Ekpo, and D. George, "4-8 GHz LNA design for an adaptive small Satellite Transponder using InGaAs PHEMT Technology," *in Proceedings of the 11th IEEE Wireless & Microwave Conference*, Melbourne, FL, 2010, pp. 1-4.

[15] Astrium Company, "Dissecting a communications satellite: what are all the parts for?" pp. 1, September 2011. http://www.astrium.eads.net/en/news2/dissecting-a-communications-satellite-parts.html.

[16] D. Barnhart, T. Vladimirova, and M. Sweeting, "Very-small-satellite design for distributed space missions," *Journal of Spacecraft and Rockets*, vol. 44, no. 6, pp. 244-257, November-December 2007.

[17] S. Ekpo, and D. George, "Reconfigurable cooperative intelligent control design for space missions," *Recent Patents on Space Technology*, vol. 2, no. 1, pp. 2-11, April 2012.

[18] B. Jackson, and K. Epstein, "A Reconfigurable multifunctional architecture approach for next generation nanosatellite design," *in Proceedings of the IEEE Aerospace Conference*, vol. 7, 2000, pp. 185-188.

[19] S. Ekpo, and D. George, "A Highly adaptive small satellites experiment for space missions modelling," *International Journal of Satellite Communication Policy and Management*, vol. 2, pp. 1-18, 2013.

[20] Lucente, E. Re, T. Rossi, E. Cianca, C. Stallo, M. Ruggieri, and A. Jebril, "IKNOW Mission: Payload Design for In-Orbit Test of W Band Technology," *IEEE Aerospace Conference*, 2008, pp. 1-10.

[21] C. Brown, "Elements of spacecraft design", Virginia: AIAA, Inc., 2002.

[22] T. James, and D. Shah, "*Transponder Tuning and Mapping*," U.S. 7950038, May 2011.

[23] F. Santoni, and F. Piergentili, "Analysis of the UNISAT-3 Solar Array In-Orbit Performance," *Journal of Spacecraft and Rockets*, vol. 45, pp. 142-148, January-February 2008.

[24] S. Ekpo, and D. George, "An adaptive radar design for small satellite missions," *in Proceedings of the World Congress on Engineering*, London, U.K, 5-8 July 2011, vol. 2, pp. 1380-1383.

[25] C. C. Wang, T. M. Nguyen, and G. W. Goo, "Satellite payload architectures for wideband communications systems," *IEEE Military Communications Conference Proceedings, (MILCOM 1999)*, vol. 2, 1999, pp. 865-869.

[26] S. R. Cvetkovic, and G. J. Robertson, "Spacecraft design considerations for small satellite remote sensing," *IEEE Trans. on Aerospace and Electronic Systems*, vol. 29, pp. 391-403, 1993.

[27] T. Vladimirova and C. Bridges, "Dual core system-on-a-chip design to support intersatellite communications," *NASA/ESA Conference on Adaptive Hardware and Systems*, 2008, pp. 191-197.

[28] W. C. Boncyk, "Revolutionary Design meets spacecraft reality: lessons learned," *Aerospace and Electronic Systems Magazine, IEEE*, vol. 25, pp. 25-31, 2010.

[29] F. Boltz, "Low-cost small-satellite delivery system" *Engineering Notes, Journal of Spacecraft*. vol. 39, no. 5, pp. 818-820, 2002.

[30] S. Ekpo, "Receiver G/T ratio improvement for space communications missions," *ARMMS RF & Microwave Society Conference*, UK, April 2011, pp. 1-2.

[31] Actel, "Radiation-hardened FPGAs," Ver.3.1, *Actel Corporation, California*, 2005.

[32] S. Rao, and D. Bressler, "*Multibeam and multiband antenna system for communication satellites*," U.S. 7868840, January 2011.

[33] L. Idkhajine, E. Monmasson, M. W. Naouar, A. Prata, and K. Bouallaga, "Fully integrated fpga-based controller for synchronous motor drive," *IEEE Transactions on Industrial Electronics*, vol. 56, pp. 4006-4017, 2009.

[34] Q. Liu, G. A. Constantinides, K. Masselos, and P. Y. K. Cheung, "Data-reuse exploration under an on-chip memory constraint for low-power FPGA-based systems," *Computers & Digital Techniques, IET*, vol. 3, pp. 235-246, 2009.

[35] J. J. Wang, R. B. Katz, J. S. Sun, B. E. Cronquist, J. L. McCollum, T. M. Speers, and W. C. Plants, "SRAM based re-programmable FPGA for Space Applications," *IEEE Transactions on Nuclear Science*, vol. 46, pp. 1728-1735, 1999.

[36] H. M. Quinn, P. S. Graham, M. J. Wirthlin, B. Pratt, K. S. Morgan, M. P. Caffrey, and J. B. Krone, "A test methodology for determining space readiness of xilinx SRAM-based FPGA devices and designs," *IEEE Transactions on Instrumentation and Measurement*, vol. 58, pp. 3380-3395, 2009.

[37] V. Agarwal, H. Arya, and S. Bhaktavatsala, "Design and development of a real-time DSP and FPGA-based integrated GPS-INS system for compact and low power applications," *IEEE Transactions on Aerospace and Electronic Systems*, vol. 45, pp. 443-454, 2009.

[38] H. Hsu-Chih and T. Ching-Chih, " FPGA implementation of an embedded robust adaptive controller for autonomous omnidirectional mobile platform," *IEEE Transactions on Industrial Electronics*, vol. 56, pp. 1604-1616, 2009.

[39] B.R. Bhat, "New radiation dose model for geostationary orbit," *Journal of Spacecraft and Rockets*, vol. 46, pp. 712-715, May-June 2009.

[40] Z. Shu, Y. Guo, and J. Lian, "Steady-state and dynamic study of active power filter with efficient FPGA-based control algorithm," *IEEE Trans. on Industrial Electronics*, vol. 55, No. 4, pp. 1527, 1528, April 2008.

[41] J. Saleh, "Flawed metrics: satellite cost per transponder and cost per day," *IEEE Trans. on Aerospace and Electronic System*, vol. 44, pp. 147-156, 2008.

[42] Y. Bentouton, "A real-time low complexity codec for use in low earth orbit small satellite missions," *IEEE Transactions on Nuclear Science*, vol. 53, pp. 1022, 1023, 2006.

[43] R. Hassan, and W. Crossley, "Spacecraft reliability-based design optimization under uncertainty including discrete variables," *Journal of Spacecraft and Rockets*, vol. 45, pp. 394-405, 2008.

[44] B.H. Calhoun, J. F. Ryan, S. Khanna, M. Putic, and J. Lach, "Flexible circuits and architectures for ultralow power," in *Proceedings of the IEEE*, vol. 98, pp. 267-282.

[45] P. C. Green, and R. F. Filipowsky, "Payload integration for space experimentation," *IEEE Trans. on Aerospace and Electronic Systems*, vol. AES-2, pp. 256-270, 1966.

[46] J. Zhenhua, L. Shengyi, and R. A. Dougal, "Design and testing of Spacecraft Power Systems using VTB," *IEEE Transactions on Aerospace and Electronic Systems*, vol. 39, pp. 976, 2003.

[47] J. Yancey, and Y. Kuo, "*Reconfigurable Communications Infrastructure for ASI Networks*," U.S. 7921323, April 2011.

[48] S. Ekpo and D. Kettle, "Mm-wave LNAs design for adaptive small satellite applications," *Proceedings of the Joint 5th ESA Workshop on Millimetre Wave and 31st ESA Antenna Workshop*, Noordwijk, Netherlands, 2009, pp. 843-847.

[49] L. Eunjeong, "Microsatellite combined attitude/energy systems," *IEEE Aerospace and Electronic Systems Magazine*, vol. 19, pp. 27-32, 2004.

[50] T. W. Kerslake, F. M. Haraburda, and J. P. Riehl, "Solar power system options for the radiation and technology demonstration spacecraft," *IEEE Aerospace and Electronic Systems Magazine*, vol. 16, pp. 9-19, 2001.

[51] R., Statnikov, and .A. Statnikov, "The Parameter space Investigation method," Artech House Publishers, Inc., London, 2011, pp. 13-94.

[52] D. Moon, and S. Song, "*Integrated Circuit Package System for Stackable Devices*," U.S. 7919871, April 2011.

[53] L. Tay, H. Bathan, and Z. Camacho, "*Integrated Circuit Package with Improved Connections*," U.S. 7919360, April 2011.

[54] A. Wang, "System and Method for Continuous Broadcast Service from Non-geostationary Orbits," U.S. 7877089, January 2011.

3.2.10 Paper 10 [SE10]

A Deterministic Multifunctional Architecture Design for Highly Adaptive Small Satellites, *International Journal of Satellite Communication Policy and Management***,** Vol. 1, No. 2/3, pp. 174–194, 2012.

DOI: https://doi.org/**10.1504/IJSCPM.2012.049543**.

Sunday Ekpo[1] and Danielle George[2]

[1]Department of Engineering, Manchester Metropolitan University, UK

[2]School of Electrical & Electronic Engineering, The University of Manchester, UK

This subsection is an exact copy of Paper 10

174 *Int. J. Satellite Communications Policy and Management, Vol. 1, Nos. 2/3, 2012*

A deterministic multifunctional architecture for highly adaptive small satellites

Sunday Ekpo* and Danielle George

Microwave and Communication Systems Research Group,
School of Electrical and Electronic Engineering,
The University of Manchester,
Manchester, M60 1QD, UK
E-mail: Sunday.Ekpo@postgrad.manchester.ac.uk
E-mail: scekpo@theiet.org
E-mail: Danielle.George@manchester.ac.uk
*Corresponding author

Abstract: A deterministic multifunctional architecture design approach for a highly adaptive small satellite system is proposed in this paper. It enables five levels of design customisation of all categories of highly adaptive small satellites; adaptive functional modules implement higher-level customised and reconfigurable mission functions. Each adaptive multifunctional structural unit (AMSU) supports the subsystem functions as a 'structural and functional block' and comes either as a baseline or hybrid. Associated functional sub subsystem components are contained in each AMSU. This removes the conventional structural and functional subsystem boundaries. A meteorology spacecraft mission using a highly adaptive nanosatellite reveals, besides more advanced mission capabilities, 0.6 kg and 1 W mass- and power-savings respectively over a conventional nanosatellite system implementation. This novelty results in adaptive, reconfigurable and multifunctional architectures with economies of scale, timely launch, system-level reliability, flexible integration and test options, cost-effective mass production, post-mission reapplication and optimal performance at the desired mission objectives.

Keywords: adaptive architectures; dynamic redundancy; field programmable gate array; functional reliability; highly adaptive small satellites; in-orbit adaptation; multifunctional; post-space mission reapplication; reconfigurable; spacecraft design customisation.

Reference to this paper should be made as follows: Ekpo, S. and George, D. (2012) 'A deterministic multifunctional architecture for highly adaptive small satellites', *Int. J. Satellite Communications Policy and Management*, Vol. 1, Nos. 2/3, pp.174–194.

Biographical notes: Sunday Ekpo obtained his BEng (Hons) in Electrical and Electronic Engineering at the Federal University of Uyo, Nigeria in 2001 and MSc in Communication Engineering at The University of Manchester, UK in 2008. He proceeded for a PhD study in Electrical and Electronic Engineering at The University of Manchester, UK with specialty in low noise amplifier design for satellite transponders, adaptive intelligent satellite constellations control and highly adaptive small satellite design for space applications. He has published technical papers in communications engineering and space satellite systems engineering. He is also a member of the American Institute of Aeronautics and Astronautics.

Copyright © 2012 Inderscience Enterprises Ltd.

Danielle George is a Senior Lecturer with the School of Electrical and Electrical Engineering, University of Manchester, Manchester, UK. She is the UK Lead Academic in the field of low noise amplifier research and has worked on radio astronomy telescope projects including the square kilometre array and the EU-funded FARADAY One Centimetre Radio 100-beam Array programme. She was part of the technical team to develop the low frequency instrument for the successfully launched PLANCK Space Telescope. Her research collaborations include Rolls Royce, The European Space Agency, The Indian Space Research Organization and The Chinese Academy of Science for Space Studies.

1 Introduction

The concept of highly adaptive small satellites (HASS) (Ekpo and George, 2010a, 2010b) for space applications is becoming more attractive with increasing possibilities for all frontiers of the space world (Ekpo and Kettle, 2009; Ekpo and George, 2010a, 2010b; Castillo et al., 2010; Franklin et al., 2006; Wittig, 2000; Vladimirova and Bridges, 2008; Schmitz, 2010; Actel, 2005; Jackson and Epstein, 2000; Shoer and Peck, 2009; Low and Zheng, 2007). Satellite systems operate in an unpredictable space environment and require system-level reliability for the onboard complex electronic components. For instance, cosmic rays coming from outside our solar system and charged particles streaming out from the sun in the solar wind impact device reliability in space applications. These react with gases in the upper atmosphere to produce high energy neutrons that interact with semiconductors to produce permanent failures in space satellites (Schmitz, 2010; Actel, 2005). Radiation-tolerant devices are inevitable for a reliable space operation. Hence, an adaptive device technology that fulfils this requirement is a plus for a successful space mission. Field programmable gate array (FPGA) architectures have been studied and qualified for the highly adaptive small satellite applications. Antifuse, static random-access memory (SRAM) and flash memory cells were analysed. The HASS system favours the Flash architecture because it is reprogrammable and retains its configuration when power is removed from the FPGA. Furthermore, a Flash-based FPGA is not affected by alpha particles and neutron-induced errors such as single-event upsets (SEUs). A high performance, robust, and reliable FPGA architecture combines the key features of existing radiation-tolerant FPGAs. Thus, a typical HASS system implements a highly reliable, radiation-tolerant, reprogrammable, non-volatile, low power (for space applications), and high speed (over 350 MHz) FPGA architecture (Schmitz, 2010; Actel, 2005). A key feature of the HASS system architecture is the high-level integration of different device-level technologies. Studies involving Si/SiGe and GaAs-based subsystem integration have been done. Two techniques have been identified for a possible HASS subsystem integration. These are area-efficient soldering bonding technique and flip-chip approach. The advantages of using the GaAs-based radio frequency (RF)/microwave subsystems on a Si-based (CMOS) (or GaAs-based) FPGA substrate are enormous. These include low interface bandwidth (due to a reduced number of possible external connections), super-high reconfiguration speed, increased useable gate density, 'radiation hardness', and reduced parasitic properties of electrical interconnections (resistance, capacitance and skin effect) (Ekpo and George, 2010b; Castillo et al., 2010; Vladimirova and Bridges, 2008; Schmitz, 2010; Actel, 2005;

Jackson and Epstein, 2000). A HASS is a reconfigurable, multifunctional and deterministic small space satellite that has capabilities for dynamic space applications and operations while retaining its designed optimal performance (Ekpo and George, 2010a). The obvious characteristics of a HASS system are complex system of systems (SoS), adaptability, multifunctionality, reconfigurability, and SoS's foundational attributes. It is envisaged as the key to realising reliable and optimal structural and functional reconfigurations for cost-effective small satellites (Ekpo and George, 2010a, 2010b; Castillo et al., 2010; Franklin et al., 2006; Wittig, 2000; Vladimirova and Bridges, 2008; Schmitz, 2010; Actel, 2005; Jackson and Epstein, 2000; Shoer and Peck, 2009). Thus, the HASS concept spans all categories of small satellites and supports space applications with very stringent requirements (Castillo et al., 2010; Franklin et al., 2006; Vladimirova and Bridges, 2008). The HASS architecture is built upon the existing design objectives for small satellites such as a nanosatellite (i.e., a satellite with a total mass of 1 to 10 kg). This novelty is expected to serve as a technology platform for the space community. The individual capabilities of HASSs are far greater than the conventional and existing reconfigurable small satellite architectures (Jackson and Epstein, 2000; Xuwen et al., 1998; Cvetkovic and Robertson, 1993; Lucente et al., 2008). This holds a great prospect for an expanding HASS constellations applications, robust inherent fault-tolerance, and reduced cost per satellite (Hassan and Crossley, 2008; Saleh, 2008; Saleh et al., 2002).

Figure 1 The highly adaptive small satellite design methodology

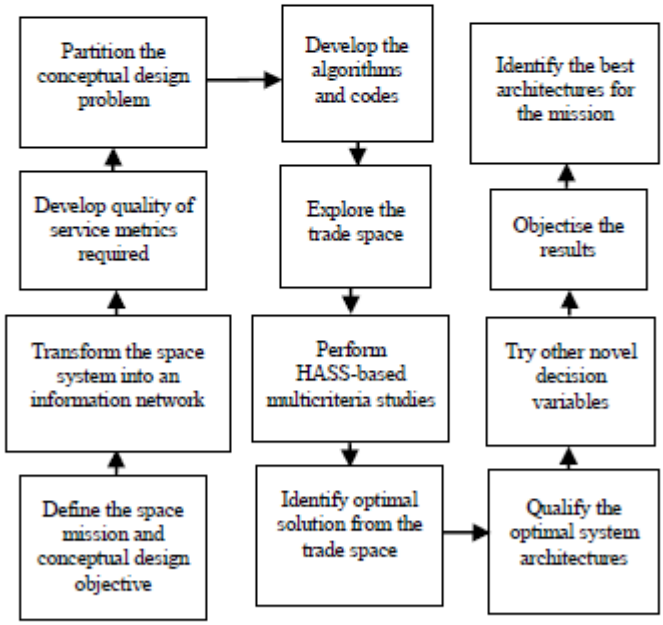

The design methodology (Ekpo and George, 2010a) for a HASS system is shown in Figure 1. This methodology addresses the space mission and conceptual design objectives with recourse to the service metrics. It also explores the system trade space for the best architecture for the mission.

This paper presents a functional design approach called the deterministic multifunctional architecture (DMA) concept. It is organised as follows. Traditional small satellite design techniques and challenges and the adaptive reconfiguration principle are presented in Section 2. Various scaling strategies are explained with emphasis on their respective applications and limitations at the subsystem and system-levels in Section 2. Section 3 addresses the functional design concept and the functional modules that constitute a typical small satellite. The emerging small satellite design technologies are discussed in Section 4. The building block of the proposed DMA follows in Section 5. Section 6 explains a case study of a meteorology spacecraft mission employing highly adaptive nanosatellite (HAN) and traditional nanosatellite. Section 7 concludes this paper.

2 Adaptive reconfiguration principle and miniaturisation strategies for small satellites

A discrete component-oriented concept has been the bane of conventional satellite design with a core structure serving as a mounting platform for single-function subsystems units. These units are electronic boxes and other discrete components that require heavy and bulky wire connections. Considerable difficulties spanning wire harness fabrication, shorts/breaks with the wire harness, installation, and testing characterise this technique. These challenges render this approach unreliable, uneconomical, and failure-prone (Jackson and Epstein, 2000; Xuwen et al., 1998). A scaled-down version of a conventional small satellite can be a feasible platform to start from using existing design paradigms. However, the resultant outcome yields a decreased satellite size with a corresponding disproportionately reduced structural overhead (Jackson and Epstein, 2000). The differing design objectives of traditional satellite components also limit the use of completely commercial off-the shelf (COTS) devices for the construction of satellite systems.

The principle of adaptive reconfiguration beacons on integrating the concepts of kinematics and passive dynamics (Shoer and Peck, 2009) with adaptive multifunctional structural units (AMSUs) (Ekpo and George, 2010a, 2010b). In the former, deterministic kinematic constraints are used to realise a stable process of configurations. This reconfigures the small satellite system to a desired end state without any recourse to an active control or power inputs. The proposed adaptive reconfiguration system leverages on the enabling structural reconfiguration of the flux-pinning interactions (FPI) technology and the functional reconfiguration of the DMA concept.

Consider a multicell HASS system with each AMSU comprising a matrix of adaptive and reconfigurable elements. The adaptive incidence matrix (Shoer and Peck, 2009) of the system is akin to the FPI-based structural reconfiguration mechanism but with an allowance for functional reconfiguration. The developed adaptive incidence matrix of a modular HASS system is given by:

$$S_A = \begin{array}{c} \\ C_o \\ C_1 \\ \vdots \\ C_i \\ \vdots \\ C_n \end{array} \begin{array}{c} \begin{array}{cccccc} u_1 & u_2 & \cdots & u_a & \cdots & u_n \end{array} \\ \begin{pmatrix} +1 & 0 & \cdots & 0 & \cdots & 0 \\ -1 & \delta^1_{2A} & \cdots & \delta^1_{aA} & \cdots & \delta^1_{nA} \\ \vdots & \vdots & & \vdots & & \vdots \\ 0 & \delta^i_{2A} & \cdots & \delta^i_{aA} & \cdots & \delta^i_{nA} \\ \vdots & \vdots & & \vdots & & \vdots \\ 0 & \delta^n_{2A} & \cdots & \delta^n_{aA} & \cdots & \delta^n_{nA} \end{pmatrix} \end{array} \tag{1}$$

and

$$S_{HASS} = \begin{array}{c} \\ S_{A0} \\ S_{A1} \\ \vdots \\ S_{Ai} \\ \vdots \\ S_{An} \end{array} \begin{array}{c} \begin{array}{cccccc} u_1 & u_2 & \cdots & u_a & \cdots & u_n \end{array} \\ \begin{pmatrix} +1 & 0 & \cdots & 0 & \cdots & 0 \\ -1 & \delta^1_{2A} & \cdots & \delta^1_{aA} & \cdots & \delta^1_{nA} \\ \vdots & \vdots & & \vdots & & \vdots \\ 0 & \delta^i_{2A} & \cdots & \delta^i_{aA} & \cdots & \delta^i_{nA} \\ \vdots & \vdots & & \vdots & & \vdots \\ 0 & \delta^n_{2A} & \cdots & \delta^n_{aA} & \cdots & \delta^n_{nA} \end{pmatrix} \end{array} \tag{2}$$

$u_{nA} = u_1, u_2, \ldots u_a \ldots u_n$ of AMSU m and $n = 1, \ldots m$; $C_0, \ldots, C_n$ represent each cell in an AMSU, S_A (where C_o is a fictitious base cell; $u_1, \ldots u_n$ represent the joints connecting each cell); S_A is an adaptive multifunctional structural unit incidence matrix; S_{HASS} is a highly adaptive small satellite system multicell incidence matrix; a_A is the adaptive incidence matrix joint index; i, j, k are the adaptive incidence matrix cell indices. δ^i_{aA} is the FPI (linking) activity state parameter (Shoer and Peck, 2009); it defines the process state of the flux-pinned interface specified by joint a_A. Consider interface u_{1A} linking AMSU blocks S_{Ai} with S_{Aj}, then the values of the activity state parameters in column A become:

$$\delta^i_{aA} = -1, \quad \delta^j_{aA} = +1, \quad \delta^k_{aA} = 0; \quad k \neq i, j \tag{3}$$

Furthermore, n cells with interfaces require n^2 activity state parameters to adaptively "connect any two bodies and reconfigure the incidence matrix" (Shoer and Peck, 2009). Flux-pinned joints with multiple degrees of freedom have been developed and include revolute, cylindrical, and prismatic joints (Shoer and Peck, 2009). It can be deduced from the above analysis that both functional and structural reconfigurations can be adaptively realised by integrating the FPI and the proposed AMSU technologies. This would enhance the design of next generation/future small satellites for capability-based, robust, and reliable space applications. This paper focuses on the adaptive multifunctional reconfiguration architecture design of small satellites; the interested reader is referred to (Shoer and Peck, 2009) for an in depth treatment of structural reconfiguration and incidence matrix generation.

There are various existing lightweighting techniques (Ekpo and George, 2010a; Jackson and Epstein, 2000; Ekpo and Kettle, 2009; Xuwen et al., 1998; Cvetkovic and Robertson, 1993) that have been developed to scale down conventional satellite design

concepts to suit the small satellite system. The following section gives the existing and emerging scaling strategies for small satellite systems. The implication(s) of each lightweighting approach is explained relative to the reported DMA concept.

2.1 High-level integration

This strategy implements multiple advanced satellite functions on a single circuit card or within a single electronics box. The fixed architecture of this lightweighting technique limits the flexibility of missions operations. Thus, emergent missions and requirements would be difficult to implement. The DMA design concept overcomes this by using an adaptable architecture that reconfigures the satellite functionally and structurally with no subsystem boundaries.

2.2 Low-level integration

This lightweighting practise implements multiple functions of a satellite within a single monolithic microwave integrated circuit (MMIC). This design technique has favoured customised systems and applications as evident in application-specific integrated circuits and multichip modules technologies. This design strategy makes missions flexibility difficult. The HASS system architecture performs in-orbit substrate-level reconfigurations without the need for a physical module replacement. Thus, once the size of a HASS system architecture is agreed upon, various missions and capabilities can be implemented onboard it.

2.3 Modularisation

This technique segments a satellite into function- or subsystem-specific discrete units. The presence of subsystems boundaries that characterise traditional small satellite systems is absent from a HASS system. In the latter, the modularity is achieved remotely at the functional and structural reconfiguration levels. Instead of having a dedicated module for a major subsystem, the HASS architecture uses AMSUs to implement its unique subsystem function for an emergent mission requirement.

2.4 Microtechnology

This involves the use of advanced and high-density electromechanical and micromachined devices. The HASS system architecture favours small microtechnology applications due to its adaptive structural and functional reconfigurations. In this case, no substantial volumetric inefficiency is obtained. The respective microtechnology applications for the HASS system are adaptively reconfigured with an excellent electrical and volumetric efficiency.

2.5 Nanotechnology and microelectronics

This strategy implements satellite functions using devices that operate at the molecular and/or atomic level. The last decade has witnessed unprecedented developments in space-qualified nanoscale technologies. However, the design technique that reaps the full benefits of nanotechnology and microelectronics is lacking. Hence, the proposed DMA

design enables beyond-state-of-the-art capabilities of the space-qualified nanotechnology and microelectronics systems.

2.6 Repackaging

This involves structural repackaging by achieving a lighter redesign of the chassis and enclosures, using different materials or completely removing them. This scaling strategy reduces the structural overhead of conventional subsystem-oriented design techniques. The HASS architecture implements most of its electronics on a 'common-substrate' and so adapts existing mission functionalities within a reconfigured subsystem module.

The above scaling techniques have advantages and disadvantages. Hence, each strategy cannot be wholly suitable for achieving a reliable and efficient small satellite design. Merits such as substantial size, weight, and power reductions can be realised in a number of subsystem functions. Other feasible subsystem advantages include increased reliability, robustness, inherent redundancy, and lower recurring cost. The obvious challenges include, but not limited to, immature technologies and devices for space applications, adaptability constraints, and mission-specific limitations.

The space community has continued to respond responsibly to the ever-widening demand for cost-effective space missions using high performance and reliable satellite architectures. This has orchestrated unprecedented research and development activities in very small satellites technologies for distributed space missions and operations. Consequently, very small satellites technologies such as microelectromechanical systems and microfabrication, co-orbiting satellite assistant concept, multichip module, SpaceChip, CubeSat, and printed circuit board satellite (PCBSat) have been developed (Barnhart et al., 2007, 2009). These focus on satellites with masses below nanosatellites and have received enormous research efforts and investments across the globe. The HASS system can be adaptively reconfigured to handle sub-kilogram spacecraft applications within its functional substrate network.

3 The functional design concept

This section addresses the functional design concept (Ekpo and George, 2010a; Shoer and Peck, 2009) that serves as a beacon for the DMA. It is opposed to the subsystem-oriented design approach and leverages on the scaling techniques discussed in the previous section. The design process eliminates conventional subsystem boundaries but realises functions. It focuses on the identification and specification of subsystem-level functional requirements. In this approach, the functions of several subsystems are implemented on a single circuit card.

The DMA uses the modularity and high/low integration lightweighting strategies to achieve an efficient small satellite design. It uses functional modules to realise high-level mission-specific and non-specific functions. Subsystem functions are implemented on structural building blocks called AMSUs.

Figure 2 shows the functional modules of a small satellite that employs the functional design paradigm (Ekpo and George, 2010a; Wittig, 2000; Jackson and Epstein, 2000). A typical DMA design encompasses four functional modules (Figure 2). These modules give the satellite system modularity that supports high-level functionality required for customised space missions. Each adaptive multifunctional structural unit comprises a

composite panel that provides mechanical, electrical and thermal functionalities (Jackson and Epstein, 2000).

Figure 2 Functional modules of a functionally designed small satellite

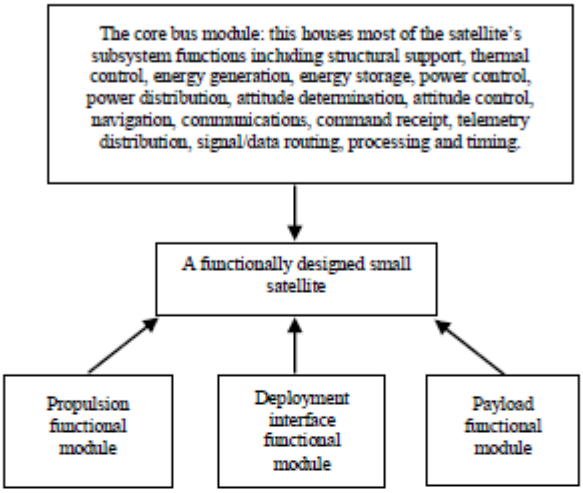

4 The emerging space system design platform

Underlying technologies and techniques for developing lightweight satellite systems for space missions have been discussed and the respective merits and demerits identified. Though some of these strategies can be used for building simple small satellites, the enabling design for implementing a highly adaptive high performance and reliable space system is lacking. It is therefore indispensable that a new design approach that harnesses the volumetric and electrical efficiency of the strategies with flexibility be developed.

Figure 3 Levels of HASS system design customisation

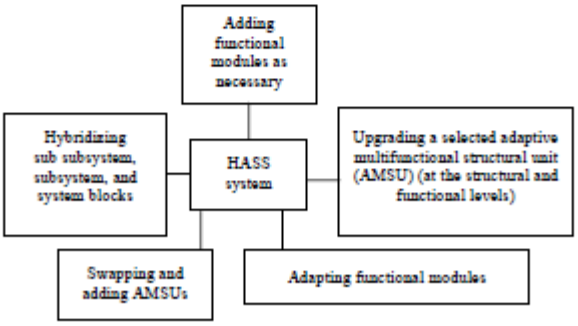

The proposed DMA is a functional design approach that offers and/or permits five levels of design customisation (Figure 3) for a spacecraft system. It integrates and incorporates the scaling strategies and technologies within a highly adaptive and reconfigurable platform. The following discussions explain the HASS technology framework. Figure 4 shows the system-level technologies and design variables sources for developing the architecture of the HASS system.

Figure 4 The HASS technology framework/architecture

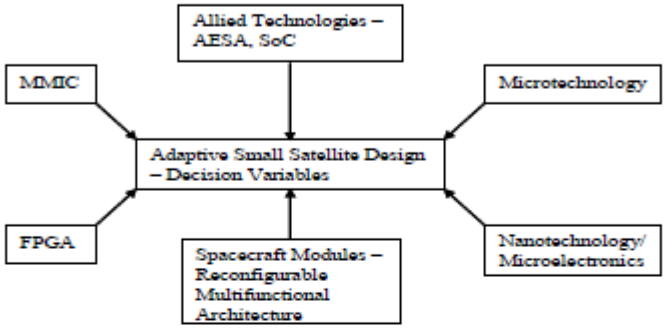

Microwave integrated circuit design technologies have greatly advanced due to the novel research development efforts in circuit fabrications technologies and stringent RF performance requirements (Ekpo and Kettle, 2009; Ekpo and George, 2010a, 2010b; Castillo et al., 2010; Vladimirova and Bridges, 2008; Xuwen et al., 1998; Barnhart et al., 2007, 2009). The MMIC technology enables RF and microwave (active and passive components) systems designs on the same semiconductor substrate. It has been applied in many space systems (Ekpo and Kettle, 2009; Vladimirova and Bridges, 2008; Xuwen et al., 1998). The HASS system architecture sustains the MIC technologies within its AMSUs without any rigid subsystem boundaries.

FPGA is an adaptive technology device that contains a matrix of reconfigurable gate array logic circuitry. It is highly deterministic and characterised by high speed, high reliability, and parallel hardware. A FPGA chip contains a finite number of configurable blocks (predefined elements) with programmable interconnects geared at implementing a reconfigurable digital circuit. The HASS system architecture is based on a monolithic FPGA architecture with allowance for RF and microwave and MEMS integration within a common substrate platform.

System-on-a-chip (SoC) technology has found a tremendous patronage for distributed satellite systems including formation flying, clustering missions, and virtual satellite missions (Vladimirova and Bridges, 2008). A SoC implementation in an FPGA has been reported for a picosatellite test mission (Vladimirova and Bridges, 2008; Schmitz, 2010; Actel, 2005). This has enabled the development of deterministic processors for in-orbit autonomous operations of space satellites. The integration of the FPGA-SoC-based design concept promises to enhance the data and signal processing capability of the HASS system.

Microtechnology applications that would benefit immensely from the adaptive multifunctional structural unit design concept of HASS are summarised in Table 1

(Jackson and Epstein, 2000). The HASS system architecture provides the associated onboard resources that support these various microtechnology applications at the subsystem-level.

Table 1 Microtechnology applications in a HASS system

Subsystem	*Microtechnology applications*
Structure	Adaptive damping structures and microlaminate structures
Mechanism	Micromirror actuators and millimachined actuators
Thermal control	Microlouvers
Propulsion	Mcironozzle array
Electrical power	Microturbine and micro switches
Attitude determination and control	Micro magnetometer, accelerometer, and gyros
Communication	Micro filters, delay lines, and configurable array antennas
Command and data handling	Micromechanical computer

Various microelectronic and nanotechnology systems that scale down the size, power consumption and weight margins of a space satellite have been proposed (Jackson and Epstein, 2000; Xuwen et al., 1998). These include molecular, nanomechanical, and quantum computers, single electron transistors, quantum dot cells, conducting molecular wires, self-assembling circuit arrays, and nanomanipulators (Jackson and Epstein, 2000). They can be realised onboard a HASS system due to the substrate configurations that embrace the key application potentials of microelectronics and nanotechnology (Ekpo and George, 2010a, 2010b).

Active electronically scanned array (AESA) technology is an emerging radar system platform that has received a fast growing popularity from the aerospace community in the last decade (Moore, 2010). AESA is an airborne radar technology that has advanced capabilities such as fast electronic scanning, flexible transmit power, multiple receive channels, electronic scan array architecture, and adaptive functionality. An AESA radar comprises several transmit/receive (T/R) array modules with distributed power capabilities for multiple air-to-air and air-to-ground coverage onboard an aircraft. Respecting the HASS structural framework, AESA architecture design is highly reliable and holds prospects for ease of integration with RF and microwave systems on a common substrate. GaAs technology is the current driving technology for AESA radar design for aircraft surveillance applications; this favours spacecraft missions due to its 'radiation hardness' (Ekpo and Kettle, 2009; Moore, 2010).

Furthermore, the adaptive reconfigurable multifunctional architecture (ARMA) concept (Ekpo and George, 2010a, 2010b; Jackson and Epstein, 2000) has been proposed for designing and developing the HASS architecture. ARMA is a modular design technique with recourse to high/low level integration of RF and microwave components.

5 The building blocks of a DMA

AMSUs are the building blocks of the DMA concept. In this section, the enabling technologies, architecture and functionality of the AMSUs are discussed in detail. The functional design concept provides a network of functionality whereby the divers intrinsic functions constitute nodes within it (Ekpo and George, 2010a; Wittig, 2000).

Single and multiple components-based functions and single/multipurpose components are possible. The proposed DMA employs this design philosophy in its AMSU architecture. Thus, each AMSU board can implement virtually all of the HASS functions. Since the various functions interact in an adaptive manner with one another through a common bus, the AMSU architecture promises great design modularity, flexibility, reliability, and cost benefits. The reprogrammable interconnects of the integrated FPGA (National Instruments, 2009) blocks can be 'soft-wired' for an adaptive and predictive performance. The programmable FPGA blocks' interconnects are borne on the MMIC of the AMSU. Allied technologies such as radio frequency identification (RFID) and RF-MEMS (Chazelas and Merlet, 2009) can also be used to transfer data within and between AMSUs thereby eliminating bulky wire harnesses. Figure 5 shows the two AMSU architectures proposed for the HASS system: Figure 5(a) and Figure 5(b) represent the baseline and hybrid DMA building blocks respectively. The baseline adaptive multifunctional structural unit has a dedicated non-signal processing and control section delineated from the FPGA block on a common substrate. The hybrid adaptive multifunctional structural unit contains a matrix of FPGA chip blocks with the rest of the RF and microwave components on the same substrate platform.

Figure 5 The building block of DMA, (a) a baseline AMSU (b) a hybrid AMSU (see online version for colours)

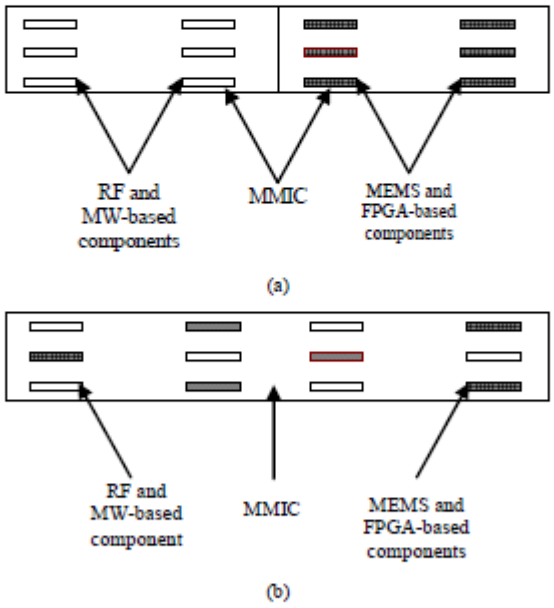

Figure 6 illustrates a multichip AMSU module design with vertical and horizontal module (or cluster) configurations. The AMSU upgradeable components include, but not limited to, RF and microwave subsystems, FPGAs, processors, and discretes. Compared with traditional and existing functional design-based satellites (Ekpo and George, 2010a; Wittig, 2000; Vladimirova and Bridges, 2008), physically replaceable/upgradeable components of the AMSU are fewer; this is a huge cost benefit for any space mission.

Figure 6 A multichip design of an AMSU module, (a) a vertical baseline AMSU module configuration (b) a horizontal baseline AMSU module configuration (see online version for colours)

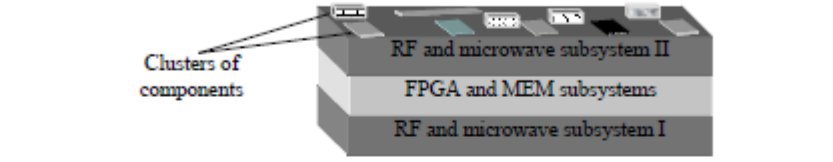

(a)

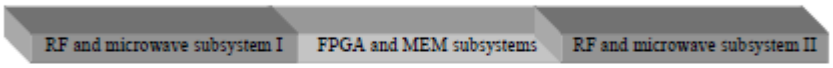

(b)

A top-level candidate DMA conceptual design consists of six AMSUs: a top deck (for providing separation and mounting interfaces), a bottom deck (for providing further mounting surfaces), a power control AMSU, an attitude/navigation AMSU, a communications AMSU, and a data processing AMSU. Each AMSU board is reprogrammable and/or reconfigurable at the functional level. With appropriate kinematic mechanisms, structural-level transformations (Shoer and Peck, 2009) are possible with the DMA block for a full-scale reliable autonomous HASS system. Moreover, each AMSU block can exhibit '3-D adaptive configuration and reconfiguration'. Thus, data and information flows can be volumetric and planar; the HASS architecture enables the various sub subsystems and subsystems to share signals and intelligence in a N-dimensional space through its inherent novel vertical, horizontal, and oblique substrate orientations.

A network functionality of the AMSUs reveals one common bus and one internode bus for a reliable, uninterruptible, and efficient interoperation of functional modules. Figure 7 illustrates the functional nodes of a HASS system based on the DMA concept.

Figure 7 A dynamic network of functions

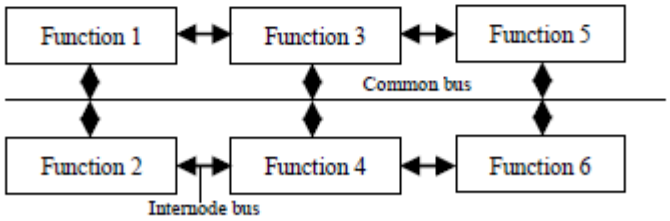

The proposed DMA concept for designing HASS enhances in-orbit space satellite reconfiguration at the functional and structural levels. Three regimes of adaptive reconfiguration are possible based on the intended/emergent application and orbital parameters: F (functional), S (structural) and FS (functional and structural). These regimes of highly adaptive small satellite reconfiguration can be performed at the adaptive multifunctional structural unit cell and block levels. Table 2 summarises the key features of a HASS system.

Table 2 A summary of the characteristics of a HASS system

Parameter	*HASS system applications*
Basic design concept	Structural and functional
Adaptive design paradigm	Adaptive reconfigurable multifunctional architecture
ARMA configurations	Baseline and hybrid
Advanced ARMA configurations	Multilayered baseline and hybrid
Building blocks of ARMA	Adaptive multifunctional structural unit
Transponder system	Adaptive and reconfigurable
Model platform	Basic systems engineering design process and generalised information network analysis
HASS technologies	FPGA, MMIC, SoC, AESA, microtechnology, nanotechnology, and microelectronics
Modules supported	Payload, core bus, propulsion and deployment interface
Top applications benefits	Parallelism and pipelining, high reliability, high determinism, in-orbit/remote reconfiguration, design flexibility, satellite reuse and cost-effectiveness

6 A case study of a spacecraft mission

A case study of a meteorology spacecraft mission detailing a possible application of the DMA concept is reported in this section. It is benchmarked with two contemporary design approaches. The obvious benefits of the highly adaptive small satellite system is judiciously presented and discussed. Table 3 compares two existing small satellite architectures (Jackson and Epstein, 2000; Xuwen et al., 1998) with the HASS system employing the DMA. Technology is not the issue but an enabling architecture to harness the functionalities and capabilities that existing device, subsystem and system-levels technologies offer.

System engineering analyses for conventional nanosatellite and HAN designs for a meteorology satellite (METSAT) mission are presented in this paper. Two critical resources (power and mass) are considered for a 10 kg nanosatellite design in each case. Furthermore, cost and reliability analyses are done to assess the competitive advantage of the HASS system over the existing small satellite systems. Figure 8 illustrates an application of the DMA concept to a nanosatellite design. The baseline AMSU configuration is used. Table 4 gives the key elements of the design for both the conventional small satellite and HASS designs.

Table 3 A comparison of traditional small satellites and HASS architectures

Spacecraft parameters	*Satellite design architecture*		
	Silicon solid-state	*Reconfigurable multifunctional architecture*	*Deterministic multifunctional architecture*
Category	Nanosatellite	Nanosatellite	Nanosatellite
Design concept	Non-functional (module-based)	Functional (non-adaptive)	Functional (adaptive)
Technology platform	ASIC and silicon solid-state	ASIC and silicon solid-state	Radiation-tolerant flash-based FPGA and GaAs RF/microwave MMIC
Subsystem boundary	Present	Absent (only at the functional module level)	Absent
In-orbit/remote partial reconfiguration	No	No	Yes
Transponder system	Non-adaptive	Non-adaptive	Adaptive
System data flow	One common bus	One common bus	One common and one secondary buses
Functional modules	4	4	4
Dynamic redundancy	No	No	Yes
Levels of design customisation	1	3	5

Figure 8 A nanosatellite design using the DMA concept

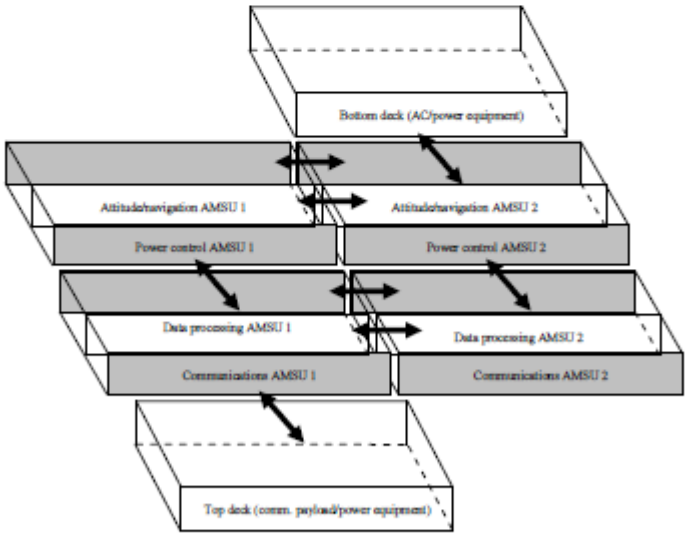

Table 4 Key parameters of the case study small satellite designs

Design parameter	*Description/value*
Category	Nanosatellite
On-orbit dry mass (kg)	10
Class of design	2 (i.e., next-generation satellites with an expanded capability based on an existing category)
Formal customer review	Conceptual design phase
Payload power (W)	10
Spacecraft mission	Meteorology
Orbit	Low-earth

A system engineering analysis to ascertain the mass and power budgets for both case study designs was done. Table 4 reveals that the maximum allowable on-orbit dry mass of the satellite is peaked at 10 kg; this can be worked back to ascertain the propellants and the launch vehicle adapter required given the launch weight capability (Brown, 2002). From the AIAA guidelines (Brown, 2002), category AW, conceptual design review stage, class 2 contingency is 25%. Thus, the total subsystem mass for allocation = 10/1.25 = 8 kg; the mass margin = (10 – 8) kg = 2 kg. Table 5 summarises the subsystem mass budget for the considered conventional nanosatellite.

Table 5 Subsystem mass allocation for a conventional nanosatellite

Subsystem	*Allocation, %*	*Allocated mass, kg*
Structure	20	1.6
Thermal control	3	0.3
Attitude determination and control	9	0.7
Power	16	1.3
Cabling	8	0.6
Propulsion	5	0.4
Communications	4	0.3
Command and data handling	4	0.3
Payload	31	2.5
Budget total		8.0
Mass margin		2.0
Maximum on-orbit dry mass		10.0

The payload power of the case study METSAT mission is 10 W (Table 4). The total satellite power is a strong function of the payload power based on a statistical analysis of past spacecraft. This is used for estimating the initial power requirements of conventional satellites (Brown, 2002; Helvajian and Janson, 2008). The presented total nanosatellite power profile is based on a four-panel array design for past and existing LEO operations; it is suitable for an accurate power estimation of existing nanosatellite systems (Brown, 2002; Helvajian and Janson, 2008).

Figure 9 Nanosatellites power distribution in LEO for a meteorology mission

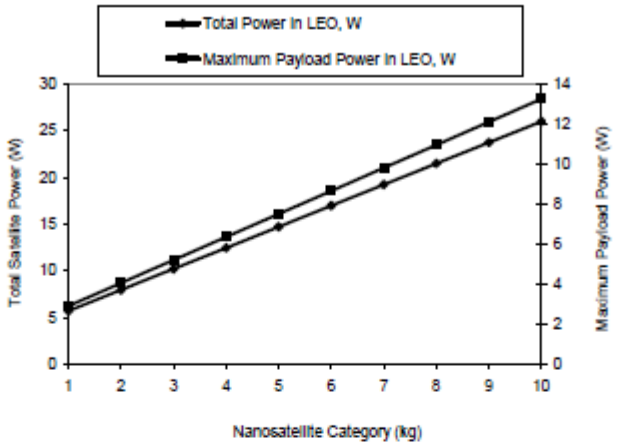

The payload power, P_{pl}, is mission-specific and varies based on the requirements set by the customer. Hence, while the total nanosatellite power, P_{total}, profile (Figure 9) can be applicable to any LEO mission, the payload and bus power regimes are mission-specific (Brown, 2002; Helvajian and Janson, 2008). Figure 9 shows the result of a statistical analysis of a nanosatellite power profile in LEO for a meteorology mission.

Furthermore, the power margin or contingency is the difference between the total capability and current best estimate while the subsystem power requirement is the difference between the total estimated power and the payload power. Mathematically, the power estimating relationship for a METSAT mission (Brown, 2002). is given by:

$$P_{total} = 1.96 P_{pl} \tag{4}$$

From Table 4 and equation (4), the subsystem power allocation is 9.6 W. From the AIAA guidelines, the recommended contingency for conceptual design stage, class 2 is 25%. Thus, the subsystem (bus) power contingency is 9.6 * 0.25 W = 2.4 W. Table 6 summarises the subsystem power budget for the case study traditional nanosatellite.

Table 6 Subsystem power budget of the conventional nanosatellite

Subsystem	*Allocation, %*	*Allocated power, W*
Thermal control	48	4.6
Attitude determination and control	19	1.8
Power	5	0.5
Command and data handling	13	1.3
Communications	15	1.4
Propulsion	0	0
Mechanism	0	0
Total		9.6

The HAN system employs the DMA concept which eliminates cabling. The conceptual design analysis resulted in a mass reduction of 0.6 kg compared with the conventional nanosatellite (Vladimirova and Bridges, 2008; Jackson and Epstein, 2000; Xuwen et al., 1998; Brown, 2002). Hence, the equivalent HAN category for the same conventional 10 kg METSAT mission is 9.4 kg. A HAN system has additional data and information collection, processing and transmission functionalities. This enhances the achievement of more payload capabilities and reliability.

Table 7 gives the total subsystem mass allocation of a HAN system (Jackson and Epstein, 2000; Brown, 2002). It is obvious from the analysis that a lesser category of nanosatellite is required to achieve a better performance that the conventional one for the same mission. Given the conditions in Table 4 and class 2 contingency of 25%, the total subsystem mass for allocation is 7.5 kg. This results in a mass margin of 1.9 kg.

Table 7 Subsystem mass allocation for a HAN

Subsystem	*Allocation, %*	*Allocated mass, kg*
Structure	20	1.5
Thermal control	3	0.2
Attitude determination and control	9	0.7
Power	16	1.2
Propulsion	5	0.4
Communications	4	0.3
Command and data handling	4	0.3
Payload	39	2.9
Budget total		7.5
Mass margin		1.9
Maximum on-orbit dry mass		9.4

For a 9.4 kg HAN, the total power available using a four panel solar array is 24.8 W (Helvajian and Janson). From Table 4 and equation (4), the power estimating relationship yields a total subsystem power of 9.6 W. The complete subsystem (bus) power budget of a HAN system is shown in Table 8. The communication subsystem power includes cabling losses as well. These account for about 10% of the total subsystem power consumption and over 15% of the total spacecraft power (Jackson and Epstein, 2000; Brown, 2002). Hence, the HAN power budget reduces by this margin within the communication subsystem. Actual total subsystem power is $9.6 - 0.1 * 9.6 = 8.64$ W. The actual total power of the HAN system is therefore 18.64 W. From the AIAA guidelines, class 2 contingency is 25% and hence, the total subsystem power contingency of HAN is $8.64 * 0.25 = 2.16$ W. The first-pass analysis reveals a power-saving of 1 W using the DMA concept for the HAN design (Jackson and Epstein, 2000; Brown, 2002; Helvajian and Janson, 2008). Moreover, the reported HAN has the capability to accommodate a 12 kg microsatellite mission with a 21.7% mass-saving and an expendable surplus maximum power margin of 74.5% (Meerman et al., 2003).

Table 8 Subsystem power budget of a HAN

Subsystem	*Allocation, %*	*Allocated power, W*
Thermal control	53	4.60
Attitude determination and control	21	1.80
Power	6	0.50
Command and data handling	15	1.30
Communications	5	0.44
Propulsion	0	0.00
Mechanism	0	0.00
Total		8.64

Spacecraft's cost function relates to its size, complexity, technology maturity, lifecycle, pre- and post-mission objectives, schedule, and other discrete and/or categorical design variables (Saleh, 2008; Saleh et al., 2002; Barnhart et al., 2007; Helvajian and Janson, 2008). Based on past space missions, spacecraft's costs have been documented for all categories of spacecraft (Saleh et al., 2002; Barnhart et al., 2007). This has enabled cost estimating relationships (CERs) to be developed based on the physical, technical, system requirements, and mission/conceptual design objectives. A given CER comprises recurring and non-recurring costs (Saleh et al., 2002). Space systems have cost-per-unit weight of the order of \$70,000/kg (Saleh et al., 2002; Barnhart et al., 2007). Though specific costs are insufficient for predicting the actual cost of spacecraft, a cost-saving of \$42,000 in favour of the HAN over the conventional nanosatellite is realised. Figure 10 gives the current approximate nanosatellites' cost profile used within the space community (Barnhart et al., 2007). Though the actual cost profile of spacecraft is non-linear, this serves the initial conceptual design estimate for space missions planning and development. Based on this historical database of nanosatellites, the HAN yields a cost-saving of \$120,000 over its conventional nanosatellite category (Xuwen et al., 1998; Saleh et al., 2002; Barnhart et al., 2007).

Figure 10 A mass-based cost profile for nanosatellites

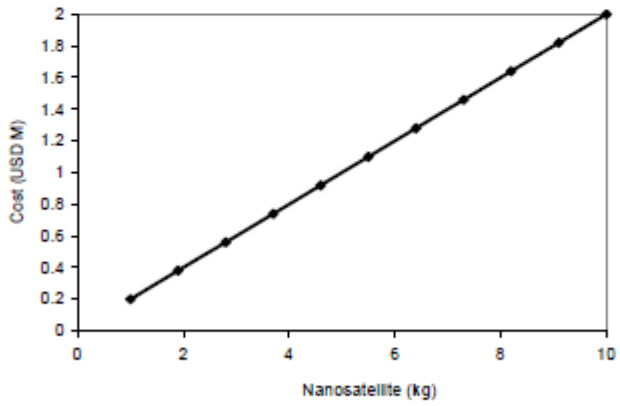

Furthermore, launch costs have a great impact on a spacecraft's cost to initial operating capability (IOC) and cost per operational day (Saleh, 2008; Saleh et al., 2002). This is derived based on the average specific cost to orbit. For a LEO nanosatellite, the specific cost to orbit for both USA and European launchers is about $10,000 (Saleh et al., 2002). This reveals a cost-saving of $6,000 in favour of the HAN system over its conventional nanosatellite category (Jackson and Epstein, 2000; Saleh et al., 2002; Barnhart et al., 2007; Brown, 2002; Xuwen et al., 1998).

Another aspect of system engineering analysis for a spacecraft is its system-level reliability. This is a function of the payload and bus modules reliabilities. Spacecraft reliability calculations are used to avoid undue high safety margins and system oversizing. Past spacecraft missions show that an average of 1.7 failures per spacecraft within the first 30 days of operation; thereafter, each spacecraft records an average of less than 0.2 failures per month (Hassan and Crossley, 2008). For the purpose of comparing the conventional spacecraft and HASS architectures, each bus subsystem is assigned a reliability of 0.9999 (Hassan and Crossley, 2008). The payload subsystem is assumed to contain a solid-state power amplifier (R = 0.9994) and an antenna (R = 1) (Hassan and Crossley, 2008). Equation (5) gives the spacecraft reliability, $R_{spacecraft}$, estimating relationship (RER) that currently determines the system-level reliability margin of spacecraft (Hassan and Crossley, 2008).

$$R_{spacecraft} = R_{payload} R_{structure} R_{ADCS} R_{EPS} R_{thermal} R_{propulsion} R_{harness} \quad (5)$$

Due to the existence of subsystem boundaries, conventional spacecraft reliability calculations are subsystem-based. Based on the published reliability parameters and from (5), a conventional nanosatellite has a system-level reliability of 93.74% at the end of the 30th day of operation (Xuwen et al., 1998; Hassan and Crossley, 2008). The absence of the subsystem boundaries (at the functional level only) results in a reliability of 99.89% (Jackson and Epstein, 2000; Hassan and Crossley, 2008). The absence of subsystem boundaries in a HASS system translates the reliability calculation to a functional module-based one. Assuming each AMSU-borne functional module has a reliability factor of 0.9999, (5) yields a system-level reliability of 99.97% for the HASS system (Jackson and Epstein, 2000; Hassan and Crossley, 2008).

7 Conclusions

A new design approach for small satellites called the DMA has been proposed. This new design concept leverages on the existing scaling techniques and technologies but has the functional design concept as its beacon. The identification and specification of the functional and structural requirements of the system initiate the design process. Five design customisation levels characterise the DMA approach. Moreover, AMSUs are the building blocks of its design paradigm. By sustaining the adaptive technology on the same 'substrate' platform with lightweighting strategies, a completely robust and reliable architecture is realised. Associated thermal control, embedded electronics, signal processing and control units and relevant discrete components are contained in each AMSU.

A case study analysis of a METSAT mission reveals mass- and power-savings of 0.6 kg and 1 W respectively by a HAN compared with its conventional nanosatellite

category. Furthermore, cost to IOC and launch cost reveal huge cost-savings of $120,000 and $6,000 respectively in favour of the HAN over its conventional nanosatellite counterpart.

The DMA concept successfully integrates the various satellite modules adaptively. For instance, the payload subsystems can be seamlessly implemented from the core bus in an event of module failure. This introduces a sort of dynamic redundancy for the entire satellite system while maintaining an uncompromised optimal performance throughout the mission. Hence, real-time space applications/missions and post-mission reapplications are possible with this concept.

References

Actel (2005) *Radiation-Hardened FPGAs*, Ver.3.1, Actel Corporation, California.

Barnhart, D., Vladimirova, T. and Sweeting, M. (2007) 'Very-small-satellite design for distributed space missions', *Journal of Spacecraft and Rockets*, Vol. 44, No. 6, pp.1294–1304.

Barnhart, D., Vladimirova, T. and Sweeting, M. (2009) 'Satellite miniaturization techniques for space sensor networks', *Journal of Spacecraft and Rockets*, Vol. 46, No. 2, pp.469–472.

Brown, C. (2002) *Elements of Spacecraft Design*, pp.1–43, AIAA, Inc., Virginia.

Castillo, L. et al. (2010) 'Flexible electronic assemblies for space applications', *IEEE Aerospace and Electronic Systems Magazine*, Vol. 25, No. 6, pp.25–29.

Chazelas, J. and Merlet, T. (2009) 'Potential technological breakthroughs for phased array antennas', *IEEE Aerospace and Electronic Systems Magazine*, Vol. 24, No. 11, pp.22–27.

Cvetkovic, S.R. and Robertson, G.J. (1993) 'Spacecraft design considerations for small satellite remote sensing', *IEEE Trans. on Aerospace and Electronic Systems*, Vol. 29, No. 2, pp.391–403.

Ekpo, S. and George, D. (2010) '4–8 GHz LNA design for a highly adaptive small satellite transponder using in GaAs pHEMT technology', *11th IEEE Wireless & Microwave Conference*, pp.1–4, Melbourne FL, USA.

Ekpo, S. and George, D. (2010) 'A system-based design methodology and architecture for highly adaptive small satellites', *4th Annual IEEE International Systems Conference*, pp.516–519, San Diego CA, USA.

Ekpo, S. and Kettle, D. (2009) 'Mm-wave LNAs design for adaptive small satellite applications', *Proceedings of the Joint ESA Workshop on Millimetre Wave and 31st ESA Antenna Workshop*, Part 2, pp.843–847, Noordwijk, Netherlands.

Franklin, S. et al. (2006) 'The space technology 8 mission', *IEEE Aerospace Conference*, p.10.

Hassan, R. and Crossley, W. (2008) 'Spacecraft reliability-based design optimization under uncertainty including discrete variables', *Journal of Spacecraft and Rockets*, Vol. 45, No. 2, pp.394–405.

Helvajian, H. and Janson, S.W. (2008) *Small Satellites: Past, Present, and Future*, p.773, AIAA, Inc., Virginia.

Jackson, B. and Epstein, K. (2000) 'A reconfigurable multifunctional architecture approach for next generation nanosatellite design', *Proceedings of the IEEE Aerospace Conference*, Vol. 7, pp.185–188, DOI: 10.1109/AERO.2000.879287.

Low, K. and Zheng, C. (2007) 'Virtual instrument for a micro-satellite power supply system', *IEEE Instrumentation and Measurement Technology Conference Proceedings, IMTC 2007*, pp.1–6, DOI: 10.1109/IMTC.2007.379406.

Lucente, M. et al. (2008) 'IKNOW mission: payload design for in orbit test of w band technology', *IEEE Aerospace Conference*, pp.1–10.

Meerman, M.J.M., Unwin, M.N., Gleason, S., Jason, S., Sweeting, M.N. and Curiel, A.S. (2003) 'A nanosatellite to demonstrate GPS oceanography reflectometry', *Space Technology Journal*, Vol. 23, No. 4, p.245.

Moore, S. (2010) 'UK airborne AESA radar research', *IEEE Aerospace and Electronic Systems Magazine*, Vol. 25, No. 2, pp.29–35.

National Instruments (2009) 'Introduction to FPGA technology: top five benefits', *National Instruments Conference and Exhibition*, London, UK.

Saleh, J. (2008) 'Flawed metrics: satellite cost per transponder and cost per day', *IEEE Trans. on Aerospace and Electronic System*, Vol. 44, No. 1, pp.147–156.

Saleh, J., Hastings, D. and Newman, D. (2002) 'Spacecraft design lifetime', *Journal of Spacecraft and Rockets*, Vol. 39, No. 2, pp.244–257.

Schmitz, H. (2010) *Application Examples: How to Use FPGAs in Satellite Systems*, pp.1–7, Actel Corporation, California.

Shoer, J. and Peck, M. (2009) 'Reconfigurable spacecraft as kinematic mechanisms based on flux-pinning interactions', *Journal of Spacecraft and Rockets*, Vol. 46, No. 11, pp.466–469.

Vladimirova, T. and Bridges, C. (2008) 'Dual core system-on-a-chip design to support intersatellite communications', *NASA/ESA Conference on Adaptive Hardware and Systems*, pp.191–195.

Wittig, M. (2000) 'Satellite onboard processing for multimedia applications', *IEEE Communications Magazine*, p.135.

Xuwen, L. et al. (1998) 'Silicon solid-state small satellite design based on IC and MEMS', *Proceedings of the Solid-State and Integrated Circuit Technology*, pp.932–935.

3.2.11 Paper 11 [SE11]

A System Engineering Consideration for Future-Generations Small Satellites Design, *in Proc. First IEEE European Satellite Telecommunications Conference*, Rome, Italy, October 2012, pp. 1–4.

DOI: https://doi.org /**10.1109/ESTEL.2012.6400067**.

Sunday Ekpo[1] and Danielle George[2]

[1]Department of Engineering, Manchester Metropolitan University, UK

[2]School of Electrical & Electronic Engineering, The University of Manchester, UK

This subsection is an exact copy of Paper 11

A System Engineering Consideration for Future-Generations Small Satellites Design

Sunday C. Ekpo, *Member, IEEE* and Danielle George, *Member, IEEE*

Abstract—**The conventional point-based satellite system engineering design procedure is insufficient to address the dynamic operations and post-mission reuse of capability-based small satellites. Emerging space systems and missions require an adaptive architecture(s) that can withstand the radiation-prone flight environment and respond to in-situ environmental changes using onboard resources while maintaining its optimal performance. This proactive and reactive response requirement poses an enormous conceptual design task in terms of the trade space – which can be too large to explore, study, analyse and qualify – for a future-generation adaptive small satellite system.**

This paper involves a careful study of the current and emerging space system technologies, architectures and design concepts for realising adaptive small satellites for future space applications. Adaptive multifunctional structural units (AMSUs) that eliminate subsystem boundaries and enable five levels of in-orbit customisations at the system level have been qualified for highly adaptive small satellites (HASSs). The initial system engineering (SE) analyses reveal that the HASS system has mass, cost and power savings over the conventional small satellite implementation. The reported novel research findings promise to enable capability-based, adaptive, cost-effective, reliable, multifunctional, broadband and optimal-performing space systems with recourse to post-mission re-applications. Furthermore, the results show that the developed system engineering design process can be extended to implement higher satellite generation missions with economies of scale.

Index Terms—**adaptive system, low earth orbit, satellite system engineering, system-level design.**

I. Introduction

THE current advances in space and allied technologies that enable the design, production and operation of capability-based subsubsystems, subsystems and modules onboard a satellite system necessitate a re-evaluation and reassessment of the conventional satellite SE margins. Spacecraft SE involves the specification of the conceptual design and mission objectives of a satellite system and the qualification of the subsubsystems and subsystems needed to fulfil its requirements cost-effectively. This includes an uncompromising development of the detailed engineering tasks in the functional design of a spacecraft. The SE process is initiated by the validation of the complete requirements that should characterise the satellite system; this includes the choice of key aspects that satisfy those requirements. In satellite SE, observed system-level changes are used to track and assess key performance parameters [1 – 8].

The system-level focus of the conceptual design phase for any given spacecraft mission requires optimality and not feasibility. Hence, the design model of the spacecraft must have cost and performance elasticity to changes in system requirements and applications for optimal results. The fundamental motivations for the HASS concept are, but not limited to, on-orbit adaptability, reliability, multifunctionality, enhanced portability, system-level simulation of spacecraft, reduced manufacturing and integration complexities, cost-effectiveness, safety, low carbon footprint, post-mission re-application and flexibility in deployments. This capability-based space system design will gain increasing and expanding applications in future deployments of constellations of small satellites. The novel HASS system architecture has an in-built dynamic redundancy and radiation shield for onboard semiconductor components which can be reengineered while in orbit. The categories of HASSs are highly adaptive microsatellites (HAMs), highly adaptive nanosatellites (HANs), highly adaptive picosatellites (HAPs), highly adaptive femtosatellites (HAFs) and highly adaptive attosatellites (HAAs); this paper focuses on the first four categories. Moreover, the mass of each category follows the mass classification convention used for traditional small satellites [3, 5, 8, 9].

This paper is organised as follows. Section II explains the operations of future-generations satellites with emphasis on adaptive small satellites. The SE of future-generations small satellites focusing on the mass and power properties are stated in section III. A case study of the SE of four categories of HASSs for a meteorology mission is given in section IV. Section V features the conclusion of this paper.

II. Future-Generations Satellites Operations

Considerable works have been ongoing for over ten years in achieving adaptive circuits for microwave subsubsystems, subsystems and systems. For instance, a power amplifier that

Manuscript received May 15, 2012.

The authors are with the MACS Research Group, School of Electrical & Electronic Engineering, The University of Manchester, Manchester, M60 1QD, United Kingdom (Tel.: +4479 5047 8245; e-mail: cookey_sunday@ieee.org; Danielle.George@manchester.ac.uk).

978-1-4673-4688-7/12/$31.00 ©2012 IEEE

operates on any frequency band adds value to the spacecraft system reliability and availability. Hence, achieving the same performance at broadband as in narrowband frequencies is highly desirable. Adaptive amplifiers onboard a spacecraft enable remote reconfigurations to support different spacecraft mission objectives (such as switching from communication to radar applications), onboard tuning after manufacturing and selectable nominal operating conditions as opposed to worst case design margins [7 – 9].

Radiation impacts negatively on semiconductor devices onboard spacecraft in orbits. Cosmic rays and heavy charged particles streaming out from the sun in the solar wind react with gases in the upper atmosphere to produce high energy neutrons. These neutrons impact on the onboard semiconductor devices to produce unpredictable in-orbit failures. As a result of this, the space systems in LEO have potential replacement timeframe of 10 years. This translates into a huge investment cost that could be avoided through a judicious system-level reengineering. Radiation-tolerant adaptive and reconfigurable devices have been developed and qualified as independent and integrated subsubsystems for control, signal processing and remote switching applications. Examples include field programmable gate array (FPGA) and reconfigurable micro-electromechanical systems (RMEMs). The monolithic integration of FPGA, RMEMs and GaAs-based RF/microwave subsystems promise to enable reliable deterministic satellite operations [3 – 5, 9 – 16].

The future space activities and payloads spanning satellites, probes, capsules, space shuttle missions and international space station (ISS) assembly hardware across the globe has been assessed and predicted using the Worldwide Mission Model (WMM) for the past 20 years. The WMM snapshot of future payloads for the period 2011 – 2030 (released in 2011) indicates that 2,315 proposed payloads are underway; this is 14 % and 4 % greater than the 2009 and 2010 figures respectively. These are payloads that have been announced and intended to be launched. Small satellite programmes spanning mini-, micro-, nano-, pico- and femtosatellites will spur up space payloads market growth in the next 20 years. This increasing number of spacecraft launched each year and technical and environmental constraints call for a reassessment of the current system engineering (SE) margins governing their design, production and operation [5, 7, 10].

Highly adaptive space subsubsystems and subsystems are expected to form the architecture of the core bus, payload and propulsion modules of future-generation spacecraft [5, 7, 11, 12, 17 – 21]. Consequently, radiation-resistant adaptive and active devices technologies have been analysed and qualified for developing a deterministic multifunctional architecture (DMA) with five levels of in-orbit spacecraft customisations [18]. Adaptive multifunctional structural units (AMSUs) form the building blocks of the HASS thereby eliminating subsystem boundaries at the system level [18]. The design methodology established for the HASS helps to enhance the conceptual design of future-generations spacecraft at the subsystem and system levels [5]. A HASS is a reconfigurable, multifunctional and deterministic small space satellite that has capabilities for dynamic space applications and operations while retaining its designed optimal performance. The architecture a HASS system implements a digitised monolithic microwave integrated circuit with an analog functions capability. The advantages are, but not limited to, very small subsubsystem footprint, reduced system weight, synthesisable digital cores, technology-independent implementations, very low power consumption, ease of application, absence of analog blocks and integrated radiation hardness. Existing SE procedures are insufficient to give a complete analysis of this type of space system. Hence, the need to review the existing SE with respect to the emerging satellite designs technology(s) and applications.

III. SE of Future-Generations Small Satellites

TABLE 1
SPACECRAFT SE PROCEDURE

Requirements definition
Resource budgeting
System-level trade studies
System integration
Operational margins
Post-mission reapplication assessment

TABLE 2
SPACECRAFT PROJECT REVIEWS

Conceptual design review
Preliminary design review
Critical design review
Preshipment readiness review
Flight readiness review
Assembly, test, and launch operations
Mission operations
Completion of mission
Post-mission capability review

In any given space development programme, the customer's requirement drives the choice of technology(s) to meet it. The major elements of the HASS SE process implements the phases of a HASS mission (Table 1). Table 2 depicts the major formal customer reviews that must be conducted in the course of a HASS mission project development. Each phase details the technological basements of the functional modules. Power and weight affect operating and insertion costs exponentially and so are always critically examined for optimal budget parameters. In this paper, mass and power properties are the two major spacecraft resources of consideration [14, 17, 21].

A. *Space Satellite Mass Budget Analysis*

The parameters for developing spacecraft's mass budget include design phase, class of design, launch weight capability and propellant mass [14]. These specifications are used to ascertain the on-orbit dry mass of a spacecraft and the corresponding mass margin. Mathematically, the on-orbit dry mass of the spacecraft is given by:

$$M_{ODM} = M_{LVC} - M_{LVA} - M_P \quad (1)$$

where,
M_{ODM} = on-orbit dry mass, kg
M_{LVC} = launch vehicle mass capability, kg
M_{LVA} = launch vehicle adapter mass, kg
M_P = propellant mass, kg

The launch vehicle adapter scales with the launch vehicle mass. Based on past spacecraft analysis, this is given by:

$$M_{LVA} = 0.076 M_{LVM} + 50 \quad (2)$$

From the American Institute of Aeronautics and Astronautics (AIAA) guidelines, the mass margin is given by:

$$M_{margin} = \frac{C_f M_{ODM}}{1 + C_f} \quad (3)$$

where M_{margin} is the mass margin in kg and C_f, the mass contingency factor [14].

Equation 3 holds true if the payload is developed along with other core bus subsystems. In the event that the customer provides the payload subsystem, (3) becomes:

$$M_{margin} = \frac{C_f (M_{ODM} - M_{pl})}{(1 + C_f)} \quad (4)$$

where M_{pl} is the payload mass in kg. The corresponding core bus subsystems mass, M_{CBS}, in kg is thus:

$$M_{CBS} = \frac{M_{ODM} - M_{pl}}{1 + C_f} \quad (5)$$

The next step in the spacecraft subsystem mass budget analysis is the mass allocation to the individual subsystems. To develop the mass budget model of a HASS, a knowledge of the cabling factor, C_{MF}, contingency factor and on-orbit dry mass is required. From (4) and (5), the equivalent on-orbit dry mass, M_{HODM}, of the HASS is given by: [14, 21]

$$M_{HODM} = M_{ODM}(1 - C_{MF}) \quad (6)$$

B. Space Satellite Power Budget Analysis

TABLE 3
MASS-BASED SPACECRAFT POWER ESTIMATING RELATIONSHIPS IN LEO

Satellite Category (kg)	Power Estimating Relationship
Microsatellite (10 – 100)	P_L (W) = 1.044M + 15.56
Nanosatellite (1 – 10)	P_L (W) = 2.26M + 3.44
Picosatellites (0.1 – 1)	P_L (W) = 5M + 0.7
Femtosatellites (0.01 – 0.1)	P_L (W) = 10.3M + 0.167

Table 3 gives the PERs of past spacecraft in LEO reveals based on a statistical analysis carried out in this research [17]. This analysis is based on a four-panel solar array and yields the total power, P_L of a satellite as a function of its mass, M.

The total spacecraft power (PER-based) can be expressed as a function of the satellite mass and payload power thus: [21]

$$P_L = f(P_{pl}) + kf(M) + C \quad (7)$$

where k is the specific power constant (W/kg) for each satellite category and C is a power constant (W).

A nanosatellite designed for a meteorology satellite (METSAT) mission in LEO revealed a PER and payload power given by (8) and (9) respectively:

$$P_L = 1.13M + 0.98P_{pl} + 1.72 \quad (8)$$

$$P_{pl} = 1.153M + 1.755 \quad (9)$$

For a 10-kg nanosatellite, (8) becomes:

$$P_L = 13.02 + 0.98P_{pl} \quad (10)$$

TABLE 4
METHOROLOGY SPACECRAFT POWER ESTIMATING RELATIONSHIPS IN LEO

Satellite Category (kg)	Power Estimating Relationship
Microsatellite (10 – 100)	P_L (W) = 0.522M +0.98P_{pl} + 7.78
Nanosatellite (1 – 10)	P_L (W) = 1.13M +0.98P_{pl} + 1.72
Picosatellites (0.1 – 1)	P_L (W) = 2.5M +0.98P_{pl} + 0.35
Femtosatellites (0.01 – 0.1)	P_L (W) = 5.15M +0.98P_{pl} + 0.0835

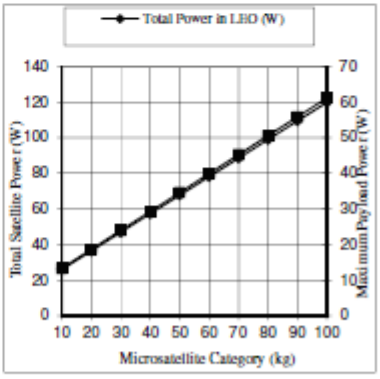

Fig. 1. Microsatellite power profile in LEO

Hence, the payload power constraint for (10) is $P_{pl} \leq 13.29$ W. Table 4 gives the derived PERs of small METSATs in

LEO based on past spacecraft missions. Figures 1 and 2 show the corresponding power profiles for microsatellites and nanosatellites in LEO respectively. They indicate the maximum feasible payload powers for each satellite classification [17, 18, 21].

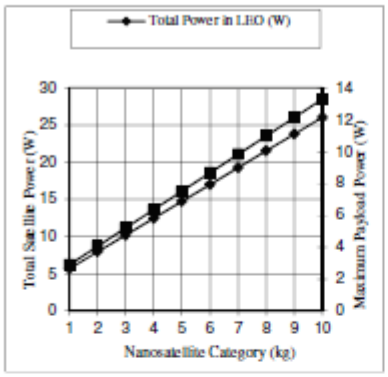

Fig. 2. Nanosatellite power profile in LEO

From (7), the total in-orbit power, P_T, of a HASS system is given by:

$$P_T^{'} = P_{pl} + P_{bus} + P_{margin}^{'} \quad (11)$$

The corresponding power contingency is given by:

$$P_{margin}^{'} = P_{margin} + \delta P \quad (12)$$

where δP is the maximum differential power (W) resulting from the dynamic operation and application of a HASS system. Since P_{margin} is defined for the conventional spacecraft without any obvious recourse to the adaptive power regimes, P'_{margin} must be greater or equal to P_{margin}. Hence, the constraint on (11) for a HASS system is given by:

$$P_{margin} \le P_{margin}^{'} \le \left(P_{margin} + \delta P\right) \quad (13)$$

Consequently, for a HASS system, (7) becomes:

$$P_T = f\left(P_{pl}\right) + kf(M) + C_T P_{bus} + \delta P + C \quad (14)$$

Equation 14 represents the complete in-orbit total spacecraft power budget function for the conceptual design of a highly adaptive small satellite system. With (14), the design point of (7) is satisfied and can be modelled reliably with accuracy. Hence, undue electrical power system redundancy and equipment oversizing can be avoided. This serves to enhance the reliable SE analysis of small satellites in the congested and radiation-prone LEO environment [4, 15, 21].

Given that a HASS design lifetime (in years) is T_{life} and post-mission re-application years, T_{pm}, its conceptual system engineering design would require a system parameters estimate for T_{HASS} given by:

$$T_{HASS} = 2\sqrt{(T_{life} * T_{pm})} \quad (15)$$

where, T_{HASS} is the overall mission and post-mission re-application lifetime of the HASS system in years. From (15) and for a three-year post-mission reuse, the maximum capability-based design lifetime (CDL) for a 18.72 kg HAM is approximately seven years eight months.

Table 5 features the highly adaptive satellite subsystems mass allocation for the communication and planetary missions for payload is customer-furnished (CF) or spacecraft team's payloads. The values are based on past spacecraft missions analysis and emerging space technologies [14, 17, 18, 21].

TABLE 5
HIGHLY ADAPTIVE SATELLITE SUBSYSTEMS MASS ALLOCATION

	Subsystems mass allocation of spacecraft missions (%)			
	Communication		Planetary	
Subsystem	STP	CFP	STP	CFP
Structure	21.6	30.2	27.8	31.5
Thermal control	4.1	6.3	3.3	3.3
ADC	7.2	10.4	9.7	10.9
Electrical power	26.8	36.4	20.4	22.8
Propulsion	7.2	10.4	14.0	16.3
Communications	-	-	6.5	7.6
CDH	4.1	6.3	6.5	7.6
Payload	29.0	-	11.8	-

Given a 10-year LEO mission, the EOL power of a 50-kg microsat is approximately 50 W. A reengineering of this microsat would successfully enable and sustain a corresponding 10-kg nanosat LEO mission. For an extra 5-year LEO mission, the life degradation of the microsat's GaAs-based solar array yields 0.87. This translates into an EOL of approximately 43.50 W. Since the EOL is the design point, (15) yields a mission of approximately 50 months. For propulsive missions' requirements, on-orbit robotic refuelling can be implemented.

Since AMSUs enable satellite payloads to be standardised to form multifunctional modules (MFMs) which can be customised while on orbit, the quality level of the HASS system is comparable with the units pass. Hence, subsubsystems are integrated onto a common platform such that multiple functions can be derived from the same unit. The obvious reduction in the materials list of AMSUs implies that thermal drift issues can be reduced. Moreover, the

developments in microfabrication and micromachining techniques such as low-temperature cofired ceramic (LTCC) and laser volumetric exposure processing (LVEP) for materials such as photosensitive glass ceramics (PSGC) hold a great promise for digitised MMICs such as AMSUs.

IV. Case Studies of Spacecraft Missions

Tables 6 and 7 are respectively the power and mass budgets for a METSAT mission in LEO using a 18.4-kg HAM. The SE analyses can be extended to cover HAP, HAF and HAA categories based on the mission requirements [21]. The advanced capabilities and mass, power and cost savings recorded with the HASS compared with the traditional small satellite systems make HASSs the obvious choice for future spacecraft missions. Table 8 shows the mission comparison analysis of meteorology, planetary (PLASAT) and communication (COMSAT) missions using a 10-kg highly adaptive nanosatellite (HAN), 30-kg highly adaptive microsatellite (HAM) and 50-kg HAM respectively has been done; the masses are stated with respect to their conventional small satellite mass margins. The mass and cost savings realisable using HASS systems rather than their corresponding conventional small satellites implementations are given in Table 8.

TABLE 6
HIGHLY ADAPTIVE SMALL SATELLITE POWER BUDGET ANALYSIS

HASS System Engineering		
Analysis: Power Budget; Mission: Meteorology; $P_t(W) = 1.96P_{pl}$		
Orbit: LEO; Design Phase: Conceptual Design		
Power contingency (C_f): 25%; Class of Design: 2 (Next-generation)		
Satellite Category: Highly adaptive microsatellite (HAM) (20 kg)		
Core Bus Subsystem Power Allocation		
Core Bus Subsystem	Allocation (%)	Power (W)
Thermal control	53	6.87
Attitude control	21	2.72
Electrical Power	6	0.78
Command and data handling	15	1.94
Communications	5	0.65
Propulsion	0	0
Mechanics	0	0
In-orbit Total Power Summary		
Parameter		Power (W)
Maximum available payload power in LEO		18.60
Required payload power		15.00
Maximum core bus power		17.85
Calculated core bus power		12.96
Power margin		3.24
Total required power		31.2
Power savings		1.80
Max. power of a 20 kg Microsat in LEO		36.45
Max. available core bus power in LEO		14.28
Max. available power margin in LEO		3.57

TABLE 7
HIGHLY ADAPTIVE SMALL SATELLITE MASS BUDGET ANALYSIS

HASS System Engineering
Analysis: Mass Budget; Mission: Meteorology; Orbit: LEO
Design Phase: Conceptual Design; Mass contingency: 25%
Class of Design: 2 (Next-generation); Cabling mass factor, C_{mf}: 8%
Small Satellite Category: Highly Adaptive Microsatellite (HAM)
Conventional on-orbit dry mass (kg): 20
Subsystem mass reduction (kg) = 1.6
Equivalent on-orbit dry mass of a HAM = 18.4
Total subsystem mass for allocation (kg) = (18.4/1.25) = 14.72

Subsystem Mass Allocation		
Subsystem	Allocation (%)	Allocated mass (kg)
Structure	21.7	3.194
Thermal control	3.3	0.486
Attitude control	9.8	1.443
Power	17.4	2.561
Propulsion	5.5	0.810
Telecom	4.3	0.633
CDS	4.3	0.633
Payload	33.7	4.960
HAM Mass Allocation Summary		
Parameter		Value (kg)
Subsystem budget total		14.72
Mass margin		3.68
Mass-saving		1.60
Maximum on-orbit dry mass		18.40
Launch cost-saving ($)		16000.00

TABLE 8
METSAT, PLASAT AND COMSAT MISSIONS USING HASS SYSTEMS

Small satellite category	HAN	HAM	HAM
Mission	Meteorology	Planetary	Communication
On-orbit dry mass (kg)	9.20	27.90	48.50
Subsystems mass (kg)	7.36	22.32	38.80
Mass margin (kg)	1.84	5.58	9.70
Mass-saving (kg)	0.80	1.50	2.10
Specific cost-saving ($)	56000	105000	147000
Launch cost-saving ($)	8000	15000	21000

It is obvious from Tables 6 and 7 that no power and 5.5 % of subsystem mass have been allocated to the propulsion subsystem of the METSAT mission respectively. This follows past historical database and based on the AIAA guidelines [14, 21]. Contemporary mission programmes employing advanced space technology breakthroughs in subsystem design and integration have also lent credence to this analysis [17]. Current miniaturised thrusters and MEMS-based thruster systems are able to support translational and rotational velocities changes of spacecraft. A cold-gas micropropulsion that yields 34 m/s velocity increment can enable the required manoeuvrings and/or orbit changing. A typical LEO mission can use 30 m/sec ΔV to easily meet the propulsion requirements. Based on the rocket equation, HASSs missions can be accommodated. The given margins are for the initial conceptual design stage of the spacecraft development programme. Appropriate propulsion technology mass and power margins can always be derived to reflect the propulsive mission requirements [17, 21].

On the mission accomplishment front, charged couple device (CCD) chip is the preferred sensors technology since it can withstand the unpredictable harsh space environment and has the capability to integrate several functions in the image sensor. Furthermore, CCD chips are smaller, consume less power and have higher SNR and better resolution than CMOS cameras.

Moreover, the cost of a satellite is usually scaled with its mass as a first approximation. Other factors such as payload complexity, maturity of the design, lifecycle, pre- and post-

mission objectives and schedule have a direct impact on cost. Based on past space programmes, each satellite cost estimating relationship (CER) comprises recurring and nonrecurring costs. Spacecraft have cost-per-unit weight of the order of $70,000/kg. Though specific costs are insufficient for predicting the actual cost of spacecraft, HAM, HAN, HAP, and HAF implementations have achieved cost savings over their conventional counterparts [21]. Furthermore, launch costs have an obvious influence on the cost to initial operating capability (IOC) and cost per operational day of a spacecraft. For a LEO satellite, the specific cost to orbit for both the United States and European launchers is about $10,000/kg. Table 7 shows the appreciable cost savings for a HAM compared with its conventional counterpart. At the conceptual design stage, Tables 6 and 7 help the spacecraft system engineer to allocate resources to the various subsystems of a spacecraft's functional modules [18].

While the presented SE process and/or analysis is for the conceptual design of small satellites based on past spacecraft missions and emerging space systems design and manufacturing technologies, there is an intrinsic recourse to specific mission objectives during the development phase of the satellite project. Any spacecraft sizing model is traditionally optimised for low power, mass and cost. For instance, the power requirement for the microsat category is more than the power budget of the nanosats. For the same technology platform, this is expected and the respective single mission objectives would definitely be different except where both satellite categories work cooperatively within a constellation or formation flying system. The presented modular SE design process for small satellites serves to enable the transitions of satellite generations for emergent missions and post-mission reapplications. This is the philosophy behind the functional design concept adopted for HASS systems.

V. Conclusion

A system engineering process for future-generations small satellites has been presented in this paper. Appropriate power and mass estimating relationships have been derived and explained for small satellite missions in the low Earth orbit.

Mass and power savings have been recorded by implementing the highly adaptive small satellite missions rather than the traditional small satellite systems. Furthermore, appreciable cost savings have been realised for the initial specific and launch costs of highly adaptive small satellites.

The analysis can be applied to study any spacecraft mission with an established past history/database. The reported system engineering promises to enhance a holistic design and development of next generation satellite missions and constellations. Technical computing and application programmes such as MATLAB and MS Excel can be used to develop the SE tool based on the derivations given in this paper. Furthermore, limited frequency spectrum and spatial capacity (orbital slots), high equipment cost, increased space debris, and expanding global broadband connectivity require adaptive, reconfigurable and multifunctional space systems. This work can be extended to provide a ready spacecraft system engineering reference handbook for the space community.

References

[1] M. Steer, "Microwave and RF Design: A systems approach," SciTech Publishing Inc., Raleigh, NC, pp. 101, 2010.

[2] B. E., White, "Complex Adaptive Systems Engineering," *IEEE Aerospace and Electronic Systems*, vol. 25, no. 12, pp. 16–22, Dec. 2010.

[3] S. Ekpo and D. George, "Mm-wave LNAs design for adaptive small satellite applications," in *Proceedings of the Joint ESA Workshop on Millimetre Wave and 31st ESA Antenna Workshop*, Noordwijk, Netherlands, May 2009, pp. 843–837.

[4] B. Elbert, "Introduction to satellite communications," Artech House, Inc., London. Third Edition. pp. 1–38, 69–107, 195–205, 389–393, 257–289, 291–297, 337–345, 389–405, 418, 2008.

[5] S. Ekpo and D. George, "A system-based design methodology and architecture for highly adaptive small satellites," in *Proceedings of the 4th Annual IEEE International Systems Conference*. San Diego CA, USA., April 2010, pp. 516–519.

[6] R. Hassan and W. Crossley, "Spacecraft reliability-based design optimization under uncertainty including discrete variables," *Journal of Spacecraft and Rockets*, vol. 45, pp. 394–405, March–April 2008.

[7] M. Steer and W. D. Palmer, "Multifunctional adaptive microwave circuits and systems," SciTech Publishing Inc., Raleigh, NC, pp. 106–154, 208–237, 2009.

[8] S. Ekpo and D. George, "4 – 8 GHz LNA design for a highly adaptive small satellite transponder using InGaAs pHEMT technology," in *Proceedings of the 11th IEEE Wireless & Microwave Conference*. Melbourne FL, USA, April 2010, pp. 1–4.

[9] S. Ekpo and D. George, "Impact of noise figure on a satellite link performance," *IEEE Communications Lewers*, Vol. 15, No. 9, pp. 977 – 979, 2011.

[10] M. Cáceres, "Mission model offers snapshot of space payloads," *Aerospace Magazine*, AIAA, pp. 24–27, June 2011.

[11] D. Barnhart, T. Vladimirova and M. Sweeting, "Very-small satellite design for distributed space missions," *Journal of Spacecraft and Rockets*, vol. 44, pp. 244–257, November-December 2007.

[12] D. Barnhart, T. Vladimirova and M. Sweeting, "Satellite miniaturization techniques for space sensor networks," *Journal of Spacecraft and Rockets*, vol. 46, pp. 469–472, March–April 2009.

[13] Mario, P., "Study of a cube-sat mission," M.S. Thesis, Karl Franzens University of Graz, Graz, Austria, pp. 56–82, Spring 2005.

[14] C Brown, "Elements of spacecraft design," Virginia: AIAA, Inc. 2002, pp. 1–43.

[15] M. Brogley, "FPGA reliability and the sunspot Cycle," pp.4 – 13, September 2011. http://www.actel.com/documents/FPGA_Reliability_WP.pdf.

[16] H. Schmitz., "Application Examples: How to Use FPGAs in Satellite Systems," *Acael Corporation, California*, 2010.

[17] H. Helvajian and S. W. Janson, "Small satellites: past, present, and future," AIAA., Inc., Virginia, pp. 559–560, 773, 2008.

[18] S. Ekpo and D. George, "A deterministic multifunctional architecture design for highly adaptive small satellites," *International Journal of Satellite Communication Policy and Management*; accepted for publication, IJSCPM-2011052501, 2012.

[19] S. Ekpo and D. George, "Reconfigurable cooperative intelligent control design for space missions," *Recent Patents on Space Technology*, Vol. 2, No. 1, pp. 2 – 11, 2012.

[20] I. D. Robertson and S. Lucyszyn, "RFIC and MMIC design and technology," The Institution of Electrical Engineers, London, pp. 1–81, 2001.

[21] S. Ekpo and D. George, "A System engineering analysis of highly adaptive small satellites," *IEEE Systems Journal*; accepted for publication, ISJ_858, pp. 1–8, April 2012.

3.2.12 Paper 12 [SE12]

A System-based Design Methodology and Architecture for Adaptive Small Satellites, *in Proc. 4th Annual IEEE International Systems Conference*, San Diego CA, USA, April 2010, pp. 516–519.

DOI: https://doi.org /**10.1109/SYSTEMS.2010.5482323**.

Sunday Ekpo[1] and Danielle George[2]

[1]Department of Engineering, Manchester Metropolitan University, UK

[2]School of Electrical & Electronic Engineering, The University of Manchester, UK

This subsection is an exact copy of Paper 12

A System-based Design Methodology and Architecture for HighlyAdaptive Small Satellites

Mr Sunday Ekpo, *Member, IEEE* and Dr Danielle George, *Member, IEEE*
Microwave & Communication Systems Research Group, School of Electrical & Electronic Eng.,
The University of Manchester, Manchester, M60 1QD, United Kingdom
Sunday.Ekpo@postgrad.manchester.ac.uk; Danielle.George@manchester.ac.uk

Abstract—**System-level conception, design and analysis are fundamental to ensuring the reliability and operability of complex systems. The ever-expanding and demanding global space activity requires, amongst other performance metrics, multifunctional, reconfigurable and adaptive system architectures. Consequently, there is need for developing a systems engineering tool/platform for assessing multipurpose space applications and decommissioned satellite systems reapplication. This paper presents a system-based design methodology and architecture for highly adaptive small satellites (HASSs). The developed HASS methodology beacons on the basic systems engineering design process and generalised information network analysis (GENA) model. The HASS methodology and architecture address the space mission and conceptual design objectives. The iterative process provides options for mission(s) definition and combinations and space system transformation. It also allows the designer to choose from available device technologies for specific and integrated applications with allowance for trade-offs and evaluation. Depending on the unique attributes of interest, the small satellite subsystem components can be selected for a specific mission. Furthermore, mission-defined quality of service metrics are assigned prior to the system trade space exploration. HASS-based multicriteria studies are then performed for qualifying the optimal system architectures. This adaptive space system-level platform allows the designer to optimize device technologies, systems and subsystems configurations and architectures in an integrated environment. The attendant benefits, are reduced design, launch and operations costs, reliability, adaptive remote monitoring and support for broadband and/or multimedia applications.**

Keywords- adaptive small satellite; architecture; methodology; multifunctional; reconfigurable; system-based design

I. INTRODUCTION

Space communications technology [1 – 6] has continued to evolve due to advances in allied technologies that characterize the device standards onboard space equipment. Advances in system and subsystem design, device architecture and technology and the need to enhance portability, cost-effectiveness, safety, reliability and flexibility in deployments all testify to this assertion. Adaptive small satellites design represents a complex system design that requires enormous systems engineering modelling and analyses. Starting from the baseline device technologies to subsystems and systems integration, the fundamental systems engineering design routine are required. It involves problem definition, exploration of appriopriate solution sets, development of options, evaluation of alternatives and choice of architecture. Design processes such as the generalised information network analysis (GENA) model [1] and Hall's methodology [2] have been developed for studying, designing and developing complex space systems. The GENA model has been applied in the multiobjective, multidisciplinary design optimisation methodology for the conceptual design of distributed satellite systems. Hall's methodology involves seven steps: problem definition, value system design, system synthesis, system modelling, system evaluation, decision making and planning for action. Furthermore, reconfigurable multifunctional architecture approach has been developed for nanosatellite missions [3]. Other small satellite design and cost models have been developed for design-to-cost goals for conceptual design [4]. This paper describes a systems-based design methodology and architecture for adaptive small satellites. Though space systems and subsystems technologies have recorded unprecedented advances in the last thirty years, the system-level focus of the conceptual design phase for any given spacecraft requires optimality and not feasibility. Thus, the small satellite system design must have cost and performance elasticity to changes in system requirements and applications for optimal results. This is why system resources adaptability and optimisation must be ensured for reliable space applications. The adaptive small satellite design methodology seeks to bridge this gap within the space systems design suites. It addresses the rudiments of the GENA model and Hall's methodology while allowing reconfigurable and multifunctional operations and design-to-cost analysis.

II. THE HASS METHODOLOGY

Fig.1 shows the developed methodology for highly adaptive small satellites design for space applications. First, the mission and conceptual design objectives are defined. This is followed by the transformation of the satellite system into an information network with nodes. Mission-specific quality of service metrics are then stated. The conceptual design problem is partitioned to allow for algorithms and codes

978-1-4244-5883-7/10/$26.00 ©2010 IEEE

and specification of subsystem-level functional requirements.

Adaptive multifunctional structural units (AMSUs) are the building blocks of the ARMA concept. This paper presents the enabling technologies, architecture and functionality of the AMSUs in detail. A prototype AMSU design for a nanosatellite is also shown. Fig. 3 shows the two AMSU architectures proposed for the HASS system: Figs. 3a and 3b represent the baseline and hybrid ARMA building blocks respectively. The represented AMSUs are meant to serve the communication subsystem function of the HASS system.

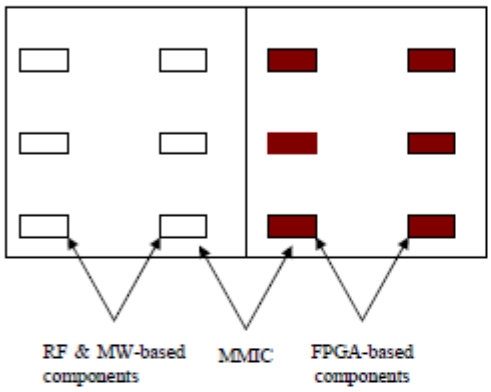

(a) Baseline AMSU

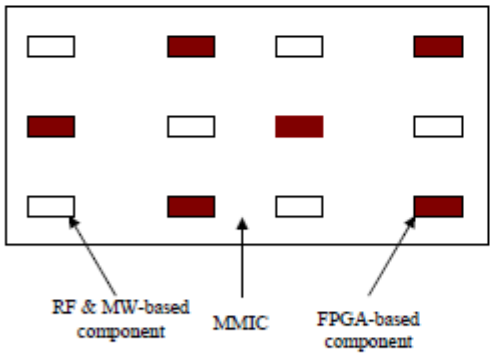

(b) Hybrid AMSU

Figure 3. The Building Block of ARMA

The functional design concept provides a network of functionality whereby the various intrinsic functions constitute nodes within it [3]. The beauty of the functional design approach is in the possibility of implementing single and multiple components-based functions and single/multipurpose components. The ARMA deign employs this design philosophy in its AMSU architecture. Thus, each AMSU board can implement virtually all of the HASS functions. The various functions interact on a common bus; the AMSU architecture promises great design modularity, flexibility, reliability and cost benefits. The reprogrammable interconnects of the integrated FPGA blocks can be "software-wired" for real-time performance. The programmable FPGA blocks' interconnects are borne on the MMIC of the AMSU. Allied technologies such as RFID can be used to transfer data between AMSUs thereby eliminating bulky wire harnesses.

The AMSU upgradeable components include, but not limited to, FPGAs, EPROM, RAM, processors, surface mount devices and discretes. Compared with traditional and existing functional design-based satellites [5, 6], physically replaceable/upgradeable components of the AMSU are fewer; this is a huge cost benefit for any space mission.

A top-level candidate ARMA conceptual design consists of six AMSUs: a top deck (for providing separation and mounting interfaces), a bottom deck (for providing further mounting surface), a power control AMSU, an attitude/navigation AMSU, a communications AMSU and a data processing AMSU. Each AMSU board is reprogrammable and/or reconfigurable at the functional level. With appropriate kinematic mechanisms, structural-level transformations are possible with the ARMA block for a full-scale reliable autonomous HASS system.

Radiation-hardened FPGAs are required for the successful implementation of space-based ARMAs for HASSs. The adaptive devices are expected to exhibit high total dose radiation capability, low single events and latch-up immune and high dose rate survivability. Though these key stringent requirements have been met to a great extent by some available FPGA manufacturers [7], this new design paradigm presents a completely new space qualification challenge. Realising space-qualified MMICs with GaAs substrates is a trivial issue since radiation-hardened GaAs-based devices are an existing and mature technology. It is expected that with the advancement in active device and substrates integration technologies, the proposed adaptive multifunctional structural unit architecture based on the ARMA design concept will be a reality.

IV. CONCLUSION

This paper has explained a novel design methodology and architecture for highly adaptive small satellites systems. It promises to serve as a technology platform for the space community in the design of next-generation space systems. A key benefit of the design routine is that it takes into account the space environment where the candidate mission

development; this involves the generation of subsystem design modules and integration. The space system design variables are then explored with recourse to performing HASS-based multicriteria studies. The methodology next identifies optimal solutions from the trade space and qualifies them. Other mission-goaled candidate decision variables are tried and sensitivity analysis done. The best architectures for the mission are chosen and the design advanced to the next stage of the space satellite procurement programme.

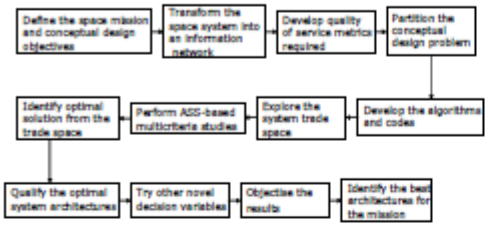

Figure 1. The HASS methodology

III. THE HASS ARCHITECTURE

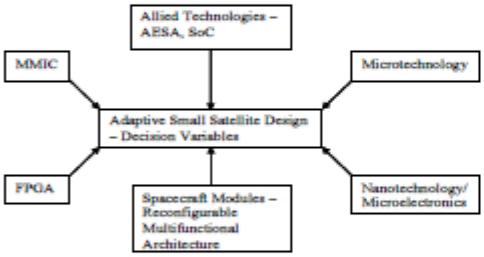

Figure 2. The HASS framework/architecture

The highly adaptive small satellite architecture is shown in Fig. 2. The driving technologies [5] for the adaptive, reconfigurable and multifunctional architecture (ARMA) are: field programmable gate arrays (FPGAs), monolithic microwave integrated circuits (MMICs), microtechnology, nanotechnology, active electronically scanned array (AESA) and system-on-chip (SoC). Monolithic microwave integrated circuit is a microwave circuit technology in which the active and passive components are fabricated on the same semiconductor substrate. MMIC technology has found tremendous applications in the military (phased array radar, electronic warfare, passive imaging, active electronically scanned array), civil (global positioning system, radio frequency identification tagging, medical systems, and cellular/handheld devices) and space (astronomy, radiometers, communication, remote sensing, reconnaissance and passive imaging) [6]. Microtechnology involves the use of advanced, high density devices such as application-specific integrated micromachines (ASIMs), microelectromechanical systems (MEMs), micro-optoelectromechanical systems (MOEMs) and other micromachined devices. Nanotechnology covers molecular or atomic scale devices. Examples are molecular computers, nanomechanical computers, quantum computers, single-electron transistors, quantum dot cells, conducting molecular wires, self-assembling circuit arrays and nanomanipulators. FPGA is a device that contains a matrix of reconfigurable gate array logic circuitry. Once it is configured, the internal circuitry yields a hardware realization of the code application. Top benefits are software reconfigurable, high reliability, high speed, highly deterministic and parallel hardware. AESA (radar) consists of several small transmit/receive (T/R) antenna modules with distributed power capabilities. These technologies form the standard subsystem-level components selection suite for the HASS design concept. The beauty of this architecture lies in its being the enabling platform for developing the result of the HASS methodology. An integrated systems engineering design tool requires adaptability in the program run and development platform. This has been satisfied by incorporating the HASS-based multicriteria studies in the design methodology and/or process.

The bulk of the space systems work has been on individual spacecraft and constellations designs and management issues without an obvious recourse to technology-based system-level adaptability. Thus, a new approach is required that addresses time dimension of space systems, subsystem- and system-levels technologies, cost and system-level performance, multifunctionality, reconfigurability and/or adaptability.

Technologies and strategies for developing lightweight satellite systems for space missions include repackaging, modularization, high-level integration, low-level integration, microtechnology, and nanotechnology. Though some of these strategies can be used for building simple small satellites, the enabling design for implementing a highly adaptive high performance and reliable space system is lacking. It is therefore indispensable that a new design approach that harnesses the volumetric and electrical efficiency of the strategies with flexibility be developed. The adaptive, reconfigurable multifunctional architecture integrates and/or incorporates the scaling strategies and technologies within a highly adaptive and reconfigurable platform.

The functional design concept [3] serves as a beacon for the adaptive, reconfigurable multifunctional architecture. It is a system-oriented design approach and leverages on the scaling strategies. Conventional subsystem boundaries are absent in the design process. It focuses on the identification

architecture(s) must operate. The HASS methodology will be applied in modelling multipurpose small satellites missions.

A new design approach for small satellites called the adaptive, reconfigurable multifunctional architecture has been proposed. The ARMA concept beacons on the existing scaling strategies and the functional design concept. The identification and specification of the functional and structural requirements of the system initiate the design process. Five design customization levels characterise the ARMA approach. Moreover, adaptive multifunctional structural units are the building blocks of the ARMA design paradigm. By sustaining the adaptive technology (FPGA) on the same "substrate" platform with lightweighting techniques such as high/low level integration and modularity, a completely modular, robust and reliable architecture is realised. Two AMSU designs/architectures have been proposed for the HASS system: baseline and hybrid. The AMSU development offers great design reliability and flexibility; its implementation transcends the space community and provides a new design platform for other signal processing and control applications. Parallelism and pipelining, high reliability, high determinism and reconfigurability are amongst the top inherent technologies and applications benefits of the ARMA concept. The cost benefits also include a huge reduction of space mission planning logistics constraints.

REFERENCES

[1] C. Jilla, "A multiobjective, multidisciplinary design optimisation methodology for the conceptual design of distributed Satellite systems," A PhD Thesis, Massachusetts Institute of Technology. pp. 33 – 44, May 2002

[2] G. Ashby and S. Kramer., "Integrated design, evaluation, and decision making for small Satellite design," in 1997 IEEE International Conference on Systems, Man, and Cybernetics. Computational Cybernetics and Simulation. vol. 3, pp. 2341 – 2346, October 1997.

[3] B. Jackson and K. Epstein, "A reconfigurable multifunctional architecture approach for next-generation Nanosatellite design, in *Aerospace Conference Proceedings, 2000 IEEE*, vol.7, pp. 185 – 188, 2000.

[4] T. Mosher, M. Barrera, D. Bearden and N. Lao, "Integration of small Satellite cost and design models for improved conceptual design-to-cost.," pp. 97 – 103, 1998.

[5] S. Ekpo and D. Kettle, "Mm-wave LNAs design for adaptive small Satellite applications," Joint 5th ESA Workshop on Millimetre Wave and 31st ESA Antenna Workshop, Netherlands, Part 2, pp. 843 – 847, May 2009.

[6] D. Kettle, "Microwave Systems," MSc communication engineering lecture notes, The University of Manchester. pp. 37 – 50, 2007

[7] Actel, Radiation-Hardened FPGAs, Ver.3.1. 2005. www.actel.com

Chapter Four

Conclusion and Future Work

4.1 Overview of Research Contributions

This thesis/analytical commentary provides a parametric system engineering analysis of capability-based small satellite missions respecting the enabling and emerging space satellite technologies. A new subsystem design approach for highly adaptive small satellites called the adaptive multifunctional architecture has been developed. This new design concept leverages on the existing scaling techniques and technologies but beacons on the functional design concept. This is important because of the increasing dependence on cost-effective, reconfigurable space-borne assets (especially in the low-earth orbit) to complement terrestrial radio access technologies [SE1, SE5–SE7]. The novel system engineering process and design methodology developed in this research for current and future-generation satellites is currently being adopted and/or applauded by experts in the space community. The presented adaptive small satellites SE design process and analysis have been utilised to design and validate a solar thermal power propulsion system and communication link budget for small satellite missions.

Furthermore, the HASS system has been developed as a network of functions with reconfigurable intra- and inter-subsystem and module links. This eliminates a single point of failure, enhances a deterministic operation and/or helps to sustain a real-time performance [SE5].

This research work has significant and coherent contributions to knowledge and scholarship. The following are some of the novel inputs to the archive of space satellite programmes development for the space community thus:

- capability-based adaptive small satellites systems engineering design process to support additively manufactured components and reduce SWaP-C penalties;
- design routine and architecture for multifunction small satellite structures for significant mass, volume, power consumption and cost savings;
- small satellites systems engineering analysis for sustainable mission applications and post-mission re-use;
- integrated adaptive small satellite electronic subsystems design, modelling, simulation, development and validation;
- reconfigurable small satellites' operational times and ubiquitous data relay analyses;
- advanced beamforming algorithm and beamformer subsystems development for low-cost earth-space communication applications;
- small satellites communication link margins refinements and enhancements; and
- multicriteria optimisation techniques development for sustainable small satellites design and applications.

4.2 Future Work

This research promises to advance the capability-based space systems designs for next-generation and future spacecraft missions. An aspect of the future work includes a full-scale implementation of the adaptive multifunctional architecture at the component-, subsystem- and system-levels. Moreover, developed adaptive multifunctional structural units will be tested for satellite link improvement and post-mission re-applications.

A further research extension of this work will focus on implementing the relevant active and adaptive devices technologies in the additive manufacturing of HASS subsubsystems, subsystems, modules and systems.

The presented HASS design methodology features a multicriteria design variables study. The parameter space integration (PSI) method has been used for establishing the correct statement and solution of real-life optimisation problems. Space shuttles, aircraft, rockets and unmanned vehicles have been designed with this optimisation concept. The PSI technique will be implemented in a HASS system multicriteria study for 5G-enabled earth-space communications.

An investigation of the possibility of implementing heterogeneous space-based adaptive wireless sensor networks (SAWSNs) shall be carried out for various formation-flying and constellation satellites. Finally, Advanced radio access technologies (such as the 5G communication standard) will be investigated for a sustainable multi-standard satellite broadband backhaul for integrated earth-space communications.

References

[1] Clements, J., Josh George, Rapid Manufacturing of Satellite Structures and Heat Pipes using Ultrasonic Consolidation, *in Proc. Small Satellite Conference*, 03 April 2013, pp. 1–7.

[2] Horais, Brian J., Love, Lonnie J. and Dehoff, Ryan R., The Use of Additive Manufacturing for Fabrication of Multifunction Small Satellite Structures, *in Proc. Small Satellite Conference*, 01 August 2013, pp. 1–7.

[3] Càceres, M., Mission Model Offers Snapshot of Space Payloads, *Aerospace Magazine*, AIAA, pp. 24–27, June 2011.

[4] Barnhart, D., Vladimirova, T. and Sweeting, M., Very-Small-Satellite Design for Distributed Space Missions, *Journal of Spacecraft and Rockets,* vol. 44, pp. 244–257, November-December 2007.

[5] Bin, L. Zheng, Y., Chenguang, Z. and Xiaomin, Z., Design and Experiment on Small Satellite Formation Flying Simulation Platform, in *Proceedings of the IEEE Aerospace Conference,* 2005, pp. 244–247.

[6] Cvetkovic, S. R. and Robertson, G. J., Spacecraft Design Considerations for Small Satellite Remote Sensing, *IEEE Trans. on Aerospace and Electronic Systems*, vol. 23, pp. 391–403, 1993.

[7] Barnhart, D., Vladimirova, T. and Sweeting, M., Satellite Miniaturization Techniques for Space Sensor Networks, *Journal of Spacecraft and Rockets,* vol. 46, pp. 469–472*,* March–April 2009.

[8] Xuwen, L., Li, L., Huawang, L., Yinjian, C., Dexin, S. and Genqing, Y., Silicon Solid-state Small Satellite Design Based on IC and MEMS, in *Proceedings* of the *Solid-State and Integrated Circuit Technology,* 1998, pp. 932–935.

[9] Jackson, B. and Epstein, K., A Reconfigurable Multifunctional Architecture Approach for Next Generation Nanosatellite Design, in

Proceedings of the IEEE Aerospace Conference, vol. 7*,* 2000, pp. 185–193.

[10] Vladimirova, T. and Bridges, C., Dual Core System-on-a-Chip Design to Support Intersatellite Communications, in *Proceedings of the NASA/ESA Conference on Adaptive Hardware and Systems*, 2008.

[11] Hassan, R. and Crossley, W., Spacecraft Reliability-Based Design Optimization under Uncertainty Including Discrete Variables, *Journal of Spacecraft and Rockets*, vol. 45, pp. 394–405, March–April 2008.

[12] Schmitz, H., Application Examples: How to Use FPGAs in Satellite Systems, *Actel Corporation, California*, 2010.

[13] Brown, C., Elements of Spacecraft Design. Virginia: AIAA, Inc. 2002, pp. 1–43, 315–368.

[14] Alvarado, S., Reduce design risk for low-Earth orbit satellites and other new space applications, A Texas Instruments Publication, 2019..

[15] Helvajian, H. and Janson, S. W., Small Satellites: Past, Present, and Future, AIAA, Inc., Virginia. pp. 95–110, 455–475, 527, 559–569, 622,623, 773, 2008.

[16] Elbert, B., Introduction to Satellite Communications, Artech House, Inc., London. Third Edition. pp. 1–38, 69–107, 195–205, 389–393, 257–289, 291–297, 337–345, 389–405, 418, 2008.

[17] Actel Corporation, Radiation-Hardened FPGAs, Ver. 3.1, 2005. Available from www.actel.com (Accessed: Jan.18, 2010).

[18] National Instruments, Introduction to FPGA Technology: Top Five Benefits, *National Instruments conference and exhibition*, London, United Kingdom, 2009.

[19] Turnbull, W., Beyond Awareness: Moving Towards Comprehensive Space Situational Knowledge. *A Research Report,* Air University, Alabama. pp. 9–30, April 2008.

[20] Wittig, M., Satellite Onboard Processing for Multimedia Applications, *IEEE Communications Magazine*, pp. 135*,* 2000.

[21] Steer, M and Palmer, W. D., Multifunctional Adaptive Microwave circuits and Systems, SciTech Publishing Inc., Raleigh, NC, pp. 106 – 154, 208–237, 2009.

[22] Robertson, I. D. and Lucyszyn, S., RFIC and MMIC Design and Technology, The Institution of Electrical Engineers, London, pp. 1–81, 2001.

[23] Quinn, H. M., Graham, P. S., Wirthlin, M. J., Pratt, B., Morgan, K. S., Caffrey, M. P., and Krone, J. B., A Test Methodology for Determining Space Readiness of Xilinx SRAM-Based FPGA Devices and Designs, *IEEE Transactions on Instrumentation and Measurement,* Vol. 58, pp. 3380–3395, 2009.

[24] Pisarevsky, D. M. and Gurfil, P., Optimizing Multiple-Flyby Orbits for Increasing the Resolution of Space Telescopes. *Journal of Spacecraft and Rockets.* Vol. 46, pp. 373– 80, March–April 2009.

[25] Saleh, J., Hastings, D. and Newman, D., Spacecraft Design Lifetime, *Journal of Spacecraft and Rockets,* Vol. 39, No. 2, pp. 244–257, March-April 2002.

[26] Steer, M., Microwave and RF Design: A Systems Approach, SciTech Publishing Inc., Raleigh, NC, pp. 101, 2010.

[27] White, B. E., Complex Adaptive Systems Engineering, *IEEE Aerospace and Electronic Systems*, vol. 25, no. 12, pp. 16–22, Dec. 2010.

[28] Biemer, S. M., Systems Engineering for Large-scale System of Systems, *4th Annual IEEE International Systems Conference Tutorial*, Part 1: pp. 1–84 & Part 2: pp. 1–154, San Diego CA, USA, April 5–8, 2010.

[29] Jackson, P. Getting Design Right: A Systems Approach, CRC Press, ISBN 978-1-4398-1115-3, Florida, USA, 2010.

[30] Roddy, D and Coolen, J., Electronic Communications, Prentice-Hall, Inc., New Jersey, Fourth Edition. pp. 711–753, 1995.

[31] Jilla, C., A Multiobjective, Multidsiciplinary Design Optimisation Methodology for the Conceptual Design of Distributed Satellite Systems. *A PhD Thesis, Massachusetts Institute of Technology.* pp. 33–44, May 2002.

[32] Ashby, G. and Kramer, S., Integrated Design, Evaluation, and Decision Making for Small Satellite Design, *in 1997 IEEE International Conference on Systems, Man, and Cybernetics. Computational Cybernetics and Simulation.* Vol. 3. pp. 2341–2346, October 1997.

[33] Valero, J. L., "Space Situational Awareness at the European Union Satellite Centre," in *Proceedings of the Near Space Security Conference*, Amsterdam, March 2010.

[34] AESA Radar: Revolutionary Capabilities for Multiple Missions, *A publication of Northrop Grumman,* pp. 1–5, 2009.

[35] Anwar, A., Fundamentals and Application of AESA Radar, *A Strategy Analytics Webinar*, pp. 36–42, 2010.

[36] Teague, G., GaAs in Space, *A Triquint Semiconductor Gmbh Publication*, pp. 1–4, 2009.

[37] Bessemoulin, A. et al, High Gain 110-GHz Low Noise Amplifier MMICs using 120-nm Metamorphic HEMTs and Coplanar Waveguides. *13th GAAS Symposium, Paris*. pp. 1–4, 2005.

[38] Kelly, M., Angelov, I., Starski, J. P., Wadefalk, N. and Zirath, H., 4 – 8 GHz Low Noise Amplifiers using metamorphic HEMT Technology, *Proceedings of the 1st European Microwave Integrated Circuits Conference*, pp. 118–121, September 2006.

[39] Scavennec, A., Sokolich, M. and Baeyens, Y., Semiconductor Technologies for Higher Frequencies, *IEEE Microwave Magazine*, Vol. 10, No. 2. pp. 77–86, April 2009.

[40] Kuo, Y. L., Kumar, K. D., Behdinan, K., and Fawaz, Z., Open-Loop Optimal Attitude Control of Miniature Spacecraft Using MEMS

Actuators, *IEEE Transactions on Aerospace and Electronic Systems*, Vol. 44. pp. 1381-1390, 2008.

[41] Roberts, S. C. and Aglietti, G. S., Design of a Multifunctional Spacecraft Structure using Plastic Lithium-Ion Batteries. *12th AIAA/ISSMO Multidisciplinary Analysis and Optimization Conference,* Victoria, British Columbia Canada, p. 1, 2008.

[42] Burgon, R., Roberts, P. C., Roberts, E. J. A. and Ankersen, F., Science Operations Planning Optimization for Spacecraft Formation Flying Maneuvers. *Journal of Spacecraft and Rockets.* Vol. 46. pp. 634 – 644, May–June 2009.

[43] Haddad, N., McWilliams, H. and Wagoner, P., NASA Engineering Design Challenges: Spacecraft Structures. Educational Product, R. Garson, Ed. Somerville, MA: National Aeronautics and Space Administration. pp. 1–78, 2007.

[44] Saleh, J. H., Flawed metrics: Satellite Cost Per Transponder and Cost Per Day, *IEEE Transactions on Aerospace and Electronic System.,* Vol. 44. pp. 147–156, 2008.

[45] Corso, D. et al, Architecture of a Small Low-Cost Satellite. *10th Euromicro Conference on Digital System Design Architectures, Methods and Tools* (DSD). pp. 1 – 4, 2007.

[46] Rodrigues, G. and Santiago-Prowald, J., Qualification of Spacecraft Equipment: Random-Vibration Response Based on Impedance/Mobility Techniques. *Journal of Spacecraft and Rockets*. Vol. 45, pp. 104–115, January–February 2008.

[47] Dainelli, V., Giannantoni, G. and Muscinelli, M., W Band Multi-Applications Payload for Space and Multiplanetary Missions, *Satellite Communications and Navigation System*, Oerlikon Contraves SpA. pp. 433, 2009.

[48] Paschalidis, N. P., Advanced System-on-a-Chip Microelectronics for Spacecraft and Science Instruments. *Acta Astronautica*, Vol. 52. pp. 411–420, March 2003.

[49] Dan, F., Shye, A., Bhattacharya, S., Connors, D. A. D. and Wichmann, S., An Adaptive Fault-Tolerant Memory System for FPGA-based Architectures in the Space Environment. *Second NASA/ESA Conference on Adaptive Hardware and Systems 2007 (AHS 2007).* pp. 250-257, 2007.

[50] Shu, Z., Guo, Y. and Lian, J., Steady-State and Dynamic Study of Active Power Filter With Efficient FPGA-Based Control Algorithm, *IEEE Trans. on Industrial Electronics*, Vol. 55, no. 4, pp. 1527, 1528, April 2008.

[51] Liu, Q., Constantinides, G. A., Masselos, K. and Cheung, P. Y. K., Data-reuse exploration under an on-chip memory constraint for low-power FPGA-based Systems, *Computers & Digital Techniques, IET,* Vol. 3, pp. 235-246, 2009.

[52] Wang, J. J., Katz, R. B., Sun, J. S., Cronquist, B. E., McCollum, J. L., Speers, T. M., and Plants, W. C., SRAM based re-programmable FPGA for space applications, *IEEE Transactions on Nuclear Science,* Vol. 46, pp. 1728-1735, 1999.

[53] Ekpo, S. and George, D., A Power Budget Model for Highly Adaptive Small Satellites, Recent Patents on Space Technology, Vol. 3, No. 2, pp. 118–127, 2013; DOI:10.2174/1877611611303020003.

[54] Gonzalez, I. et al, Classification of Application Development for FPGA-Based Systems, in *IEEE National Aerospace and Electronics Conference 2008*, pp. 203–208, 2008.

[55] Brogley, M., FPGA reliability and the Sunspot Cycle, *A White Paper Publication by Microsemi Corporation,* California, pp. 3–13, September 2011.

[56] Radiation Hardened FPGA Technology for Space Applications, *IEEE Aerospace Conference*, pp. 1–7, March 2007.

[57] Aeby, C. A., Space Systems Survivability – The Protection Environment, *IEEE Aerospace and Electronic Systems Magazine*, Vol. 26, No. 7, pp. 37–41, July 2011.

[58] Boncyk, W. C., Revolutionary Design Meets Spacecraft Reality: Lessons Learned, *IEEE Aerospace and Electronic Systems Magazine*, Vol. 25, No. 11, pp. 25–31, November 2010

[59] Castillo, L. D., Moussessian, A., McPherson, R., Zhang, T. and Hou, Z., Flexible Electronic Assemblies for Space Applications, *IEEE Aerospace and Electronic Systems Magazine*, Vol. 25, No. 6, pp. 25–29, 2010.

[60] Jones, P. S. and Spence, B. R., Spacecraft Solar Array Technology Trends, *IEEE Aerospace and Electronic Systems Magazine*, Vol. 25, No. 8, pp. 17–28, August 2011.

[61] Meerman, M. J. M, Unwin, M. N., Gleason, S, Jason, S., Sweeting, M. N., and Curiel A. S., A Nanosatellite to Demonstrate GPS Oceanography Reflectometry, *Space Technology Journal*, Vol. 23, No. 4, pp. 245, 2003.

[62] Lucente, M., et al, IKNOW Mission: Payload Design for In-Orbit Test of W Band Technology, *IEEE Aerospace Conference, 2008,* pp. 1–10, 2008.

[63] Bhat, B. R., New Radiation Dose Model for Geostationary Orbit, *Journal of Spacecraft and Rockets*, Vol. 46, pp. 712–715, May–June 2009.

[54] Moore, S., UK Airborne AESA Radar Research, *IEEE Aerospace and Electronic Systems Magazine*, Vol. 25, No. 2, pp. 29–35, 2010.

[65] Firestone, D., Atkin, R., Hooks, C. and Klein, P. A., Low-Cost, Automated Ground Station for LEO Mission Support, *IEEE Aerospace and Electronic Systems Magazine*, Vol. 26, No. 3, pp. 12–18, March 2011.

[66] Lu, D and Zhou, Z., Integrated Solutions for Testing Wireless Communication Systems, *IEEE Communications Systems Magazine*, Vol. 49, No. 6, pp. 97, June 2011

[67] Friedman, A. et al, (ASUSat1): Low-Cost, Student-Designed Nanosatellite, *Journal of Spacecraft and Rockets* Vol. 39, No. 5. pp. 740–748, September–October 2002.

[68] Benedict, B., Satellite Payload Arrangement, a Device for and Method of attaching a Piggyback Satellite Payload and Adapter to be used for a Payload Arrangement for launching the Piggyback Satellite, U.S 7,866,607, January 2011.

[69] Statnikov, R. and Statnikov, A. The Parameter Space Investigation Method: Toolkit, Artech House, London, 2011.

[70] Ekpo, S. C., Kharel, R. and Uko, M. (2018), A Broadband LNA Design in Common-Source Configuration for Reconfigurable Multi-standards Multi-bands Communications," *in Proc., ARMMS RF & Microwave Society Conference, Double Tree by Hilton Oxford Belfry, Thame, UK, 01 & 02 April 2018*, pp. 1-10.

Appendices

Appendix 1

A. Statistical Analysis of Mass-based PERs for LEO Satellites

To validate the mass-based PERs for LEO satellites, a statistical analysis technique is employed. Consider the data below:

$$\begin{pmatrix} X_{11} & X_{12} & . & . & . & X_{1N} & . & Y_1 \\ & & & & . & & & \\ X_{M1} & X_{M2} & . & . & . & X_{MN} & . & Y_M \end{pmatrix} \quad \text{(A1.1)}$$

For a 1-D space, Eqn. A1.1 becomes:

$$f(X) = W_1 X + W_O \quad \text{(A1.2)}$$

For a high-dimensional space, Eqn. 3.13 becomes:

$$f(X) = WX + W_O \quad \text{(A1.3)}$$

where W and X are the vectors and $W.X$ is the inner product of vectors W and X.

The loss function [130] is the amount of residual error obtained after fitting the linear function. The residual error is the sum of all dependent (system's resource) variable values, Y_j (target design parameter), minus the prediction which is $W_1X_j - W_o$ to the square. Mathematically, the loss function is given by: [130]

$$Loss = \sum_i \left(Y_i - W_1 X_i - W_o\right)^2 \tag{A1.4}$$

This gives the quadratic error between the target tables and what the best hypothesis can produce. The minimising of loss is used for the linear regression of a new linear regression problem and can be written as follows: [130]

$$W^* = \arg\min_{\omega} Loss \tag{A1.5}$$

The next step involves the minimisation of the quadratic loss [130].

Let
$$\min \sum_{\omega} \left(Y_i - W_1 X_i - W_o\right)^2 = L \tag{A1.6}$$

Differentiating Eqn. A1.6 with respect to W_0 and equating the result to zero yields:

$$\partial L / \partial W_o = -2\sum \left(Y_i - W_1 X_i - W_o\right) = 0 \tag{A1.7}$$

From Eqn. A1.7, the W_0 term is given by:

$$\sum Y_i - W_1 \sum X_i = M W_o$$

or,

$$W_o = \left(1/M\right)\sum Y_i - \left(W_1/M\right)\sum X_i \tag{A1.8}$$

where M is the size of the data.

Similarly, differentiating Eqn. A1.6 with respect to W_1 and equating the result to zero yields:

$$\partial L / \partial W_1 = -2\sum (Y_i - W_1 X_i - W_o) X_i = 0 \qquad \text{(A1.9)}$$

$$\sum X_i Y_i - W_o \sum X_i = W_1 \sum X_i^2$$

$$\sum X_i Y_i - (1/M)\sum Y_i \sum X_i + \left(W_1 / M\right)\left(\sum X_i\right)^2 = W_1 \sum X_i^2$$

Thus, the term W_1 can be obtained from Eqn. A1.9 as:

$$W_1 = \frac{M\sum X_i Y_i - \sum X_i \sum Y_i}{M\sum X_i^2 - \left(\sum X_i\right)^2} \qquad \text{(A1.10)}$$